Localization and Functional Analysis of Two-Pore Channel Proteins

A thesis submitted to board of the faculty of Medical Sciences, University of Oxford, for the degree of Doctor of Philosophy in Michaelmas Term 2011.

Keiko Watanabe

St. Catherine's College

THE LOCALIZATION AND FUNCTIONAL ANALYSIS OF TWO-PORE CHANNEL PROTEINS

Keiko Watanabe, St. Catherine's College
A thesis submitted for the degree of Doctor of Philosophy in Michaelmas Term 2011

ABSTRACT

Nicotinic acid adenine dinucleotide phosphate (NAADP) is the most recently characterized Ca^{2+} mobilizing second messenger, joining inositol 1,4,5-trisphosphate (IP_3) and cyclic ADP-ribose (cADPR). Previous pharmacological and biochemical studies have suggested that NAADP targets acidic Ca^{2+} stores rather than the ER, which releases Ca^{2+} in response to IP_3 or cADPR. Although NAADP receptors are proposed to be distinct from those for IP_3 and cADPR, the molecular identity of NAADP receptors has remained elusive. This study focuses on establishing whether two-pore channels (TPCs), a family of intracellular Ca^{2+}-release channels, function as NAADP receptors.

In this thesis, TPC proteins have been investigated as potential NAADP receptors in the sea urchin, *Strongylocentrotus purpuratus*, whose genome encodes three potential TPC proteins, namely *Sp*TPC1, *Sp*TPC2 and *Sp*TPC3, and in the social amoeba, *Dictyostelium discoideum*, which encodes only one TPC2 (*Dd*TPC2). These channels were analyzed in multiple model systems namely the sea urchin egg, human cell lines (HEK cells and HeLa cells), an insect cell line (sf9) and *Dictyostelium*. Analytical approaches including the generation of anti-TPC antibodies, localization studies, ligand binding assays and Ca^{2+} release studies were employed.

*Sp*TPC1 and *Sp*TPC2 were predominantly localized to the ER and the lysosome, respectively. Endogenous sea urchin protein immunoprecipitated with anti-*Sp*TPC3 antibody showed enhanced NAADP binding. However, no correlation between NAADP binding and expression levels of TPCs in HEK cells or Sf9 cells was detectable. In *Dictyostelium*, TPC2 was localized to the contractile vacuole and the ER, whereas *Dd*TPC2 localized to the lysosome and Golgi apparatus when expressed in HeLa cells. Protein expression of *Dd*TPC2 is regulated developmentally, reaching a peak in the late stages of development. A *tpc2* null strain exhibited abnormal post-aggregative development, consistent with a role for *Dd*TPC2 at later stages of development. No high affinity NAADP binding sites or NAADP-induced Ca^{2+} release were detected in *Dictyostelium* membranes isolated either at the early or late development stages in these studies. However, NAADP-induced Ca^{2+} release from vesicle fractions prepared from vegetatively growing cells was observed.
On the other hand, arachidonic acid (AA) induced Ca^{2+} release from vesicles prepared from growing cells and from cells developed for 4 hours or 20 hours. AA-induced Ca^{2+} release was altered in *tpc2* null cells. In sea urchin egg homogenate, AA also elicited Ca^{2+} release with an EC_{50} value of approximately 8 μM. Low concentrations of AA effectively inhibited NAADP-induced Ca^{2+} release.

It was not possible to produce evidence of TPCs being NAADP-sensitive Ca^{2+} channels in the systems investigated. In *Dictyostelium*, TPC2 does not appear to be responsible for NAADP-induce Ca^{2+} release. However, TPC2 may play a role in AA-induced Ca^{2+} release.

ABBREVIATIONS

AA	arachidonic acid
ACA	adenylyl cyclase
ACS	Acidic calcium store
ADPR	ADP-ribose
ARC	ADP-ribosyl cyclase
ARC channels	arachidonate-regulated calcium selective channels
ATP	adenosine 5'-triphosphate
Baf	bafilomycin A1
β-NAD	β-nicotinamide adenine dinucleotide
BLAST	basic local alignment search tool
bp	base pair
bs	blasticidin
BSA	bovine serum albumin
bsR	blasticidin resistance
cADPR	cyclic adenosine diphosphate ribose
cAMP	adenosine 3', 5'- cyclic monophosphate
cAR	cAMP receptor
CCCP	carbonyl cyanide *m*-chlorophenyl-hydrazone
CCD	central core disease
cDNA	complementary DNA
cGMP	guanosine 3′,5′ monophosphate
CHAPS	3-[(3-cholamidopropyl) dimethylammonio]-1 propanesulfonate
CICR	calcium-induced calcium release
CMA	concamycin A
CRAC	cytosolic regulator of adenylyl cyclase
CRAC channel	calcium-release activated calcium channel
CV	contractile vacuole
DAG	diacylglycerol
DAPI	4', 6-diamino-2-phenylindole
DIF	differentiation inducing factor
DMEM	Dulbecco's Modified Eagle's medium
DMSO	dimethyl sulfoxide
DNA	deoxyribonucleic acid
DTT	dithiothreitol
ECL	enhanced chemiluminescence
EDTA	ethylenediaminetetra-acetic acid disodium salt
EGTA	ethyleneglycol-bis-(β-amino ethyl ether)-N,N,N',N' tetra-acetic acid
ER	endoplasmic reticulum
ERK2	extracellular-signal regulated kinase 2
ETI	eicosatriynoic acid
ETYA	eicosatetraynoic acid
FA	fatty acid
FBS	foetal bovine serum
gDNA	genomic DNA
G418	geneticin
GFP	green fluorescent protein

Glu-IM	glucamine intacellular medium
GPCR	G protein-coupled receptor
GPN	glycyl-phenylalanine-2-naphthylamide
GTP	guanosine 5'-triphosphate
GST	glutathione S-transferase
HA	haemagglutinin
HEK cells	Human Embryonic Kidney cells
HEK293T	Human Embryonic Kidney 293 large T antigen cells
HEPES	N-2-hydrozyethyylpiperazine-N'-2-ethanesulphonic acid
His	histidine
HPLC	high performance liquid chromatography
HRP	horseradish peroxidase
IMCD	mouse inner medullary collecting duct
IP_3	inositol 1,4,5-trisphosphate
IplA	IP_3 receptor–like protein (*Dictyostelium*)
IPTG	isopropyl β-D-thiogalactopyranoside
IP_3R	inositol 1,4,5-trisphosphate receptor
kDa	kilodaltons
KLH	keyhole limpet haemocyanin
kV	kilovolts
LA	linoleic acid
LB	lysogeny broth
LGCC	ligand-gated calcium channel
LvsA	large volume sphere A
Mb	megabases
MBS	*m*-maleimidobenzoyl-*N*-hydroxysuccinimide ester
MCR	mutiple cloning site
MDCK	Madin-Darby canine kidney
mRNA	messenger RNA
MW	molecular weight
NAADP	nicotinic acid adenine dinucleotide phosphate
NADP	nicotinamide adenine dinucleotide phosphate
NCKXs	Na^+/Ca^{2+}-K^+ exchangers
NCXs	Na^+/Ca^{2+} exchangers
NLS	nuclear localization signal
NP-40	nonidet P-40
OA	oleic acid
ORF	open reading frame
P	phosphate
PA	palmitic acid
PBS	phosphate buffered saline
PCR	polymerase chain reaction
PEG	polyethylene glycol
PIP_2	phosphatidylinositol 4,5-bisphosphate
PIP_3	phosphatidylinositol 3,4,5-trisphosphate
PI3K	phosphatidylinositol-3-kinase
PKA	cAMP-dependent protein kinase A
PLA_2	phospholipase A_2

PLC	phospholipase C
PMCAs	plasma membrane Ca^{2+}-ATPases
PMSF	phenylmethylsulphonyl fluoride
PTEN	phosphatase tensin type domain-containing protein
PTP3	protein tyrosine phosphatase-3
P2X receptor	purinergic receptor
PUFAs	polyunsaturated fatty acids
RFP	red fluorescent protein
RNA	ribonucleic acid
ROC	receptor-operated channel
RT	reverse transcriptase
RyR	ryanodine receptor
SDS	sodium dodecyl sulphate
SDS-PAGE	sodium dodecyl sulphate polyacrylamide gel electrophoresis
SERCA	sarco (endo) plasmic reticulum calcium ATPase
SMOC	second messenger operated Ca^{2+} channel
SOC	store-operated channel
SOCE	store-operated calcium entry
SPCAs	secretor-pathway Ca^{2+}-transport ATPases
SPF rabbit	specific pathogen free rabbit
STAT	signal transducer and activator of transcription
STIM	stromal interaction molecule
TAE	Tris-acetate-EDTA buffer
tBHQ	*tert*-Butylhydroquinone
Tg	thapsigargin
TGN	trans Golgi network
TKR	tyrosine-kinase receptors
TMD	transmembrane domains
TPC	Two-pore channel
Tris	2-amino-2-(hydroxymethyl-)1,2-propanediol
TRP	transient receptor potential
TRPA	transient receptor potential ankyrin
TRPC	transient receptor potential canonical
TRPM	transient receptor potential melastatin
TRPML	transient receptor potential mucolipin
TRPN	transient receptor potential no mechanoreceptor potential C
TRPP	transient receptor potential polycystin
TRPV	transient receptor potential vanilloid
VGCC	voltage-gated calcium channel
XeC	xestospongin C
X-gal	5-bromo-4-chloro-3-indolyl-β-D-galactoside

TABLE OF CONTENTS

ABSTRACT ..... **i**
TABLE OF CONTENTS ..... **ii**
ABBREVIATIONS ..... **vi**

CHAPTER 1: GENERAL INTRODUCTION **1**
1.1. Calcium signalling **2**
1.1.1. Ca^{2+} as an intracellular messenger 2
1.1.2. Ca^{2+} homeostasis 2
1.1.3. Ca^{2+} entry through the plasma membrane 3
1.1.3.1. Store-operated Ca^{2+} entry (SOCE) 3
1.1.3.2. Arachidonate-regulated Ca^{2+}-selective (ARC) channels 5
1.1.3.3. Transient receptor potential (TRP) channels 7
1.1.3.4. Voltage-gated calcium channels (VGCCs) 9
1.1.3.5. Receptor-operated channels (ROCs) 12
1.1.4. Ca^{2+} mobilization from intracellular stores 13
1.1.4.1. Endoplasmic reticulum (ER) 13
1.1.4.2. Intracellular acidic stores 19
1.1.4.3. Mitochondria 29
1.1.4.4. Golgi apparatus 30
1.1.5. Removal of calcium 31
1.1.6. G protein-coupled receptors 31
1.1.7. Sea urchin egg as a model system for investigating Ca^{2+} mobilization 32
1.2. *Dictyostelium discoideum* (*Dictyostelium*) **36**
1.2.1. Developmental cycle of *Dictyostelium* 36
1.2.2. *Dictyostelium* as a model system 40
1.2.3. Signalling molecules in *Dictyostelium* proposed to work through Ca^{2+}-dependent pathways 41
1.2.3.1. cAMP-induced signalling pathways during early development 41
1.2.3.2. The role of cAMP during post-aggregative development 45
1.2.3.3. Differentiation inducing factor in *Dictyostelium* 45
1.2.4. Cell fate and intracellular Ca^{2+} concentration in *Dictyostelium* 47
1.2.5. Global or transient changes of $[Ca^{2+}]_i$ 49
1.2.6. Ca^{2+} oscillations 50
1.2.7. Known Ca^{2+} mobilising agents in *Dictyostelium* 51
1.2.7.1. cAMP 51
1.2.7.2. Differentiation-inducing factor 1 (DIF-1) 52
1.2.7.3. Inositol 1,4,5-trisphosphate (IP_3) 52
1.2.7.4. Fatty acids as Ca^{2+} mobilizing agents 53
1.2.8. Intracellular Ca^{2+} stores in *Dictyostelium* 55
1.2.9. Ca^{2+} transporters and channels in *Dictyostelium* 57
1.2.9.1. PMCA-type Ca^{2+}-ATPase (PAT1) 57
1.2.9.2. IP_3 receptor-like protein 57
1.2.9.3. Polycystin-2-like protein 59
1.2.9.4. P2X receptors 59
1.2.9.5. Mucolipin 60
1.2.9.6. Two-pore channel-2 (TPC2) 60
1.2.10. *Dictyostelium* as a model system for studying TPC2 61

CHAPTER 2: MATERIALS AND METHODS **62**
2.1. Cell lines and consumables **63**
2.2. Molecular and biochemical techniques **63**

2.2.1. DNA manipulations 63
2.2.2. Competent cells 63
2.2.3. Transformation 65
2.2.4. Primers and sequencing 66
2.2.5. Quantification of DNA / RNA 66
2.3. Protein analysis 67
2.3.1. Quantifying protein concentration 67
2.3.2. SDS-polyacrylamide gel electrophoresis and Western blot analysis 68
2.4. Microscopy 70
2.4.1. Fluorescence microscopy 70
2.4.2. Laser scanning confocal microscopy 70
2.5. [^{32}P]-NAADP experiments 71
2.5.1. [^{32}P]-NAADP synthesis 71
2.5.2. High-performance liquid chromatography (HPLC) 72
2.6. Sea urchin (*Lytechinus pictus*) 72
2.6.1. Collection of sea urchin eggs 73
2.6.2. Preparation of sea urchin egg homogenate (50% v/v) 73
2.6.3. Microsome preparation 74
2.6.4. Binding assays 74
2.6.5. Calcium uptake experiments 74
2.7. Mammalian cells 75
2.7.1. Cell culture 75
2.7.2. Transfection for immunohistochemistry experiments 76
2.7.3. Immunohistochemistry 76
2.7.4. Transfection: calcium phosphate method 77
2.7.5. Whole cell lysate (sonication) 77
2.7.6. Membrane preparation 79
2.7.7. NAADP binding 80
2.8. *Spodoptera frugiperda* (Sf9) cells 80
2.8.1. Cell culture 80
2.8.2. Co-transfection of transfer vector DNA and bacmid DNA 81
2.8.3. Producing recombinant baculovirus 81
2.8.4. Test for gene expression 82
2.8.5. Infecting cells to amplify further stocks of recombinant virus. 82
2.8.6. Extraction of recombinant protein by solubilization 82
2.8.7. Membrane preparation for binding assay (homogenate) 83
2.8.8. Binding assay 83
2.8.9. Purification of His fusion proteins 84
2.9. *Dictyostelium discoideum* 85
2.9.1. Cell culture 85
2.9.2. *Dictyostelium* development 86
2.9.3. Transformation of *Dictyostelium* by electroporation 87
2.9.4. Genomic DNA (gDNA) preparation 88
2.9.5. Isolation of *Dictyostelium* RNA 89
2.9.6. cDNA (complementary DNA) synthesis 90
2.9.7. Calcium release assays 92
2.9.8. NAADP binding assay 93
2.9.9. Immunofluorescence 93
2.9.10. Sample preparation for Western blot analysis 94

CHAPTER 3: LOCALIZATION AND NAADP BINDING ACTIVITY OF RECOMBINANT TPC PROTEINS 95
3.1. Introduction 96
3.2. Aims 97

3.3. Results 97
3.3.1. Putative *Sp*TPCs 97
3.3.2. Production of anti-*Sp*TPC polyclonal antibodies 98
3.3.3. Overexpression of *Sp*TPCs 102
3.3.3.1. *Sp*TPC expression in mammalian cells 102
3.3.3.2. Detection of transient expression of *Sp*TPCs 105
3.3.3.3. Characterization of anti-*Sp*TPC antibodies using recombinant protein 107
3.3.3.4. Efficiency of immunoprecipitation using anti-*Sp*TPC antibodies 107
3.3.4. Localization of *Sp*TPCs in starfish oocytes 109
3.3.4.1. Heterologous expression of *Sp*TPCs in starfish oocytes 111
3.3.4.2. Localization of *Sp*TPCs in starfish oocytes 111
3.3.5. Localization of transiently expressed *Sp*TPCs in HEK293 cells 114
3.3.6. NAADP binding to sea urchin egg proteins 120
3.3.6.1. NAADP shows high affinity binding to sea urchin egg homogenate 121
3.3.6.2. NAADP binding to membrane fractions 122
3.3.6.3. Correlation between NAADP binding and the presence of *Sp*TPCs 122
3.3.7: NAADP binding in cells expressing recombinant *Sp*TPCs 124
3.3.7.1. NAADP binding in HEK293T cells transiently expressing mRFPmars *Sp*TPCs 124
3.3.7.2. NAADP binding in HEK293 cells expressing HA-tagged *Sp*TPCs 126
3.3.8. Bac-to-Bac baculovirus expression system (insect cell, Sf9 expression) 128
3.3.8.1. Expression of TPCs in insect cells 128
3.3.8.2. Confirmation of integration of TPCs into bacmid DNA 130
3.3.8.3. Infection of insect cells with recombinant baculovirus particles 130
3.3.8.4. Expression levels of TPC recombinant proteins in Sf9 cells 133
3.3.9. NAADP binding activity of membranes prepared from Sf9 cells expressing TPCs 133
3.3.9.1. Purification of *Hs*TPC2 using a nickel column 135
3.3.9.2. NAADP binding assay applied to purified recombinant protein 135
3.4. Discussion 137
3.4.1. Expression of *Sp*TPC recombinant proteins 137
3.4.2. Localization studies 138
3.4.3. NAADP binding 139
3.5. Summary 142

CHAPTER 4: ANALYSIS OF TWO PORE CHANNEL (TPC) PROTEIN AND NAADP BINDING ACTIVITY IN *DICTYOSTELIUM DISCOIDEUM* 143

4.1. Introduction 144
4.2. Aims 147
4.3. Results 148
4.3.1. Putative TPC2 in *Dictyostelium* 148
4.3.2. Developmental delay in GPN-treated *Dictyostelium* cells 152
4.3.3. Levels of *Dd*TPC2 mRNA during development 156
4.3.4. NAADP binding activity in *Dictyostelium* cells 159
4.3.4.1. Fractionation of intracellular Ca^{2+} stores 159
4.3.4.4. NAADP binding to membrane fractions 159
4.3.5. Detection of endogenous *Dd*TPC2 at the protein level 166
4.3.5.1. Production of anti-*Dd*TPC2 polyclonal antibody 166
4.3.5.2. Antigen peptide synthesis in *E. coli* 167
4.3.5.3. Reactivity of serum to endogenous or heterologous antigens 171
4.3.5.4. Antibody purification 171
4.3.5.5. Endogenous protein recognized by purified antibody throughout development of *Dictyostelium* 174
4.3.6. The localization of endogenous *Dd*TPC2 177
4.3.7. Overexpression of *Dd*TPC2 177
4.3.7.1. Expression of synthetic recombinant *Dd*TPC2 179
4.3.8. Localization of exogenously-expressed *Dd*TPC2 in *Dictyostelium* 184

4.3.9. The localization of *Dd*TPC2 in HeLa cells....184
4.3.10. Generation of *tpc2*$^-$ cells....186
4.3.10.1. Construction of *Ddtpc2* disruption vector....188
4.3.10.2. Screening potential disruptant clones....188
4.3.10.3. Development of the *Ddtpc2*$^-$ cells....190
4.4. Discussion....195
4.4.1. The involvement of acidic Ca^{2+} stores in *Dictyostelium* development....195
4.4.2. *Ddtpc2* mRNA levels are developmentally regulated....196
4.4.3. Protein levels....197
4.4.4. Localization study....199
4.4.5. The role of *Dd*TPC2 during development....202
4.4.6. NAADP binding activity in *Dictyostelium* cells....202
4.5. Summary....205

CHAPTER 5: CALCIUM RELEASE FROM INTRACELLULAR VESICLES ISOLATED FROM SEA URCHIN EGGS AND *DICTYOSTELIUM*....206
5.1. Introduction....207
5.1.1. Ca^{2+} release in sea urchin egg homogenate....207
5.1.2. Ca^{2+} release from *Dictyostelium* membranes....207
5.2. Aims....209
5.3. Results....209
5.3.1. Ca^{2+} release studies in vesicle preparations from *Dictyostelium*....209
5.3.1.1. Ca^{2+} uptake into intracellular Ca^{2+} stores requires ATP....209
5.3.1.2. Arachidonic acid-induced Ca^{2+} release....211
5.3.1.3. Ability of other fatty acids to cause Ca^{2+} release from T4P1 vesicles....214
5.3.1.4. Release of Ca^{2+} from vesicles by NAADP....214
5.3.1.5. The role of *Dd*TPC2 in NAADP-induced Ca^{2+} release....218
5.3.1.6. The role of *Dd*TPC2 in AA-induced Ca^{2+} release....221
5.3.1.7. Ca^{2+} mobilising activity of differentiation inducing factor (DIF) in T4P1 vesicles....221
5.3.2. Ca^{2+} release studies in sea urchin eggs....224
5.3.2.1. NAADP-induced Ca^{2+} release in sea urchin egg homogenate....224
5.3.2.2. Ca^{2+} mobilizing ability of AA....226
5.3.2.3. Ca^{2+} stores targeted by NAADP, IP_3 and AA....229
5.3.2.4. The effect of Ca^{2+} channel blockade on AA responses in sea urchin egg homogenate....229
5.3.2.5. Effect of AA on NAADP and IP_3-induced Ca^{2+} release....233
5.3.2.6. Inhibitory effect of Ned-19 on Ca^{2+} release in sea urchin egg homogenate....236
5.4. Discussion....236
5.4.1. Ca^{2+} release studies using *Dictyostelium* vesicles....236
5.4.2. Biological role of DIFs in *Dictyostelium*....237
5.4.3. Biological role of AA in *Dictyostelium*....238
5.4.4. AA-induced Ca^{2+} release in sea urchin egg homogenate....240
5.5. Summary....242

CHAPTER 6: GENERAL DISCUSSION....244
6.1. Are TPCs NAADP receptors?....246
6.2. Fatty acid-induced Ca^{2+} release....249
6.3. Future directions....251

APPENDICES....252

REFERENCES....281

CHAPTER 1

GENERAL INTRODUCTION

1.1. Calcium signalling

1.1.1. Ca^{2+} as an intracellular messenger

Among the intracellular messengers, the versatility of the calcium ion (Ca^{2+}) is remarkable in transducing extracellular stimuli to intracellular responses. Receptors and transducers of various stimuli activate a variety of channels, which produce specific and rapid changes in the intracellular concentration of Ca^{2+} and in its spatio-temporal patterning. The effectors recruited by Ca^{2+} possess different sensitivities to this ion. Ca^{2+} signalling is accomplished through protein-enzyme interactions activated through Ca^{2+}-sensitive proteins, which possess EF-hand domains. The classical sensory proteins for Ca^{2+} are troponin C (TnC), calmodulin (CAM) and S100. The binding of Ca^{2+} to the EF-hand causes conformational changes in these proteins and leads to the activation of various downstream effectors. The evolution of such mechanisms in organisms allows Ca^{2+} to control numerous cellular processes as diverse as exocytosis, muscle contraction, metabolism, secretion, fertilization, transcription, proliferation and apoptosis (Berridge *et al*., 2003).

1.1.2. Ca^{2+} homeostasis

Cells maintain their intracellular free Ca^{2+} concentration at a level about 20,000-fold lower than that of extracellular Ca^{2+}; at rest, the intracellular free Ca^{2+} concentration is about 100 nM, but this rises to approximately 1000 nM in response to various external stimuli. High levels of Ca^{2+} precipitate phosphate and show a high toxicity to the cell itself, therefore cytosolic Ca^{2+} must be carefully controlled, with increases

in Ca^{2+} concentration localized when appropriate, and Ca^{2+} extruded speedily and effectively as required (Clapham, 2007). In addition, cytosolic Ca^{2+} buffer proteins, such as parvalbumin, calbindin-D28K and calretinin, play important roles in Ca^{2+} homeostasis by rapidly binding free cytosolic Ca^{2+} (Berridge *et al.*, 2000).

1.1.3. Ca^{2+} entry through the plasma membrane

The distribution of Ca^{2+} channels in the plasma membrane usually depends on whether the cell is excitable or non-excitable. In excitable cells, like nerves and muscle cells, voltage-gated Ca^{2+} channels (VGCCs) comprise the preponderate route for Ca^{2+} influx, with some contribution from Ca^{2+}-permeable ligand-gated channels (LGCCs). In non-excitable cells on the other hand, voltage-gated Ca^{2+} channels are generally absent. Instead, Ca^{2+} entry is achieved largely by store-operated calcium channels (SOCCs) and second-messenger operated Ca^{2+} channels (SMOCs).

1.1.3.1. Store-operated Ca^{2+} entry (SOCE)

Store-operated Ca^{2+} entry (SOCE) is a major Ca^{2+} entry pathway across the plasma membrane. In many cell types, extracellular stimuli activate phospholipase C (PLC) by stimulating cell surface receptors, which leads to the production of inositol 1,4,5-trisphosphate (IP_3); this intracellular messenger can initiate the release of Ca^{2+} from the ER. Ca^{2+} release may also be amplified through the mechanism of calcium-induced calcium release (CICR), whereby an initial transient rise of $[Ca^{2+}]_i$ (e.g. a small amount of Ca^{2+} influx through the plasma membrane, or IP_3-mediated Ca^{2+} release) elicits further Ca^{2+} release from the ER. The depletion of Ca^{2+} from the ER triggers Ca^{2+} influx through store-operated channels (SOCs) in a wide variety of cell

types (Lewis, 2007). One well-characterized SOC is the Ca^{2+} release-activated Ca^{2+} (CRAC) channel, which is expressed in mast cells, T cells and related hematopoietic cells (Lewis, 2001).

The molecular mechanism of SOCE has been revealed following the identification of stromal interaction molecule 1 (STIM1) as the ER Ca^{2+} sensor (Liou *et al.*, 2005; Roos *et al.*, 2005) and Orai1 as the pore-forming subunit of the CRAC channel (Feske *et al.*, 2006). The ER luminal N-terminal region of STIM1 includes an ER signalling peptide, a Ca^{2+}-sensing region, consisting of an EF-hand pair, and a sterile α motif domain (SAM), whereas the cytosolic portion consists of two coiled-coil domains and two C-terminal domains: a proline/serine-rich region and a lysine-rich region (Stathopulos *et al.*, 2008). STIM1 oligomerization is the key event that triggers the redistribution of STIM1 and Orai1, translating changes in ER [Ca^{2+}] into graded activation of the CRAC channel, through binding of the CRAC activation domain of STIM1 to the Orai1 N- and C-termini (Feske *et al.*, 2006; Kawasaki *et al.*, 2009; Park *et al.*, 2009).

CRAC channels mediate important biological functions including gene expression during T cell activation, release of histamine and serotonin from mast cells, and the exocytosis of lytic granules from cytotoxic T cells during target cell killing (Park *et al.*, 2009). Antigen stimulation of immune cells triggers CRAC channels, promoting the immune response to pathogens by activating the transcription factor NFAT (nuclear factor of activated T cells). Severe combined immune deficiency (SCID) syndrome is defective in store-operated Ca^{2+} entry and CRAC channel function (Lewis, 2007). Two unbiased genome-wide approaches, a modified linkage analysis

with single-nucleotide polymorphism arrays, and a *Drosophila* RNA interference screen designed to identify regulators of store-operated Ca^{2+} entry and NFAT nuclear import, converged on a novel protein that was termed Orai1, which contains four putative transmembrane segments and was proposed as an essential component, or regulator, of the CRAC channel complex (Feske *et al*., 2006). Interestingly, orai1, on chromosome 12, was found to be mutated in patients with severe combined immunodeficiency disease, and expression of wild-type Orai1 restored Ca^{2+} influx and CRAC channel activity in the T cells of patients (Prakriya *et al*., 2006; Yeromin *et al*., 2006).

1.1.3.2. Arachidonate-regulated Ca^{2+}-selective *(ARC) channels*

ARC channels are highly Ca^{2+} selective; they are some 50 times more Ca^{2+} selective than CRAC channels (Mignen *et al.*, 2003). The ARC channel in mammalian systems is located on the plasma membrane. ARC channels and CRAC channels share many features, for instance, high selectivity for Ca^{2+}, a small conductance and voltage-independent gating. The most fundamental difference between ARC and CRAC channels is that activation of the ARC channel is entirely independent of intracellular Ca^{2+} store depletion and specifically dependent on arachidonic acid (AA) (Mignen and Shuttleworth, 2000). The activation of ARC channels occurs at low concentrations of exogenously applied AA (2 - 8 μM), whereas higher concentrations of AA (> 25 μM) induce large, highly nonselective conductances that are indicative of a breakdown in membrane integrity as a result of the detergent-like actions of the fatty acid at high concentrations (Mignen *et al.*, 2003).

More recently, molecular details of ARC and CRAC Ca^{2+} channels have been elucidated using transiently expressed, recombinant Orai subunits in a HEK293 cell line, stably expressing STIM1. The pore of the functional ARC channel comprises a heteropentamer of three Orai1 and two Orai3 subunits, whilst the pore of the functional CRAC channel is formed by a tetrameric arrangement of Orai1 subunits (Thompson *et al*., 2010). The N-terminal region of the second Orai3 subunit is critical for switching the channel to one that functions as an ARC channel, whereby the conductance is regulated selectively by AA. The full-length cytosolic N-terminal domain is required; in particular a glutamate at position 81 (E81) is important since the replacement of this residue with glutamine dramatically reduces the AA-activated current in Orai proteins transiently expressed in HEK cells (Mignen *et al*., 2008; Thompson *et al*., 2010).

For the operation of SOCE, STIM1 has been reported to be located on ER membranes and translocate to the plasma membrane in response to store depletion. Interestingly, STIM1 is also constitutively expressed on the plasma membrane, and this STIM1 specifically regulates ARC channel conductance. Interfering with the N-terminal domain of STIM1, either by antibody blocking or by mutation of an N-linked glycosylation site, markedly inhibited current through the ARC channels (Shuttleworth *et al*., 2007), indicating a role for STIM1 in ARC channel regulation.

Of relevance to this thesis, it is interesting to note that there are no genes predicted to code for orthologues of STIM1, Orai1 or Orai3 in the *Dictyostelium discoideum* genome. Instead, AA is thought to target intracellular Ca^{2+} stores through other mechanisms, although the physiological role of this Ca^{2+} signalling system is not

known (Malchow *et al*., 2006; Schaloske *et al*., 1998). The AA-mediated Ca^{2+} response in sea urchin egg homogenate is also consistent with an action at intracellular stores, although the precise mechanisms remain to be elucidated. As fatty acids are hydrophobic substance, it is often assumed that they might act by altering either the interaction of channels with the lipid bilayer or membrane fluidity, although, as far as I am aware, no evidence for these hypotheses has been reported to date.

1.1.3.3. Transient receptor potential (TRP) channels

TRP channels tend to contribute smaller amplitude and longer duration Ca^{2+} signalling than Voltage-gated calcium channels (VGCCs), and thereby control relatively slow cellular processes such as smooth-muscle contraction and cell proliferation (Berridge *et al*., 2003). TRP channels were first discovered in *Drosophila* (Hardie, 2007) and now more than 20 genes coding for mammalian TRP channels have been identified, forming the largest family of ion channels known. The TRP superfamily comprises seven related protein families, TRPC (canonical), TRPV (vanilloid), TRPM (melastatin), TRPA (ankyrin), TRPN (no mechanoreceptor potential C), TRPML (mucolipin) and TRPP (polycystin), which were identified based on their homology (Clapham, 2003; Hardie, 2007). The sequence identity between each sub-family is as low as 20% (Clapham, 2003). TRP channels often contain six putative transmembrane domains (TMDs) and assemble as tetramers to form cation-permeable channels (Clapham, 2007).

The majority of the mammalian TRPCs comprise plasma membrane channels that depolarize cells and increase intracellular concentrations of Na^{+} and Ca^{2+}; however,

gating mechanisms and functions of the TRPC family are diverse (Clapham, 2007). TRPC channels are mainly potentiated by phospholipase C (PLC), which is activated by G protein-coupled or tyrosine-kinase receptors (TKR). TRPC2, 3, 6 and 7 have been show to be activated through a diacylglycerol (DAG)-dependent mechanism. TRPV channels respond to environmental signals including light, heat and pH (Clapham, 2003). TRPV1 is activated by capsaicin and heat, and TRPV2, 3 and 4 are also heat activated (Clapham, 2003; Venkatachalam and Montell, 2007). TRPM2 is suggested to act as a sensor of intracellular oxidation/reduction. TRPM5 is a Ca^{2+}-activated non-selective cation (CAN) channel found in taste receptor cells, and is involved in the production of taste sensations (Pérez *et al*., 2002; Zhang *et al*., 2003). TRPA and TRPN are characterized by long chains of ankyrin (ANK) repeats. TRPA1 is probably sensitive to noxious cold temperature (< 15°C) as well as pungent chemicals such as wasabi and garlic (Hardie, 2007; Story *et al*., 2003).

TRPPs were earlier recognized as polycystins. There are two known subgroups, polycystin 1 and 2, which possess eleven and six TMDs, respectively. In humans, mutations of the gene *pkd2* cause autosomal dominant polycystic kidney disease (ADPKD), characterized by progressive formation and enlargement of cysts in both kidneys. Endogenous *Hs*PKD2 has been found in the plasma membrane and the primary cilium of mouse inner medullary collecting duct (IMCD) cells, and Madin-Darby canine kidney (MDCK) cells, heterologously expressed *Hs*PKD2 shows a predominant ER localization (Luo *et al*., 2003). Despite confirmation of their role in ADPKD, the precise functions of polycystins 1 and 2 remain to be determined. Mucolipins (mucolipin 1, 2 and 3) belong to the TMPML sub-family. Since there is evidence that these TRP channels are localized intracellularly to organelles of the

endolysosomal system, these are discussed later.

In *Drosophila*, there are several known TRP channels. TRPL and TRPγ are activated by polyunsaturated fatty acids (PUFAs), such as AA or linoleic acid (Chyb *et al*., 1999; Jors *et al*., 2006). Mouse TRPV3 is distantly related to dTRPγ and dTRPL are found to be activated by AA and monounsaturated and polyunsaturated fatty acids, as well as eicosatetraynoic acid (ETYA) and eicosatriynoic (ETI), when this murine TRP channel was expressed in HEK cells in which Ca^{2+} transients were measured with fura-2 AM (Hu *et al*., 2006). TRPV4 is also potentiated by the endocannabinoid, anandamide, and its metabolite AA in an indirect way (Watanabe *et al*., 2003). Despite sensitivity to AA and other fatty acids, none of these TRPs are likely to represent the currently known mammalian ARC channel (Mignen *et al.*, 2003). Of relevance to this thesis, it should be noted that the orthologues of TRPV3, TRPV4, TRPL and TRPγ are not found in the *Dictyostelium* genome.

1.1.3.4. Voltage-gated calcium channels (VGCCs)

VGCCs are Ca^{2+} (and, to a much lesser extent, Na^{+}) permeable ion channels in excitable cells that activate in response to depolarization of the cell membrane. Activation of these channels allows Ca^{2+} to enter the cell in order to elicit a response, such as contraction of smooth and cardiac muscle, release of hormones and neurotransmitters, and alteration of gene-expression. VGCCs activate rapidly, allowing changes in intracellular Ca^{2+} concentration to occur within a millisecond timescale.

VGCCs are formed by a complex of several subunits, namely α_1, α_2, β, γ and δ

(Figure 1.1). The α_1 subunit is the primary subunit essential for VGCC function, containing the Ca^{2+}-selective pore, the voltage sensor and the binding sites for the majority of drugs that influence VGCC function. This subunit contains four homologous domains, each with six, transmembrane α-helices and has a molecular mass of approximately 170 kDa. The remaining subunits have been postulated to contribute several roles, including enhancing expression levels of the α_1 subunit and thus influencing current amplitude, the activation and inactivation kinetics and the voltage-dependence of activation and inactivation.

There are five main classes of VGCC, distinguished by their α_1 subunit type: L-type (Ca_V 1.1, 1.2, 1.3, 1.4), P/Q-type (Ca_V 2.1), N-type (Ca_V 2.2), R-type (Ca_V 2.3), and T-type (Ca_V 3.1, 3.2, 3.3). These subtypes may also be distinguished on the basis of their pharmacology. L-type VGCCs are predominantly found in skeletal, cardiac and smooth muscle as well as in bone osteoblasts, whereas T-type VGCCs are found in cells that exhibit pacemaker activity, such as cardiac sino-atrial node cells and certain neurones, as well as in bone osteocytes. N-type VGCCs are widely distributed in the central and peripheral nervous systems, and P/Q and R-types are also found in certain neurones (Berridge *et al*., 2003; Clapham, 2007).

Interestingly, the function of the $Ca_V1.1$ L-type Ca^{2+} channel differs significantly from that of the other Ca_V1 family members. In skeletal muscle, $Ca_V1.1$ couples directly to the ryanodine receptor (RyR1) to mediate the voltage-induced Ca^{2+}-release mechanism that underlies contraction of this muscle, and does not function as a Ca^{2+} channel. In cardiac and smooth muscle, the other Ca_V1 isoforms act as conventional voltage-gated Ca^{2+} channels, contributing trigger Ca^{2+} for CICR (Striessnig *et al*.,

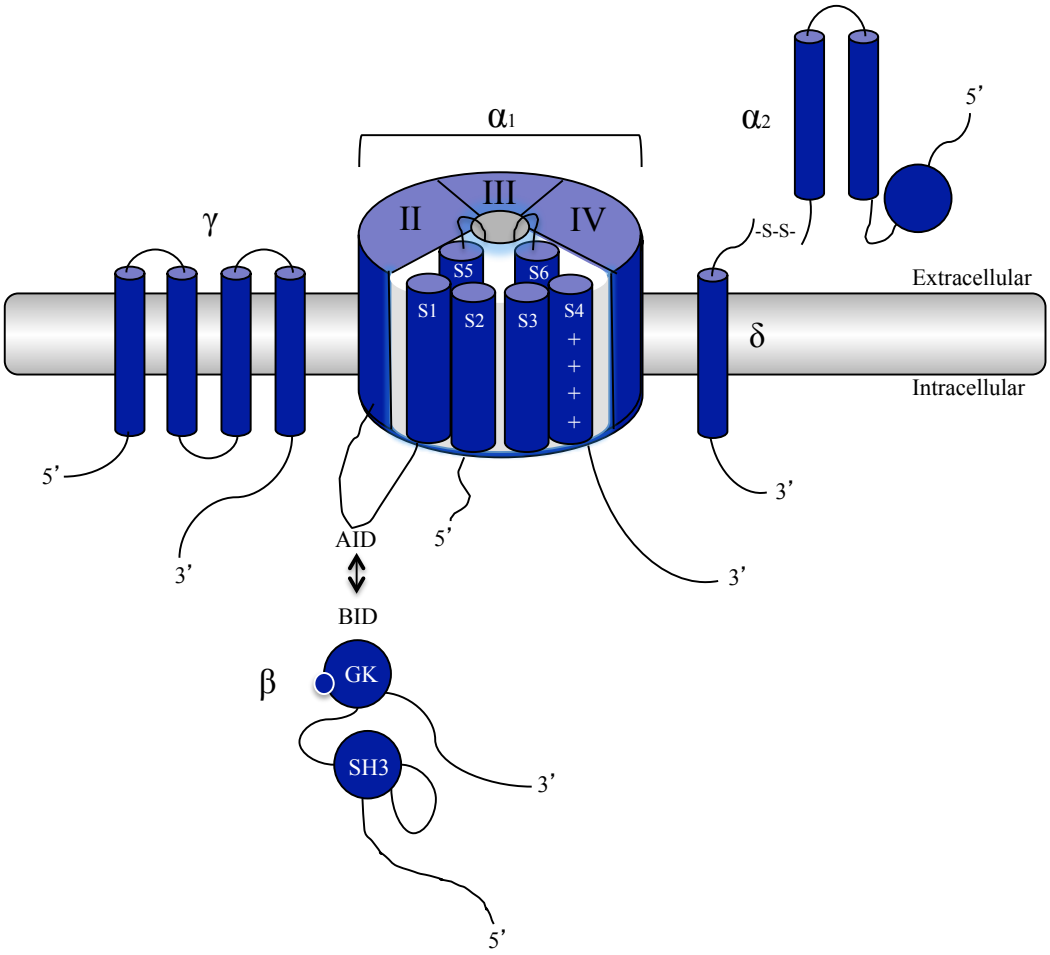


Figure 1.1. Structure of voltage-gated Ca^{2+} channels (VGCCs)
VGCCs comprise five components, a pore-forming α_1 subunit (170 kDa), α_2 (150 kDa), β (52 kDa), δ (17-25 kDa) and γ (32 kDa) (Dolphin, 2006). α_1 subunit contains four homologous domains, each of which includes six transmembrane segments (S1-S6). β subunit contains two conserved domains, *src* homology-3 (SH3) domain and a guanylate kinase (GK)-like domain (Hanlon *et al*., 1999) and interacts with the alpha interaction domain (AID) on the I-II loop of the α_1 subunit via its GK domain indirectly (Chen *et al*., 2004). $\alpha_2\delta$ subunit is encoded by a single gene, whose polypeptide product is post-translationally cleaved into an α_2 and a δ moiety, α_2 is entirely extracellular (Klugbauer *et al*., 2003). γ subunit is co-purified with skeletal muscle Ca^{2+} channels (Takahashi *et al*., 1987), however, whether it could be subunits is unknown.

2010). N-type and P/Q-type channels, knows as Cav2.1 and Cav2.2 respectively, in neurones are coupled to soluble *N-ethylmaleimide*-sensitive fusion protein-attachment protein receptor proteins (SNARE proteins) at the synapse, which allows for increased speed of downstream signal transfers (Fox *et al*., 2008).

1.1.3.5. Receptor-operated channels (ROCs)

ROCs are multimeric proteins that act as ion channels gated by ligands, such as neurotransmitters and hormones. Although these channels are generally permeant to various ions, including Na^+ and K^+, and therefore can influence membrane potential, several ROCs are also permeant to Ca^{2+} and thus can influence intracellular Ca^{2+} signalling by altering Ca^{2+} entry into the cell (Berridge *et al*., 2003).

There are three main types of ROC: cysteine loop receptors, glutamate receptors and P2X receptors. The former group includes nicotinic acetylcholine receptors (nAChRs), 5-hydroxytryptamine-3 receptors (5-HT_3Rs), γ-aminobutyric acid (GABA) receptors and glycine receptors (GlyRs). Glutamate receptors comprise α-amino-3-hydroxy-5-methylisoxazole-4-propionic acid (AMPAR) receptors, *N*-methyl-D-aspartate (NMDA) receptors and kainate receptors. P2X receptors are sensitive to ATP. These various ROCs serve a wide variety of functions and it is of relevance to note that certain isoforms of nAChRs, 5-HT_3Rs, glutamate receptors and P2X receptors can permit significant entry of Ca^{2+} into the cell, contributing to the effects the respective agonists elicit in the tissue (Berridge *et al*., 2003).

1.1.4. Ca^{2+} mobilization from intracellular stores

Receptor-mediated Ca^{2+} release from the ER (or sarcoplasmic reticulum, SR, in muscle) has been well characterized, and is elicited by IP_3Rs or RyRs which are activated, respectively, by IP_3 or Ca^{2+} itself, with cyclic ADP-ribose (cADPR) believed also to activate RyRs either directly or indirectly (Figure 1.2). In addition to the ER, other intracellular organelles are now recognized to act as stores of intracellular Ca^{2+}, including lysosome-related acidic organelles, mitochondria and the Golgi network. These various intracellular Ca^{2+} stores, and the second messenger operated Ca^{2+} channels (SMOCs) relevant for their function, are discussed below.

1.1.4.1. Endoplasmic reticulum (ER)

The ER is, perhaps, the best-known and most classic intracellular Ca^{2+} store. The ER spreads like a vast three-dimensional inter-connected network within cells, acting as a framework for Ca^{2+}-binding proteins and actively sequestering Ca^{2+} into its intra-organellar space using sarco/endoplasmic reticulum Ca^{2+}-ATPases (SERCA). SERCAs belong to the class of P-type ATPases and are the products of three different genes. These proteins are known as SERCA1, SERCA2 and SERCA3, expressed in fast-twitch skeletal muscle, cardiac and slow-twitch skeletal muscle, and non-muscle tissues respectively (Clapham, 1995; Pozzan *et al*., 1994).

The SERCA pump is inhibited by thapsigargin (Tg) as well as vanadate. IP_3-induced and cADPR-induced Ca^{2+} release are known to be inhibited by Tg, vanadate, carbonyl cyanide *m*-chlorophenyl-hydrazone (CCCP), and are pH and K^+-sensitive in the sea urchin egg (Genazzani and Galione, 1996; Genazzani *et al.*, 1997).

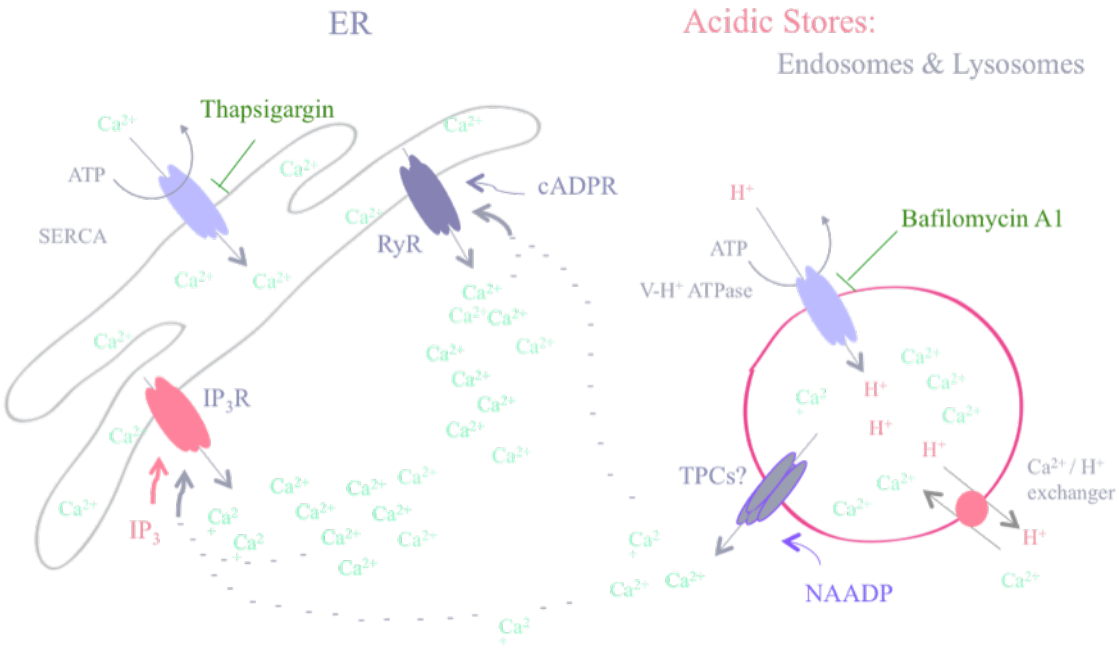


Figure 1.2. Ca^{2+} mobilization from intracellular stores
The endoplasmic reticulum (ER) and the acidic stores (comprised of endosomes and lysosomes) are the major Ca^{2+} storage organelles of cells. The ER releases Ca^{2+} in response to inositol 1,4,5-trisphosphate (IP_3) and cyclic ADP-ribose (cADPR) through IP_3 receptors (IP_3Rs) and ryanodine receptors (RyRs) respectively, whereas the acidic stores are targeted by NAADP. Ca^{2+} activates IP_3Rs and RyRs through a Ca^{2+}-induced Ca^{2+} release mechanism. The ER contains a sarco/endoplasmic reticulum Ca^{2+}-ATPase (SERCA) that is inhibited by thapsigargin, whereas the acidic stores contain a V-type H^+-ATPase that is sensitive to bafilomycin A1.

1.1.4.1.1. Ryanodine receptors (RyRs)

RyRs are a family of homotetrameric Ca^{2+} release channels, consisting of about 5000 amino acids for each monomer with various multiple transmembrane domains (TMDs), in which TMD1-2 in RyR1 has been suggested to include ER retention signals (Meur *et al.*, 2007). Three genes coding for RyRs have been identified in the human genome. RyR1 (NP_000531.2) is found mainly in skeletal muscle and RyR2 (NP_001026.2) is found mainly in cardiac muscle, whereas RyR3 (NP_001027.3) is more widely distributed (including the brain); they share 65 - 70% amino acid sequence identity (Furuichi *et al.*, 1994; Giannini *et al.*, 1995). RyR proteins share significant homology with IP_3Rs, mainly in the putative pore region (Bosanac *et al.*, 2005; Furuichi *et al.*, 1989).

Mutations in the gene for RyR1 (on 19q13) cause a variety of clinical conditions that affect skeletal muscle, including malignant hyperthermia and central core disease (CCD) in humans (Robinson *et al.*, 2006), whereas mutations in the gene for RyR2 (on 1q43) can cause catecholaminergic polymorphic ventricular tachycardia. Unfortunately, mice lacking the RyR1 or the RyR2 die during early embryonic development (Takeshima, 1994; Takeshima *et al.*, 1998), limiting the use of such knockout techniques to study RyR function.

It is well established that RyRs are activated by Ca^{2+} (including Ca^{2+} entry through VGCCs, in response to depolarization of the cell membrane), as well as cADPR - although it is not known whether this latter effect is direct or indirect (Thomas *et al*., 2001; Thomas *et al*., 2002). Ca^{2+} release following the activation of RyRs is modulated by phosphorylation of the receptors, as well as by the associated proteins,

calmodulin (CaM), the Ca^{2+}-binding protein calsequestrin (CSQ), and FK506-binding proteins (FKBPs). Ca^{2+}-free CaM (apoCaM) activates RyR1 and RyR3, but not RyR2, and all three subtypes are inhibited by Ca^{2+}-bound CaM (Ca^{2+}-CaM) (Chen *et al*., 1997; Fruen *et al*., 2000). In sea urchin egg, caffeine-, ryanodine- or cADPR-induced Ca^{2+} release from microsomal vesicles is enhanced by the presence of exogenously added CaM (Lee *et al*., 1995). CSQ is the major Ca^{2+}-binding protein located in the terminal cisternae of skeletal and cardiac muscle SR. CSQ acts as a Ca^{2+} buffer in the lumen of SR Ca^{2+} storage pools to lower free Ca^{2+} concentrations, and Ca^{2+} released from the SR lumen dissociates from the CSQ-Ca^{2+} complex after activation of the RyR (Ozawa *et al*., 2010). FKBP12 has been shown to associate with RyR1 on the SR of skeletal muscle and stabilize the closed conformation of the Ca^{2+} channel, and to be dissociated from the RyR1 complex by phosphorylation of the receptor by PKA (Timerman *et al*., 1993; Reiken *et al*., 2003). There is also evidence that FKBP12.6 may be involved in mediating the actions of cADPR on the RyR (Wang *et al.*, 2004).

RyR function may also be affected by a number of pharmacological agents. For example, caffeine has been shown to increase the open probability of RyRs in sheep cardiac SR (Sitsapesan and Williams, 1990). The plant alkaloid, ryanodine has been reported to have differing effects depending on the concentration used; low concentrations of ryanodine (< 10 μM) have been demonstrated to increase the frequency of RyR channel openings, whereas higher concentrations (> 200 μM) cause complete closure of the channel (Buck *et al*., 1992).

1.1.4.1.2. Inositol trisphosphate receptors (IP_3Rs)

The IP_3R was originally identified during extensive studies of P400 protein, which was subsequently found to be the IP_3R (Maeda *et al.*, 1988; Mikoshiba *et al.*, 1979). Three isoforms have now been reported, namely IP_3R1 (NP_001093422), IP_3R2 (NP_002214.2) and IP_3R3 (NP_002215.2). They consist of 5028, 2701 and 4870 amino acids, respectively. Overall, the homology between the isoforms is 60 - 80%. The primary sequence of the IP_3R has been determined and shown to possess six transmembrane domains. The recombinant protein exhibited high affinity binding of IP_3 with a K_d value of 21.7 nM. Ca^{2+} release activity was also examined and this was shown to be localized to the ER (Furuichi *et al.*, 1989; Miyawaki *et al.*, 1990; Parker *et al.*, 2004). The three isoforms of the IP_3R have different affinities for IP_3. The isoform-specific 'tuning' of IP_3-binding is due to the N-terminal side of the binding core, encompassing residues 226 - 576 and a binding suppressor region containing residues 1 - 225 (Iwai *et al.*, 2005; Iwai *et al.*, 2007; Newton *et al.*, 1994). The crystal structures of the IP_3-binding core domain (224 - 604) and the repressor domain have been determined (Bosanac *et al.*, 2002; Bosanac *et al.*, 2005). Site-directed mutagenesis studies have identified 10 conserved arginine and lysine residues, distributed throughout the IP_3-binding core domain, which are crucial for IP_3 binding (Iwai *et al.*, 2007; Yoshikawa *et al.*, 1996; Yoshikawa *et al.*, 1999). The differences in affinity of IP_3 binding among the isoforms varies depending on the study; for instance, the rank order of affinity for IP_3 was Type I > II > III (K_d values for types I, II and III of approximately 1, 2 and 40 nM, respectively) in one study (Wojcikiewicz and Luo, 1998) and Type II >I (K_d values for types Ia, Ib and II of 55±12, 65±10 and 15±35, respectively) in another (Newton *et al.*, 1994). It should be noted that the former study used a recombinant protein that included the IP_3-binding region,

expressed in bacteria, whereas the latter used endogenous IP_3Rs purified using anti-IP_3R antibodies from mammalian cell lines. Thus, the physiological relevance of different IP_3 affinities among the IP_3R isoforms has not been established unequivocally (Newton *et al.*, 1994).

The IP_3-mediated Ca^{2+} release is also modulated by intracellular Ca^{2+} concentration in rat pancreatic islets, illustrating the Ca^{2+} dependence of the mechanism by which IP_3 triggers Ca^{2+} release (Wolf *et al.*, 1986). It has been reported that IP_3Rs are regulated, not only by IP_3, but also by Ca^{2+} itself, with half-maximal activating and inhibitory Ca^{2+} concentrations of 210 nM and 54 μM, respectively (Mak *et al*., 1998). In addition, it has been shown that the Ca^{2+} sensor proteins, CaBPs, can engage IP_3 receptors and promote channel opening in the absence of IP_3 (Yang *et al*., 2002). These data suggest the involvement of the IP_3Rs in CICR.

IP_3R1 deficient mice exhibit severe ataxia and tonic/tonic-clonic seizures and die by the weaning period (Matsumono *et al.*, 1996). Deletion of the IP_3R2 was found to abolish the positive inotropic and arrhythmogenic effects (abnormal electrical activity) of endothelin in cardiac atrial myocytes (Li *et al.*, 2005). Despite the unveiled details of the IP_3R, including its binding proteins, for instance, ERp44 which senses the luminal environment of the ER, the details of the molecular mechanisms responsible for the amplification of local Ca^{2+} signals and more widely distributed global Ca^{2+} signals remain unknown. The localization of IP_3Rs to specific regions of cells is now considered an important factor in the spatial regulation of Ca^{2+} release.

1.1.4.1.3. Ca^{2+}-induced Ca^{2+} release (CICR)

CICR is a mechanism by which local rises in cytosolic Ca^{2+} levels trigger more substantial intracellular Ca^{2+} release from the ER through RyRs or IP_3Rs, thus generating more global Ca^{2+} signals. RyRs are well known to play a central role in CICR (for example, in the heart), but the involvement of IP_3Rs in CICR is still controversial. The process of CICR plays a central role in generating Ca^{2+} signals, whereby a small amount of Ca^{2+} crossing the plasma membrane (for example, in response to an external stimulus) or Ca^{2+} release from intracellular stores (for example, in response to the action of IP_3) can act to set up propagating, intracellular Ca^{2+} signals that, in turn, activate numerous cellular processes.

At the most fundamental level, opening of individual RyRs or IP_3Rs elicits quarks and blips, which are highly localized, small Ca^{2+} signals originating from individual channels. Co-ordinated opening of clusters of channels results in sparks (for RyRs) and puffs (for IP_3Rs). When clusters of channels activate their neighbouring channel clusters, global Ca^{2+} signals may propagate as waves, which is called CICR (Berridge *et al.*, 2000).

1.1.4.2. Intracellular acidic stores

Acidic stores are comprised of the lysosome, endosome, acidocalcisome, yolk platelet, exocytotic vesicle and pigment granule, according to the cell type (Galione *et al.*, 2010). Lysosomal pH has been estimated to be 4.64 in a mouse macrophage cell line - calculated by a combination of membrane potential determinations and the pH gradient (Koivusalo *et al.*, 2011; Steinberg *et al.*, 2010). More recently, an acidic compartment, thought to be a lysosome-related organelle, has been suggested to play

a role in Ca^{2+} storage and Ca^{2+} release elicited by nicotinic acid adenine dinucleotide phosphate (NAADP) (Figure 1.2). NAADP-sensitive acidic stores are refilled in an indirect manner; stores are believed to be acidified by a V-type H^+-ATPase, then the generated proton gradient drives Ca^{2+} into the stores using a Ca^{2+}/H^+ exchanger. In the sea urchin genome, a coding sequence for a Ca^{2+}/H^+ exchanger has not yet been identified; instead, sequences for both Na^+/H^+ and Na^+/Ca^{2+} exchangers have been determined, thus it is possible that Ca^{2+} uptake into acidic stores may be achieved by the utilization of several exchangers (Roux *et al.*, 2006). Generation of a proton gradient across the lysosomal membrane has been shown to be sensitive to apyrase (indicating a requirement for ATP), bafilomycin A1 (a known V-type H^+-ATPase inhibitor), protonophores (FCCP and nigericin) and the weak base, NH_3 (Churchill *et al.*, 2002; Gross, 2009). Furthermore, disruption of the proton gradient has been reported to prevent Ca^{2+} uptake into acidic vesicles (Patel and Docampo, 2010).

The acidocalcisome is a conserved organelle found from bacteria to man (where it has been identified in platelets). In sea urchin eggs, the acidocalcisome contains a large amount of Ca^{2+} and a bafilomycin A1-sensitive ATPase, and also possesses Ca^{2+}/H^+ and Na^+/H^+ exchange activities; however, it has been suggested that NAADP-sensitive Ca^{2+} store is not the acidocalcisome (Ramos *et al.*, 2010).

1.1.4.2.1. NAADP (nicotinic acid adenine dinucleotide phosphate)

NAADP was first discovered as a contaminant in a solution of NADP (Clapper *et al.*, 1987). Since this first report of its Ca^{2+} mobilizing ability in sea urchin egg microsomes, NAADP has been identified as the most potent Ca^{2+} mobilizing

messenger known to date (Billington and Genazzani, 2000; Chini *et al.*, 1995; Churchill *et al.*, 2003). Chemical analysis showed that NAADP is a nicotinic acid derivative of NADP, with a hydroxyl group replacing the amino group (Figure 1.3). Nanomolar concentrations of NAADP, as opposed to NADP, were found potently to release Ca^{2+} from intracellular stores (Lee and Aarhus, 1995; Lee and Aarhus, 1997). Soon after these observations, it was confirmed that pancreatic acinar cells have the ability to produce NAADP (Cancela *et al.*, 1999). In sea urchin egg, NAADP has been reported to exhibit a unique self-desensitization mechanism; subthreshold concentrations of NAADP inhibited NAADP-mediated Ca^{2+} release in response to a subsequent saturating concentration of NAADP, in a concentration- and time-dependent manner (Aarhus *et al.*, 1996). Another unique feature of responses to NAADP is that the concentration-response relationships are bell-shaped in Jurkat T-cells (Berg *et al.*, 2000) and pancreatic β-cells (Masgrau *et al.*, 2003). In addition, desensitization experiments demonstrated that cauliflower tissue contained low levels of NAADP and that vegetable tissue homogenates were capable of NAADP synthesis, when suitable precursors were provided (Navazio *et al.*, 2000). These findings illustrate that NAADP may be important in plant as well as animal cells, and hence be widely conserved as an intracellular messenger.

It has been reported that activation of certain cell surface receptors by their agonists is coupled to an increase in NAADP levels (Galione, 2010). *In vitro*, ADP-ribosyl cyclases (ARCs), including CD38, have been shown to be capable of catalyzing the formation of cADPR from NAD at neutral pH, and of NAADP from NADP at acidic pH via a base-exchange reaction, if a high concentration of nicotinic acid and low pH (~ pH 5) environment are provided (Figure 1.3) (Aarhus *et al.*, 1995). However, CD38 and the base-exchange reaction are unlikely to be the only mechanism involved

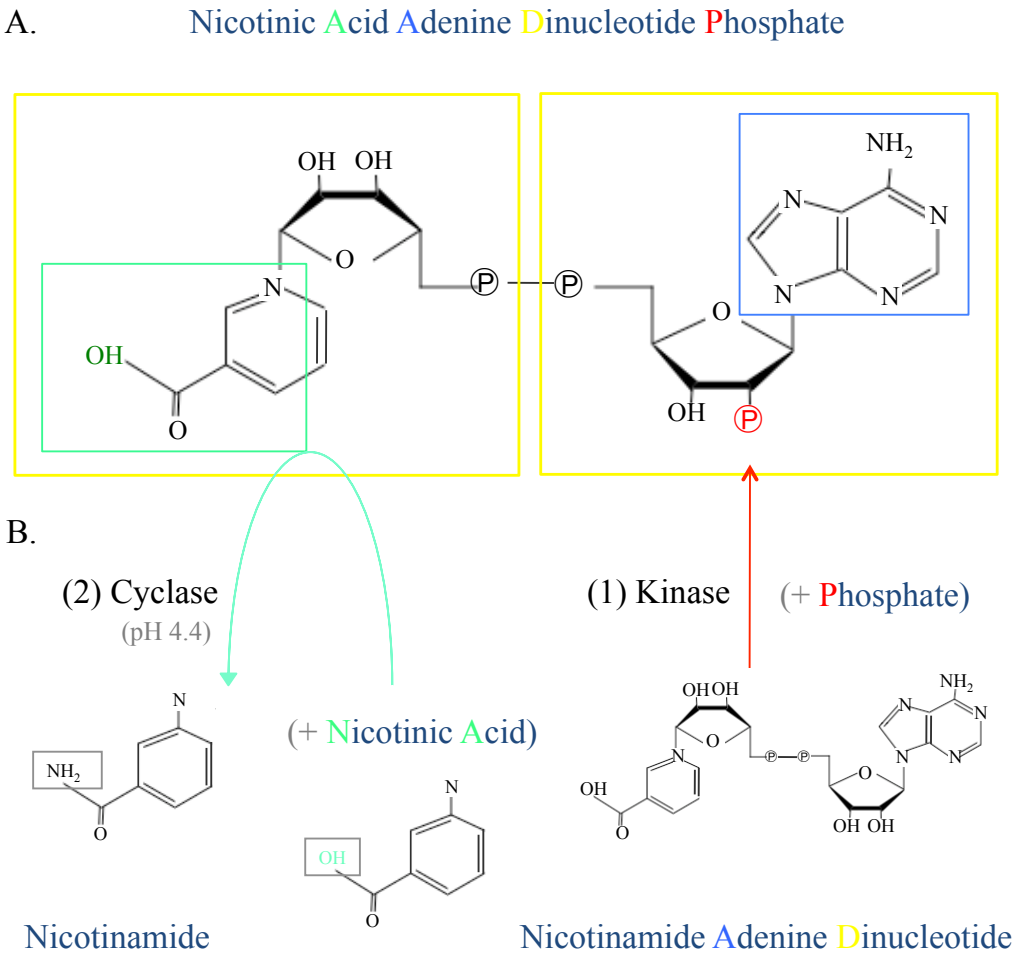


Figure 1.3. Nicotinic Acid Adenine Dinucleotide Phosphate (NAADP)
A. The chemical structure of NAADP.
B. *In vitro* synthesis of NAADP. The phosphorylation of NAD is catalyzed by NAD kinase (1), then NADP is converted into NAADP, using a base-exchange reaction, by ADP-ribosyl cyclase (2). Nicotinic acid, adenine, two nucleotides and phosphate are indicated with green, blue and yellow boxes and a red circle, respectively.

in the generation of NAADP in mammalian systems, since, endogenously produced NAADP was detected in $CD38^{-/-}$ mice (Soares *et al*., 2007). The role of CD38 could be compensated by other gene, thus, alternative pathways have been also proposed for NAADP biosynthesis, in which cADPR acts as a precursor, or enzymes other than CD38 are utilized (Soares *et al*., 2007; Palade, 2007).

In the sea urchin, three isoforms of ARC namely ARC1, 2 and 3 are found in the *Strongylocentrotus purpuratus (Sp)* genome; in sea urchin eggs, the ARCs are localized exclusively to the luminal side of cortical granules and act to synthesize cADPR. Although these ARCs are theoretically able to synthesize NAADP via the base-exchange reaction, it has not yet been shown that *Sp*ARCs are capable of NAADP production (Davis *et al*., 2008). On the other hand, endogenous NAADP levels increase in the egg following contact of sperm with egg jelly, suggesting an ability of sea urchin sperm to synthesize NAADP (Churchill *et al.*, 2003). Recently, NAADP biosynthesis by an enzyme isolated from sea urchin sperm has been convincingly demonstrated (Vasudevan *et al.*, 2008).

1.1.4.2.2. Actions and pharmacology of NAADP

In sea urchin egg homogenate, NAADP activates a Ca^{2+}-release channel that is quite distinct from the well-characterized inositol 1,4,5-trisphosphate receptor (IP_3R) and the ryanodine receptor (RyR) (Clapper *et al.*, 1987; Lee and Aarhus, 2000). The ER SERCA inhibitor, thapsigargin (Tg), inhibited Ca^{2+} release induced by either IP_3 or cADPR but did not reduce NAADP-induced Ca^{2+} release in either sea urchin egg homogenate or the intact egg (Churchill and Galione, 2001; Genazzani *et al.*, 1996). NAADP-mediated Ca^{2+} release was sensitive to nigericin (an ionophore that antiports

H^+ and K^+), bafilomycin A1 (a specific inhibitor of vacuolar-type H^+-ATPase) and glycyl-L-phenylalanine 2-naphthylamide (GPN), which is hydrolysed by lysosomal cathepsin C and causes osmotic lysis of lysosomes. These data are consistent with lyososome-related acidic organelles being the target for NAADP.

The L-type Ca^{2+} channel blockers diltiazem, nifedipine and verapamil have been reported to block the NAADP-sensitive Ca^{2+} channel with IC_{50} values of approximately 7.5 μM, 10 μM and 20 μM respectively, however, these agents did not alter NAADP binding in the sea urchin egg (Genazzani *et al.*, 1997; Genazzani *et al.*, 1996). Interestingly, diltiazem had no effect on the NAADP response in cauliflower membrane vesicles (Navazio *et al.*, 2000).

Heparin is known to block IP_3-mediated Ca^{2+} release from IP_3Rs, and ruthenium red and 8-NH_2-cADPR (an antagonist of cADPR actions) are known to block Ca^{2+} release from RyRs, but none of these agents inhibited NAADP-mediated Ca^{2+} release (Galione and Churchill, 2002). Ned-19, the most recently synthesized NAADP antagonist (Naylor *et al.*, 2009), blocks both NAADP-mediated Ca^{2+} release and NAADP binding in sea urchin egg homogenate (Rosen *et al.*, 2009). In sea urchin egg homogenate, the fluorine and the carboxylic acid groups of Ned-19 are vital for inhibition of NAADP binding and inhibition of NAADP-induced Ca^{2+} release, respectively (Rosen *et al.*, 2009).

A model has been proposed for the actions of NAADP at its receptor in the sea urchin egg, in which two affinity binding sites were posited. This hypothesis gained support from the discovery of two binding sites in a mammalian system (Calcraft *et al.*, 2009).

Multiple NAADP binding sites were also found in rabbit heart microsomes, with K_d values of 130 pM and 4 nM for high affinity sites and 323 nM for a low affinity site (Bak *et al*., 2001). The authors suggested that these results may reflect either, the presence of a single class of binding site whose affinity changes with receptor occupancy, or expression of different subtypes of the NAADP receptor - although the lower affinity binding site may represent an NADP binding site.

1.1.4.2.3. Two-pore channel (TPC) proteins

TPCs were first identified as channels in rat kidney and were thought to be similar to voltage-gated Ca^{2+} and Na^{+} channels; they have since been shown to have similar pharmacological properties to the NAADP receptor (Genazzani *et al.*, 1997; Ishibashi *et al.*, 2000). Plant (*Arabidopsis thaliana*) TPC1 (*At*TPC1) was not only described to be a Ca^{2+}-release channel but was also commonly found in the plant cell equivalent of the acidic organelle, namely the vacuole (Peiter *et al.*, 2005).

TPCs are predicted to possess two homologous domains, each consisting of 6 trans-membrane regions forming a putative pore-forming domains. A list of TPCs found in a variety of species is shown in Table 1.

1.1.4.2.4. Human TPCs (HsTPCs)

*Hs*TPCs have been intensively studied recently in terms of the Ca^{2+} mobilizing ability of NAADP. *Hs*TPCs are localized to the endo-lysosomal compartment. The lysosomal targeting motif, dileucine [(D/E)XXXL(L/I)], is found in both *Hs*TPC1 and *Hs*TPC2. Disruption of the dileucine motif in truncated *Hs*TPC2 redirected *Hs*TPC2

Table 1. TPC isoforms

Species	TPC	STIM	Orai	TRPC	Mucolipin	Polycystin
Homo sapiens (*Hs*)	1, 2	1, 2	1, 2, 3	1 - 7	1, 2, 3	1, 2
Mus musculus (*Mm*)	1, 2	1, 2	1, 2, 3		2, 3	1, 2
Ruttus norvegicus (*Rn*)	1	1	1, 2, 3		2, 3	1, 2
Danio rerio (*Dr*)	2, 3	1				
Gallus gallus (*Gg*)	3	1	1, 2			
Saccharomyces cerevisiae (*Sc*)	1, 2, 3	-	-			
Strongylocentrotus purpuratus (Sp)	1, 2, 3	-	-	-	-	-
Dictyostelium discoideum (*Dd*)	2	-	-	-	1	2
Dictyostelium purpureum (*Dp*)	-	-	-		1	2
Arabidopisis thaliana (*At*)	1	-	-			

TPC: Two-pore channel
STIM: Stromal interaction molecule
Orai: Calcium release-activated calcium channel protein
TRPC: Transient receptor potential canonical channels - indicates no gene coding for the protein predicted

to the plasma membrane (Brailoiu *et al.*, 2010b). Homologously expressed *Hs*TPC2 has previously been shown to enhance NAADP binding (Calcraft *et al.*, 2009) and recently to function as a NAADP-sensitive Ca^{2+} release channel in artificial lipid bilayers (Pitt *et al.*, 2010). Introducing mutations in the pore-forming domains caused dysfunction of the NAADP-sensitive channel, indicating that *Hs*TPCs are the pore-forming subunits of the NAADP-gated Ca^{2+} channel (Brailoiu *et al.*, 2009; Schieder *et al.*, 2010). *Hs*TPCs are glycosylated and N-glycosylation in *Hs*TPC1 serves to inhibit TPC1 channel function (Hooper *et al.*, 2011).

1.1.4.2.5. Strongylocentrotus purpuratus TPCs (SpTPCs)

*Sp*TPC bioinformatics analysis suggests that *Strongylocentrotus purpuratus* has 3 TPC isoforms (Sodergren *et al*., 2006)

At the amino acid level, the homology between each isoform is about 30%. Endogenous and heterologously expressed *Sp*TPC2 was shown to be glycosylated (Ruas *et al.*, 2010). The authors reported that heterologously expressed *Sp*TPCs were distributed in the endo-lysosomal compartment, and that *Sp*TPC1 and *Sp*TPC2 mediated NAADP-induced Ca^{2+} release. By contrast, *Sp*TPC3 had an inhibitory effect on NAADP-induced Ca^{2+} release, but this effect was not observed in another *Sp*TPC3 variant (Brailoiu *et al.*, 2010a). On the other hand, all isoforms of endogenous *Sp*TPCs, which were immuno-precipitated using anti-*Sp*TPC antibodies, showed increased specific NAADP binding (Ruas *et al.*, 2010).

A model has been developed, proposing that the Ca^{2+} signal induced by NAADP contributes to the trigger responsible for global CICR responses from the ER, depending on the relative positions of the ER Ca^{2+} release channels. In HEK cells

expressing *Sp*TPC2, a biphasic Ca^{2+} response was elicited by NAADP application; that is, an early, small Ca^{2+} release followed by a much larger one. Bafilomycin A1 treatment abolished both phases whereas the IP_3R antagonist, heparin, blocked the second phase only (Galione *et al.*, 2010; Ruas *et al.*, 2010), consistent with NAADP inducing an initial Ca^{2+} release from an acidic compartment that was subsequently amplified by Ca^{2+} release from the ER.

1.1.4.2.6. Mucolipin

TRPML1 is predicted to be an intracellular late endosomal and lysosomal ion channel protein containing six transmembrane domains. TRPML1 is a lysosomal Ca^{2+}-permeable TRP channel, and mutations in this channel cause mucolipidosis type IV (MLIV), a neurodegenerative lysosomal storage disease characterized by psychomotor retardation and ophthalmological abnormalities, including corneal opacities, retinal degeneration and strabismus in humans (Bach, 2001; Piper and Luzio, 2004). Gastric parietal cells isolated from *trpml1*$^{-/-}$ mice showed no alteration in Ca^{2+} signalling (Chandra *et al.*, 2011), whereas *trpml1*$^{-/-}$ cells obtained from the patients with MLIV exhibited either lysosome over-acidification (Soyombo *et al.*, 2006) or elevated lysosomal pH (Bach *et al*., 1999); a disturbance in the regulation of a mutant mucolipin-1 cation channel by pH has also been reported, suggesting that the pH-sensitive regulatory mechanism is important for vesicular function (Raychowdhury *et al*., 2004). Therefore, TRPML1 is more likely to play an important role in membrane trafficking and fusion events. In sea urchin, the function of mucolipin has not been investigated.

Mucolipin has been suggested to function as a NAADP-sensitive Ca^{2+} channel in lysosomes, on the basis that anti-TRPML1 polyclonal antibody was found to attenuate NAADP-induced increases in lysosomal Ca^{2+} release channel activity (Zhang and Li, 2007). However, the molecular basis for NAADP-mediated Ca^{2+} release remains controversial, since NAADP-induced Ca^{2+} oscillations in pancreatic acinar cells in TRPML1$^{-/-}$ mice were identical compared to those of wildtype (Yamaguchi *et al*., 2011).

1.1.4.3. Mitochondria

Mitochondria possess highly sophisticated mechanisms for energy production (ATP) as well as various cellular signalling processes, including Ca^{2+} handling and the generation of local and global Ca^{2+} signals. Mitochondria themselves constitute a target for Ca^{2+}, as metabolic enzymes, such as the dehydrogenases of the Krebs cycle, are Ca^{2+} sensitive, and translate an elevation of Ca^{2+} in the mitochondrial matrix into increased respiration and ATP production. Mitochondria accumulate Ca^{2+} up to a level of 0.5 mM in the mitochondrial matrix, owing to a large electrochemical gradient created by mitochondrial hydrogen exchange (Malli and Graier, 2010).

The voltage-dependent anion channel (VDAC) controls Ca^{2+} permeation to prevent free diffusion across the outer mitochondrial membrane, whereas the mitochondrial calcium uniporter (MCU), a non-MCU mechanism and possibly the mitochondrial RyR (mRyR) mediate calcium uptake across the inner mitochondrial membrane (IMM) (Hoppe, 2010). In rat heart, antibodies against mitochondrial RyRs are found predominantly in the cristae of the inner mitochondrial membrane (Beutner *et al*.,

2001). In liver mitochondria, an initial rapid Ca^{2+} uptake is followed by a slower Ca^{2+} sequestration mode. The rapid mode of mitochondrial Ca^{2+} uptake (RAM) was found to drop the external Ca^{2+} to 100 nM in about 0.75 s, whereas MCU contributed to the latter slow sequestration (Sparagna *et al*., 1995). On the other hand, Ca^{2+} outward transport is regulated by the Na^+-dependent mitochondrial Na^+/Ca^{2+} exchanger (mNCX) and a Na^+-independent Ca^{2+} efflux mechanism.

Excessive mitochondrial Ca^{2+} load causes cell death by triggering either apoptosis or necrotic cell death.

1.1.4.4. Golgi apparatus

The Golgi apparatus acts as an agonist-sensitive intracellular Ca^{2+} store. The Golgi complex possesses Ca^{2+} releasing channels, Ca^{2+} binding proteins and Ca^{2+} uptake mechanisms (Van Baelen *et al*., 2004), and may store up to 5% of the total cellular Ca^{2+} at significantly higher Ca^{2+} concentrations (1 - 2 mM) than other regions of the cell.

Ca^{2+} release from the Golgi apparatus has been shown to be induced by IP_3 and agonists that couple with IP_3 production in HeLa cells (Pinton *et al*., 1998), and the IP_3R1 has been reported to co-distribute to the ER and the Golgi apparatus in HeLa cells (Lin *et al*., 1999). The Golgi apparatus possesses Tg-sensitive SERCA and Tg-insensitive secretory-pathway Ca^{2+}-transport ATPases (SPCA), which play an important role in cytosolic and intra-Golgi Ca^{2+} and Mn^{2+} homeostasis. The relative contribution of the SERCA and SPCA1 Ca^{2+} pumps to total Ca^{2+} uptake by the Golgi apparatus is cell-type dependent. The ER and the part of the Golgi apparatus expressing the SERCA are reported to be involved in the setting up of cytosolic Ca^{2+}

signals, in contrast, the SPCA1-based part of the Golgi complex does not contribute to cytosolic Ca^{2+} signalling (Van Baelen *et al*., 2004). Mutation in the gene coding for the SPCA1 pump (ATP2C1) causes Hailey-Hailey disease (familial benign chronic pemphigus), which is a genetic disorder that causes blisters to form on the skin in humans (Wuytack *et al*., 2003).

1.1.5. Removal of calcium

Unlike other intracellular messengers, Ca^{2+} is not degraded. Therefore, cytosolic Ca^{2+} is removed, either by extrusion to the extracellular space or by uptake into intracellular storage compartments. The main extrusion mechanisms used by a given cell differ depending on the cell type. Several mechanisms pump out Ca^{2+} cross the plasma membrane, including plasma membrane Ca^{2+}-ATPases (PMCAs), Na^{+}/Ca^{2+} exchangers (NCXs) and Na^{+}/Ca^{2+}-K^{+} exchangers (NCKXs) (Guerini *et al.*, 2005). Various intracellular Ca^{2+} stores contribute to the rapid removal of cytosolic Ca^{2+}, for instance, Ca^{2+} is re-sequestered by the endoplasmic reticulum (ER), mitochondria and the Golgi apparatus by SERCAs, by flow through Ca^{2+} channels driven by a large electrochemical gradient (in turn created by mitochondrial H^{+} exchange), and SERCA and secretory-pathway Ca^{2+}-transport ATPases (SPCAs), respectively (Clapham, 2007; Malli and Graier, 2010; Wuytack *et al.*, 2003).

1.1.6. G protein-coupled receptors

Extracellular stimuli often increase the intracellular Ca^{2+} concentration, and many of these stimuli operate through the recruitment of G protein-coupled receptors (GPCRs). GPCRs are proteins with seven transmembrane domains that transduce

extracellular signals to intracellular signals by activation or inactivation of enzymes or channels. The binding of agonists to GPCRs exposes the intracellular sites of GPCRs, which are involved in the interaction with the G protein heterotrimer α, β and γ subunits. The replacement of GDP by GTP, which binds to the Gα subunit, leads to dissociation of Gα from the Gβγ subunit complex. Both Gα and the Gβγ subunit complex activate several downstream effectors through $G_{q/11}$, G_s, $G_{i/o}$ and $G_{12/13}$ pathways. One $G\alpha_q$ family activates phospholipase C (PLC), which cleaves phosphatidylinositol bisphosphate (PIP_2) into diacylglycerol (DAG) and inositol trisphosphate (IP_3), which in turn elicits Ca^{2+} release from the ER. $G\alpha_s$ activates adenylyl cyclase (AC) and increases levels of cyclic adenosine monophosphate (cAMP), whereas $G\alpha_i$ inhibits AC and decreases cAMP levels. $G\alpha_{12}$ and $G\alpha_{13}$ have been shown to control the activity of key intracellular signal-transducing molecules, through activation of Rho guanine nucleotide exchange factors (RhoGEFs), which stimulates the Rho family of small GTPases (Buhl *et al*., 1995). More recently, it has been discovered that the Gβγ complex can also act as an intracellular effector: the Gβγ subunit complex has been reported to activate MAPKs through the small GTPase Ras, PLC-β, K^+ channels, AC and phosphatidylinositol-3-kinase (PI3K) (Neves *et al.*, 2002).

1.1.7. Sea urchin egg as a model system for investigating Ca^{2+} mobilization

The sea urchin egg has a long and extremely successful history as a model organism, and continues to be an ideal system to study mechanisms of general biological importance such as egg activation, fertilization, Ca^{2+} signalling, the cell cycle and exocytosis (Swann and Parrington, 1999). Together with the hemichordates, sea urchins represent basal groups of non-chordate invertebrate deuterostomes that

occupy a key position in bilaterian evolution. Because sea urchin embryos are also amenable to functional studies, the sea urchin system has emerged as one of the leading models for the analysis of the function of genomic regulatory networks that control development.

In particular, the sea urchin egg has been an excellent system to study Ca^{2+} release from intracellular stores, since the Ca^{2+} mobilizing abilities of IP_3, ryanodine, NAADP and cADPR are highly reproducible and the pharmacology has been well established (Table 2). Ca^{2+} responses are remarkably robust and display a high signal-to-noise ratio, providing an extremely effective and convenient system to study Ca^{2+} release mechanisms. In addition, these advantages are retained not only in intact eggs, but also in egg homogenate or purified microsomes (Churchill *et al.*, 2002; Clapper and Lee, 1985). Importantly, egg homogenate can be stored at -80°C, for decades, without losing its biological activities, and large quantity of eggs and sperm are available during the gravid season.

The sequence of the sea urchin (*Strongylocentrotus purpuratus; Sp)* genome was completed and annotated in 2006 (Sodergren *et al.*, 2006); it encodes about 23,300 genes.

In evolutionary terms, sea urchins are more closely related to humans than to flies or worms. The sea urchin genome is also the first genome of a non-chordate marine animal, of any kind, to be sequenced (Sodergren *et al.*, 2006). The completion of the sea urchin genome project has opened up many new valuable lines of research.

Table 2.1. Summary of results of Ca^{2+} transient experiments

Calcium release (Reference)	Sea urchin (1, 2, 3, 4)					*Sp*TPCs (5,6)*	*Hs*TPC1 *Hs*TPC2 (7,8)*	Pancreatic acinar cells (9)	β cells (9)	Plant *Brassica oleracea* (10)
Pharmacology	SERCA	V-H^+-ATPase	IP_3R	RyR	NAADP	NAADP	NAADP / CICR	NAADP	NAADP	NAADP
Ryanodine (> 10 μM)				●						
Heparin			●			● Global				
8-NH_2-cADPR				●						
Ruthenium red				●						●
NAADP (< 3 nM)					●	●				●
Diltiazem					●					
GPN					●			●		
Ned-19 & Ned-19.4						●				
Apyrase	●	●	●	●	●					
Thapsigargin	●		●	●			● Global			
Nigericin					●					
Bafilomycin A1		●			●	●	● Small	●	●	
Modulation			Ca^{2+}, pH	pH						

Table 2.2. Summary of results of NAADP binding experiments

NAADP Binding (Reference)	*Sea urchin* (4,11,12)	*Sp*TPCs (5) *	*Hs*TPC2 (8)*	Rat/Mouse brain (13)
K_d	540 pM	*Sp*TPC1 1.4 nM *Sp*TPC3 0.9 nM	5.0 nM, 7.2 μM	200 nM
Modulation	K^+ Phospholipid			
Antagonist	Ned-19 & Ned-20			
Inhibitory effect	Palmitoleic acid Arachidonic acid			

(1) Galone & Churchill, 2002
(2) Genazzani *et al*., 1996
(3) Genazzani *et al*., 1997
(4) Rosen *et al*., 2009
(5) Ruas *et al*., 2010
(6) Brailoius *et al*., 2010a
(7) Brailoius *et al*., 2010b
(8) Calcraft *et al*., 2009
(9) Yamasaki *et al*., 2003
(10) Navazio *et al*., 2000
(11) Patel *et al*., 2000a
(12) Churamani *et al*., 2005
(13) Patel *et al*., 2000b *expressed in HEK cells

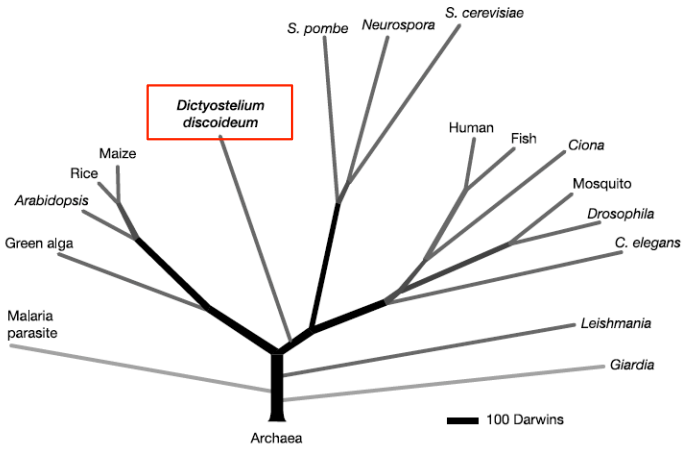
1.2. Dictyostelium discoideum

Dictyostelium discoideum is a species of soil-living amoebae belonging to the phylum *Mycetozoa*, one of the earliest branches from the last common ancestor of all eukaryotes (Figure 1.4A) (Eichinger *et al*., 2005).

1.2.1. Developmental cycle of *Dictyostelium*

The most striking feature of *Dictyostelium* is its unusual asexual lifecycle (Figure 1.4B and Figure 1.5). Under starved conditions, *Dictyostelium* exists as single cells on bacteria, respond chemotactically to cell-generated waves of cyclic adenosine - 3',5'- monophosphate (cAMP); cAMP relay signals induce chemotaxis and cell-cell contacts, resulting in streams of cells moving towards the aggregation centre. The independent amoebae generate multicellular structures of up to 100,000 cells and a tip forms approximately 12 hours after the initiation of development of the tight aggregates. Then, this multicellular structure forms a first finger and can either culminate where it is, involving a final round of differentiation and morphogenetic cell movement to form a mature fruiting body, or collapse onto the stratum to form a slug, allowing migration towards attractants, for instance, light, heat and humidity, and thus a move to a place more suitable for future spore dispersal and germination before culmination. The slug consists of different cell types that are defined by the expression of cell-type specific genes. The rear four-fifths of the slug consists mainly of prespore cells while the anterior of the slug contains prestalk cells. After a variable period of migration, the slug cells terminally differentiate during culmination to generate two major cell types, namely spore cells and stalk cells, as part of a fruiting body (Kay, 1992).

A.



B.

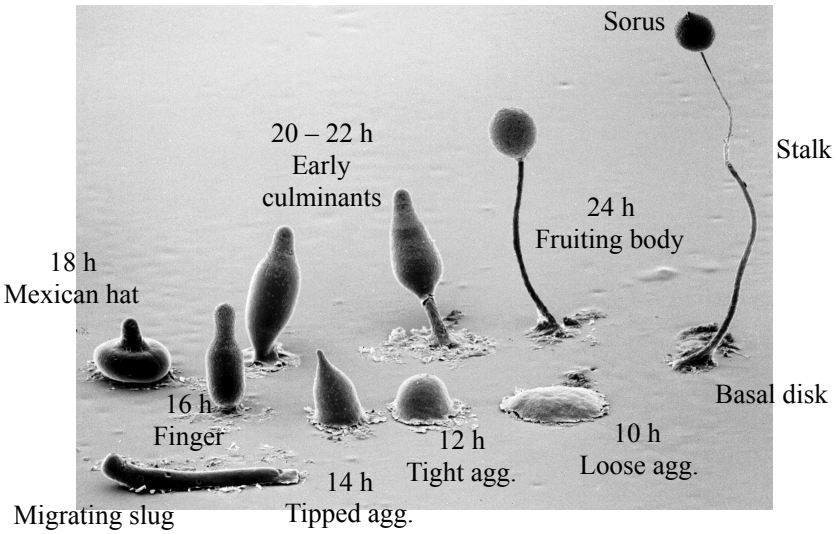


Figure 1.4. Phylogenetic tree and life cycle of *Dictyostelium discoideum*
A. Proteome-based eukaryotic phylogeny. The phylogenetic tree was reconstructed from a database of 56,279 orthologous protein clusters drawn from the proteomes of the17 eukaryotes shown, and was rooted on 159 protein clusters that had representatives from six archaebacterial proteomes. The relative lengths of the branches are given as Darwins (where 1 Darwin = 1/2,000 of the divergence between *S. cerevisiae* and humans). *Dictyostelium* diverged between plant and yeast, one of the earliest branches from the last common ancestor of all eukaryotes (Eichinger *et al.*, 2005).
B. The life cycle of *Dictyostelium* consists of four stages: vegetative growth (not shown), aggregation, slug migration and culmination (Grimson and Blanton, dictyBase: http://dictybase.org/). Images of stages were taken by a scanning electron microscope, and the approximate times after the onset of development are shown. Stalk cells form the stalk itself, as well as the conical basal disc, into which the foot of the stalk is embedded. Sorus indicates the top of the fruiting body in which spores are contained.

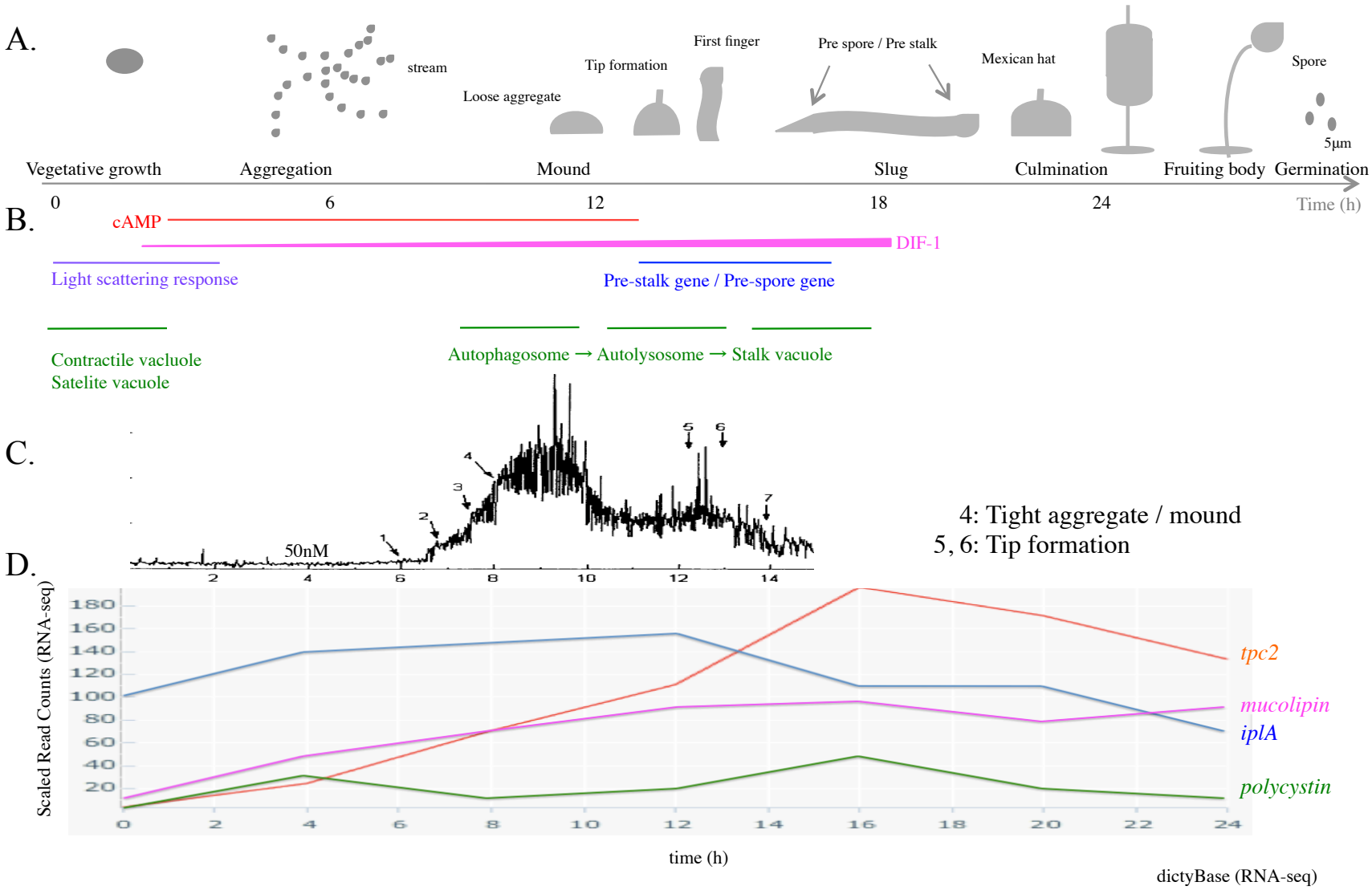


Figure 1.5. Life cycle of *Dictyostelium discoideum*

Figure 1.5. Life cycle of *Dictyostelium discoideum*
A. During vegetative growth, *Dictyostelium* lives unicellularly. Under food deprivation, individual amoebae migrate guided by a chemo-attractant cAMP, and form aggregates consisting of approximately 10^5 cells. The loose mound becomes tight and develops a tip, which elongates to form the first finger. This structure either culminates to form a fruiting body or collapses onto the stratum to form a slug, which moves towards heat and light (for example) in order to migrate to a place presumably more suitable for future spore dispersal and germination. Approximately 80% of cells differentiate into spores, supported by stalk cells, which are vacuolated and destined for death. Spores can remain dormant for long periods of time until nutritional and environmental conditions become suitable for germination and new life. Time (h) indicates the approximate times after the initiation of development.
B. Developmental changes in the levels of cAMP (red) and DIF-1 (pink), light scattering (purple) and timing of gene expression (blue). Differentiation of the contractile vacuole and the stalk vacuole are indicated by the green lines (Uchikawa *et al.*, 2011).
C. Intracellular Ca^{2+} levels as measured by stably expressed apoaequorin (Cubitt *et al.*, 1995).
D. The abundance of mRNA encoding putative Ca^{2+} channels during development is shown for *tpc2* (orange), *mucolipin* (pink), *iplA* (blue) and *polycystin-2* (green). mRNA-seq data were obtained from dictyBase.

1.2.2. *Dictyostelium* as a model system

The National Institutes of Health has included *Dictyostelium* on the list of biochemical model organisms. *Dictyostelium* is a haploid organism, containing a total of about 34 Mb of DNA (Eichinger *et al*., 2005). The haploid genome contains approximately 12,500 genes on six chromosomes. For comparison, the diploid human genome has 20,000 - 25,000 genes (represented twice) on 23 chromosome pairs. The *Dictyostelium* genome has been sequenced and many of the identified genes show a high degree of sequence similarity to genes in vertebrate species. Interestingly, *Dictyostelium* has more genes homologous to disease-related human genes than yeast (Eichinger *et al*., 2005).

Recent advances in technology have allowed detailed molecular biological analysis of much more complex organisms; however, using *Dictyostelium* as a model system has permitted novel experimental approaches, compared to those used in higher eukaryotic organisms, to understand human disease, and provided useful tools to facilitate drug screening and drug discovery (King *et al*., 2010). Particularly valuable is the fact that cells differentiate into fruiting bodies within 24 hours, allowing the timely study of all life stages. Taken together, these factors make the simple and unusual life cycle of *Dictyostelium* a valuable model system in which to investigate, amongst other mechanisms, cell differentiation, chemotaxis, regulation of gene expression, DNA repair pathways and programmed cell death. Importantly, *Dictyostelium* is haploid, allowing for relatively easy genetic manipulations to be made, including gene ablation. Thus, the functions of genes of interest can be exhibited as phenotypes in appropriate biological assays.

1.2.3. Signalling molecules in *Dictyostelium* proposed to work through Ca^{2+}-dependent pathways

1.2.3.1. cAMP-induced signalling pathways during early development

An overview of likely cAMP signalling pathways is shown in Figure 1.6. cAMP was shown to act as a chemo-attractant that could trigger the aggregation of *Dictyostelium* cells (Darmon *et al*., 1975). During the early developmental stages, cAMP is formed from ATP by ACA in a few starved cells, and then secreted in a pulsatile manner to act on surrounding cells in aggregation centres. In many cell types throughout the animal kingdom, the binding of an agonist to a GPCR causes the dissociation of the α-subunit from the $\beta\gamma$-subunit complex and it is the α-subunit that regulates intracellular cAMP production by activating ACA (Neves *et al*., 2002). The cAMP generated by ACA subsequently acts intracellularly to influence cellular function, either by activating cAMP-dependent protein kinases, which in turn phosphorylate target proteins, or by binding to exchange proteins activated by cAMP (Epac) that in turn activate Ras-like GTPase proteins (Bolourani *et al*., 2008). However, in *Dictyostelium*, the secreted cAMP binds to the extracellular domain of the GPCR, cAR1 (Klein *et al*., 1988; Saxe *et al*., 1991), resulting in the release of the $\beta\gamma$-subunit complex (Jin *et al*., 1998; Lilly *et al*., 1993) which in turn activates ACA in conjunction with the cytosolic regulator of adenylyl cyclase (CRAC) protein (Insall *et al*., 1994; Lilly and Devreotes, 1994). Most of the cAMP generated is secreted to relay the signal. Activation of the cAMP signalling pathway tells not only surrounding cells to synthesize cAMP in waves, produced by activation/desensitization of cAMP receptors (cARs) (Caterina *et al*., 1995), but also initiates several signalling cascades which ultimately lead to chemotaxis and

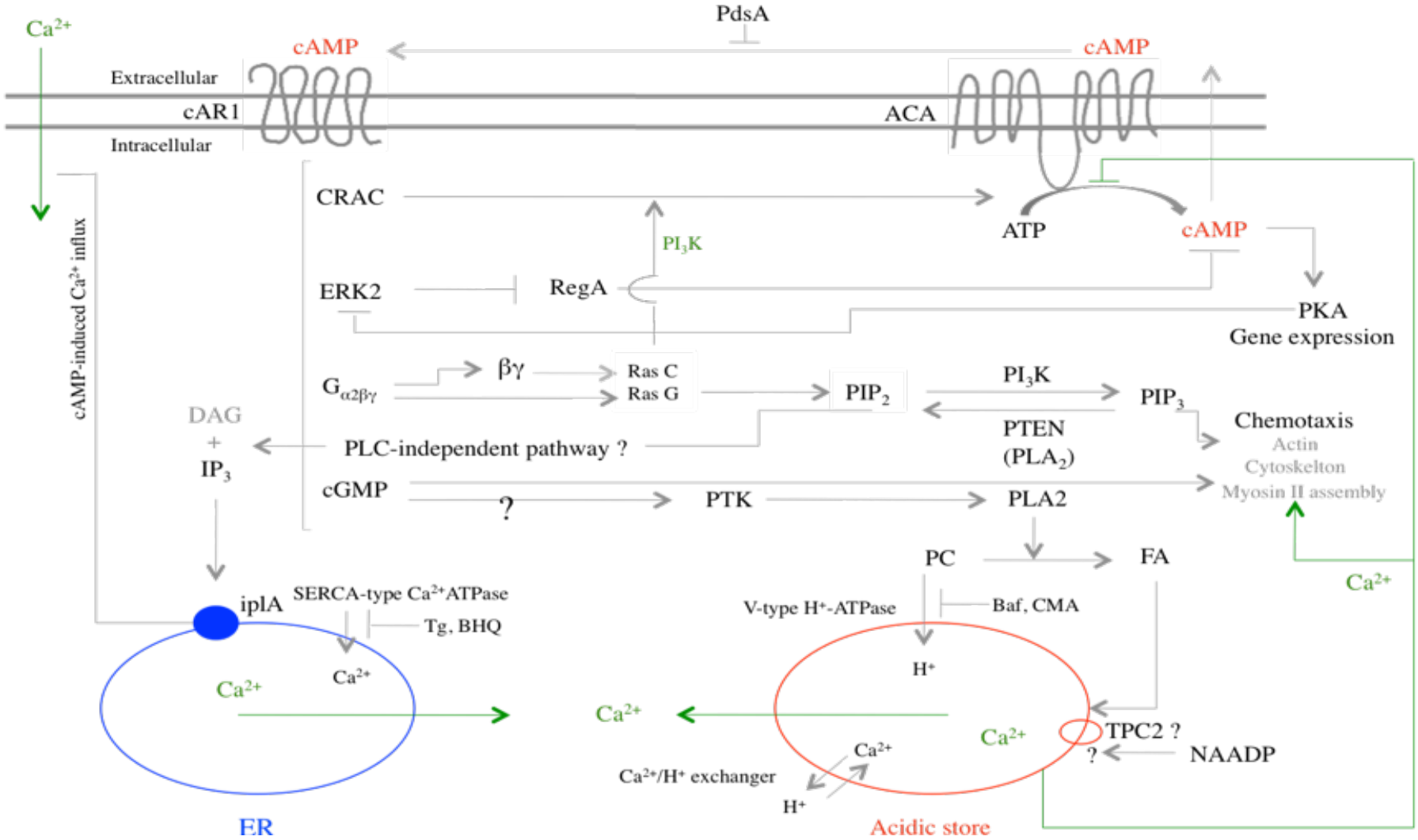


Figure 1.6. Model of the cAMP-dependent signalling network in *Dictyostelium*

Figure 1.6. Model of the cAMP-dependent signalling network in *Dictyostelium*
Binding of extracellular cAMP to the cAR1 receptor (Klein *et al.*, 1988; Saxe *et al.*, 1991) allows the Gα subunit to exchange GDP for GTP, resulting in the release of the Gβγ subunit (Lilly *et al.*, 1993; Jin *et al.*, 1998). Gβγ activates adenylyl cyclase (AC) through RasC and the cytosolic regulator of adenylyl cyclase (CRAC), resulting in the synthesis of cAMP (Insall *et al.*, 1994; Lilly and Devreotes, 1994, Bolourani *et al.*, 2008). To prevent accelerated development, cAMP is inactivated by hydrolysis by several phosphodiesterases (PDE). In addition, global Ca^{2+} elevation inhibits cAMP production (Malchow *et al.*, 2004; Schaloske *et al.*, 1976). Ligand-bound cAR1 also activates the MAP kinase ERK2 (Knetsch *et al.*, 1996) which further aids cAMP accumulation by inhibiting the cAMP PDE, RegA (Shaulsky *et al.*, 1996, 1998; Thomason *et al.*, 1998). Most of the cAMP synthesised is secreted whilst the remainder stays within the cell and is able to bind to the PKA regulatory subunit, resulting in increased PKA activity that instigates changes in developmental gene expression. Activated PKA also targets ERK2, resulting in decreased cAMP levels as a consequence of increased RegA PDE activity (Aubry *et al.*, 1997). After activation of the cAMP receptor, gradient sensing is proposed to occur in the section between the activated heterotrimeric G protein and the activation of RasG (Bolourani *et al.*, 2008). The resultant PIP_3 production is controlled by parallel pathways, through PI_3K and PTEN (Chen *et al.*, 2007; Bolourani *et al.*, 2008). Binding of extracellular cAMP to the cAR1 receptor also activates phospholipase A_2 (PLA_2), which liberates fatty acid (FA) and elicits Ca^{2+} influx (Schaloske *et al.*, 1997; Schaloske *et al.*, 1998). FA induces Ca^{2+} release from acidic stores, which is inhibited by V-type H^+-ATPase inhibitors (bafilomycin A1 and concanamycin A). Ca^{2+} uptake into the ER is inhibited by SERCA-type Ca^{2+}-ATPase inhibitors (BHQ and thapsigargin, Tg) and a cell-permeable inhibitor of IP_3 receptor-mediated Ca^{2+} release (xestospongin C, XeC) (Rooney *et al.*, 1992; Flaadt *et al.*, 1993a; Rooney *et al.*, 1994; Schaloske *et al.*, 2000; Malchow *et al.*, 2006). Other pathways implicated in the control of Ca^{2+} responses are increases in the production of IP_3 and cGMP (Bominaar *et al.*, 1994). IP_3 elicits Ca^{2+} release from the ER and disruption of a putative IP_3R (*iplA*) abolishes cAMP-induced Ca^{2+} release. The mechanism of Ca^{2+} release by FA, and whether NAADP or *Dd*TPC2 are involved in Ca^{2+} signalling, remain unknown.

developmental gene expression. The binding of cAMP to cell surface receptors triggers production of phosphatidylinositol (3,4,5)-trisphosphate (PIP_3) and cyclic guanosine monophosphate (cGMP), which are the key molecules involved in cell movement during chemotaxis. PIP_3 levels are controlled by the regulation of enzymes involved in PIP_3 synthesis (phosphoinositide 3'-kinase, PI3K) or its degradation (phosphatase tensin type domain-containing protein, PTEN) (Chen *et al*., 2007). cGMP, which regulates myosin II assembly (Parent, 2004; Van Haastert and Devreotes, 2004), is produced by guanylyl cyclase from GTP.

A genetic screen in *Dictyostelium*, to identify pathways which regulate chemotaxis in the absence of PI3K, revealed the importance of a gene with homology to patatin-like phospholipase A_2 (PLA_2). Patatin is a glycoprotein found in potatoes (*Solanum tuberosum*); the main function of patatin is as a storage protein, but it also has lipase activity and can cleave fatty acids from membrane lipids. Loss of PLA_2 in *Dictyostelium* did not alter PIP_3 regulation, but chemotaxis became sensitive to inhibition of PI3K (Chen *et al*., 2007). Similarly, cells deficient in PI3K activity were more sensitive to inhibition of PLA_2 activity. Deletion of the *pla2* gene homologue and two of five genes for PI3K (*pi3k*s) caused a strong defect in chemotaxis, and a reduction in receptor-mediated actin polymerization. In wild-type cells pre-loaded with ^{3}H-arachidonic acid, chemo-attractants stimulated a rapid burst in release of free arachidonic acid (AA), consistent with PLA_2 activation. This response was absent in cells lacking the *pla2* homologue, and exogenous AA reduced their dependence on PI3K signalling (Chen *et al*., 2007). Therefore, not only PIP_3 but also metabolites of PLA_2 may be important mediators involved in chemotaxis. It has been reported that

there is no AA in *Dictyostelium* (Weeks, 1976), but another fatty acid could act as the endogenous signal.

1.2.3.2. The role of cAMP during post-aggregative development

The levels of extracellular cAMP rise to around 1 mM at the mound stage and cease to be pulsatile. *Dictyostelium* cells express different types of cARs with different affinities for cAMP, dependent on the particular developmental stage (Johnson *et al*., 1993; Saxe III *et al*., 1991). *Car2* (the gene for cAR2) is expressed only during post-aggregative development, and deletion of *car2* leads to a block of tip formation, and the strain arrests at the mound stage of development (Saxe *et al*., 1993). *Car3* is expressed at low levels during early development, and maximally during tight aggregate formation (Johnson *et al*., 1993). Studies with *car4* have suggested that cAMP signalling continues during the post-aggregative stage. Thus, the mRNA of *car4* is initially expressed during tip formation and continues to increase toward culmination, whereas *car4* null cells exhibit aberrant cellular patterns after tip formation (Louis *et al*., 1994). Although cAMP signalling has been investigated in some detail, no studies have examined the role of Ca^{2+} signalling during the later stages of development.

1.2.3.3. Differentiation inducing factor in *Dictyostelium*

Another well-studied extracellular signalling molecule, which has been proposed to function through changes in intracellular Ca^{2+} levels in *Dictyostelium*, is differentiation inducing factor (DIF). DIF-1 was originally discovered as a morphogen that was necessary for prestalk/prespore cell pattern formation in

Dictyostelium (Morris *et al*., 1987) and which induced prestalk cell differentiation in monolayer assays. Slugs that formed from cells, which were blocked from carrying out DIF-1 synthesis, were deficient in PstO (prestalk type O) cells, one of the subtypes of prestalk cell (Thompson and Kay, 2000). DIF-2 and DIF-3 were identified soon after (Morris *et al*., 1988). DIF-1 plays a crucial role in the early events before the fate of the cell is determined (Wurster and Kay, 1990). DIF-1 is synthesized endogenously by prespore cells from a C_{12} polyketide precursor by chlorination and methylation reactions (Kay and Thompson, 2001; Neumann *et al*., 2010). The synthesis and metabolism of DIF-1 is developmentally regulated and increases towards the end of development (Figure 1.5B). At the beginning of development (about 2 hours), DIF-1 levels are initially very low, but they gradually increase during tip formation (e.g. 2.5 nM after 6 hours), followed by a dramatic increase around 13 - 16 hours after the initiation of development (e.g. 62 nM in the slug) (Kay, 1998). DIF-1 is inactivated by DIF-1 dechlorinase (Insall *et al*., 1992). The biological activity of the first metabolite, DIF-3, drops to 3.5% compared to that of DIF-1 (Kay *et al*., 1999). On the other hand, DIF-2 has been suggested to be produced as a side reaction of DIF-1 biosynthesis, and possesses 40% of the specific activity of DIF-1 (Masento *et al*., 1988), but is 2-10 fold more potent in causing the light-scattering response (*infra vide; light scattering*) (Wurster and Kay, 1990). It has been suggested that DIF-1 and DIF-2 play different roles in development, namely inhibition and enhancement of chemotaxis, respectively (Kuwayama and Kubohara, 2009). It has also been posited that there are specific DIF receptors, since solubilized membrane fractions of *Dictyostelium* showed a single class of DIF-1 binding site with high affinity (a K_d of 1.8 nM). However, the molecular identity of this putative

receptor class remains to be elucidated (Insall and Kay, 1990). The chemical structures of DIFs are shown in Figure 1.7.

The regulation of gene expression by DIF-1 has been extensively studied, the best known effect being induction of STATc (signal transducer and activator of transcription-c) tyrosine phosphorylation, a primary DIF-1 response that reaches a peak some 3 - 5 min after DIF-1 treatment, by inhibition of protein tyrosine phosphatase-3, PTP3 (Araki *et al*., 2008). STATc localises to nuclei of pstO (prestalk type O) cells, one of the prestalk cell subtypes, where it acts to prevent ectopic expression of the *ecmA* gene, a marker of pstA (prestalk type A) cell differentiation (Fukuzawa *et al*., 2001). It is not known whether tyrosine phosphorylation is a direct response to DIF-1 or due to a downstream effect of DIF-1-induced signalling, e.g. an alteration in Ca^{2+} levels. Ca^{2+} has been shown to be involved in STATc activation, whereby the elevation of intracellular Ca^{2+} levels caused by BHQ (a selective inhibitor of the endoplasmic reticulum Ca^{2+}-ATPase) results in an increase in tyrosine phosphorylation of STATc by repressing dephosphorylation through the inhibitory effect of PTP3 (Araki *et al*., 2010).

1.2.4. Cell fate and intracellular Ca^{2+} concentration in *Dictyostelium*

Measuring stable cytosolic Ca^{2+} levels in cells that expressed apoaequorin, showed that intracellular Ca^{2+} levels are normally kept around 50 nM during chemotaxis (about 6 - 7 hours), and rise 20-fold at the stream stage (Figure 1.5C). A further dramatic increase follows at the mound stage some 8 - 10 hours later. The second peak accompanies tip formation at around 12 hours (see Figure 1.5) (Cubitt *et al*., 1995). Sustained $[Ca^{2+}]_i$ elevation eventually leads to stalk cell death, indicating that

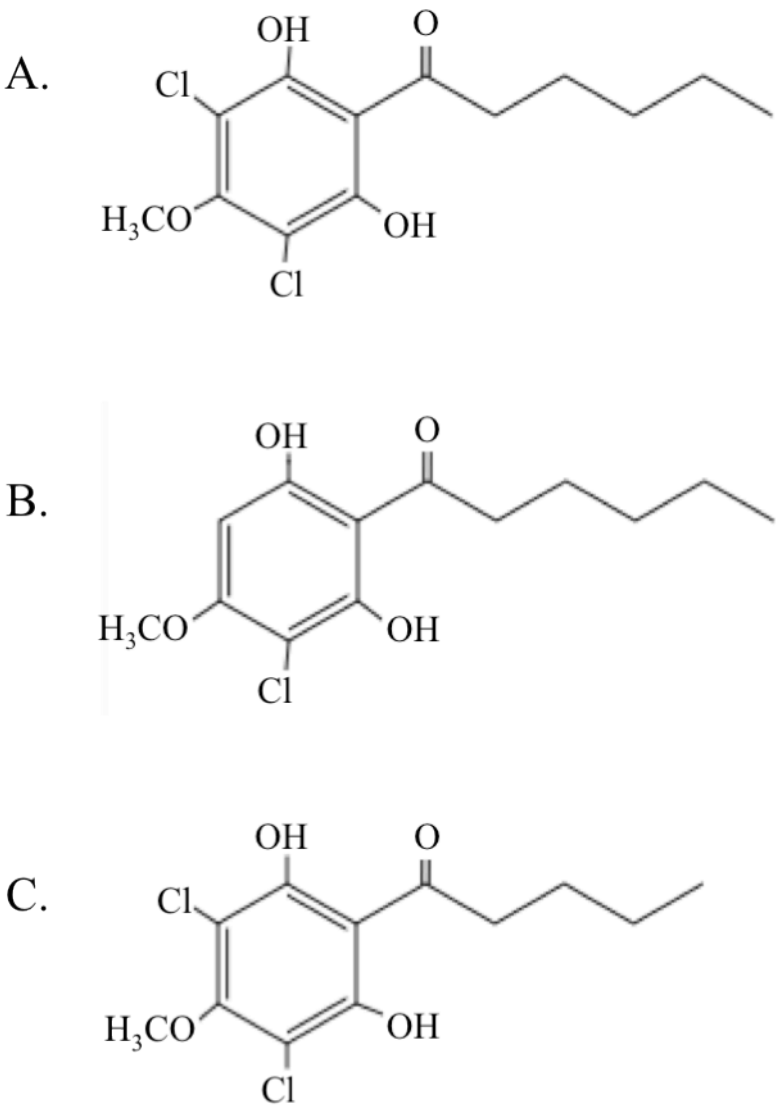


Figure 1.7. Differentiation inducing factors from *Dictyostelium*
Chemical structures of DIF-1 (A), DIF-2 (B) and DIF-3 (C) are shown (Morris *et al*., 1987, 1988).

there may be a developmentally regulated Ca^{2+} mobilizing system throughout the life cycle of *Dictyostelium.* The recent manufacture of a calcium-sensitive dye which detects brief, small Ca^{2+} transients (induced by Ca^{2+} mobilizing agents), permits the study of Ca^{2+} signalling in *Dictyostelium* throughout the developmental cycle, including cAMP-induced Ca^{2+} influx or receptor-mediated Ca^{2+} release from intracellular Ca^{2+} stores. These studies have been mainly carried out using *Dictyostelium* cells starved for 2 - 6 hours (Flaadt *et al*., 1993a; Schaloske *et al*., 1997); however, no studies of Ca^{2+} signalling have been carried out on cells in the late developmental stages.

1.2.5. Global or transient changes of $[Ca^{2+}]_i$

The interaction of cAMP with its cell surface receptor also causes extracellular Ca^{2+} influx into intact cells, as measured with a Ca^{2+}-sensitive electrode or using $^{45}Ca^{2+}$ (Flaadt *et al*., 1993b), but the mechanisms involved remain to be elucidated. The Ca^{2+} signals triggered by cAMP eventually lead to global increases in Ca^{2+}, which involve CICR mechanisms. CICR has been demonstrated in *Dictyostelium* by Malchow and colleagues, who showed that CICR was largely dependent on the function of acidic stores, which comprise the contractile vacuole, the acidocalcisome and endosomal compartments; it is noteworthy that CICR was not dependent on the intact function of the ER (Malchow *et al*., 2008). CICR was reduced in two strains lacking functional acidic stores: HGR8, which has an impaired proton gradient across the CV membrane, and *lvsA*$^-$ cells which lack the gene encoding large volume sphere A (LvsA), causing failure of calmodulin to associate with the contractile vacuole (CV) (Malchow *et al*., 2008). In contrast, CICR was unchanged in the *iplA*$^-$ strain that lacks the putative IP_3 receptor on the ER (Malchow *et al*., 2008). Similar results were

obtained by pharmacological disruption of intracellular Ca^{2+} stores; inhibition of acidic stores was achieved using W7 (a calmodulin antagonist) or concamycin A (CMA, a V-type H^{+}-ATPase inhibitor) and disruption of ER function was achieved using thapsigargin (Tg, a SERCA-type Ca^{2+}-ATPase inhibitor) and xestospongin C (XeC, a membrane permeable inhibitor of IP_3-mediated Ca^{2+} release).

Pharmacologically-induced global elevation of basal $[Ca^{2+}]_i$, caused either by CMA, Tg or XeC, was found to arrest the cAMP relay signal (Malchow *et al*., 2004; Schaloske *et al*., 2000). However, Ca^{2+} transients caused by W7 were of low magnitude and had no impact on excitability but nevertheless increased cAMP synthesis (Malchow *et al*., 2004). A small, artificial, elevation of Ca^{2+} by calmidazolium (a calmodulin antagonist) caused pseudopods to extend over the whole circumference of cells, whereas a larger Ca^{2+} elevation induced full contraction. How *Dictyostelium* cells produce elevations in Ca^{2+}, from small transients to a large global response that leads to excitable biological events, and the identity of the Ca^{2+} stores responsible, remain unknown.

1.2.6. Ca^{2+} oscillations

Periodic spikes of decreased optical density (light scattering) can be recorded in cell suspensions of *Dictyostelium*. These are believed to represent signal transmission in aggregating cells of *Dictyostelium* (Gerisch and Hess, 1974). Spike-like oscillations are an indicator for the operation of the cAMP relay mechanism. Oscillations in cAMP levels are accompanied by Ca^{2+} oscillations, and a disturbance of Ca^{2+} regulation affects the cAMP relay as well as light scattering oscillations. Spike-shaped light scattering oscillations, without any elevation of extracellular cAMP

concentrations, have been measured using Ca^{2+}-sensitive electrodes in cells that had been starved for 5 hours. This finding suggests that cAMP is not the pacemaker for cellular oscillations in light scattering, but rather Ca^{2+} itself (Malchow *et al*., 1996; Wurster and Kurzenberger, 1989). However, the mechanisms underlying light scattering in *Dictyostelium* are not fully understood (Lusche *et al*., 2004).

1.2.7. Known Ca^{2+} mobilising agents in *Dictyostelium*

1.2.7.1. cAMP

As described above, cAMP is a natural chemo-attractant of the social amoeba, *Dictyostelium*, detected by specific, cell surface cAMP receptors that activate intracellular messenger cascades. In addition to the signalling cascade involving phosphatidylinositol 3,4,5-trisphosphate (PIP_3), an involvement of Ca^{2+} signalling in chemotaxis has also been suggested (Chen *et al*., 2007). Whether Ca^{2+} signalling is necessary for chemotaxis to occur, and if so, the potential pathways responsible for chemotaxis, are subjects of great interest in this field. The relationship between extracellular cAMP levels and transient increases in cytosolic Ca^{2+} levels has been studied extensively during the aggregation stages of development (Gross, 2009; Malchow *et al*., 2004; Malchow *et al*., 2006; Schaloske *et al*., 1997; Schaloske *et al*., 2005; Traynor *et al*., 2000). The cAMP-mediated Ca^{2+} transients may be indirect, produced by activation of signalling pathways rather than due to cAMP itself acting directly as a ligand at Ca^{2+} mobilising channels in intracellular compartments. Binding of cAMP to its receptor activates several downstream pathways related to Ca^{2+} signalling, including the production of IP_3, cGMP (Bominaar and Van Haastert, 1994) and fatty acids by PLA_2 activation (Schaloske *et al.*, 1997). IP_3 and fatty acids

are potential mediators to induce Ca^{2+} release from intracellular Ca^{2+} stores, the ER and acidic stores, respectively (Flaadt *et al*., 1993a; Schaloske *et al*., 1998).

1.2.7.2. Differentiation-inducing factor 1 (DIF-1)

DIF-1 rapidly induces expression of the prestalk gene, *ecmB*, in cells starved for up to 8 hours. *EcmB* expression is also upregulated by an increase in $[Ca^{2+}]_i$, produced by BHQ, and inhibited by the Ca^{2+} chelator, BAPTA (Schaap *et al*., 1996). Consistent with an important role for Ca^{2+} in stalk cell induction, regions of future stalk or stalk-like cells are coincident with high Ca^{2+} level regions in multicellular structures (Cubitt *et al*., 1995). Furthermore, stalk cell differentiation is induced by elevation of $[Ca^{2+}]_i$, mediated by cAMP (via unknown mechanisms) or Ca^{2+} release from intracellular Ca^{2+} stores elicited by Tg and BHQ (Cubitt *et al*., 1995; Kubohara *et al*., 2007; Kubohara and Okamoto, 1994). It is noteworthy that lowering $[Ca^{2+}]_i$, by using either BAPTA or EGTA, decreases the ratio of stalk cells to spore cells (Cubitt *et al*., 1995; Jaffe, 1999). These studies provide evidence to support the hypothesis that $[Ca^{2+}]_i$ plays an intermediate messenger role in DIF-induced gene expression, without producing an alteration (decrease) in cytosolic pH (Kay *et al*., 1986). Spatiotemporal Ca^{2+} signalling patterns may be involved in this mechanism, enabling a single substance, such as DIF, to control complicated cellular processes, for instance, gene expression.

1.2.7.3. Inositol 1,4,5-trisphosphate (IP_3)

IP_3-induced Ca^{2+} release has been demonstrated using permeabilised *Dictyostelium* cells, which had been starved for 4 - 6 hours (Flaadt *et al*., 1993a). In general, IP_3

together with DAG (diacylglycerol) are produced as metabolites of PIP_2 (phosphatidylinositol 4,5-bisphosphate) hydrolysis by phospholipase C. *Dictyostelium* possesses one phospholipase C-like orthologue (Drayer *et al*., 1994) as well as enzyme activities capable of synthesizing IP_3 through a PLC-independent pathway (Van Dijken *et al*., 1995). This novel mechanism was identified in *plc* null cells (lacking the gene for phospholipase C), which exhibited virtually normal levels of IP_3 produced from endogenous precursors (Drayer *et al*., 1994). With regard to function, disruption of *plc* had no detectable effects on development (Drayer *et al*., 1994). In addition, cAMP-induced Ca^{2+} influx was normal in cells starved for 4 - 8 hours (Schaloske *et al*., 1998). Interestingly, cAMP-mediated Ca^{2+} influx was abolished in *iplA*$^-$ cells, in which an IP_3 receptor-like protein was ablated, however there was no alteration of development was apparent (Traynor *et al*., 2000). On the other hand, *stmF* mutants, lacking cGMP-specific phosphodiesterase activity, exhibited prolonged cAMP-mediated changes in intracellular Ca^{2+} levels (Nebl *et al*., 2002). The cGMP-dependent Ca^{2+} response to cAMP was present in the vegetative and early post-starvation stages. However, the molecular basis for this response is not known.

1.2.7.4. Fatty acids as Ca^{2+} mobilizing agents

Deletion of a *pla*$_2$ gene homologue and two of five genes for PI3K (*pi3k*s) caused a strong defect in chemotaxis and a reduction in receptor-mediated actin polymerization (Chen *et al*., 2007). This phenotype was rescued by overexpression of PLA_2, or by adding AA extracellularly, giving rise to the possibility that Ca^{2+} elevation, especially that mediated by fatty acids, may play an important role in chemotaxis in the absence of PIP_3 signalling. The hydrophobicity of fatty acids is increased with increasing

saturation and chain length; long chain, saturated fatty acids are the least soluble in water. Biological activity varies and depends on the structure of the fatty acids and the systems involved. In *Dictyostelium*, the unsaturated long chain fatty acids, linoleic (LA) and oleic acid (OA), were found to activate the Ca^{2+}/calmodulin-dependent phosphatase, calcineurin. In contrast, arachidic acid, also known as eicosanoic acid, a saturated fatty acid with a 20-carbon chain, had no effect on calcineurin activity (Kessen *et al*., 1999). LA and AA induced a transient increase in $[Ca^{2+}]_i$, followed by Ca^{2+} influx into cells developed for 5 - 7 hours (T5 - T7) and electroporated at T2 - T3 to permit the introduction of a Ca^{2+} indicator dye (Schaloske *et al*., 1997). Palmitic acid was found to induce Ca^{2+} release from intracellular Ca^{2+} stores in permeabilized cells (Schaloske *et al*., 1998). More recently, AA-induced Ca^{2+} release has been detected using both permeabilized cells and vesicular fractions containing intracellular Ca^{2+} stores (Malchow *et al*., 2006). Pharmacological studies have indicated that AA-induced Ca^{2+} release is blocked by inhibitors of Ca^{2+} transport- and V-type H^+-ATPases (Schaloske *et al*., 1998). Inhibition of V-type H^+-ATPases with concanamycin A (CMA, 5 μM) reduced AA-induced Ca^{2+} influx; similarly, bafilomycin A1 (5 μM) reduced the AA effect by 20% but was less effective than CMA (Schaloske *et al*., 1998). AA-induced Ca^{2+} influx was reduced in HGR8 cells, which exhibited a lower capacity for the acidification of endolysosomes, and in the *lvsA*$^-$ strain in which Ca^{2+} uptake into intracellular stores was reduced (Malchow *et al*., 2006). All these results are consistent with the targeting of acidic Ca^{2+} stores by AA. However, AA is not endogenously synthesized in *Dictyostelium* (Weeks, 1976). The mechanism of AA-induced Ca^{2+} release, and whether exogenous AA is mimicking an endogenous Ca^{2+} mobilizing agent, remain unknown. In

addition, the molecular identity of the AA receptor is yet to be revealed in *Dictyostelium.*

1.2.8. Intracellular Ca^{2+} stores in *Dictyostelium*

cAMP elicits an initial Ca^{2+} influx though the plasma membrane and subsequent Ca^{2+} release from intracellular stores, followed by resequestration (Flaadt *et al*, 1993a). Several organelles have been identified as potential intracellular stores of Ca^{2+} in *Dictyostelium*. The ER is widely believed to be the IP_3-sensitive store, and Ca^{2+} uptake has been shown to be inhibited by the SERCA-type Ca^{2+}-ATPase inhibitors, BHQ and Tg, as well as by a cell-permeable inhibitor of IP_3 receptor-mediated Ca^{2+} release, XeC (Schaloske *et al*., 2000). Acidic stores comprising the CV, acidocalcisomes and endosomal compartments - which accumulate Ca^{2+} using the ATP-dependent Ca^{2+}/H^+ exchanger in conjunction with a V-type H^+-ATPase (Heuser *et al*., 1993; Nolta and Steck, 1994) - are sensitive to the V-type H^+-ATPase inhibitors, bafilomycin A1 and CMA, and to weak bases (Flaadt *et al*., 1993b; Malchow *et al*., 2006; Rooney and Gross, 1992; Schaloske *et al*., 2000). A summary of these experiments is shown in Table 3.

Dictyostelium is known to possess large vacuoles and small satellite vacuoles (Quiviger *et al*., 1978); however, the luminal pH of these vacuoles is unclear, except for the endosomes, which have been reported to be 5.7 (Bof *et al*., 1992). Only recently, the origin of the stalk cell vacuole, which is distinct from the CV and enriched in H^+-ATPase (as are plant cell vacuoles), was revealed. Acidic vesicles and autophagosomes - smaller neutral vesicles - fuse to form large acidic structures called autolysosomes, about 8 hours after the development initiation (Figure 1.5B). The

Table 3. Summary of Ca^{2+} influx/release experiments in *Dictyostelium*

Chemical	Influx (Whole cell)	Inhibitor	Reduced / Abolished (strain)	Reference	Release from intracellular Ca^{2+} stores (Vesicles)	Inhibitor	Reduced (strain)	Reference
cAMP	●	BHQ	*iplA*$^-$ *lvsA*$^-$	1,2,3,4				
AA	●	CMA Bafilomycin A1	*lvsA*$^-$	1,2,4	●		HRG8 *lvsA*$^-$	2
PA	●			1,2	●			2
LA					●			2
IP_3	● (ER)			5				
Ca^{2+} (ICIR)					● (CV)	W7 CMA	HRG8 *lvsA*$^-$	6
Ca^{2+} uptake						(ER) Tg, BHQ (CV) CMA		4
Nigericin	●			7				

1. Schaloske & Malchow, 1997
2. Schalske *et al*., 1998
3. Traynor *et al*., 2001
4. Malchow *et al*., 2006
5. Flaadt *et al*., 1993b
6. Malchow *et al*., 2008
7. Rooney & Gross, 1994

continuously fused acidic compartment expands within the cellulosic cell wall and eventually forms the stalk cell vacuole (Uchikawa *et al*., 2011).

1.2.9. Ca^{2+} transporters and channels in *Dictyostelium*

There are a number of genes encoding putative Ca^{2+} transporters and channels in *Dictyostelium*, including the PMCA-type Ca^{2+}-ATPase (PAT1), IP_3 receptor-like protein (IplA), two-pore channel 2 (TPC2), mucolipin, polycystin-2 like protein (polycystin2) and purinergic receptors (Ludlow *et al*., 2008; Wilczynska *et al*., 2005). These candidates are summarized in Table 4, and discussed below

1.2.9.1. PMCA-type Ca^{2+}-ATPase (PAT1)

PAT1 (DDB0214945) is a P-type Ca^{2+}-ATPase comprised of 10 predicted transmembrane domains. The localisation of PAT1 on the CV indicates a potential function, not only in osmoregulation but also in Ca^{2+} homeostasis through sequestration and extrusion of Ca^{2+} when fused to the plasma membrane (Moniakis *et al*., 1995; Moniakis *et al*., 1999).

1.2.9.2. IP_3 receptor-like protein

Dictyostelium has only one gene coding for a protein with high homology to the IP_3R, and none encoding potential ryanodine receptors (RyR) (Wilczynska *et al*., 2005). Expression of *iplA* mRNA is low during growth and rises to a peak after about 9 hours of development when chemotactic aggregation, driven by cAMP, is near its zenith, before declining throughout the rest of development (Figure 1.5D). There are some reports that IP_3 can induce Ca^{2+} release from internal stores (Europe-Finner and

Table 4. Putative Ca^{2+} transporters and channels in *Dictyostelium*

Transporter or channel	dictyBase accession number	Protein product	Number of transmembrane domains	Subcellular location (Reference)	Putative calcium- or calmodulin-binding regulatory sites	Functional roles
Transporters	DDB0214945	*PatA*	10	Vacuolar membrane	Calmodulin-binding helical peptide IQ motif (642-661)	Ca^{2+} homeostasis
	DDB0188438	PMCA or SERCA	10	Plasma membrane or ER	Calmodulin-binding helical peptide IQ motif (683-702)	Ca^{2+} homeostasis
	DDB0186093	PMCA or SERCA	10	Plasma membrane or ER	Calmodulin-binding helical peptide IQ motif (127-146)	Ca^{2+} homeostasis
Channels	DDB0201571	*iplA* (IP_3 receptor-like protein)	5	ER membrane (Pharmacology)	Calmodulin-binding helical peptide IQ motif (148-167)	Cytosolic Ca^{2+} signalling
	DDB0216059	TPC (Two Pore Channel) (putative Ca^{2+} channel)	10	CV and ER (in this study)	Ca^{2+} -binding EF-hands (781-792 and 817-828)	Cytosolic Ca^{2+} signalling
	DDB0183788	Mucolipin (putative Ca^{2+} channel)	6 (5: TMHMM)	Lysosomes (Prediction)	Ca^{2+} -binding EF-hands (614-626)	Ca^{2+}-dependent lysosomal or vesicle biogenesis and trafficking (prediction)
	DDB0217079	Polycystin-2 like receptor (putative Ca^{2+} channel)	6	Plasma membrane (prediction)		Mechanosensory Ca^{2+} signalling in cilia
	DDBG0272004	P2X1 (ATP-gated ion channel)	1 (TMHMM)	Vacuolar membrane		May be involved in cytosolic Ca^{2+} signalling
	DDBG0275293	P2X2 (ATP-gated ion channel)	1 (TMHMM)	Vacuolar membrane (prediction).		May be involved in cytosolic Ca^{2+} signalling
	DDBG0275191	Putative P2X3 (ATP-gated ion channel)	1 (TMHMM)	Vacuolar membrane (prediction).		ATP-gated ion channel activity could not be demonstrated
	DDBG0288335	Putative P2X4 (ATP-gated ion channel)	1 (TMHMM)	Vacuolar membrane (prediction).		ATP-gated ion channel activity could not be demonstrated
	DDBG0288061	P2X5 (ATP-gated ion channel)	2 (TMHMM)	Vacuolar membrane (prediction).		May be involved in cytosolic Ca^{2+} signalling

dictyBase is an online bioinformatics resource for *Dictyostelium*.
TMHMM server v.2.0 and Motif scan / EF-hand: PROSITE were used for the structural analysis.

Newell, 1986; Flaadt *et al*., 1993b), which would suggest that the IP_3 receptor-like protein functions as an actual IP_3 receptor. The cAMP-induced rapid Ca^{2+} transient has been suggested to be mediated by IP_3 (Flaadt *et al*., 1993b), since Ca^{2+} influx, in response to cAMP, was abolished in the IP_3-like receptor ablated strain, *iplA*$^-$ (Traynor *et al*., 2000). Interestingly, in this study, *iplA*$^-$ cells aggregated and developed normally without the IP_3-like receptor (IplA). In contrast, another group reported that EGTA-induced Ca^{2+} influx was observed in *iplA*$^-$ cells. Therefore, capacitative Ca^{2+}-entry appears to be fully operative in this mutant (Schaloske *et al*., 2005).

1.2.9.3. Polycystin-2-like protein

Polycystin-2-like protein (DDB_G0272999) is a putative Ca^{2+} channel (PFAM), similar to metazoan polycystin-2 (PKD2) proteins and polycystin-like (PKD2L) proteins, and consists of 6 putative transmembrane regions. The function and localization of polycystin-2 in *Dictyostelium* is unknown.

1.2.9.4. P2X receptors

Purinergic receptors are a large family of plasma membrane proteins, to which P1, P2Y and P2X receptors belong. P2X receptors are ligand-gated cation channels that respond to the binding of extracellular adenosine 5'-triphosphate (ATP). In *Dictyostelium*, five *p2xA-E* -like genes were recently identified. *Dd*P2XA, expressed in HEK cells and localized predominantly to the plasma membrane, has been characterized as an ATP-gated cation channel (Fountain *et al*., 2007). In addition, *Dictyostelium* P2X receptors have been shown to facilitate Ca^{2+} influx mediated by

extracellular ATP and ADP in HEK cells. ATP also induces Ca^{2+} influx in *Dictyostelium* (Ludlow *et al*., 2008). However, this response remains intact in strains in which all five potential P2X receptors have been disrupted (Ludlow *et al.,* 2009). Furthermore, all five endogenous P2X proteins show an intracellular localization, being present exclusively on the contractile vacuole, suggesting an involvement of P2X receptors in osmoregulation (Fountain *et al*., 2007; Ludlow *et al*., 2009) and possibly Ca^{2+} release.

1.2.9.5. Mucolipin

Mucolipin (DDB_G029175) is a putative Ca^{2+} channel consisting of 6 predicted transmembrane domains and a Ca^{2+}-binding EF-hand. In *Dictyostelium*, a mucolipin null strain has been generated (personal communication to Professor Cosson). This mutant appeares to have endosomes of normal structure and composition, and wild-type pH values for both lysosomal and post-lysosomal vacuoles (by which undigested endocytosed material is returned to the cell surface) compartments; however, lysosome exocytosis was substantially increased, and post-lysosomal Ca^{2+} concentration was significantly lower in mucolipin null cells compared to wild type cells (Lima WC and Cosson P, meeting abstract; *Annual International Dictyostelium Conference, 2010*).

1.2.9.6. Two-pore channel-2 (TPC2)

Dictyostelium has one predicted gene encoding a potential TPC2 protein, *tpc2* (DDB_G0289105) (Wilczynska *et al*., 2005). The putative *Ddtpc2* is an orthologue of human *tpc2* (*Hstpc2*) and mouse *tpc2* (*Mmtpc2*). The gene product of *Ddtpc2*

consists of 2060 amino acids and includes about 400- and 1200-amino acid extensions at the N- and C-terminal sides respectively, compared to TPC2s of other species (Calcraft *et al*., 2009).

1.2.10. *Dictyostelium* as a model system for studying TPC2

There are several advantages to the use of *Dictyostelium* as a model system for studying the role of TPCs in Ca^{2+} signalling. First, *Dictyostelium* has only a single gene encoding TPC2 and no genes encoding other forms of TPC, so generation of a knockout strain is potentially straightforward. Second, a strain in which the single gene encoding an IP_3-like receptor has been knocked out (*iplA*$^-$) is available. *Dictyostelium* has only one gene coding for a protein with high homology to the IP_3R and no potential RyRs (Wilczynska *et al*., 2005). Therefore, this *iplA*$^-$ strain, which aggregates and develops normally without the IP_3-like receptor, has limited mechanisms for generation of calcium transients through release of Ca^{2+} from intracellular organelles - possibly only via the TPC2 (Traynor *et al*., 2000). In addition, it is easy to grow large numbers of cells for pharmacological and biochemical analysis. Therefore, *Dictyostelium* was chosen as a suitable model system for the current study.

CHAPTER 2

MATERIALS AND METHODS

2.1. Cell lines and consumables

Details of the solutions, cell lines, kits, IMAGE clones, primers and chemicals used in this thesis are listed in the *Appendices*.

2.2. Molecular and biochemical techniques

2.2.1. DNA manipulations

Polymerase chain reaction (PCR) is a scientific technique in molecular biology developed by Kary Mullis in 1983 and used for amplifying DNA (Mullis, 1993). PCR was used in the experiments described in *Chapter 3* and *Chapter 4* of this thesis. The PCR steps utilized are described in Tables 5 - 7.

Other genetic engineering techniques, for instance, restriction enzyme digests, phosphatase reactions, phenol/chloroform extractions, ligations, agarose gel electrophoresis and precipitation of DNA with ethanol or sodium acetate, were all carried out using standard procedures or as recommended by the reagent manufacturer (Sambrook and Russell, 2001).

2.2.2. Competent cells

2.2.2.1. Competent cells ($CaCl_2$ method)

A single colony of *Escherichia coli* (*E. coli*), either the Top10 (Invitrogen Limited, Paisley, UK) or XL-10 (obtained from Stratagene, Cheshire, UK) strain was inoculated in 5 ml Lysogeny Broth (LB) medium for 2 - 3 h with vigorous shaking.

Table 5. PCR protocol

PCR protocol for amplification of *Hs*TPCs and *Sp*TPCs. Expand Long Range dNTPack was obtained from Roche Applied Science, Roche Diagnostics Limited, West Sussex, UK (Catalogue Number 04 829 034 001).

PCR Steps	Temperature (ºC)	Time (sec/min)	Number of cycles required
Denaturation (RT Inactivation)	92	2 min	
Denaturation	92	10 sec	
Annealing	55-65	15 sec	
Elongation	72	2 min/kbp	9
Denaturation	92	10 sec	
Annealing	55-65	15 sec	
Extension	72	6 min + 20 sec/cycle	20
Final extension	72	10 min	
Hold	4		

Table 6. PCR protocol for Bacmid DNA amplification

The Taq polymerase used in this study was obtained from Sigma-Aldrich Co. Limited, Poole, UK (Catalogue Number D4545).

PCR Steps	Temperature (ºC)	Time (sec/min)	Number of cycles required
Denaturation (RT Inactivation)	95	2 min	
Denaturation	95	30 sec	
Annealing	55	45 sec	
Extension	68	10 min	35
Final extension	72	10 min	
Hold	4		

Table 7. PCR protocol for *Dictyostelium discoideum*

The Taq polymerase used in this study was obtained from Sigma-Aldrich Co. Limited, Poole, UK (Catalogue Number D4545).

PCR Steps	Temperature (ºC)	Time (sec/min)	Number of cycles required
Denaturation (RT Inactivation)	93	3 min	
Denaturation	94	45 sec	
Annealing	45-60	45 sec	
Elongation	70	3 min/kbp	35-38
Final extension	72	10 min	
Hold	4		

(~300 rpm) at 37°C, then transferred into 200 ml LB medium (see *Appendix 1*) until it reached an optical density (OD) measurement of 0.4 - 0.6 at an absorbance wavelength of 600 nm (A_{600}). Cells were chilled on ice for 15 min and centrifuged at 4000 rpm for 10 min at 4°C. The cell pellet was resuspended in 50 ml of ice cold 0.1 M $CaCl_2$, by gentle mixing, and left on ice for 15 min. Cells were centrifuged at 4000 rpm for 10 min at 4°C, and the pellet was resuspended in 4 ml of sterile ice cold $CaCl_2$ and 15% glycerol (1:1). Competent cells were left in a cold room on ice overnight and 100 µl aliquots of competent cells were stored at -80°C.

2.2.2.2. High efficiency chemically competent cells

E. coli (Invitrogen), that were grown in 50 ml of LB medium (see *Appendix 1)* to an OD A_{600} of between 0.4 and 0.6, were placed on ice for 10 - 15 min and centrifuged at 4000 rpm for 10 min at 6°C. The pellet was resuspended in 25 ml of ice cold Transformation Buffer I (TBFI; see *Appendix 1*) and centrifuged at 4000 rpm for 10 min at 6°C. The pellet was resuspended in 2 ml of ice-cold Transformation Buffer II (TBFII; see *Appendix 1*) and 50 µl aliquots were stored at -80°C immediately.

2.2.3. Transformation

Ligated plasmid (5 µl of a ligation mixture containing approximately 100 ng of linearized, dephosphorylated plasmid vector DNA plus 300 ng insert DNA, if the vector and insert DNA were approximately the same length) or 100 ng of super-coiled plasmid was incubated with 50 µl of competent cells on ice for 30 min. Heat shock was carried out in a water bath at 42°C for 30 - 40 s and cells were immediately cooled down on ice for 2 min. 200 µl - 500 µl of Super Optimal Broth with

Catabolite Repression (SOC medium, containing 20 mM glucose; Invitrogen) was added to allow the *E. coli* to recover, and this was shaken (250 rpm) at 37°C for 1 h before being spread onto an LB plate containing appropriate antibiotics (100 μg/ml ampicillin or 50 μg/ml kanamycin) for selection.

Blue-white colour screening

40 μl of 0.1 M IPTG (isopropyl β-D-1-thiogalactopyranoside; Sigma-Aldrich Co. Limited, Poole, UK) and 40 μl of 20 mg/ml X-gal (5-bromo-4-chloro-3-indolyl-beta-D-galacto-pyranoside; Fermentas, St. Leon-Rot, Germany) were spread on solidified LB agar plates, 30 min prior to plating the transformations.

2.2.4. Primers and sequencing

Primers were synthesized by Invitrogen Limited. Sequencing was performed either by the Oxford Biochemistry Department Sequencing Laboratory, on an ABI PRISM 377 automated DNA sequencer (Applied Biosystems, Life Technologies Limited, Paisley, UK) using ABI Big-Dye terminators and the Taq-FS enzyme kit (PerkinElmer, Cambridge, UK), or by GATC Biotech (Konstanz, Germany). Sequence data received were analyzed using 4Peaks software V1.7.2 (Mekentosj.com software, Amsterdam, The Netherlands).

2.2.5. Quantification of DNA / RNA

DNA or RNA concentration was calculated using a spectrophotometer (GeneQuant pro; GE Healthcare Limited, Little Chalfont, UK) or NanoDrop (Thermo Scientific,

Cramlington, UK), measuring the intensity of absorbance of the DNA or RNA solution at a wavelength of 260 nm. The ratio of absorbance at 260 nm and 280 nm was used to assess the purity of DNA and RNA. A ratio of ~1.8 is generally accepted as 'pure' for DNA; a ratio of ~2.0 is generally accepted as 'pure' for RNA.

2.3. Protein analysis

2.3.1. Quantifying protein concentration

2.3.1.1. UV methods

The absorbance of the protein solution was measured at 280 nm and 260 nm using a GeneQuantpro spectrophotometer. The approximate concentration of the protein in the solution was calculated using the equation below, which is appropriate for protein solutions potentially contaminated with nucleic acids:

$$\text{Protein concentration (mg/ml)} = (1.55 \times A_{280}) - (0.76 \times A_{260})$$

2.3.1.2. BCA protein assay

Protein concentrations were determined spectrophotometrically using a bicinchoninic acid (BCA) assay kit according to the manufacturer's instructions (Pierce BCA Protein Assay Kit, Thermo Scientific). Absorbance at a wavelength of 595 nm was measured using a SUNRISE Absorbance Reader (Tecan Group Limited, Männedorf, Switzerland).

2.3.2. SDS-polyacrylamide gel electrophoresis and Western blot analysis

Whole cell lysate or membranes were resuspended in 4x Laemmli Loading Buffer (see *Appendix 1*). Samples were loaded into each well of an SDS-PAGE (sodium dodecyl sulphate polyacrylamide gel electrophoresis) gel alongside a pre-stained molecular marker (Fermentas; PageRulerPlus prestained protein ladder SM1811) and separated by electrophoresis. Protein was transferred to polyvinylidene fluoride (PVDF) membranes (Millipore Limited, Livingston, UK) pre-soaked in methanol, using a current of 250 mA for 2 - 3 h. PVDF membranes were incubated in Blocking Buffer (Tris-buffered saline, TBS, containing 0.2% Tween-20 and 5% non-fat dried milk; see *Appendix 1*) for 1 h at room temperature, or overnight at 4°C.

The membranes were then incubated with the primary antibodies at appropriate dilutions in Blocking Buffer for 1 - 5 h at room temperature, or overnight at 4°C, followed by five 10 min washes in Washing Buffer (TBS buffer containing 0.2% Tween-20; see *Appendix 1*). The membranes were incubated with relevant horseradish peroxidase (HRP)-conjugated secondary antibodies in Blocking Buffer, following the instructions provided by the supplier, for 1 h at room temperature. After three 20 min washing periods, the membranes were incubated in chemiluminescent detection reagent (see *Appendix 1*) and the light emission was captured using an autoradiography film (Kodak Limited, Hemel Hempstead, UK). Please refer to Table 8 for a list of antibodies used for Western blot experiments.

Stripping

Membranes were rinsed with Washing Buffer and incubated in Stripping Buffer (see *Appendix 1*) for 30 min at 50°C, in a rotating mixer.

Table 8. Antibodies used for Western blot experiments

Antibody	Manufacturer	Catalogue number	Dilution	Other information
α-mCherry (multi-Red 5F8)	Gift from Professor Heinrich Leonhardt	LMU Munich Biocenter	1:1000 in 5% Milk (HEK cells) 1:100 in 0.5% (*Dictyostelium*)	Rat monoclonal
α-HA High Affinity	Roche	11 867 423 001	50 ng/ml	Rat monoclonal
α-His_6-peroxidase	Roche	11 965 085 001	1:50/1:100	Mouse monoclonal HRP conjugated
α-polyhistidine	Sigma-Aldrich	H1029	1:3000	Mouse monoclonal
α-GFP (FL)	Santa Cruz Biotechnology	sc-8334	1:200	Rabbit polyclonal
α-actin (C-11)	Santa Cruz Biotechnology	sc-1615	1:1000	Rabbit polyclonal
α-GST	Sigma-Aldrich	G1160	1:5000	Mouse monoclonal
α-Ku	Dr Nick Lakin	Biochemistry Oxford	1:2000	Goat polyclonal / serum
α-goat IgG	DAKO	P0160	1:1000/1:2000	HRP conjugated
α-mouse IgG	DAKO	P0161	1:1000	HRP conjugated
α-rabbit IgG	DAKO	P0217	1:1000/1:20000	HRP conjugated
α-rat IgG	DAKO	P0450	1:1000/1:10000	HRP conjugated

2.4. Microscopy

2.4.1. Fluorescence microscopy

Fluorescence microscopy is capable of imaging the distribution of an intracellular component (such as a protein) labelled with specific fluorophores. This is most commonly achieved using fluorescently labelled molecules that can subsequently be detected specifically. The technique is based on the fluorescence emitted from electronically excited states of the fluorophores. The fluorophore contains electrons that can enter an excited state when a photon ('excitation light') is absorbed; this energy can be subsequently emitted as a photon with lower energy (higher wavelength), generating emitted fluorescence that may be detected with suitable detectors.

Imaging was carried out using an Olympus IX71 fluorescence microscope with a 100x oil immersion objective (numerical aperture, 1.40) (see *Chapter 4*). Excitation light was provided by a halogen lamp (in a lamphouse mounted to the top port of the microscope) and appropriate excitation filters individually selected as required. Emitted fluorescence was reflected through the side port of the microscope and collected using a camera (Hamamatsu Photonics; C10600). Images were analyzed using HCImage software.

2.4.2. Laser scanning confocal microscopy

Confocal microscopy is capable of isolating and collecting a plane of focus from within a sample, eliminating the out of focus information, and hence allowing the

capturing of fine details. This property is conferred by the presence of two pinholes (one in the excitation path and one in the emission path); each pinhole lies exactly the same distance from the object in focus, and together act to block any scattered light from the planes above and below that desired to be viewed.

For these experiments, primary antibody staining was visualized with Alexa Fluor-labelled secondary antibodies (Invitrogen), and cells were viewed on a Zeiss 510 META confocal microscope with a 63x oil immersion objective (NA 1.4), in multitrack mode to reduce bleed-through, using the following excitation/emission parameters (nm): Alexa 488 (488 / 505-530) for GFP (green fluorescent protein) and Alexa 546 (543 / > 560) for mRFPmars (see *Chapter 3)*. This system has a high spatial resolution, producing scanned images up to 1024 x 1024 pixels.

2.5. [^{32}P]NAADP experiments

Protocols were adapted from *Calcium Signaling: Methods in Signal Transduction* (Putney JW, second edition, 2005).

2.5.1. [^{32}P]NAADP synthesis

[^{32}P]NAADP was synthesized in a two-step reaction as previously described (Lewis *et al.*, 2007). In the first step, 8.06 μM [^{32}P]NAD (GE Healthcare Limited or PerkinElmer) was phosphorylated and converted to [^{32}P]NADP using 0.5 U/ml human NAD kinase (Alexis Biochemicals, Enzo Life Sciences Limited, Exeter, UK; ALX-201-236) in a reaction mixture containing 5 mM Mg^{2+}-ATP and 100 mM HEPES (pH 7.2); the reaction proceeded for 3 h at room temperature. In the second step,

[^{32}P]NADP was converted to [^{32}P]NAADP via the base-exchange reaction. Final concentrations of 100 mM nicotinic acid (pH 4.4) and 1 µg/ml ADP-ribosyl cyclase (kindly provided by Prof H.C. Lee, University of Hong Kong, Hong Kong) were added to the previous mixture, and the second reaction was carried out at room temperature for 1 - 2 h.

Alternatively, in the first step, NAD in the phosphorylation buffer was converted to [^{32}P]NADP by human NAD kinase (a phosphorylation reaction) using [^{32}P]ATP (PerkinElmer; NEG002A500UC); the reaction was carried out at 37°C for 2 h.

2.5.2. High-performance liquid chromatography (HPLC)

Anion exchange HPLC was used routinely to separate and purify synthesized compounds (Lewis *et al.*, 2007). Synthesized [^{32}P]NAADP was loaded onto an anion exchange column (AGMP-1; Bio-Rad, Hemel Hempstead, UK) and separated using a trifluoroacetic acid (TFA) gradient (0 - 100%). A radioactivity detector (LabLogic Systems Limited, Sheffield, UK) was used to detect the radioligand and [^{32}P]NAADP was collected in 1.5 ml eppendorf tubes containing 20 µl of 1 M HEPES (pH 8.0), to neutralize the eluent immediately. Purified [^{32}P]NAADP was stored at 4°C.

2.6. Sea urchin (Lytechinus pictus)

Protocols were adapted from *Calcium Signalling: Methods in Signal Transduction* (Putney JW, second edition, 2005).

2.6.1. Collection of sea urchin eggs

Sea urchins were purchased from Marinus Inc. (Long Beach, California, USA). Ovulation was induced by stimulating female sea urchins with an intracoelomic injection of 0.5 M KCl solution (up to 0.5 ml total volume) through the peristomal membrane surrounding the mouth. Eggs were collected in Ca^{2+}-free artificial seawater (Ca^{2+}-free ASW; see *Appendix 1*).

2.6.2. Preparation of sea urchin egg homogenate (50% v/v)

The jelly coat surrounding the egg was removed by filtering through 90 μm nylon mesh (Plastok Associates Limited, Merseyside, UK) and centrifuged at 300g for 1 min at 4°C. The dejellied eggs were immediately washed in 10 times their volume of ASW (see *Appendix 1*) and centrifuged at 800g for 15 min at 4°C. The washing steps were repeated twice in Ca^{2+}-free ASW, supplemented with 1 mM of the Ca^{2+} chelator ethylene glycol tetra-acetic acid (EGTA), and twice in Ca^{2+}-free ASW. The final washing step was carried out in GluIM (an intracellular medium; see *Appendix 1*) and homogenized in an equal volume of GluIM containing 2 mM ATP, 20 U/ml creatine phosphokinase, 20 mM phosphocreatine, and cOmplete EDTA-free protease inhibitor cocktail tablets (Roche, West Sussex, UK), using a dounce glass tissue homogenizer (pre-chilled on ice); homogenization was achieved with a tight pestle, size 'A', after approximately 6 strokes (the resistance increased significantly when DNA was released). Cortical granules were removed and discarded by centrifugation at 13,000g for 8 seconds at 4°C. Homogenates were stored as 0.5 ml aliquots at -80°C.

2.6.3. Microsome preparation

Resuspension of 310 µl of the 50% egg homogenate was carried out in 6250 µl GluIM supplemented with cOmplete EDTA-free protease inhibitor cocktail tablets (Roche) and centrifuged at 10,000g for 10 min. Subsequently, the supernatant was centrifuged at 100,000g for 1 h. The pellet was resuspended in GluIM, to which the proteinase inhibitor (cOmplete EDTA-free protease inhibitor cocktail tablets) was freshly added. All procedures were carried out at 4°C.

2.6.4. Binding assays

Incubation of 250 µg of microsomes in the presence or absence of unlabelled NAADP took place for 20 min at room temperature prior to incubation with 0.2 nM [^{32}P]NAADP for 1 h in GluIM at room temperature. For the competitive binding assay, various concentrations of unlabelled NAADP (10 pM – 1 mM) were made in either GluIM or sea urchin egg standard buffer (GluIM: 1.5 M $HClO_4$: 2M $KHCO_3$ at a ratio by volume of 1:1:2). The reactions were terminated by rapid filtration through Whatman GF-B filters (Whatman, Banbury, UK) using ice-cold GluIM, and bound radiolabel was quantified by either liquid scintillation counting, or a phosphor screen (Amersham Biosciences, GE Healthcare). The screen was then scanned using a Typhoon 9400 Phosphor Imager (GE Healthcare) at a resolution of 100 µm. The resulting image was analyzed using ImageQuant software (GE Healthcare).

2.6.5. Calcium uptake experiments

0.5 ml of Regeneration Medium (see *Appendix 1*) was added to the defrosted egg homogenate (50% v/v) and placed in a water bath at 17.3°C for 30 min. 1 ml of

Regeneration Medium was added and incubated for another 30 min, before an additional 3 ml of Regeneration Medium was added and incubated for a further 45 min. Finally, 5 ml of Regeneration Medium was added and incubated for at least 90 min (ideally, 2 - 3 h).

2.7. Mammalian cells

2.7.1. Cell culture

HEK293/HEK293T cells (human embryonic kidney cells) and HeLa cells (cervical cancer cells) were maintained in HEK Culture Medium, which consisted of Dulbecco's Modified Eagle's Medium (DMEM; Sigma-Aldrich Co. Limited) supplemented with 10% (v/v) fetal bovine serum (FBS; Invitrogen), 100 units/ml penicillin (Invitrogen), 100 µg/ml streptomycin (Invitrogen) and 2 mM L-glutamine (Invitrogen). The origin of these cell lines is listed in *Appendix 2.1*. Cells were grown in 25, 100 or 175 cm^3 flasks between 30% and 80% confluence at 37°C in a humidified culture incubator supplied with 5% (v/v) CO_2.

After reaching 80 - 90% confluency, cells were trypsinized using 0.05% trypsin (EDTA free; Invitrogen) at 37°C for 3 min and resuspended in HEK Culture Medium before being transferred to new flasks or dishes at the desired cell density.

Cell storage

Trypsinized mammalian cells from 100 cm^3 flasks were centrifuged at 1000 rpm for 5 min and the pellet was rinsed with HEK Culture Medium once or twice. Cells were

resuspended in 900 µl FBS, and the same volume of FBS supplemented with 10% DMSO (dimethyl sulfoxide; Sigma-Aldrich Co. Limited) was gently added. The vials were stored in an isopropanol box at -80°C overnight and then transferred to liquid nitrogen for storage.

2.7.2. Transfection for immunohistochemistry experiments

Transfection was carried out using either Lipofectamine 2000 transfection reagent (Invitrogen; 11668-027) or jetPEI (Polyplus-Transfection SA, Strasbourg, France), following the manufacturer's instructions.

HEK293 cells were plated on sterilized cover slips, coated with poly-D lysine (Sigma-Aldrich Co. Limited; P6407), whereas HeLa cells were placed directly onto cover slips at a cell density of 0.5 x 10^5 cells/ml in HEK Culture Medium not containing antibiotics, 12 h before the transfection.

2.7.3. Immunohistochemistry

24 - 48 h after the transfection, cells were washed with phosphate-buffered saline (PBS; Oxoid, Hampshire, UK) once, and fixed with 4% paraformaldehyde (Sigma-Aldrich Co. Limited) for no more than 20 min, then washed with PBS 3 times. The fixed samples could be kept at 4°C for up to 1 week in PBS. Fixed cells were permeabilized with 0.2% Triton X-100 for 10 min and washed with PBS briefly, followed by blocking with 5% or 10% serum, in which the secondary antibody was raised, in PBS for at least 30 min. Cells were again washed with PBS with 0.1% Triton X-100 3 more times prior to being incubated with appropriate antibody in

Blocking Buffer (0.5% - 10%). These blocking and antibody incubation steps were repeated for experiments requiring double staining, and then the nuclei were stained with 10 μg/ml Hoechst 33342 (Invitrogen) in PBS for 10 min. Following 3 further washes, the cover slips were mounted onto microscope slides using either Prolong Gold (Invitrogen) or Vectorshield containing DAPI (4', 6-diamidino-2-phenylindole; Vector Laboratories Limited, Peterborough, UK), a fluorescent marker that binds strongly to A-T rich regions in DNA. Slides were dried at room temperature overnight and imaged using a confocal microscope (Zeiss 510 META) or a fluorescence microscope (Olympus, IX71). The antibodies used are listed in Table 8. The percentage of serum in the Blocking Buffer varied (0.5% - 5%) depending on the quality of the primary antibody. A list of antibodies used for immunohistochemistry is shown in Table 9.

2.7.4. Transfection: calcium phosphate method

900 μl DNA (50 μg) was mixed with 100 μl 2.5 M $CaCl_2$ and this was transferred to 1000 μl 2x HBS (see *Appendix 1*) drop by drop, and immediately mixed by vortexing. The DNA mixture was incubated at room temperature for 30 min and then added to the cells in a 14 cm dish, drop by drop. The medium was changed 2 h before and about 20 h after the transfection.

2.7.5. Whole cell lysate (sonication)

HEK293 cells were harvested by centrifugation at 1500g for 10 min at 10°C, washed with PBS once and resuspended in a minimal amount of PBS on ice, followed by sonication using Vibra-cell (Sonics and Materials Inc., Connecticut, USA) with a

Table 9. Antibodies and reagents used for immunohistochemistry experiments

Antibody / reagent	Manufacturer	Catalogue number	Dilution	Other information
α-HA	Roche	11 867 423 001	100 ng/ml	Rat monoclonal
α-LAMP2 (H4B4)	Santa Cruz Biotechnology	Sc-18822	1:50	Mouse monoclonal
α-GM-130	BD Transduction Laboratories	610822	1:50	Mouse monoclonal
α-Cytochrome c	Invitrogen	33-8200	1:50	Mouse monoclonal
α-PDI (RL90)	Abcam	Ab2792	1:2000	Mouse monoclonal
α-transferrin receptor	Invitrogen	236-15375	1:50 - 1:200	Mouse monoclonal
α-rat 488	Invitrogen	A11006	5 µg/ml	Goat anti-rat IgG
α-mouse 488	Invitrogen	A31619	5 µg/ml	Goat anti-mouse IgG
α-mouse 546	Invitrogen	A11003	5 µg/ml	Goat anti-mouse IgG
ProLong Gold	Invitrogen	P36934		Anti-fade mounting reagents
Vectorshield	Vector Laboratories	H-1200		

probe (630-0422 P) pulsing for 5 sec at 20 sec intervals on ice. The breakage of cells was examined after 5 min, and an average of 20 min of sonication was required. Homogenate was divided as 3.3 ml aliquots into tubes and stored at -80°C

2.7.6. Membrane preparation

2.7.6.1. Membrane preparation using homogenization

HEK293 cells that were grown in 15 cm dishes were washed with ice-cold PBS once and scraped into PBS, and this was centrifuged at 1500g for 3 min. The pellet was resuspended in 2 ml of hypotonic buffer per plate and incubated on ice for 30 min, then homogenized with a dounce glass tissue homogenizer (loose fitting pestle) using 15 strokes. Homogenate was centrifuged at 1500g for 3 min in order to remove the nuclei and unbroken cells, and the supernatant was centrifuged at 100,000g for 1 h at 4°C. Subsequently, the pellet was washed with fresh Hypotonic Buffer (see *Appendix 1*) and centrifuged again at the same speed. The pellet was resuspended in as little volume as possible of fresh Hypotonic Buffer and aliquots were frozen in liquid nitrogen. Samples were stored at -80°C.

2.7.6.2. Membrane preparation using solubilization

Harvested cells were solubilized with 1% CHAPS (3-[(3-cholamidopropyl) dimethylammonio]-1-propanesulfonate; Sigma-Aldrich Co. Limited) or Lysis Buffer (Sigma-Aldrich Co. Limited; Nonidet P – 40), left on ice for 1 h, and then centrifuged at 15,000g for 30 min. The supernatant was analyzed by Western blotting after determining the protein concentration using BCA reagent.

2.7.7. NAADP binding

The binding assay was carried out as in sea urchin egg homogenate. Whole cell homogenate or membranes were incubated with 100 μM unlabelled NAADP for 20 min, followed by incubation with [^{32}P]NAADP for 1 h at room temperature. The binding reaction was terminated by quick filtration. GluIM was used as the binding and washing buffer for experiments involving *Sp*TPCs expressed in HEK293 cells.

2.8. Spodoptera frugiperda (Sf9) cells

2.8.1. Cell culture

Sf9 cells (obtained from Dr Cohn, Department of Biochemistry, Oxford) were maintained either as suspension cultures in 100, 250 or 500 ml glass flasks filled to one fifth of their capacity with medium, or as monolayer cultures in 3.4, 9 or 14 cm dishes at 27°C. Cells were adapted to serum-free medium (Sf900-II SFM; GIBCO, Invitrogen Limited) without any supplements. In suspension cultures, cells were cultivated in shaken cultures with the aid of an orbital shaker platform. The cell density was maintained between 1.0 to 5.0 x 10^6 cells/ml and the lids of flasks kept loose to ensure an adequate air supply. The ratio of existing culture in dishes to fresh medium was not greater than 1 to 5, and seeding densities in flasks were not lower than 1.0 x 10^6 cells/ml in a 100 ml flask and 1.5 to 2 x 10^6 cells/ml in a 500 ml flask, respectively. Detergent was not used for washing flasks.

Cell storage

3 x 10^7 cells were harvested at ~500g for 4 min and resuspended in 500 µl medium, and 500 µl of medium containing 10% DMSO was added gently. Cells were cooled down in an isopropanol box in a -80°C freezer overnight and transferred to liquid nitrogen. Frozen cells were thawed in a water bath at 27°C, immediately resuspended in 10 ml medium and put back in suspension culture.

2.8.2. Co-transfection of transfer vector DNA and bacmid DNA

pFastHT.A.TPC constructs were transformed into DH10bac *E. coli* for transposition into the bacmid. Successful transformants were selected on LB agar plates containing 50 µg/ml kanamycin (Sigma-Aldrich Co. Limited), 7 µg/ml gentamicin (Sigma-Aldrich Co. Limited), 10 µg/ml tetracycline, 100 µg/ml bluo-gal (Fermentas) and 40 µg/ml IPTG (Sigma-Aldrich Co. Limited).

2.8.3. Producing recombinant baculovirus

9 x 10^5 cells in 2 ml of the transfection buffer, in a 6-well plate, were transfected with bacmid DNA using either Lipofectamine 2000 (Invitrogen) or jetPEI (Polyplus-Transfection SA) following the manufacturer's instructions. For the former, 1 µg of purified bacmid DNA was suspended in 100 µl of unsupplemented Grace's medium (Invitrogen) and mixed with 6 µl Lipofectamine 2000 in 100 µl of unsupplemented Grace's medium. Diluted bacmid DNA was combined with the diluted Lipofectamine 2000, and incubated for 45 min at room temperature. Sf9 cells were washed once with 2 ml of unsupplemented Grace's medium, and 0.8 ml of Grace's medium was added before the DNA complex was subsequently added, drop-wise, to

the cell monolayer. 48 h after transfection, a few cells were enlarged; 72 h after transfection, it was observed that some cells started to break down.

2.8.4. Test for gene expression

96 h after the initial transfection, supernatant (P1) was taken for further virus amplification, the remaining cells were lysed with 2x SDS Sample Buffer (see *Appendix 1*) and the expression level of recombinant protein was examined by Western blotting.

2.8.5. Infecting cells to amplify further stocks of recombinant virus

Supernatant, obtained from the primary infection (P1), was transferred to a cell monolayer at a density of 1.0 x 10^6 cells in a 6-well plate, at a 1 in 10 dilution, and 4 days later supernatant was collected (P2). Diluted P2 (1 in 10 dilution) was added to the cell monolayer at a density of 8.0 x 10^6 cells per 9 cm dish, and supernatant (P3) was collected 4 days later. Finally, 1.6 x 10^7 cells per 14 cm dish were infected with P3 at a dilution of 1 in 10 and incubated for 5 - 7 days to obtain large-scale virus stock. Supernatant (P4) was kept at 4°C in the short term to enable further experimental work on a large scale.

2.8.6. Extraction of recombinant protein by solubilization

2 - 3 days after infection, Sf9 cells expressing recombinant protein were harvested at 500g for 3 min and resuspended in Sf9 Lysis Buffer or MAC buffer (see *Appendix 1*). After incubation for 1 h on ice, cells were centrifuged at 15000g for 15 min, and this

was followed by purification. CHAPS at a final concentration of ~2% was added before centrifugation.

2.8.7. Membrane preparation for binding assay (homogenate)

2 - 3 days after the infection, Sf9 cells (100 ml at 2 to 3 x 10^6 cells/ml) expressing recombinant protein were harvested by centrifugation at 500g for 3 min and washed with 50 ml PBS once, then resuspended in 20 ml Hypotonic Buffer (see *Appendix 1*) and incubated for 30 min, and this was followed by homogenization, on ice, using a Dounce glass tissue homogenizer with a tight pestle. After about 20 strokes, the breakage of cells was examined under a light microscope. Additional strokes were carried out if required. The homogenate was centrifuged at 500g for 3 min to remove unbroken cells and nuclei and then centrifuged at 1000g for 1 h. The supernatant was centrifuged at 100,000g for 1 h, then the final pellet was re-suspended in a small amount (approximately 500 μl) of Hypotonic Buffer, and aliquots snap frozen in liquid nitrogen and stored at -80°C.

2.8.8. Binding assay

250 μg of membrane prepared from Sf9 cells, expressing His-tagged fusions of *Sp*TPC1, *Hs*TPC1 and *Hs*TPC2, was resuspended in Binding Buffer (see *Appendix 1*). Whole cell homogenate or membranes were incubated with 1 mM unlabelled NAADP in Binding Buffer (20 mM Hepes, 140 mM K^+ acetate; pH 7.2) for 20 min, followed by incubation with [^{32}P]NAADP for 1 h at room temperature. The reaction was terminated by quick filtration using ice-cold Washing Buffer (20 mM HEPES; pH 7.2).

2.8.9. Purification of His fusion proteins

Membrane, prepared from solubilized Sf9 cells expressing His-tagged recombinant proteins, was purified using either HisPur™ Cobalt Resin (Pierce, Thermo Scientific) or HisTrap HP (GE Healthcare) following the manufacturer's instructions.

2.8.9.1. HisPur™ Cobalt Resin

Solubilized membrane protein was resuspended in Washing Buffer containing 10 mM imidazole (2 mM and 5 mM was also tested) and mixed with cobalt resin on an end-over-end rotator for 30 min at room temperature. The sample was centrifuged at 700g for 2 min and protein-resin complex was washed with Washing Buffer 5 times. Bound protein was eluted with Elution Buffer (see *Appendix 1*) containing different concentrations of imidazole from 20 mM to 1 M.

2.8.9.2. HisTrap HP

Homogenized Sf9 cells expressing His-tagged proteins were centrifuged at 500g for 4 min to remove unbroken cells and then at 1000g for 15 min, at 4°C. The pellet was resuspended in Binding Buffer (see *Appendix 1*) containing 20 mM imidazole and loaded onto a HisTrap column (GE Healthcare) using a screw type syringe, and unbound protein was washed out using Washing Buffer (see *Appendix 1*). Bound protein was eluted by 500 µl of Elution Buffer (see *Appendix 1*) containing different concentrations of imidazole ranging from 40 mM to 1 M. Samples and column were kept on ice throughout the procedure, and purification efficiency was immediately examined by Western dot blotting using samples taken at each step.

2.9. Dictyostelium discoideum

2.9.1. Cell culture

2.9.1.1. Axenic culture

Dictyostelium cells were grown axenically in HL5 medium (see *Appendix 1*) at 22°C in a dark room. Cells were maintained as a monolayer in 90 or 140 mm Petri dishes, or in 6, 24 or 96-well plates under an appropriate volume of HL5 medium. Cultures were transferred to fresh Petri dishes every 2 – 3 days. Alternatively, cells were shaken in 100, 250 or 500 ml glass flasks filled to one-fifth of their capacity with HL5 medium. Flasks were shaken in a darkened incubator (180 rpm) at 22°C. For experimental purposes, cells were harvested during the exponential phase of growth (i.e. 2 to 6 x 10^6 cells/ml).

2.9.1.2. Genetically modified cell lines

Ax2 cells were transformed with plasmid vectors designated to confer resistance to the antibiotics blasticidin S (BS) or geneticin (G418). Blasticidin-resistant strains (bsR) were selected for and maintained in HL5 medium containing 10 μg/ml BS (Sutoh, 1993). G418 resistant strains (neoR) were selected for by using 10 - 50 μg/ml G418 (Nellen *et al*., 1984). Mutant cell lines, which had DH1 as a parent, were maintained as a monolayer in 90 or 140 mm Petri dishes.

2.9.1.3. Liquid nitrogen stocks

Cells were frozen and stored under liquid nitrogen for long-term storage.

2 to 5 x 10^7 cells per vial (1.8 ml), or a loopful of growing edge from a bacterial plate (*Klebsiella aerogenes)* were resuspended in 0.9 ml HL5 medium containing 50% horse serum (Oxoid), and added gently, to 0.9 ml HL5 medium containing 50% horse serum and 10% DMSO. Vials were inverted a couple of times, kept on ice for 5 - 10 min and incubated at -20°C for 1 - 2 h before being stored at -80°C for 12 - 24 h. Cell stocks were stored in liquid nitrogen for long-term storage (storage in a -80°C freezer was an acceptable alternative).

New cultures of each cell line were initiated every 4 - 6 weeks by taking out an aliquot of stock from a -80°C storage vial (the vial was kept on dry ice to prevent thawing whilst the aliquot was withdrawn) and either placed onto an SM agar plate which was pre-spread with a lawn of *Klebsiella aerogenes*, or grown directly in HL5 medium containing 100 μg/ml penicillin-streptomycin.

2.9.2. Dictyostelium development

Developmental structures were observed using a Nikon SMZ-2B stereoscopic microscope and photographed using a Coolpix 4500 digital camera mounted on the microscope. The developmental cycle was observed in a number of ways, described below.

2.9.2.1. On black filter

3.5 mm filters (black filter, pore size 0.45 μm; Millipore Limited) were boiled in ddH_2O for 10 - 15 min. Harvested cells were washed twice with KK_2 Buffer (see *Appendix 1*), then resuspended in KK_2 Buffer and placed on filters (Ax2: 1.2 x 10^7

cells/filter; DH1: 2 x 10^7 cells/filter), and these were placed on filter paper soaked with KK_2 Buffer and drained of excess liquid.

2.9.2.2. On KK_2 agar (2%)

Harvested cells were washed with KK_2 Buffer twice and resuspended in KK_2 Buffer. Cells were placed on 2% KK_2 agar (~ 2 days old) in 6-well plates, with a cell density of 1.2 x 10^7 cells per well for Ax2 cells, and 2 x 10^7 cells per well for DH1 cells. Plates were stored in an airtight, lightproof, humid container and incubated at 22°C.

2.9.2.3. On a lawn of Klebsiella aerogenes

Axenically growing *Dictyostelium* cultures were spotted onto a lawn of *K. aerogenes* on SM agar plates (see *Appendix 1*) and incubated as above. The resultant plaques are formed when the bacterial lawn is cleared by *Dictyostelium*.

2.9.3. Transformation of *Dictyostelium* by electroporation

Cell membranes were transiently permeabilized with an electrical pulse, allowing cellular uptake of a variety of biological molecules including DNA. The following protocol is essentially that described by Howard and colleagues (Howard *et al*., 1988).

Ax2 cells were harvested during the logarithmic phase of growth, and washed twice in cold H5O buffer (*see Appendix 1*) prior to resuspension in this buffer to a density of 5 x 10^7 cells/ml. A 100 µl volume of the cell suspension was added to a 1 mm gap electroporation cuvette (Bio-Rad) containing 4 - 10 µg of linearized plasmid DNA

and 100 μM of specific primers. Linearized plasmid was purified using the phenol/chloroform method. Cells and DNA were mixed gently and incubated on ice for 5 min. Two consecutive pulses of 0.65 kV, with a capacitance of 25 μF, were applied to the cuvette with a 5 sec recovery between pulses, resulting in a time constant (TC) of 0.8 - 1.0 ms. After 5 min of incubation on ice, the cells were transferred to 50 ml HL5 medium (see *Appendix 1*). Cells were dispersed into five 96-well plates (100 μl/well) and incubated at 22°C. 100 μl HL5 medium supplemented with 20 μg/ml blasticidin was added to each well 12 - 15 h after transformation, and incubated at 22°C for around 10 days. For genetic ablation, single colonies were screened by PCR; for an extrachromosomal expression, a pool of single colonies was used directly for the assay (Howard *et al*., 1988; modified later by Pang *et al*., 1999).

2.9.4. Genomic DNA (gDNA) preparation

2.9.4.1. Crude genomic DNA preparation for PCR screening

The procedure for preparing gDNA for PCR screening was adapted from previously described methods (Charette and Cosson, 2004). Approximately 1 x 10^4 *Dictyostelium* cells were lysed in 100 μl of Lysis Buffer. Proteinase K was inactivated by heating it to 95°C for 1 min. 1 μl of the gDNA preparation was used as a template for a 50 μl PCR reaction.

Alternatively, gDNA was extracted using the GenElute^{TM} Mammalian Genomic DNA Miniprep kit (Sigma-Aldrich Co. Limited; G1N70) or Wizard®Genomic DNA Purification kit (Promega Limited, Southampton, UK; A1120). 5 x 10^6 *Dictyostelium*

cells were used, and 1 - 2 µl of gDNA was required as a template for a 25 µl PCR reaction.

2.9.4.2. Genomic DNA for Southern blotting

Dictyostelium cells (40 ml at 1 x 10^7 cells/ml) were collected by centrifugation at 3000 rpm for 3 min and washed twice with 0.2% NaCl. Harvested cells were resuspended in 40 ml NLB (10 mM MgOAc, 10 mM NaCl, 30 mM Hepes, 10% sucrose, 2% NP-40; pH 7.5) and incubated on ice for 10 min. The sample was centrifuged at 9000g for 10 min, or 4000g for 20 min, and nuclei were collected as a white pellet. The nuclear pellet was resuspended in 5 ml HMK (50 mM Hepes, 40 mM MgOAc, 20 mM KCl; pH 7.5) and SDS to a final concentration of 1% was added to lyse the nuclei, followed by the addition of NaCl at a concentration of 200 mM. The gDNA in the lysate was phenol/chloroform extracted until the aqueous phase became clear (about three times), before a final chloroform extraction was performed. The gDNA was precipitated at -20°C using 2.5 volumes of ice-cold ethanol (100%) and resuspended in water.

2.9.5. Isolation of *Dictyostelium* RNA

RNase AWAY (Fisher Scientific UK Limited, Leicestershire, UK) and double autoclaved pipette tips were used to decontaminate all solutions of RNases. 10^7 cells were washed with KK_2 Buffer twice and lysed with 1 ml of TRI reagent (Sigma-Aldrich Co. Limited) by pipetting. Samples were incubated at room temperature for 5 min to complete the dissociation of nucleoprotein complexes. 0.2 ml of chloroform was added to the lysate, which was then vortexed for 15 sec and left

at room temperature for 5 - 10 min. Samples were vortexed again before centrifugation at 12,000g for 15 min at 4°C. The colourless aqueous phase, containing RNA, was transferred to a new microcentrifuge tube containing 0.5 ml isopropanol. Samples were mixed well by inversion and incubated on ice, and this was followed by centrifugation at 12,000g for 20 min at 4°C. The precipitated RNA was washed with 1 ml of 75% ethanol in diethylpyrocarbonate (DEPC)-treated water and pelleted by centrifugation at 12,000g for 20 min at 4°C. The RNA pellet was dried in a fume hood and eluted with 50 µl of DEPC-treated water to obtain a final concentration of approximately 1 - 2 µg/µl. Aliquots of RNA were stored long term at -80°C. In the short term, samples were stored in isopropanol or ethanol at -20°C for 2 weeks.

2.9.6. cDNA (complementary DNA) synthesis

Contaminating DNA was removed from total RNA using the TURBO DNA-free kit (Ambion, Warrington, UK). Briefly, 50 µl total RNA (10 µg) in 1 x DNase buffer was mixed with 2 U TURBO DNase I at 37°C for 30 min, then 5 µl DNase inactivation beads were added. After 5 min incubation at 20°C, the DNase-bound beads were precipitated and the supernatant isolated.

RNA was reverse-transcribed using the Enhanced Avian HS RT-PCR kit (Sigma-Aldrich Co. Limited) following the manufacturer's instructions. Briefly, 1 µl of DNase-treated RNA (in a 50 µl final volume of RT-PCR reaction) was used as a template, and an RT-PCR protocol was employed as shown in Table 10.

Table 10. RT-PCR protocol for *Dictyostelium discoideum*

RT-PCR Steps	Temperature (ºC)	Time (sec/min)	Number of cycles required
First strand synthesis	42	50 min	
Denaturation (RT inactivation)	94	2 min	
Denaturation	94	15 sec	30 cycles for erkB 35-40 cycles for *Dd*TPC2
Annealing	55	30 sec	
Elongation	68	3 min/Kbp	
Final extension	68	5 min	
Hold	4		

SuperScript III First-Strand Synthesis System or SuperScript II First-Strand Synthesis System for RT-PCR (Invitrogen; 18080-051 or 11904-018) was also used, following the manufacturer's instructions.

2.9.7. Calcium release assays

2.9.7.1. Vesicle preparation

Vesicle preparation was adapted from the method of Malchow and colleagues (Malchow *et al.*, 2008). Vegetatively growing *Dictyostelium* cells (T0), 3.5 x 10^8 cells shaken in 25 ml KK_2 buffer containing 5 mM EGTA for 4 h (T4), or cells 20 h after the initiation of development on filter paper or 2% KK_2 agar (T20), were washed with ice-cold Washing Buffer (see *Appendix 1*) twice and resuspended in 4 ml of Washing Buffer. Samples were disaggregated, using 21 G and 23 G needles and then homogenized by passage through 0.2 µm nucleopore filters (Millipore Limited). Homogenate was immediately added to 4 ml of 2 x Buffer 1 (100 mM KCl, 2 mM $MgCl_2$, 6% sucrose, 2 x proteinase inhibitor; Roche). After centrifugation for 5 min at 200g in 2 ml eppendorf tubes, to remove intact cells, the supernatant was fractionated by centrifugation at 3800g for 5 min. Pellet P0 was resuspended in 30 µl/tube Buffer 2 (*see Appendix 1*). Pellet P1 was obtained by centrifugation at 12000g for 20 min, and this pellet was resuspended in 25 µl/tube of Buffer 2 (see *Appendix 1*). All procedures were carried out on ice in a cold room (4°C).

2.9.7.2. Ca^{2+} uptake

100 µl ice-cold Ca^{2+} uptake buffer, supplemented with 100 µM NaN_3, 1.5 mM ATP and 6 µg/ml oligomycin A, was aliquoted into a 96-well plate, and Ca^{2+} uptake was

initiated by adding freshly prepared vesicles (200 - 400 μg protein) to each well. Ca^{2+} uptake was monitored by detecting free ionized Ca^{2+} which was measured using 6.6 μM Fluo-3 (490 nm excitation and 535 nm emission), using a fluorometer (NovoStar, BMF Labtech Limited, Aylesbury, UK). Data are presented as the mean ± S.E.M.

2.9.8. NAADP binding assay

The NAADP binding assay was carried out using membrane fractions prepared in the same way as for the vesicle preparation. 250 μg of membrane per reaction was incubated with 1 mM, unlabelled, NAADP in Binding Buffer (see *Appendix 1*) for 40 min; 0.4 nM [^{32}P]NAADP was then added for 1 h at room temperature and the reaction terminated by quick filtration using ice-cold Washing Buffer (see *Appendix 1*).

2.9.9. Immunofluorescence

5 x 10^6 cells were placed on 11 mm coverslips coated with poly-L-lysine (Sigma-Aldrich Co. Limited) and allowed to settle for 10 - 20 min; subsequently, these were washed once with KK_2 buffer and dipped in super cold ethanol (a tray containing 100% ethanol was placed in liquid nitrogen) 3 times, before being mounted on glass slides using 24 - 30 μl of Vectorshield containing DAPI, and sealed with nail varnish. Slides were allowed to dry overnight, at room temperature in the dark, and cells were subsequently examined by fluorescence microscopy (Olympus IX71).

2.9.10. Sample preparation for Western blot analysis

5 x 10^6 cells were lysed in 50 µl of 4 x SDS loading buffer. 2 µl and 10 - 20 µl of whole cell lysate were used for dot blot analysis or Western blot analysis, respectively.

CHAPTER 3

LOCALIZATION AND NAADP BINDING ACTIVITY OF RECOMBINANT TPC PROTEINS

3.1. Introduction

Of all the established intracellular messengers known to be Ca^{2+} mobilising agents, NAADP is the most efficacious, and elicits the release of Ca^{2+} from acidic stores. However, the molecular identity of the NAADP receptor is unknown. Our group has been carrying out research to characterize NAADP signalling mechanisms, and this research has especially focused on two pore channel proteins as the most likely candidates to be the elusive NAADP receptor, mainly using the sea urchin (*Strongylocentroutus purpuratus*) system. Three isoforms of TPCs have been identified in the sea urchin by genome screening, and cloned from sea urchin ovary in our laboratory (Ruas *et al*., 2010). The *Rattus norvegicus* TPC1 (*Rn*TPC1) was first identified in rat kidney as a protein with similarities to voltage-gated Ca^{2+} and Na^{+} channels (Ishibashi *et al*., 2000). Previous information on TPCs concerned only plant TPC1, which functions as a Ca^{2+} channel and localizes to the contractile vacuole (CV), which is equivalent to the lysosome in animal cells (Peiter *et al*., 2005).

Several studies have suggested the presence of NAADP receptors in acidic organelles, an idea based largely on pharmacological assays. NAADP elicits Ca^{2+} release from acidic stores, which are quite distinct from the endoplasmic reticulum (ER) (Genazzani and Galione, 1996; Galione and Churchill, 2002). The NAADP-releasable store is sensitive to bafilomycin A (an inhibitor of V-type H^{+}-ATPases found in acidic organelles), but not thapsigargin (an inhibitor of Ca^{2+}-ATPases), whereas ER Ca^{2+} stores are sensitive to the latter (Churchill and Galione, 2001; Churchill *et al*., 2002).

A radioligand receptor-binding assay has been used to study the distribution of NAADP binding activity in sea urchin egg homogenates. NAADP binding sites were enriched in the microsome and particulate fractions, which contained mainly ER and lysosomes respectively. GPN treatment of the lysosome-enriched particulate fraction (to cause osmotic lysis of lysosomes) abolished NAADP-induced Ca^{2+} release (Churchill *et al*., 2002). Furthermore, pre-treatment of the intact sea urchin egg with GPN also eliminated NAADP-induced Ca^{2+} release, but not that elicited by either IP_3 or cADPR (Churchill *et al*., 2002). Controversially, it has also been proposed that NAADP acts on RyRs, in which case NAADP receptors may be localized to the ER (Gerasimenko *et al*., 2003; Hohenegger *et al*., 2002; Steen *et al*., 2007).

3.2. Aims

The aims of the research presented in this chapter are to determine if TPC proteins are NAADP receptors, or a component of NAADP receptors, by analyzing both endogenous and heterologously expressed *Sp*TPCs using immunohistochemistry to investigate their cellular distribution, and radioligand binding assay techniques to study NAADP binding.

3.3. Results

3.3.1. Putative *Sp*TPCs

The *Strongylocentroutus purpuratus* (*Sp*) genome sequence (Sodergren *et al*., 2006) was screened by a BLAST search using rat TPC sequences, and the genes encoding three potential isoforms of the two pore channel proteins, *Sp*TPC1, *Sp*TPC2 and

*Sp*TPC3, were identified. A BLAST search revealed that the overall homology, at the amino acid level, between these three proteins varied from 29 - 34% (Ruas *et al*., 2010). Putative *Sp*TPCs possess twelve transmembrane domains (Figure 3.1) and are predicted to function as ion channels by analysis using the bioinformatics resources Pfam and TMHMM. Alignment of the protein sequences in comparison to *Hs*TPCs is shown in Figures 3.2A and B, with conserved N-glycosylation sites also shown.

To further characterize these putative Ca^{2+} channels in the sea urchin, it was necessary to raise antibodies that recognized endogenous *Sp*TPCs.

3.3.2. Production of anti-*Sp*TPC polyclonal antibodies

Anti-*Sp*TPC polyclonal antibodies were generated using the custom antibody service from Covalab for *Sp*TPC2, and from Eurogentec for *Sp*TPC1 and *Sp*TPC3. Antibodies, specific for individual *Sp*TPCs, were raised by immunizing rabbits simultaneously with two specific peptides derived from the following protein sequences:

*Sp*TPC1: peptide a, CEVSRLKWKSQREERL
peptide b, AYRGTRQRTKADLSKC

*Sp*TPC2: peptide a, QKQPIHRKVYPIYGC
peptide b, CDEIYKHPHIQNLRF

*Sp*TPC3: peptide a, MEGPKDYVDSYMPKSC
peptide b, TSLDKTTFSEPSSPVC

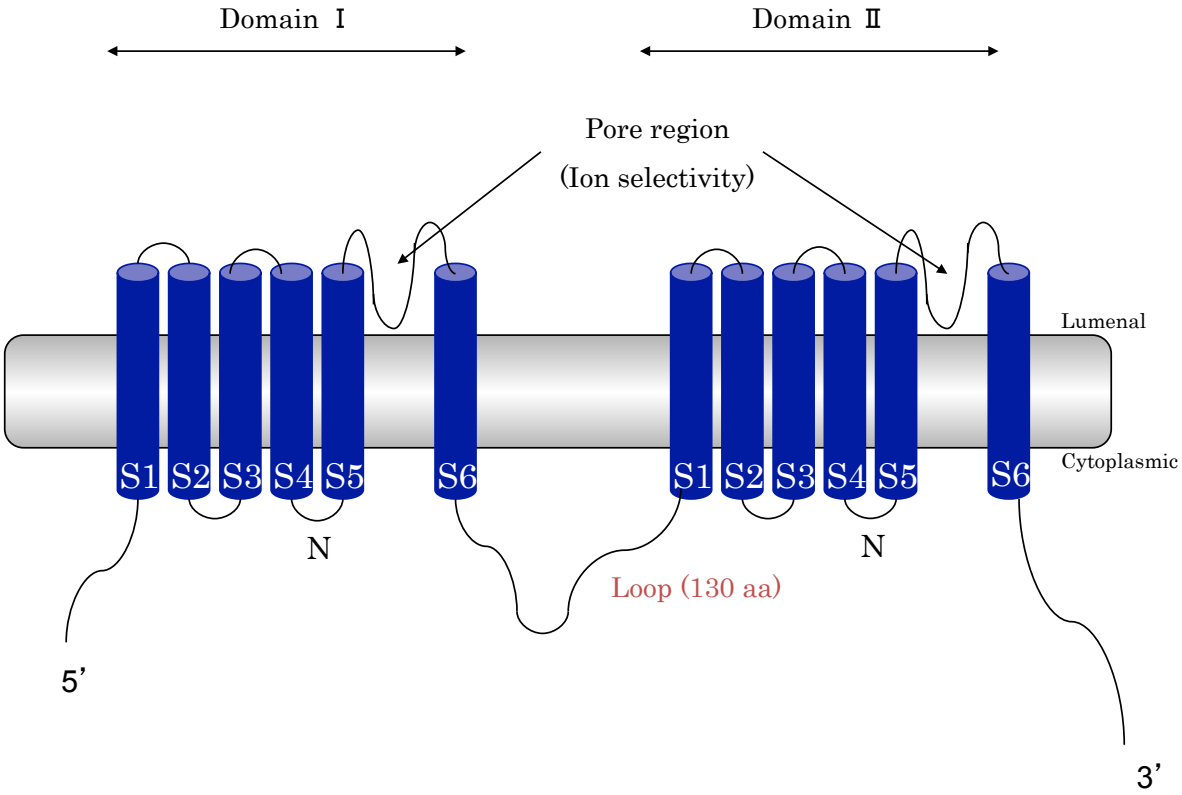
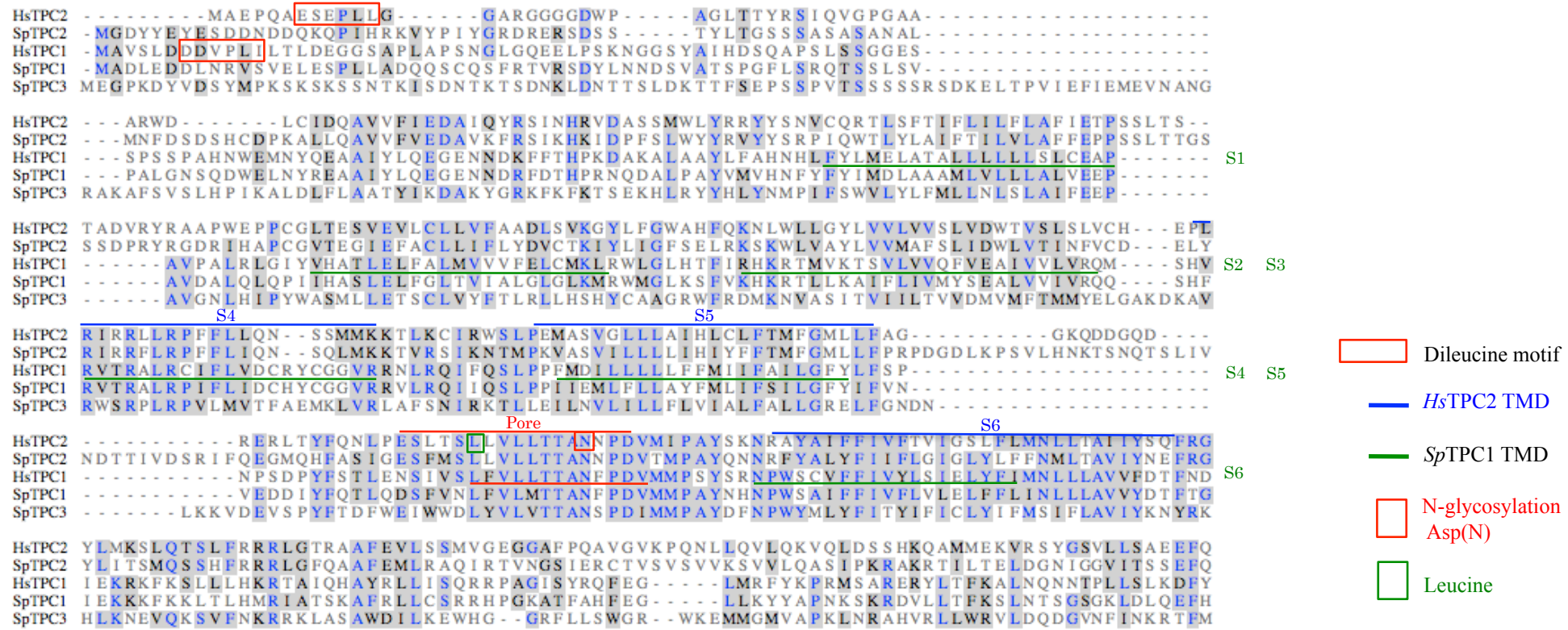


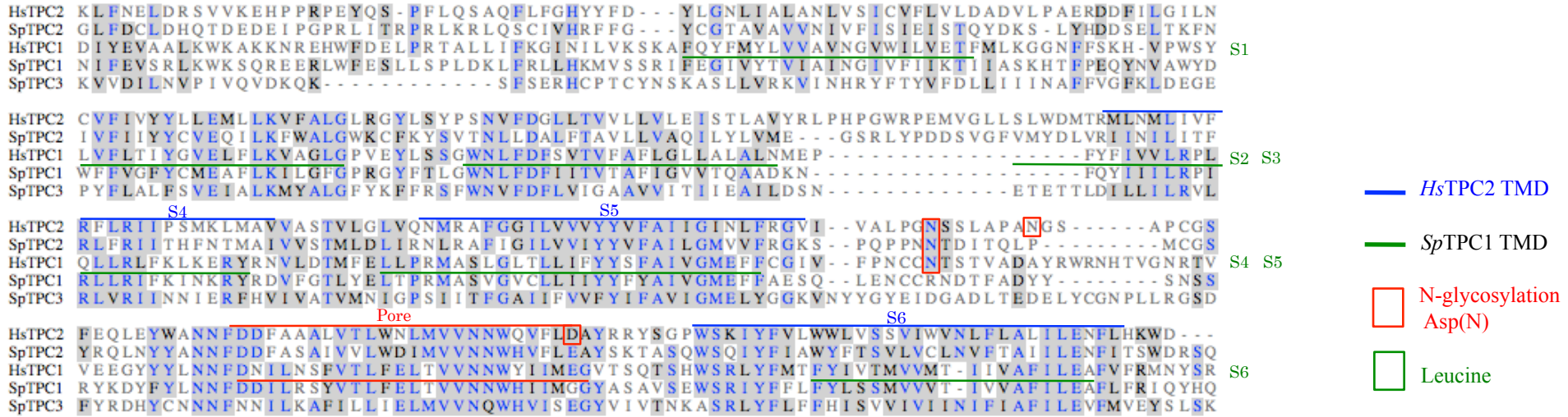
Figure 3.1. Topology of putative *Sp*TPCs
Putative *Sp*TPCs are predicted to have two domains separated by a loop (of about 130 residues) with each domain containing 6 transmembrane segments (S1 to S6). S4 is predicted to be the positively charged voltage sensor (since it contains the characteristic positively charged amino acid residues) and pore regions that function as the ion selectivity filter are thought to be between S5 and S6. N: N-glycosylation site, S4: voltage sensor.

A. *Hs*TPCs and *Sp*TPCs: Domain I



Figures 3.2A and B. Protein alignment of *Sp*TPCs and *Hs*TPCs

B. *Hs*TPCs and *Sp*TPCs: Domain II



Figures 3.2A and B. Protein alignment of *Sp*TPCs and *Hs*TPCs

Protein sequences were aligned using Mobyle portal (see *Appendix 7*). Identical residues to consensus are represented as letters in blue and a grey background indicats identical residues and similar residues to consensus. The dileucine motif, confirmed to transfer *Hs*TPC2 to the lysosome (Brailoiu *et al*., 2010b), is marked with a red rectangle, and N-glycosylation sites conserved through species and studied in *Hs*TPCs are marked with a red square. Transmembrane domains of *Hs*TPCs and *Sp*TPCs are indicated by blue and green bars respectively. No signal peptides are predicted, except in *Sp*TPC1, which suggests a nuclear localization signal. Although several dileucine motifs are found in *Sp*TPCs, they are all located far from the N- or C-terminal tails where most functional dileucine motifs are normally found. Leucine, found in the pore region and thought to be important to permit the function of the NAADP-sensitive Ca^{2+} channel, is marked with a green square (Brailoiu *et al*., 2010a).

These immunogenic peptides are located in the N- or C-terminal tails, or in the loop regions of the TPC protein (Figure 3.3). Antisera to the peptides, coupled to BSA, were raised in rabbits: rabbit 7303F and rabbit 7303C for *Sp*TPC1, rabbit 690G for S*p*TPC2, and rabbit 7302F and rabbit 7302C for *Sp*TPC3 (Ruas *et al*., 2010).

3.3.3. Overexpression of *Sp*TPCs

Anti-*Sp*TPC antibodies were tested by immunohistochemistry using sea urchin eggs (previously carried out by Dr Davis in this laboratory; data not shown), and this showed labelling of cortical regions with anti-*Sp*TPC antibodies. However, only the reactivity of anti-*Sp*TPC3 antibody was blocked by the immunizing peptide, raising questions concerning the selectivity of the other antibodies. Therefore, it was decided to produce recombinant *Sp*TPC proteins to determine the quality of the anti-*Sp*TPC antibodies used to detect endogenous proteins.

3.3.3.1. *Sp*TPC expression in mammalian cells

*Sp*TPC cDNA sequences had been previously cloned from tissue obtained from the ovaries of *S. purpuratus* (details given in Ruas *et al*., 2010). The coding sequence of each *Sp*TPC with an mRFPmars tag at the N- or C-terminus was subcloned into the mammalian expression plasmid, pcDNA5TO, to produce the over-expression vectors pcDNA5TO.mRFPmars.*Sp*TPC or pcDNA5TO.*Sp*TPC.mRFPmars. Each fragment (Figure 3.4B) was obtained by PCR using appropriate primer sets (see *Appendices 5.1 and 5.2*) and inserted in selected restriction sites of the pcDNA5TO plasmid (Figure 3.4A). The coding sequence of the red fluorescent protein mRFPmars was amplified

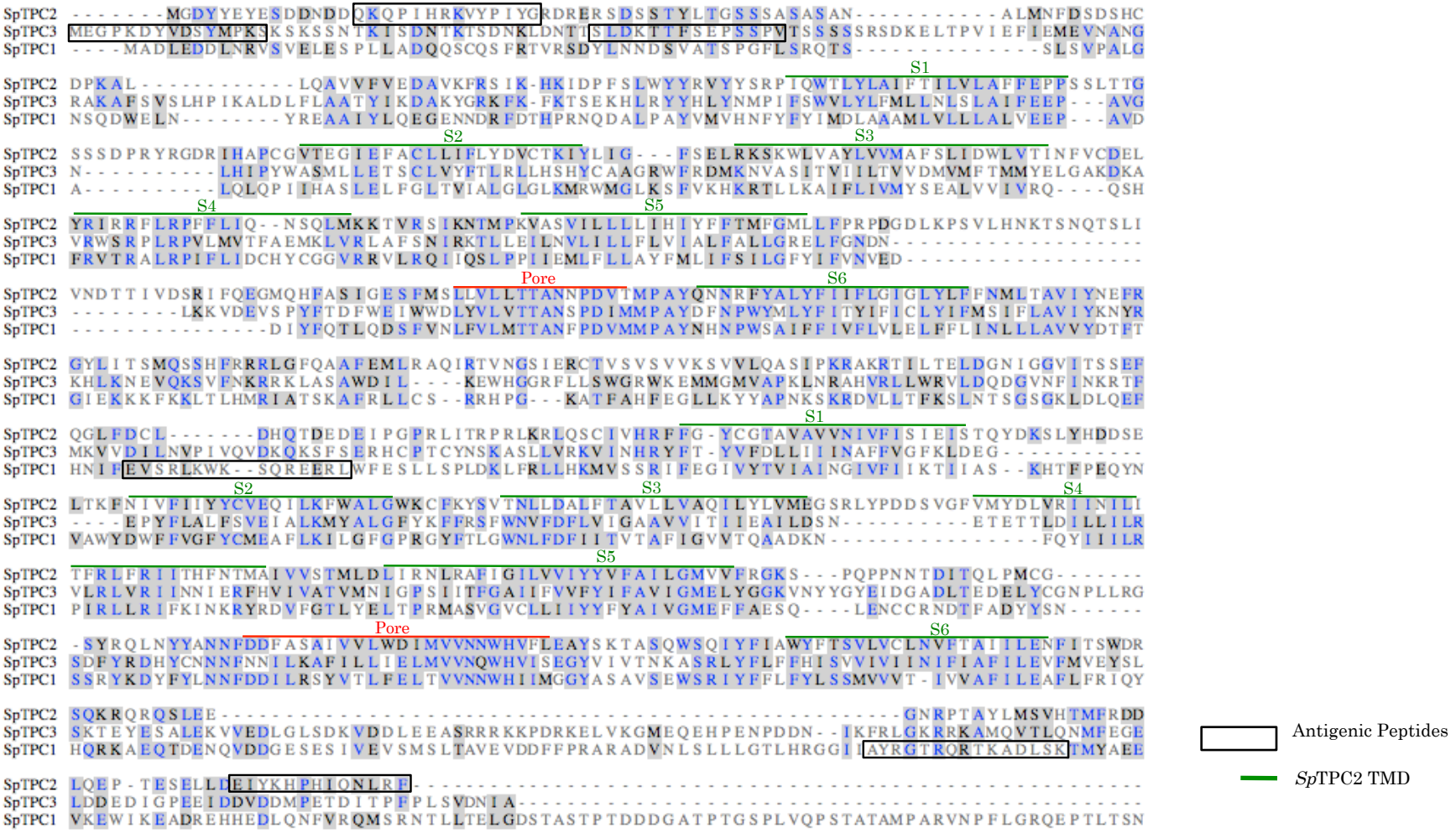
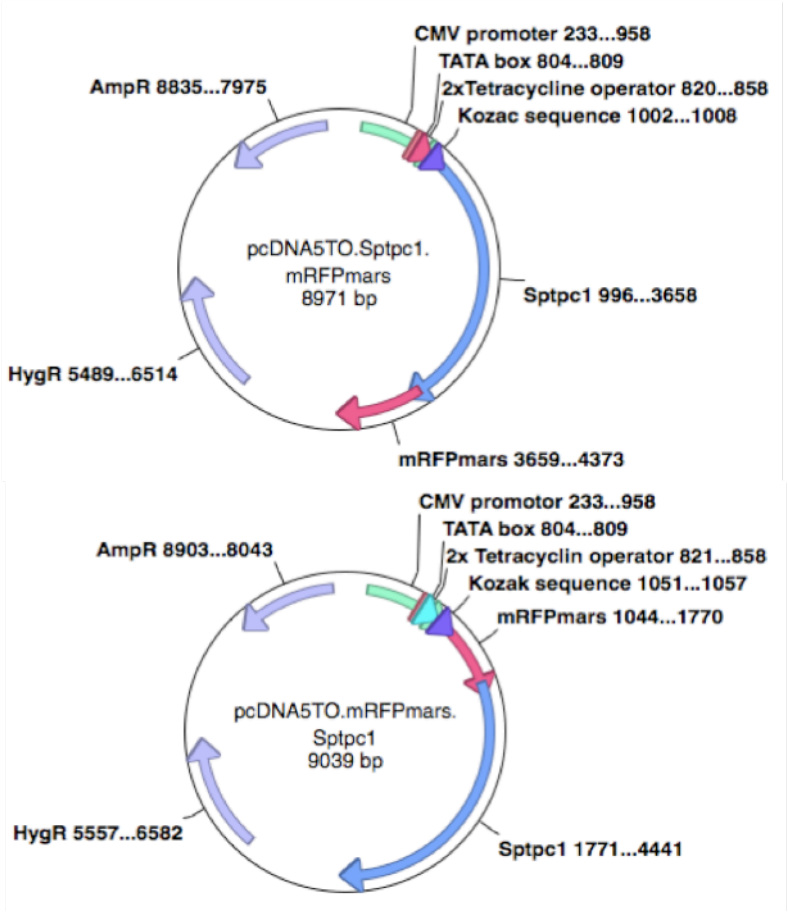


Figure 3.3. Antigenic peptides for generating anti-*Sp*TPC antibodies
Anti-*Sp*TPC antibodies were designed to recognize the loop between domain I and II in *Sp*TPC1, the N- and C-termini in *Sp*TPC2, and two parts of the N-terminal tail in *Sp*TPC3 (marked by black rectangles). The regions close to the transmembrane domain, indicated by green bars, were avoided. The protein sequence shown above was aligned using Mobyle portal (shown in *Appendix 7*). Letters representing identical residues are denoted in blue; the backgrounds for identical residues and similar residues are in grey.

A.



B.

pcDNA5TO.mRFPmars.*Sp*TPCs

*Sp*TPC1	NotI-Kozak-mRFPmars-NotI-*Sp*TPC1-Stop-ApaI
*Sp*TPC2	NotI-Kozak-mRFPmars-NotI-*Sp*TPC2-Stop-XbaI
*Sp*TPC3	NotI-Kozak-mRFPmars-NotI-*Sp*TPC3-Stop-ApaI

pcDNA5TO.*Sp*TPCs.mRFPmars

*Sp*TPC1	BamHI-Kozak-*Sp*TPC1-NotI-mRFPmars-ApaI
SpTPC2	HindIII-Kozak-*Sp*TPC2-NotI-mRFPmars-ApaI
*Sp*TPC3	BamHI-Kozak-*Sp*TPC3-NotI-mRFPmars-ApaI

Figure 3.4. Sub-cloning of *Sp*TPCs into the mammalian expression vector, pcDNA5TO

A. Maps of *Sp*TPCs expression constructs generated using pcDNA5TO as a host vector. B. The fragments of *Sp*TPCs were obtained by PCR using appropriate primer sets (see *Appendix 5.1 and 5.2*) and inserted into pcDNA5TO using the indicated restriction sites. A mRFPmars tag was inserted at the N- or C-terminal side of the *Sp*TPC coding sequence. Kozak sequence GC(C/G)ATGG was introduced before the start codon.

and ligated either upstream or downstream of the gene of interest using either NotI, or NotI and ApaI, sites respectively. In addition, a Kozak sequence (GCCATGG) was included upstream of each start codon, since most mammalian mRNAs have the short recognition sequence (GCC)n(A/G)CCATGG (Kozak sequence) at the site of translation initiation, which greatly facilitates the initial binding of the small subunit of the ribosome. The correct insertion of the gene of interest and lack of base changes introduced by PCR was confirmed by DNA sequencing.

3.3.3.2. Detection of transient expression of *Sp*TPCs

pcDNA5TO.mRFPmars.*Sp*TPCs, pcDNA5TO.*Sp*TPCs.mRFPmars and pcDNA5TO.HA.*Sp*TPCs (the latter plasmid previously constructed in this laboratory) were transfected into HEK293T cells using the Ca^{2+} phosphate transfection method (Ruas *et al*., 2010). For the construction of pcDNA5TO.HA.*Sp*TPCs, annealed double-stranded oligonucleotides coding for a haemagglutinin (HA) tag, an epitope derived from the haemagglutinin molecule, was ligated into the vector prior to the insertion of *Sp*TPC. Cells were harvested 48 h after transfection. The expression of *Sp*TPCs was confirmed by Western blot analysis using anti-mRFPmars antibody or anti-HA antibody (Figure 3.5A or B). The expected molecular weights of *Sp*TPC1, *Sp*TPC2 and *Sp*TPC3 with mRFPmars tags were 138 kDa, 120 kDa and 125 kDa, respectively, and those with HA tags were 112 kDa, 95 kDa and 99 kDa, respectively. Western blot analysis showed that full length mRFPmars or HA fusion proteins of all three *Sp*TPCs were successfully expressed in HEK293T cells (see Figure 3.5). For *Sp*TPC2, an additional band was observed at a higher molecular weight, above 250 kDa.

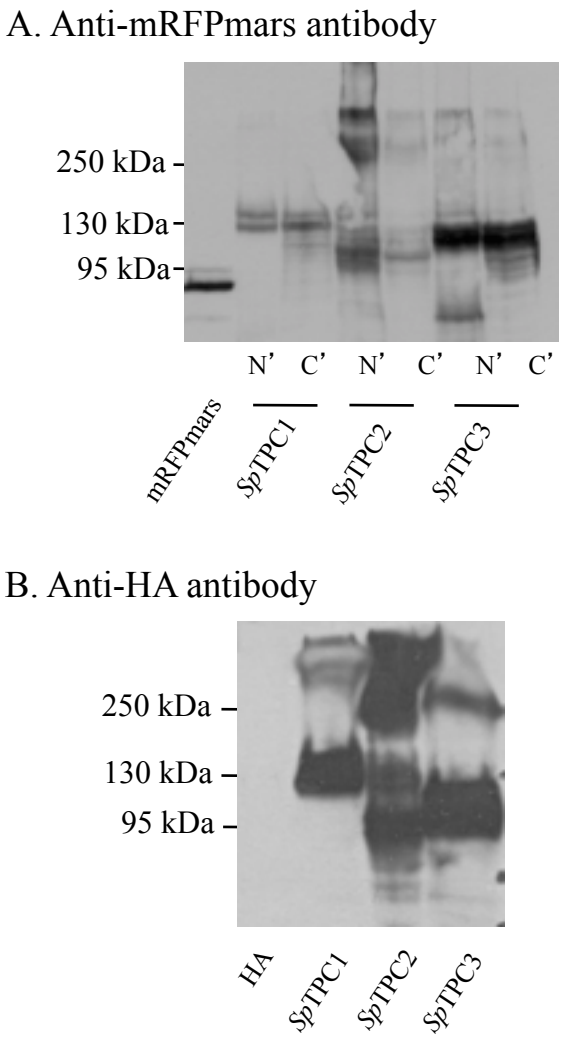


Figure 3.5. Expression of mRFPmars- or HA-tagged recombinant proteins mRFPmars fusions of *Sp*TPCs were transiently expressed in HEK293T cells and cell extracts were separated on a 10% SDS polyacrylamide gel, followed by Western blot analysis using either anti-mRFPmars antibody (A) or anti-HA antibody (B). Expressed mRFPmars alone was used as a control in the first lane. A. The bands seen at around 130 kDa in the second and the third lane correspond to fusion protein of *Sp*TPC1 with mRFPmars at the N- and C-termini, respectively. The bands for *Sp*TPC2 and *Sp*TPC3 corresponded to 120 kDa and 125 kDa respectively. B. N-terminus HA fusion proteins of *Sp*TPCs were also analyzed by Western blotting. Estimated molecular weights of these proteins were 120, 100 and 105 kDa for *Sp*TPC1, *Sp*TPC2 and *Sp*TPC3, respectively (B).

3.3.3.3. Characterization of anti-*Sp*TPC antibodies using recombinant protein

The expression plasmids, pcDNA5TO.mRFPmars.*Sp*TPC (for all three *Sp*TPCs) and pcDNA5TO.S*p*TPC.mRFPmars (for *Sp*TPC2 only) were transfected into HEK293 cells using the Ca^{2+} phosphate transfection method. Cells were harvested 48 h after transfection and lysed with either Lysis Buffer (Sigma-Aldrich Co. Limited, Poole, U.K.) or 1% CHAPS (Sigma-Aldrich Co. Limited), and protein levels were analyzed by Western blotting. Antibodies against *Sp*TPCs were affinity purified from immunized rabbit serum using Sulfo-Link agarose (Pierce Thermo Scientific, Cramlington, U.K.).

No specific bands, which were not seen in control cells were detected with anti-*Sp*TPC1 antibody (Figure 3.6A). Anti-*Sp*TPC2 antibody recognized bands above 250 kDa and at around 100 kDa; the latter band at just above 100 kDa was observed in the control lane for the N-terminus tagged protein and the this band could be detected if the equal amount of protein was loaded on control lane for cells transfected with C-terminus tagged *Sp*TPC2 (Figure 3.6B). Antibodies from both rabbit 7302F and rabbit 7302C recognized a band with an estimated size of 120 kDa on the *Sp*TPC3 blot (Figure 3.6C). Although the band detected by 7302F antisera could be non-specific as the faint band could be visible with further exposure on the control lane. Therefore, anti-*Sp*TPC3 antisera (7302C) appeared to successfully detect recombinant *Sp*TPC3 using Western blot analysis.

3.3.3.4. Efficiency of immunoprecipitation using anti-*Sp*TPC antibodies

Membranes, prepared from HEK293T cells transiently expressing HA-tagged *Sp*TPC1 and *Sp*TPC3, were incubated with purified antibodies, 7303F and 7303C for

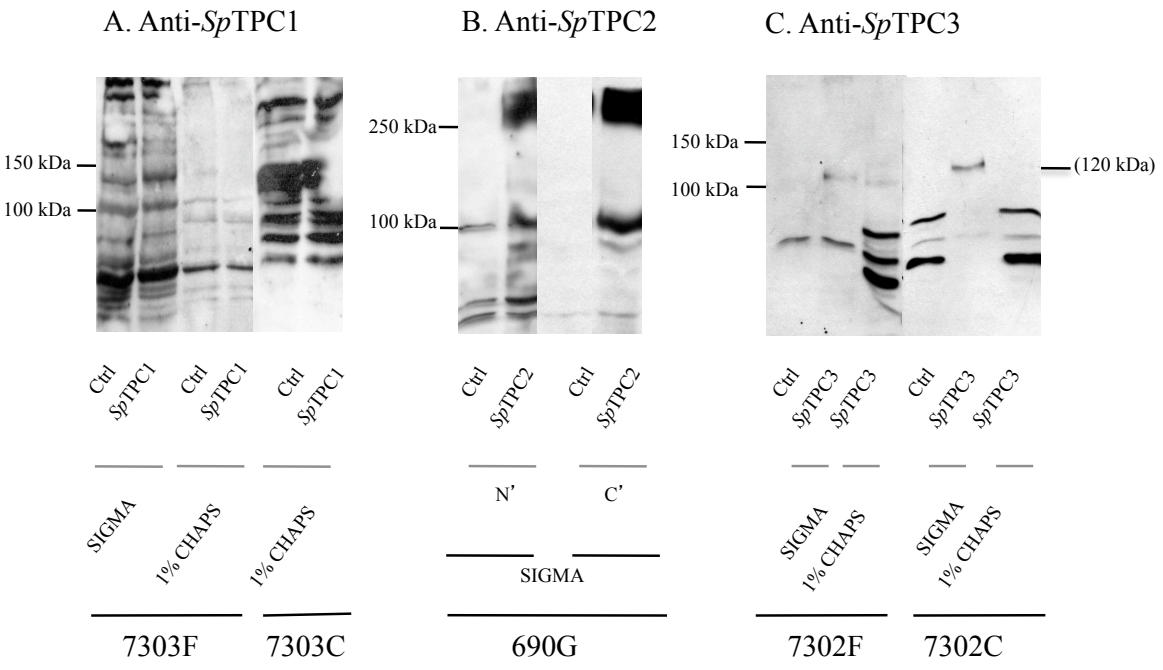


Figure 3.6. Testing anti-*Sp*TPC antibodies by Western blotting
Antibodies raised against *Sp*TPCs were tested on mRFPmars-tagged *Sp*TPCs expressed in HEK293T cells. Anti-*Sp*TPC antibodies were purified from serum of rabbits 7303F and 7303C for *Sp*TPC1 (A), 690G for *Sp*TPC2 (B), and 7302F and 7302C for *Sp*TPC3 (C). *Sp*TPC2 was tagged with mRFPmars either at the N- or C-terminus. 48 hours after transfection, using the calcium phosphate method, cells were harvested and lysed with lysis buffer (Sigma) or 1% CHAPS. Samples were resolved on an 8% or 10% SDS polyacrylamide gel, followed by immuno-blotting using the indicated antibodies. Predicted molecular weights of mRFPmars-tagged *Sp*TPC1, 2 and 3 are 130, 120 and 125 kDa respectively. The 120 kDa bar (upper right, panel C) gives an indication of the estimated molecular weight.

*Sp*TPC1, and 7302F and 7302C for *Sp*TPC3, respectively. Antibody complexes were pulled down with protein A coupled to resin, and this was followed by Western blotting using anti-HA antibody (Figure 3.7). Anti-*Sp*TPC1 antibodies did not immunoprecipitate any tagged TPC protein, consistent with the failure of this antibody to interact with recombinant *Sp*TPC1 in a Western blot. On the other hand, anti-*Sp*TPC3 antibodies from both rabbits precipitated recombinant *Sp*TPC3 successfully (Figure 3.7).

Since only the anti-*Sp*TPC3 antibody gave labelling blocked by an immunogenic peptide in the immunohistochemistry experiments designed to visualize endogenous proteins, whereas the reactivities of anti-*Sp*TPC1 and anti-*Sp*TPC2 antisera were not blocked by immunogenic peptides, it was not possible to determine the cellular distributions of the various *Sp*TPC subtypes using these antibodies. I therefore decided to investigate the distribution of epitope-tagged *Sp*TPCs using recombinant proteins expressed in heterologous systems.

3.3.4. Localization of *Sp*TPCs in starfish oocytes

Starfish (*Asterina miniata*) and sea urchins are both echinoderms, thus, the environment for protein synthesis and transportation in starfish may be more similar to that of the sea urchin system than to that of mammalian cells. In addition, the starfish is often used as a model system to study fertilization, and NAADP-induced Ca^{2+} release in this system has already been reported (Lim *et al.*, 2001). Importantly, the starfish system allows for the expression of proteins of interest to be achieved by the microinjection of mRNA, a technique, which has already been established.

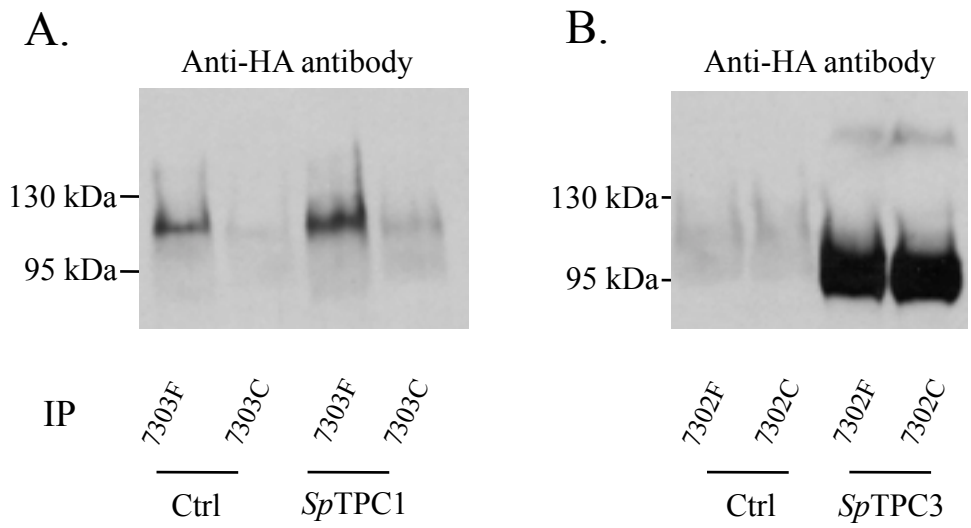


Figure 3.7. Immunoprecipitation of HA-fusion protein using anti-*Sp*TPC1 and *Sp*TPC3 antibodies

Membranes extracted from HEK293T cells expressing HA-tagged *Sp*TPC1 or *Sp*TPC3 were solubilized with 1% CHAPS, and samples were incubated with serum containing each antibody: 7303F and 7303C for *Sp*TPC1 (A), and 7302F and 7302C for *Sp*TPC3 (B). Antibody complexes were immunoprecipitated with protein A beads and after washing several times, eluted with 2x SDS loading buffer. Samples were resolved on a 10% SDS polyacrylamide gel and subjected to Western blotting using anti-HA antibody. Rabbit IgG was incubated with samples as a negative control. Estimated molecular weights of the HA fusion proteins of *Sp*TPC1 and *Sp*TPC3 were120 and 105 kDa

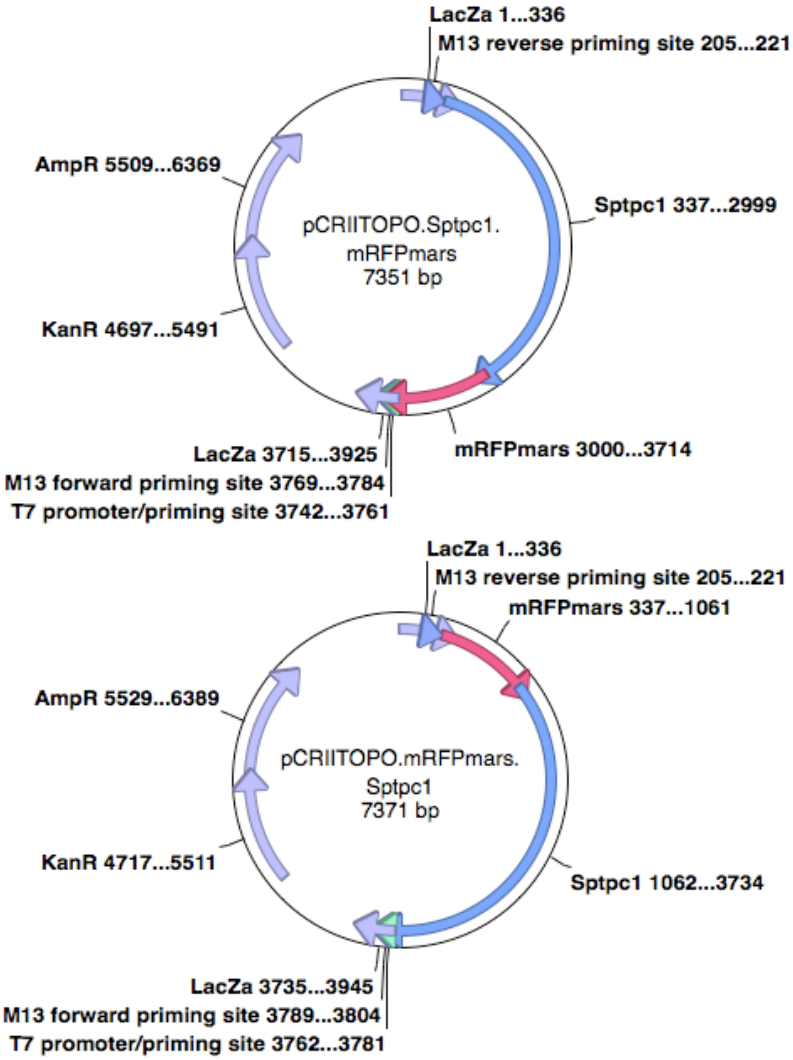
3.3.4.1. Heterologous expression of *Sp*TPCs in starfish oocytes

The distribution of *Sp*TPCs was examined after expression in starfish oocytes. pcDNA5TO.*Sp*TPC constructs with an mRFPmars tag at the N- or C-terminus were used as templates to amplify the fragments shown in Figure 3.8B and inserted into the pCRIITOPO cloning vector. The orientations, Sp6 (forward) and T7 (reverse), were successfully inserted in the donor plasmid, but the forward construct of *Sp*TPC1 with a mRFPmars tag at the 5' side was not (Figure 3.8). The primer sets used for the construction of these plasmids are listed in *Appendices 5.3 and 5.4* respectively. Insertion and orientation of the coding sequences were confirmed by restriction enzyme digestion and sequencing.

3.3.4.2. Localization of *Sp*TPCs in starfish oocytes

Following expression in starfish oocytes, *Sp*TPC localization (Figure 3.9) was shown to be predominantly in the cortex, which correlates with the sites of NAADP-dependent responses in sea urchin eggs (Ruas *et al.*, 2010; collaborative experiments performed with Dr Davis and Dr Wessel). RyRs and RyR-sensitive Ca^{2+} release regions are also located within the sea urchin egg cortex (McPherson *et al.*, 1992). Therefore, to obtain more detailed information, intracellular compartments were visualized and the localization of *Sp*TPCs was examined by following their expression in HEK293T cells.

A.



B.

pCRIITOPO.mRFPmars.*Sp*TPCs

*Sp*TPC1 (T7)	NotI-Kozak-mRFPmars-NotI-SpTPC1-Stop-ApaI
*Sp*TPC2 (Sp6 and T7)	NotI-Kozak-mRFPmars-NotI-SpTPC2-Stop-XbaI
*Sp*TPC3 (Sp6 and T7)	NotI-Kozak-mRFPmars-NotI-SpTPC3-Stop-ApaI

pCRIITOPO.*Sp*TPCs.mRFPmars

*Sp*TPC1 (Sp6 and T7)	BamHI-Kozak-SpTPC1-NotI-mRFPmars-ApaI
*Sp*TPC2 (Sp6 and T7)	HindIII-Kozak-SpTPC2-NotI-mRFPmars-ApaI
*Sp*TPC3 (Sp6 and T7)	BamHI-Kozak-SpTPC3-NotI-mRFPmars-ApaI

Figure 3.8. Sub-cloning of *Sp*TPCs with an mRFPmars tag into a TOPO cloning vector

A. Maps of SpTPCs expression constructs using pCRIITOPO as a backbone. B. Fragments amplified by PCR using Expand Long Range dNTPack (Roche). A single deoxyadenosine [A] was added to the 3′ ends of PCR products before ligation to the linearized vector, which has single, overhanging, 3′ deoxythymidine [T] residues. The correct insertion and sequence of the gene of interest was confirmed by full-length insertion sequencing.

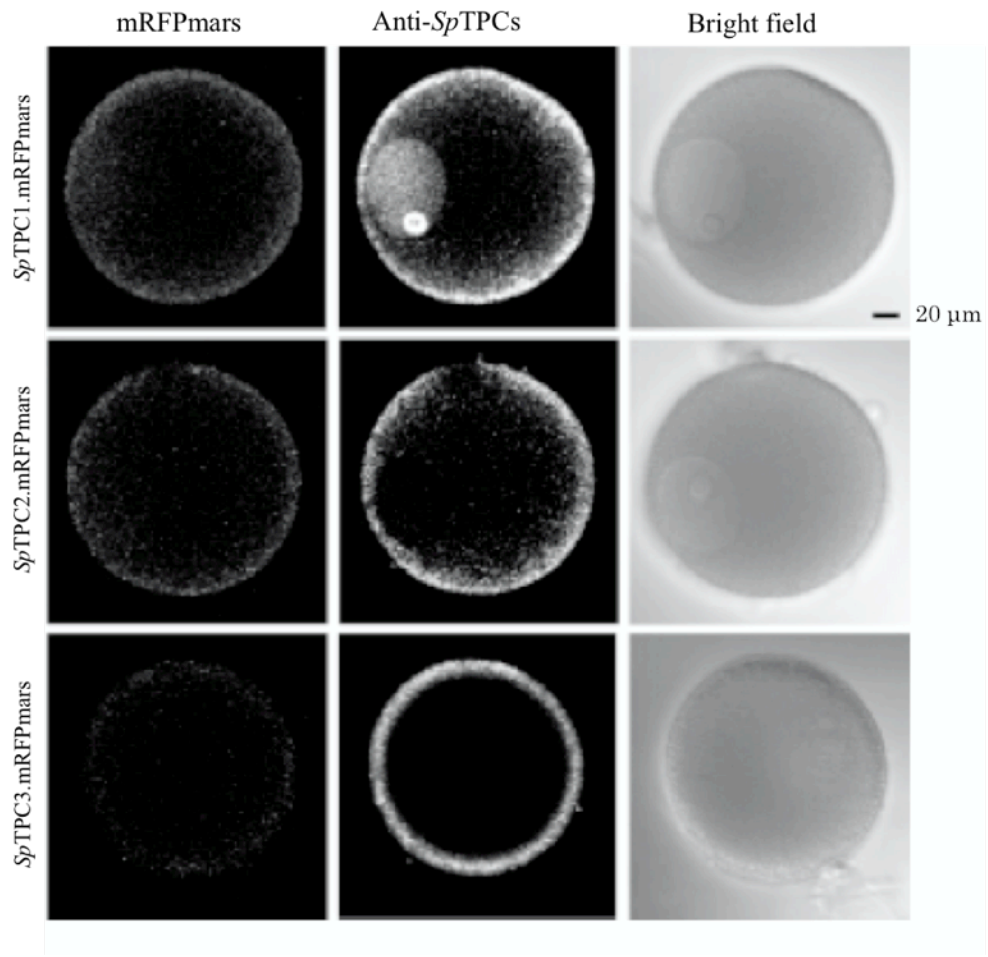


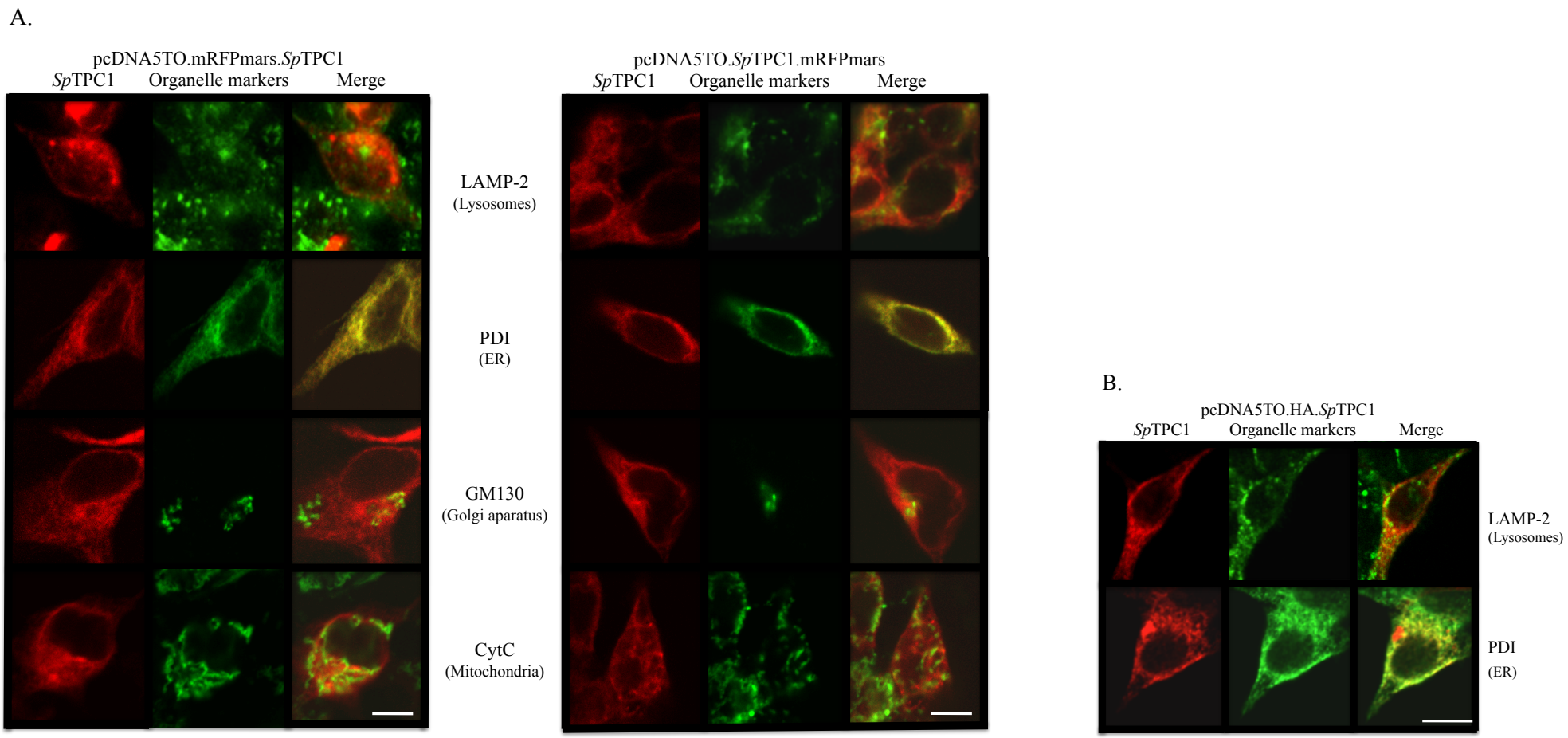
Figure 3.9. Localization of *Sp*TPCs in oocytes of starfish *Asterina miniata*
C-terminal fusion proteins expressed in oocytes were analyzed either by detection of mRFPmars fluorescence or by immunofluorescence with the corresponding anti-*Sp*TPC antibody. The figure shows that *Sp*TPC1 was found within the cortex, and partial localization of *Sp*TPC1 to the nucleus was also observed. *Sp*TPC2 and *Sp*TPC3 showed similar localization patterns to that of *Sp*TPC1, although nuclear staining was not observed for these TPCs. Similar results were obtained with the N-terminal mRFPmars fusion proteins. This was collaborative work performed with Dr Davis and Dr Wessel (Ruas *et al*., 2010).

3.3.5. Localization of transiently expressed *Sp*TPCs in HEK293 cells

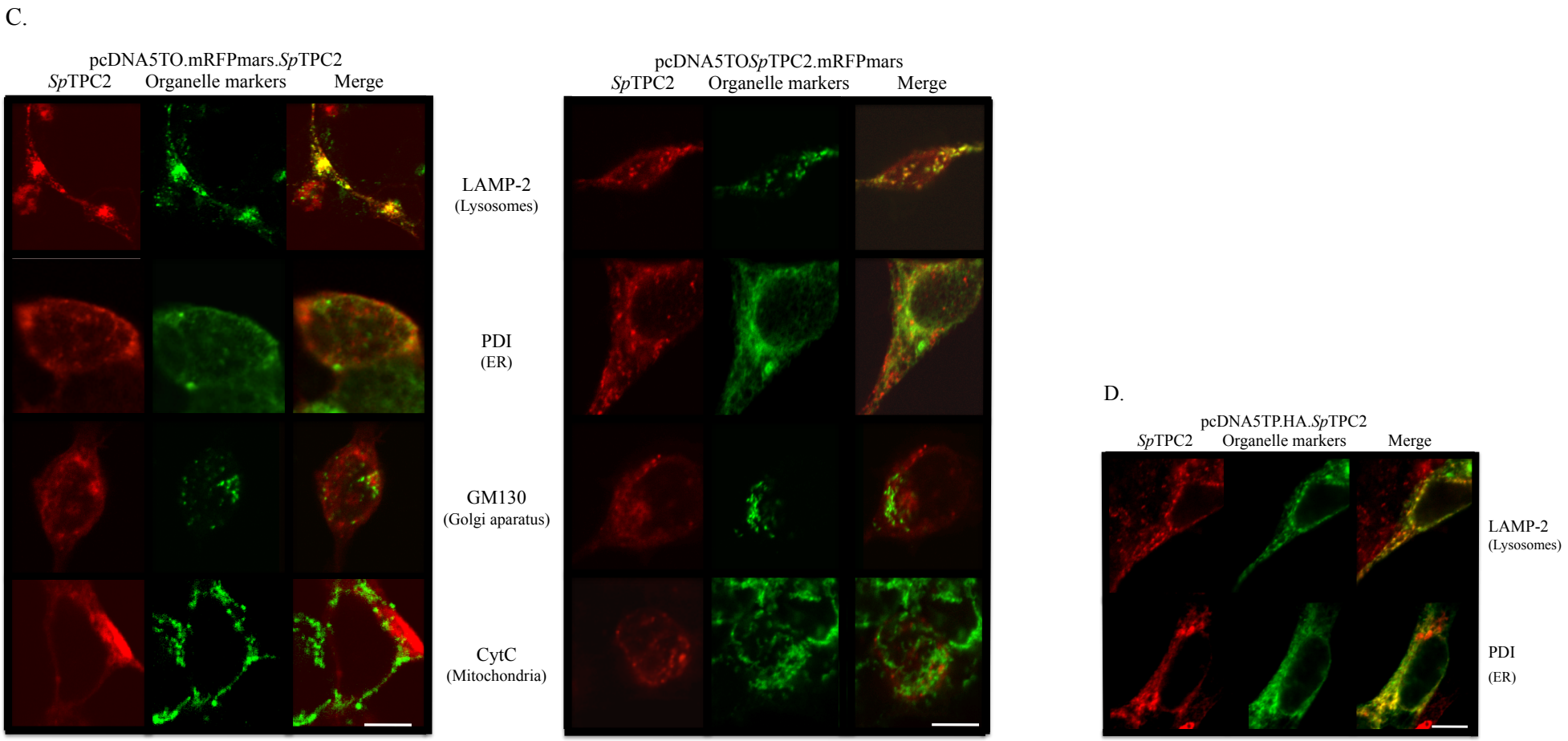
HEK293 cells expressing mRFPmars or HA fusions of *Sp*TPCs were fixed and incubated with primary antibodies (raised in mouse) for various organelle markers, namely LAMP-2 (for lysosomes), PDI (for the ER), GM130 (for the Golgi apparatus) and CytC (for mitochondria); this was followed by incubation with Alexa 488 conjugated anti-mouse antibody (Zorzato *et al*., 1990). HA fusion protein was also visualised using an anti-HA antibody and a red-fluorescent conjugated secondary antibody (Alexa Fluor 546).

Using this approach, it was found that localization of the three *Sp*TPC isoforms was not identical. *Sp*TPC1 was found on the ER (Figures 3.10A and B), whereas *Sp*TPC2 was predominantly found on lysosomes and partially distributed on ER (Figures 3.10C, D and E). Interestingly, *Sp*TPC3, although on intracellular membranes, did not co-localize with LAMP-2 or PDI (Figure 3.10F and G). No significant co-localization of any of the *Sp*TPC isoforms with the Golgi apparatus or mitochondria was detected (Figures 3.10A, C and F). Summary data are listed in Table 11.

Recombinant *Sp*TPC2 localized predominantly to lysosomes, as hypothesised, whereas most of the recombinant *Sp*TPC1 did not; however, conditional stable cell line expressing *Sp*TPC1 did show localization to lysosomes (localization of stably expressed *Sp*TPCs in HEK293 cells was examined in this laboratory; see Table 11). Having successfully demonstrated expression of *Sp*TPCs and their localization on membranes of intracellular organelles, HEK293 cells were next used to determine if increased NAADP binding could be detected due to expression of *Sp*TPCs.



Figures 3.10A and B. Localization of *Sp*TPC1 in HEK cells
*Sp*TPC1 co-localized with the ER marker. As far as the different fusion tags were concerned, mRFPmars at both the N- and C-termini, and the smaller HA-tag, gave similar localization patterns (A, B). *Sp*TPC1 did not localize to the endolysosomal compartment. Scale bars, 10 μm.



Figures 3.10C and D. Localization of *Sp*TPC2 in HEK cells
*Sp*TPC2 with N- or C- terminal fusion to mRFPmars co-localized with LAMP-2 (which identifies lysosomes or late endosomes) (C). HA-tagged *Sp*TPC2 also showed a similar staining pattern (D). *Sp*TPC2 did not co-localize with PDI, an ER marker. Scale bars, 10 μm.

E.

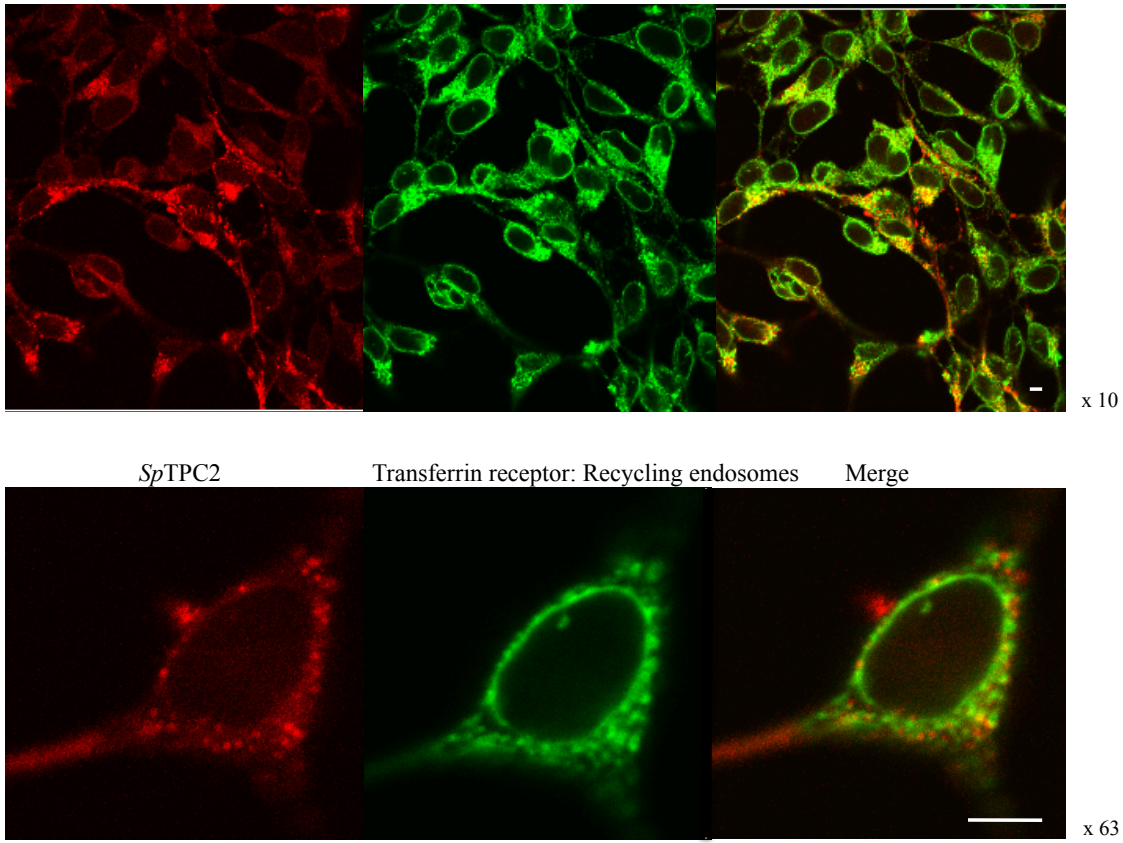
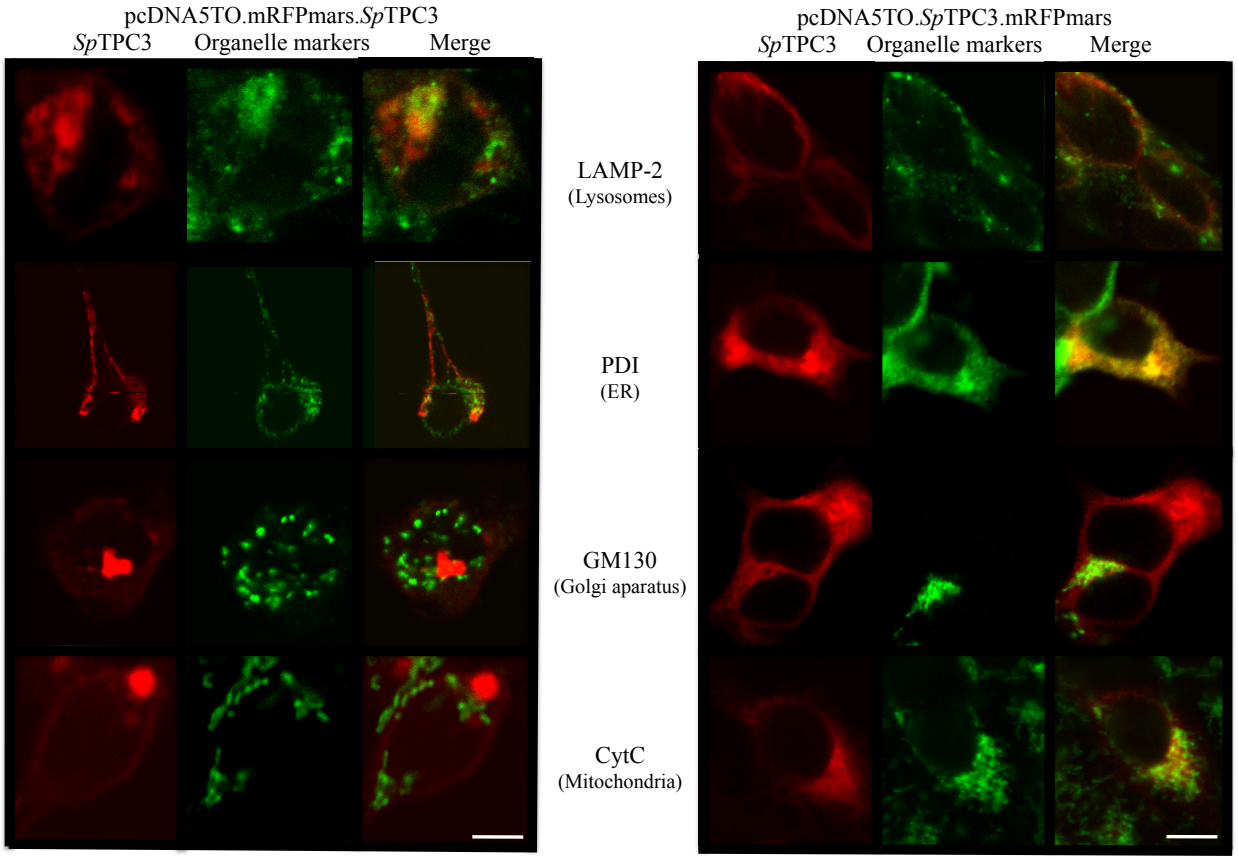
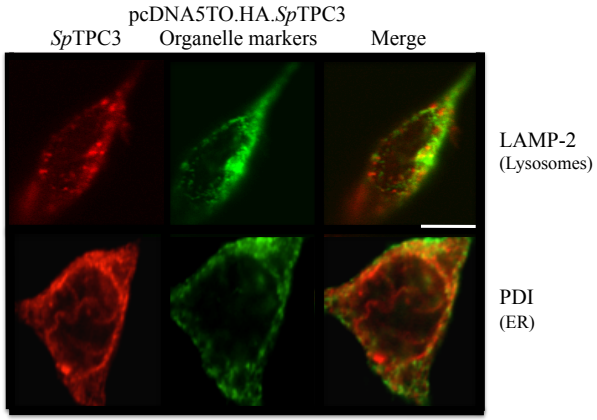


Figure 3.10E. Localization of *Sp*TPC2 in a stable HEK293 cell line expressing mRFPmars fusion protein of *Sp*TPC2. mRFPmars-tagged *Sp*TPC2 of stable cells was compared to labelling with an anti-transferrin receptor antibody as a marker for the ER. *Sp*TPC2 did not co-localize with recycling endosomes in stably expressing cells (E). Scale bars, 10 μm.

F.



G.



Figures 3.10F and G. Localization of *Sp*TPC3 in HEK cells
*Sp*TPC3 did not co-localize with either LAMP-2 or PDI. Scale bars, 10 μm.

Table 11. Localization of *Sp*TPCs in HEK cells

*** Published data**

Sp	Transient expression			Stable expression *	
	mRFPmars N	mRFPmars C	HA N	mRFPmars N	HA N
TPC1	ER			lysosome	ER
TPC2	lysosome /(ER)	lysosome	lysosome	lysosome	
TPC3	Not clear			Recycling endosome	lysosome

3.3.6. NAADP binding to sea urchin egg proteins

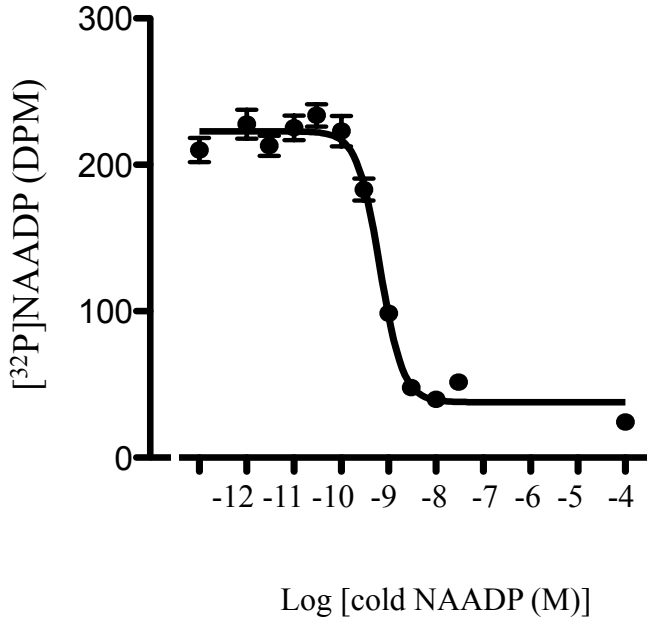
In previous studies in sea urchin egg homogenate, proteins responsible for NAADP binding have been shown to have a single, high affinity binding site with an IC_{50} value (competitive displacement assay) of 540 pM (Patel *et al*., 2000a). In contrast, the IC_{50} values for the binding of related molecules were 21 μM for NADP, 6.3 μM for NADPH, 2.5 μM for cADPR and 51 μM for NAAD, respectively (Lewis *et al*., 2007).

3.3.6.1. NAADP shows high affinity binding to sea urchin egg homogenate

To verify our assay, NAADP binding to its putative receptor was investigated in sea urchin egg homogenate using [^{32}P]NAADP. Homogenates were incubated with various concentrations of unlabelled NAADP for 10 min, prior to the addition of [^{32}P]NAADP for 20 min, both reactions being carried out at room temperature. After incubation, the free radioligand was separated from the bound ligand by rapid filtration using a cell harvester. The retention of [^{32}P]NAADP on the filter membrane was determined either by liquid scintillation counting or with a phosphor screen.

The binding of [^{32}P]NAADP was inhibited when the concentration of unlabelled NAADP was increased, suggesting that NAADP was binding to a saturable site. The binding had an IC_{50} value of 556 ± 14 pM (Figure 3.11A), a value consistent with the presence of an endogenous protein that binds NAADP with high affinity, as has been reported in sea urchin egg homogenate (Lewis *et al*., 2007; Patel *et al*., 2000a). Previous studies have shown that the NAADP binding protein was enriched in the microsome and particulate fractions prepared by percoll density gradient

A.



B.

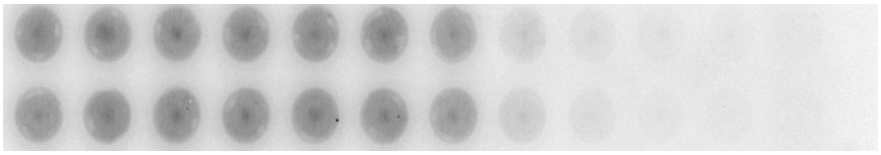


Figure 3.11. Competitive displacement NAADP binding assay in sea urchin egg homogenate

Aliquots of sea urchin egg homogenate [1% (v/v)] were simultaneously incubated with various concentrations of unlabelled NAADP and 0.2 nM [^{32}P]NAADP. Various concentrations of NAADP, up to 100 μM, were used to generate a competitive displacement curve, consistent with a single class of binding site. The IC_{50} for NAADP was 556 ± 14 pM (n = 2) with a Hill coefficient of -1.8 ± 0.02 (A). A phospho-image of a representative filter paper is shown in (B); each circle corresponds to a point in (A) and each reaction was duplicated.

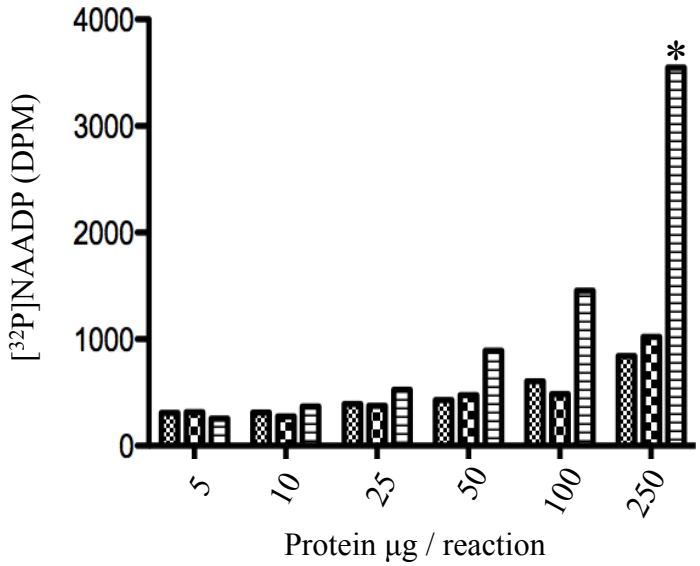
centrifugation (Churchill *et al*., 2002). Therefore, the NAADP binding assay was performed on appropriate membrane fractions prepared from sea urchin eggs.

3.3.6.2. NAADP binding to membrane fractions

Two different membrane fractions were prepared from egg homogenate: total membrane collected by centrifugation of egg homogenate at 100,000g; and microsomes, pelleted at 100,000g from the supernatant obtained after 10,000g centrifugation. The NAADP binding activity of each of these fractions was compared to that of egg homogenate using a range of protein concentrations from 5 - 250 μg per reaction. The highest [^{32}P]NAADP binding was observed in microsome fractions, and was significantly higher than that measured in either total egg homogenate or the total membrane fraction (Figure 3.12). It was therefore evident that the NAADP binding protein was enriched in the microsome fraction, which is purported to contain membranes other than the plasma membrane, including lysosomes and the ER (previously tested in our laboratory).

3.3.6.3. Correlation between NAADP binding and the presence of *Sp*TPCs

In order to examine the correlation between increased NAADP binding activity and *Sp*TPC expression, pre-labelled microsomes from *S. purpuratus* were immunoprecipitated with anti-*Sp*TPC antibodies. 1 mg of microsomes was labelled with 0.2 nM [^{32}P]NAADP in GluIM, prior to immunoprecipitation. The solubilized complex was pulled down using serum produced in non-immune rabbits or in rabbits immunized against *Sp*TPCs, and collected using protein A beads. The anti-*Sp*TPC3



(a) : Egg homogenate
(b) : Total membrane fraction (100,000g)
(c) : Microsome fraction (10,000g - 100,000g)

Figure 3.12. [^{32}P]NAADP binding to membrane fractions of sea urchin eggs
Sea urchin egg homogenate was fractionated by centrifugation
(a) Egg homogenate: total egg homogenate
(b) Total membrane fraction: egg homogenate was lysed and collected at 100,000g
(c) Microsome fraction: proteins were removed from egg homogenate by spinning at 10,000g, and microsome fractions were collected at 100,000g.
Specific binding in the presence or absence of 100 µM unlabelled NAADP with various amounts of protein (indicated) in each membrane fraction was determined. The X-axis corresponds to the amount of protein used (µg).
*Indicates statistically significance difference relative to the other fractions (a,b) $P < 0.05$.

antibody from the serum of rabbit 7302C precipitated endogenous proteins with a high associated level of labelled NAADP. This result provides strong evidence that TPC proteins are associated with the NAADP binding activity. However, sera obtained from other rabbits, immunized with *Sp*TPC1 or *Sp*TPC2, were unable to pull down any proteins associated with labelled NAADP (Figure 3.13). Although this was only a single set of experiments, one possible conclusion is that *Sp*TPC3 is responsible for the majority of NAADP binding. An alternative explanation is that the specificities of anti-*Sp*TPC antibodies against TPC1 and TCP2 were not high enough to precipitate endogenous NAADP-protein complexes. This possibility was anticipated for two reasons; firstly, the antisera against *Sp*TPC1 failed to work on a Western blot; secondly, both *Sp*TPC1 and *Sp*TPC2 immunoreactivities (in immunohistochemistry experiments) were not blocked using competing peptides. Due to the limitations of the antisera available, NAADP binding to epitope-tagged *Sp*TPCs expressed in HEK293 cells was investigated.

3.3.7: NAADP binding in cells expressing recombinant *Sp*TPCs

Due to the uncertainty of the specificity of the anti-*Sp*TPC1 antibody, and the potential expression levels of endogenous *Sp*TPC1 and *Sp*TPC2, it was decided to perform NAADP binding experiments on *Sp*TPCs expressed in HEK cells.

3.3.7.1. NAADP binding in HEK293T cells transiently expressing mRFPmars *Sp*TPCs

The [^{32}P]NAADP binding assay was performed on membranes prepared from HEK293T cells, transiently transfected with mRFPmars.*Sp*TPC constructs, followed

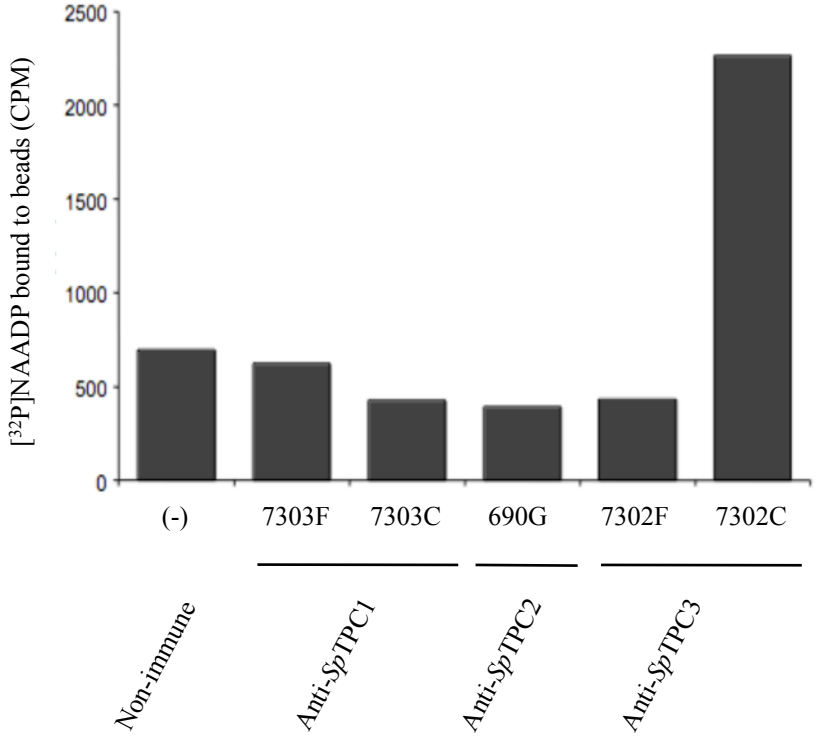


Figure 3.13. Immunoprecipitation of *Sp*TPCs from sea urchin egg microsomes pre-labelled with [^{32}P]NAADP
1 mg of the microsome fraction was labelled with 0.2 nM [^{32}P]NAADP in GluIM, this was followed by solubilization with 1% CHAPS, and the complex was then incubated with serum, from immunized or non-immunized rabbits, overnight. The immuno-complexes were collected using protein A beads. Bound material was eluted with 1% SDS, and radioactivity subsequently counted. Serum from rabbits 7303F and 7303C contained anti-*Sp*TPC1 antibodies, serum from rabbit 690G contained anti-*Sp*TPC2 antibody, and serum from rabbits 7302F and 7302C contained anti-*Sp*TPC3 antibodies. This was a collaborative experiment performed in my host laboratory (n = 1).

by PEG precipitation (details can be found in *Chapter 2*). [^{32}P]NAADP specific binding appeared to show a slight increase in binding on expression of *Sp*TPC3 or *Sp*TPC2 but the increase was not statistically significant (data not shown, as the work was collaborative within the laboratory and not solely my own). Immunoprecipitation of the NAADP binding complexes may enhance differences between control and expressing cells, so it was decided to repeat the binding assays using HA-*Sp*TPC fusion proteins, which allowed pull down of the [^{32}P]NAADP binding complexes using an anti-HA antibody.

3.3.7.2. NAADP binding in HEK293 cells expressing HA-tagged *Sp*TPCs

Specific [^{32}P]NAADP binding to HA-*Sp*TPC fusion proteins was examined. In initial experiments, microsome fractions were prepared from HEK293 cells expressing *Sp*TPCs constitutively. Unlabelled NAADP (100 μM) was added to 500 μg of membrane for 1 h prior to the addition of [^{32}P]NAADP. After further incubation for 1 h, the binding reaction was terminated by separation of the unbound [^{32}P]NAADP using a manifold. There was no significant enhancement of [^{32}P]NAADP specific binding in cells expressing *Sp*TPCs when compared to the controls (Figure 3.14). Based on information available, the binding assay conditions had been optimized with regard to incubation time, temperature, amount of protein / reaction, PEG precipitation methods and the K^+ concentration in the binding buffer and washing buffer. However, the lack of enhancement of NAADP binding may have been due to a low level of *Sp*TPC expression or to aggregation of recombinant protein, since it was often observed that mRFPmars- or HA-tagged protein formed several bright spots (detected by immunofluorescence) soon after expression level leading to cell toxic. To keep the balance of *Sp*TPCs expression level to maximize fluorescent but not

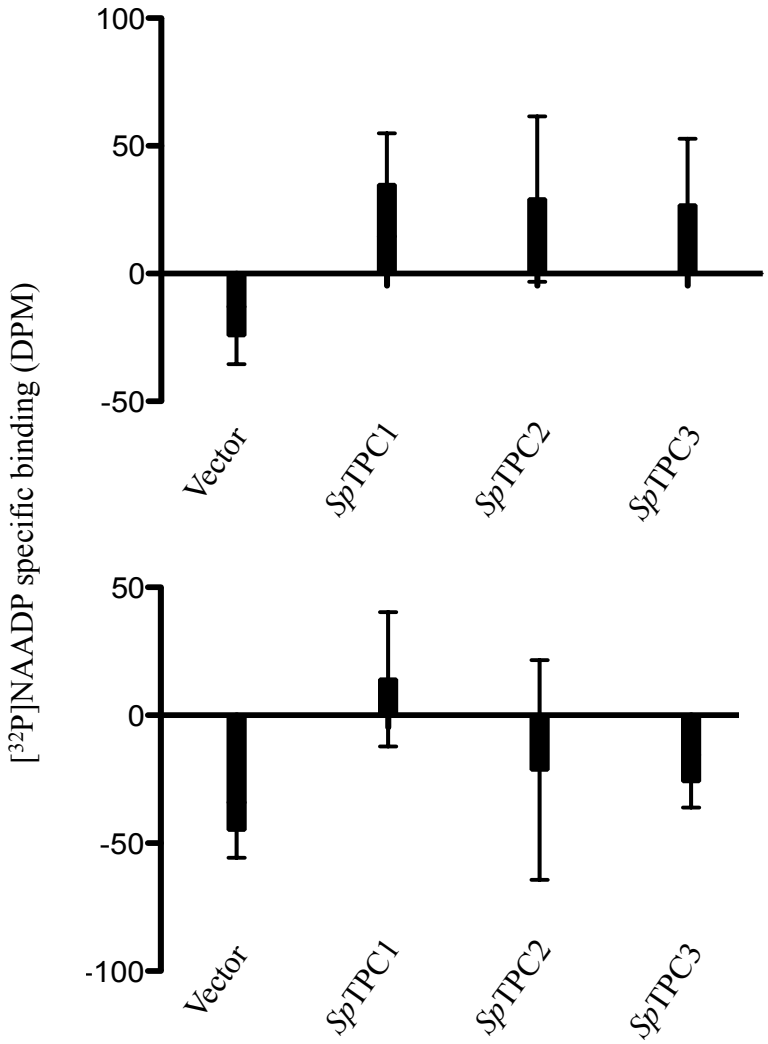


Figure 3.14. [^{32}P]NAADP binding to membranes isolated from HEK293T cells that expressed HA-tagged *Sp*TPCs

Samples were obtained from HEK293T cells transiently expressing HA-tagged *Sp*TPCs. 48 hours after transfection, using a calcium phosphate transfection method, cells were lysed with 1% CHAPS, and this was followed by membrane preparation. 500 μg / reaction of membrane protein was incubated either in the presence or absence of 100 μM unlabelled NAADP, prior to incubation with ^{32}P-labelled NAADP at room temperature for 1 hour. The binding reaction was terminated by filtration using a manifold. Cells expressing mRFPmars only, were used as a negative control (n = 6 - 7). Two independent experiments (triplicated/each) are shown. The results were analysed by analysis of variance (ANOVA) and the mean ± S.M.E shown.

toxic*, the ex*pression of *Sp*TPCs in an inducible system might be necessary.
As an alternative approach, expression in insect cells was tried. There is no gene encoding a TPC orthologue in Sf9 cells, thus the correlation between the presence of *Sp*TPCs and NAADP binding might be clearer than in HEK293 cells, particularly when levels of protein expression are low.

3.3.8. Bac-to-Bac baculovirus expression system (insect cell, Sf9 expression)

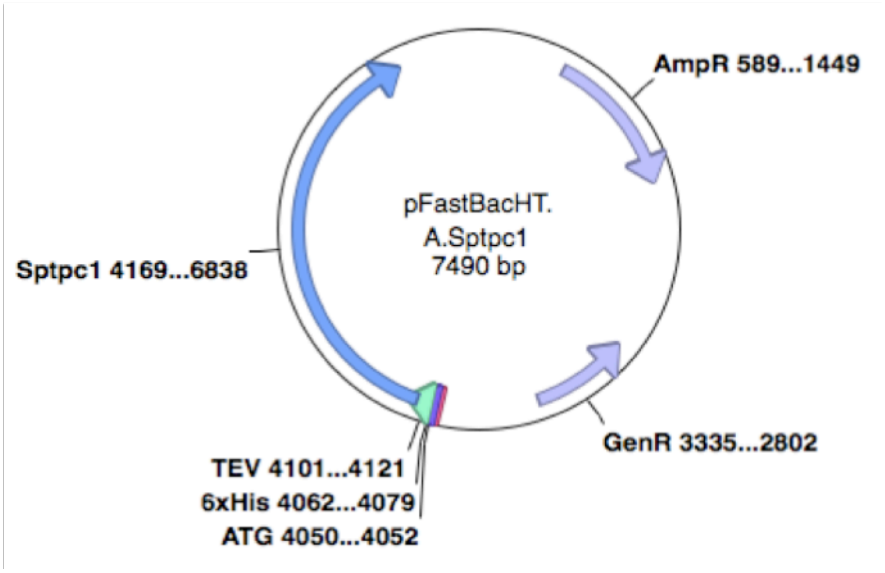
The Bac-to-Bac® Baculovirus Expression System is an efficient method for producing recombinant baculovirus for protein expression in insect cells. This system relies on the generation of recombinant baculovirus, by site-specific transposition in *E. coli*, rather than homologous recombination in insect cells.

3.3.8.1. Expression of TPCs in insect cells

pFastBacHT.A.His-TPC plasmids were generated for the expression of recombinant TPC proteins in Sf9 cells. Coding sequences for *Sp*TPC1, *Hs*TPC1 and *Hs*TPC2 were amplified using the primers shown in *Appendix 5.5* and inserted into the pFastBacHT.A vector (Invitrogen) at the appropriate restriction sites (Figure 3.15).

The correct insertion and sequence were confirmed by DNA sequence analysis. The recombinant plasmids were transformed into DH10Bac^{TM} competent cells, which contained the bacmid with a mini-attTn7 target site and the helper plasmid. The mini-Tn7 element on the pFastBac^{TM} donor plasmid can transpose to the mini-attTn7 target site on the bacmid, in the presence of transposition proteins provided by the helper

A.



B.

NotI-*Hs*TPC1-XbaI
NotI-*Hs*TPC2-XbaI
NotI-*Sp*TPC1-XhoI

Figure 3.15. Cloning of *Hs*TPCs and *Sp*TPC1 into pFastBac™ donor plasmid
A. Maps of SpTPC1 and HsTPCs expression constructs generated using pFastBacHT. B. Fragments of *Hs*TPC1, *Hs*TPC2 and *Sp*TPC1 were generated by PCR to introduce the indicated restriction sites. Full length insert sequencing confirmed the successful sub-cloning of the gene of interest. IMAGE CLONEs were purchased and used as template for *Hs*TPCs (see *Appendix 4*).

plasmid. Colonies containing recombinant bacmids were identified by disruption of the lacZα gene, which allowed the visual selection of positive colonies. Recombinant bacmid was also selected on the same plate using gentamicin, kanamycin and tetracycline.

3.3.8.2. Confirmation of integration of TPCs into bacmid DNA

Potentially recombinant bacmid DNA was isolated from selected white colonies, by high molecular weight mini-prep, and its transposition was confirmed by PCR analysis using a primer set (M13F, M13R; see *Appendix 5.5*), followed by agarose gel electrophoresis. Four clones of successful transposition for each construct were confirmed (Figure 3.16).

3.3.8.3. Infection of insect cells with recombinant baculovirus particles

Initially, 9 x 10^5 cells in 6 well plates were transfected with bacmid DNA using Lipofectamine 2000. Some 3 - 4 days later, viral supernatant was taken and used for a second infection at a 1:10 dilution. The third viral amplification was carried out in a 10 cm dish, the viral supernatant (P3) being kept at 4°C. The remaining cells were lysed with 4x SDS-PAGE buffer, and samples were separated by SDS-PAGE. The target protein was detected by the anti-6x His antibody using Western blotting (Figure 3.17A).

The expected molecular weights of *Sp*TPC1, *Hs*TPC1 and *Hs*TPC2 are 118, 100 and 91 kDa respectively. The bands detected by the anti-His antibody (Figure 3.17) were of slightly larger size than expected, although given that protein expression is

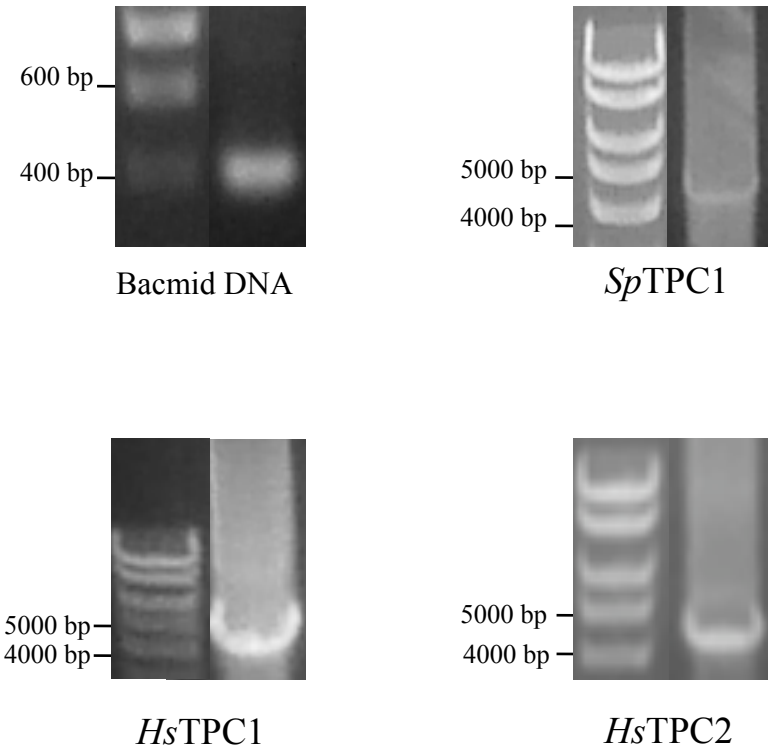


Figure 3.16. PCR analysis of recombinant bacmid
Transposition of the gene of interest was examined by PCR, using recombinant bacmid DNA isolated from white colonies as a template. PCR products from successful transposition of *Sp*TPC1, *Hs*TPC1 and *Hs*TPC2 were 4629 bp, 4431 bp and 4236 bp respectively. The size of the band from bacmid DNA without insertion was ~ 300 bp, shown as a control. The first lane, from the left on each panel, shows a DNA molecular weight marker (HyperLadder^{TM}I, BIOLINE). The screening primer set (M13F or M13Rev) for the PCR reaction is listed in *Appendix 5* (Band size: 1980 bp + gene of interest).

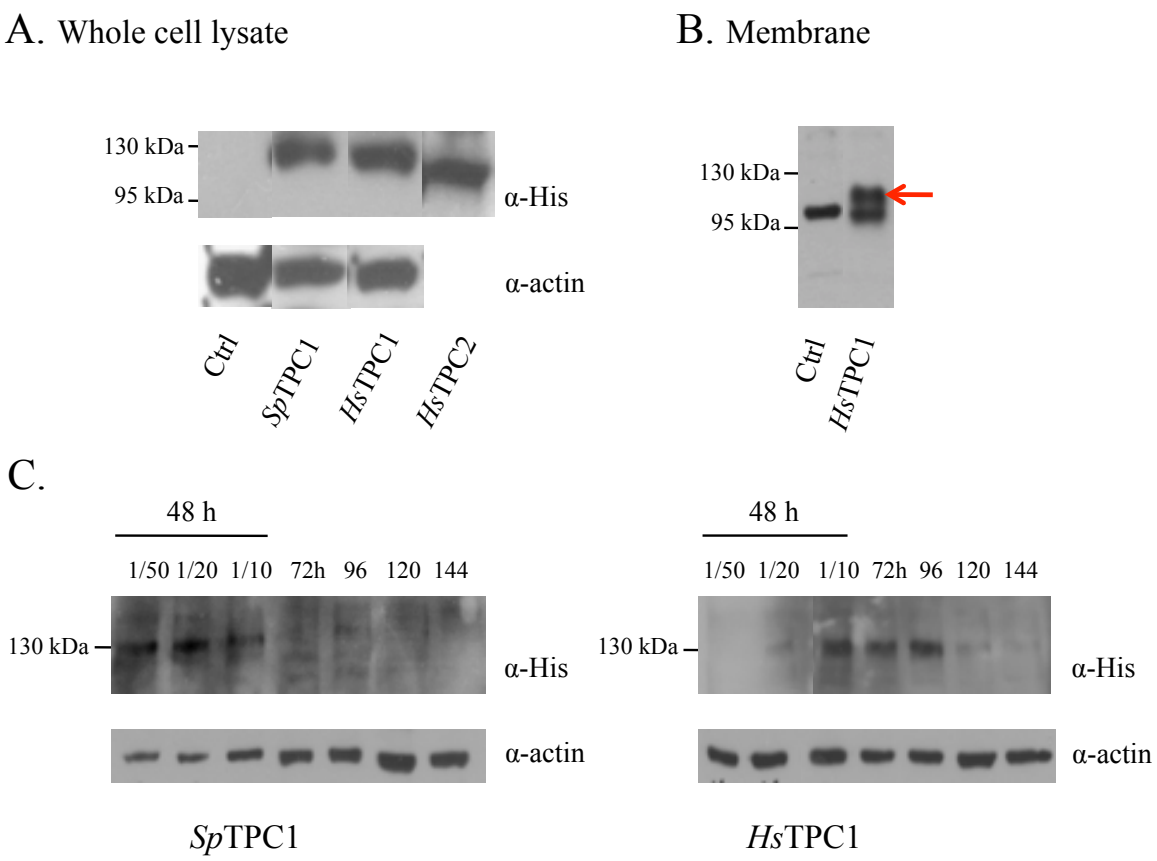


Figure 3.17. Optimization of His- tagged protein expression
Whole cell lysates were obtained after the third infection of bacmid DNA containing the gene of interest. The expression of *Sp*TPC1, *Hs*TPC1, *Hs*TPC2 and His tag only was examined by Western blotting using anti-His antibody (Roche). The expected molecular weights of *Sp*TPC1, *Hs*TPC1 and *Hs*TPC2 were 118, 100 and 91 kDa respectively. The blot was re-probed with α-actin antibody to show equal loading (A). Membrane prepared from Sf9 cells expressing *Hs*TPC1 was also detected using anti-His antibody (B), which shows that the lower band is non-specific, endogenous protein and the upper band is the protein of interest (red arrow). Expression levels of *Sp*TPC1 and *Hs*TPC1 were compared following infection by different dilutions of virus, and different incubation periods after infection. Infected cells at virus dilutions of 1:50, 1:20 and 1:10 were harvested 48 hours later, and that of the 1:10 dilution was harvested 48, 72, 96, 120 and 144 hours after infection. Reprobing with an anti-actin antibody confirmed equal loading (C).

incubation time-dependent, it was decided to analyze this result further. The proteins were detected using two different anti-His antibodies purchased from Roche and Sigma (see details in *Chapter 2*). Both anti-His antibodies recognized bands at the same molecular weight. Next, membrane was prepared from Sf9 cells expressing recombinant TPC proteins and then further separated on SDS polyacrylamide gels, followed by Western blotting analysis. Successful expression of all 3 recombinant proteins was apparent (data not shown). To obtain a larger volume of virus stock, cells plated on 15 cm dishes were infected using P3 virus at a 1:10 dilution, incubated for 5 days (P4), and used in the recombinant protein expression assay.

3.3.8.4. Expression levels of TPC recombinant proteins in Sf9 cells

In order to optimize the recombinant protein expression level, P4 virus was diluted at 1:10, 1:20 and 1:50 and the protein expression level determined, by Western blotting, after 48 h. In addition, cells infected by a 1:10 dilution of P4 virus were incubated for 48, 72, 96, 120 and 144 h respectively. As shown in Figure 3.17, His-tagged recombinant proteins of *Sp*TPC1, *Hs*TPC1 and *Hs*TPC2 were successfully expressed in Sf9 cells. The highest expression of *Sp*TPC1 appeared at a 1:20 dilution of the virus and after 48 h. On the other hand, the expression of *Hs*TPC1 increased for up to 96 h with a 1:10 dilution of the virus.

3.3.9. NAADP binding activity of membranes prepared from Sf9 cells expressing TPCs

The [^{32}P]NAADP binding assay was carried out on membranes prepared from Sf9 cells that expressed *Sp*TPC1, *Hs*TPC1 and *Sp*TPC2, in the presence or absence of

1 mM unlabelled NAADP. Although there appeared to be a trend towards some enhancement of specific binding to the membranes in the presence of TPCs, the difference in binding between Sf9 control membranes and membranes from cells expressing recombinant proteins was not significant (data not shown). In an attempt to increase the amount of specific binding, further experiments were performed to optimize the conditions of the binding assay by varying the incubation temperature (room temperature or on ice), the incubation time of the [^{32}P]NAADP binding reaction (20, 30 and 40 min), the amount of [^{32}P]NAADP (0.2, 0.4 and 0.8 nM), the amount of protein per reaction, and preparation of membranes either by solubilisation or sonication. In addition, after incubation of [^{32}P]NAADP with the membranes for 40 min, 3000-PEG or 8000-PEG was added to the reaction tube to precipitate all protein-ligand complexes, and this was followed by scintillation counting of the radioactivity associated with each pellet (data not shown). PEG precipitation was originally developed to separate antibody-bound and unbound peptide hormones by distribution into an aqueous polymer two-phase system (Desbuquois and Aurbach, 1972). This method has been successfully used for the assay of radioligand binding to soluble receptors. None of these techniques improved binding (data not shown).

In further experiments, *Hs*TPC1 and *Hs*TPC2 were co-expressed on the basis that this might stabilize *Hs*TPC complexes, since it has been suggested that *Hs*TPC may be dimerized; however, it is not known whether *Hs*TPCs form homo- or hetero-dimers (Zong *et al*., 2009). An unrelated protein, FancI, involved in DNA repair and so not a candidate for NAADP binding, was also used as a negative control. Despite these attempts to optimize conditions, analysis of the data showed that there was no significant difference in NAADP binding between uninfected cells, FancI-expressing

cells and TPC2 expressing cells (data not shown). Therefore, as an alternative strategy, NAADP binding to purified TPC proteins was investigated.

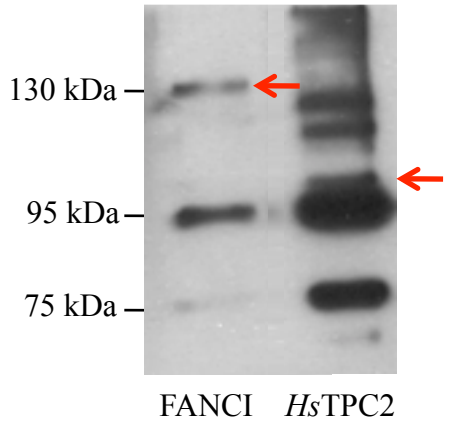
3.3.9.1. Purification of *Hs*TPC2 using a nickel column

Histidine-tagged protein has a high selective affinity for Ni^{2+}, consequently a protein containing a His tag will be bound selectively to metal ion charged media; other cellular proteins will not bind, or will only bind weakly and hence will be removed during the washing steps, depending on the buffer conditions adopted. Sf9 cells expressing histidine-TPC fusion proteins were homogenized and homogenates applied to nickel columns (HisTrapTM FF Columns: GE Healthcare). Purification efficiency was analyzed by Western blotting (Figure 3.18A). Bands of the appropriate size for FancI (negative control) and *Hs*TPC2 were detected; however, much stronger non-specific bands were observed in both cases. The purification of recombinant protein using cobalt resin (HisPur^{TM}CobaltResin: Thermo Scientific) was less successful (data not shown). Therefore, protein purified using a nickel column was employed in subsequent further analysis.

3.3.9.2. NAADP binding assay applied to purified recombinant protein

FancI and *Hs*TPC2 were purified using nickel resin columns and incubated with or without 1 mM unlabelled NAADP for 20 min prior to incubation with [^{32}P]NAADP for 40 min at room temperature. The binding reaction was terminated by filtration, using an ice cold washing buffer. There was no significant difference in specific NAADP binding between the two samples (Figure 3.18B). No correlation between over-expression of *Hs*TPC2 and [^{32}P]-NAADP specific binding was demonstrated.

A.



B.

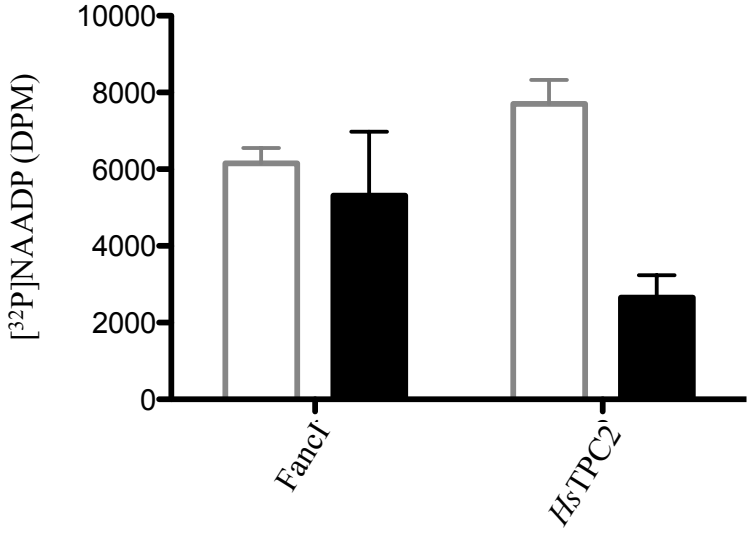


Figure 3.18. [^{32}P]NAADP specific binding of purified protein
*Hs*TPC2 and FANCI were purified using HisTrap™ FF columns (GE Healthcare Life Sciences). Purified proteins were detected with anti-His antibody. FancI and *Hs*TPC2 are indicated by the arrows (A). The results of the [^{32}P]NAADP binding assay using 10 µg / reaction of purified FANCI and *Hs*TPC2 are shown in (B). The binding reaction was carried out at room temperature and terminated by filtration using ice cold washing buffer, after 40 min incubation with 0.4 nM [^{32}P]NAADP (n = 1: tripricated).
□: Non-specific binding, ■: Specific binding

3.4. Discussion

3.4.1. Expression of *Sp*TPC recombinant proteins

Western blot analysis using either anti-mRFPmars or anti-HA antibodies demonstrated that mRFPmars and HA fusion proteins of *Sp*TPCs were successfully expressed in HEK293T cells. Appropriate molecular weight bands for each *Sp*TPC were detected (130 kDa for *Sp*TPC1, 120 kDa for *Sp*TPC2 and 125 kDa for *Sp*TPC3). In addition, there were bands above 250 kDa for mRFPmars-tagged *Sp*TPC2, and HA-tagged *Sp*TPC2 and *Sp*TPC3. These higher molecular weight bands may well be glycosylated forms of *Sp*TPC2 and *Sp*TPC3 or dimerized/aggregated form, as the former observed in heterologously expressed *Mm*TPC1 and *Mm*TPC2 in HEK cells (Zong *et al*., 2009). Recombinant *Hs*TPC2 (Calcraft *et al*., 2009), and *Hs*TPC1 and *Hs*TPC2 (Hooper *et al.*, 2011), overexpressed in HEK cells are also glycosylated, and more recently, it has been shown that both endogenous and heterologously expressed *Sp*TPC2 are modified by N-glycosylation (Galione *et al*., 2010). In the latter paper, glycosylation of *Sp*TPC3 was not shown; however, N-glycosylation sites found in *Sp*TPC2 are conserved in *Sp*TPC3, and these residues are in the same position as in *Hs*TPC1 and *Hs*TPC2. Alternatively, it is possible that the band observed at 250 kDa could represent aggregates rather than glycosylated forms of TPCs.

The conclusion that may be drawn from these data is that I have successfully generated antisera recognizing *Sp*TPC3. This finding was demonstrated by the recognition of mRFPmars or HA fusion proteins of *Sp*TPC3 using Western blot techniques, and by recognition of *Sp*TPC3 in immunoprecipitation experiments. However, the attempts to generate antibodies against *Sp*TPC1 and *Sp*TPC2 were not successful, as assessed either by Western blot or immunoprecipitation studies.

3.4.2. Localization studies

The data presented in this chapter provide strong evidence that recombinant *Sp*TPCs, expressed in HEK293 cells, are located on intracellular membranes. *Sp*TPC1 is found predominantly in the ER, *Sp*TPC2 in lysosomes and *Sp*TPC3 in an, as yet, unidentified membrane compartment. There is a predicted, lysosomal targeting signal peptide, the dileucine motif, in *Hs*TPC1 and *Hs*TPC2 consisting of [D/E]xxxL(L/I). Expression of *Hs*TPC2, lacking residues 3 - 25, including the dileucine motif, redirected *Hs*TPC2 to the plasma membrane (Brailoiu *et al*., 2010b). The same authors reported that *Hs*TPC1 and *Hs*TPC2 expressed in SKBR3 cells were located in endolysosomal and lysosomal compartments, respectively (Brailoiu *et al*., 2009), supporting the idea that correct targeting of these proteins is maintained when they are expressed in host cells. However, the dileucine motif is not found in any *Sp*TPCs.

For sea urchin TPCs, it was reported that all isoforms of *Sp*TPC, expressed in SKBR3 cells, localize to acidic organelles; furthermore, NAADP-mediated Ca^{2+} transients were also demonstrated in these cells (Brailoiu *et al*., 2010a). In the experiments presented in this chapter, the localization of mRFPmars- or HA-tagged recombinant *Sp*TPCs, transiently expressed in HEK293 cells, was determined. *Sp*TPC2 localized to lysosomes, and this was confirmed by LysoTracker Green co-localization studies in live cells, which were stably expressing *Sp*TPC2 (Ruas 2010). Transiently expressed recombinant *Mm*TPC2 protein is predominantly localized to both lysosomes and the ER, although *Mm*TPC2 expressed on the ER appears not to be functional, that is, when cells were treated with bafilomycin A1 to selectively inhibit lysosomal function, prior to the application of NAADP, no response to NAADP was observed (Zong *et al*., 2009).

The co-localization of *Sp*TPC, expressed transiently in HEK cells, with an ER marker was observed. The same localization pattern was seen in a HEK stable cell line that expressed HA-tagged *Sp*TPC1 (analyzed by Dr Davis). In contrast, stably expressed recombinant *Sp*TPC1, with an mRFPmars tag on the N-terminus, clearly associated with lysosomes (Galione *et al*., 2010). One must consider that a transiently expressed protein may distribute or function differently from a stably expressed one (Luo *et al.*, 2003). It could be that the protein, produced by ribosomes attached to the rough-surfaced endoplasmic reticulum, aggregated on the surface of the ER and could not therefore be properly transferred to the Golgi apparatus. In this case, targeting to lysosomes would not be observed. Alternatively, it could be that protein trafficking to lysosomes takes a variable amount of time and that the transiently expressed protein may not yet have reached its final destination.

The distribution of *Sp*TPC3 was not fully elucidated by the studies presented in this chapter; however, *Sp*TPC3 has subsequently been shown to co-localize with LysoTracker Green in HEK cells (Galione *et al*., 2010). A homologue of *Sp*TPC3 has not been found in humans, therefore, it may not be efficient to express *Sp*TPC3 in human cells (although *Sp*TPC3 was still expressed in intracellular compartments). It is noteworthy that transiently expressed chicken TPC3 does not co-localize with stably expressed *Hs*TPC2, which has been shown to be present in lysosomes (Calcraft *et al*., 2009).

3.4.3. NAADP binding

NAADP binding activity was successfully detected in sea urchin homogenates and was enriched in membrane fractions, as previously reported (Churchill *et al*., 2002;

Lewis *et al*., 2007). Anti-*Sp*TPC3 antibody exhibited high specificity to heterologously expressed *Sp*TPC3. NAADP binding activity could also be immunoprecipitated using antisera specific for *Sp*TPC3. This finding is an important demonstration of a link between TPCs and NAADP binding. Although the results do not directly demonstrate that the binding activity resides in the TPC protein (or an associated protein), it is likely that *Sp*TPC3 is at least in part responsible for NAADP binding in the sea urchin egg microsome fraction.

However, no statistically significant increase in NAADP binding activity was detected in HEK cells that expressed either mRFPmars-tagged (data not shown) or HA-tagged recombinant proteins of *Sp*TPCs. Despite the fact that the expression of *Sp*TPC recombinant proteins was confirmed in HEK293 cells, with *Sp*TPC2 found to localize to lysosomes, as predicted, it was not possible to demonstrate a correlation between increased NAADP binding and *Sp*TPC expression in these cells in the current study. In mammalian systems, membranes enriched with *Hs*TPC2 exhibited increased NAADP binding (Calcraft *et al*., 2009). It has been shown in our laboratory that expression of *Sp*TPC2 also enhanced NAADP binding (Ruas *et al*., 2010). NAADP binding to endogenous proteins in sea urchin egg homogenate has been extensively characterized. For instance, the binding is irreversible in the presence of K^+, is inhibited by NaCl or Ned-19, but is insensitive to pH or Ca^{2+} concentration changes (Dickinson and Patel, 2003; Patel *et al*., 2000a; Rosen *et al*., 2009). Therefore, the binding conditions (temperature during incubation, washing buffers used and the K^+ concentration in the washing buffer) were optimized in my studies, based on the currently available information, for both sea urchin and mammalian TPCs. One possible reason why it was not possible to increase NAADP binding by

expression of *Sp*TPCs may relate to the expression system itself. Transiently expressed protein often aggregates, and it is fair to say that unhealthy cells were sometimes observed. An alternative possibility is that expression levels of the recombinant proteins were too low to detect a significant difference in the binding assay. To try to overcome the last problem, *Sp*TPC1 and *Hs*TPCs were expressed in Sf9 cells but, again, there was no enhancement of NAADP binding, even when affinity-purified protein was used. In general, 1 mM unlabelled NAADP used was too high and 100 μM (100 x expected Kd value) should be optimal for binding assay.

It has been shown that NAADP binding is inhibited by peptide blocking when immunoprecipitated recombinant proteins of *Sp*TPC2 and *Sp*TPC3 were assayed (Ruas *et al*., 2010), using the antisera described in this chapter. These results indicate that the anti-*Sp*TPC2 and anti-*Sp*TPC3 antibodies are suitable for immunoprecipitation experiments, but anti-*Sp*TPC1 antibody is not, supporting the data obtained by immunoprecipitation of HA-fusion protein using anti-*Sp*TPC1 and *Sp*TPC3 antibodies. It was not able to show the evidence that TPC is the actual NAADP receptor in this study, as expression of TPC could not enhance NAADP binding, although it is possible that other proteins which are associating and stabilizing NAADP binding complex may be missing and limiting in the expression systems used in these experiments.

Data supporting the concept that TPCs are the NAADP receptors have been reported recently (Patel *et al*., 2011), from experiments in which the authors examined cells that overexpressed TPCs. However, NAADP binding activity was still present in TPC1 and TPC2 -single or -double knockout mice (experiments performed by Ms

Chuang in this laboratory; unpublished data). In addition, photoaffinity labelling of liver extracts with NAADP failed to show a difference between the wild type and the double knock out in both female and male mice, with bands observed at around 30 kDa. Therefore NAADP may not bind to TPCs directly, or requires other ancillary proteins.

3.5. Summary

NAADP binding activity was enriched in *Sp*TPC3 immunoprecipitates from sea urchin egg extracts. Recombinant *Sp*TPCs were successfully expressed in HEK293 cells, confirmed by Western blot analysis using anti-mRFPmars and anti-HA antibodies. The specificities of the anti-*Sp*TPC3 antibody were high enough to recognize their target proteins. In the present study, the localization of mRFPmars or HA fusions of *Sp*TPC1, *Sp*TPC2 and *Sp*TPC3 in HEK293 cells was predominantly on the ER, lysosomes (partially on ER) and an unknown compartment, respectively. Transiently expressed, mRFPmars-tagged *Sp*TPCs slightly, but not significantly, enhanced NAADP binding compared to the control. Expression of HA-tagged *Sp*TPCs in HEK cells, or of His-tagged *Sp*TPCs and *Hs*TPCs in Sf9 cells, did not increase NAADP binding. From these data, it is not clear whether TPCs directly bind NAADP or whether an associated protein is required.

CHAPTER 4

ANALYSIS OF TWO PORE CHANNEL (TPC) PROTEIN AND NAADP BINDING ACTIVITY IN *DICTYOSTELIUM DISCOIDEUM*

4.1. Introduction

Ca^{2+} signalling in *Dictyostelium* has been extensively studied during chemotaxis and cell differentiation following stimulation with extracellular cAMP or DIF. For the former messenger, Ca^{2+} influx or transient Ca^{2+} release in response to cAMP has been examined using whole cells or intracellular vesicles, respectively (Malchow *et al*., 2006; Schaloske and Malchow, 1997). For the latter, a sustained increase in cytosolic Ca^{2+} levels in response to DIF was shown throughout development, providing evidence of a role for intracellular Ca^{2+} as an intermediate for DIF-induced gene expression (Schaap *et al*., 1996). To date, *in vivo* NAADP synthesis in *Dictyostelium* has not been investigated. Indeed, the coding sequence for the orthologue of human cyclic ADP-ribose cyclase/hydrolase **(**CD38), which catalyzes conversion of NADP to NAADP by exchange of nicotinamide for nicotinic acid under acidic conditions *in vitro*, is not found in the *Dictyostelium* genome. Therefore, whether or not NAADP is involved in Ca^{2+} signalling in *Dictyostelium* has not yet been determined, and no studies have been carried out to investigate the role of *Dd*TPC2.

Several studies have provided evidence that intracellular Ca^{2+} levels play a significant role in *Dictyostelium* development and cell-type pattern formation. High cytosolic Ca^{2+} levels were found in stalk cells, whereas cytosolic Ca^{2+} was maintained at low levels in spore cells, in which Ca^{2+} is accumulated in intracellular vesicles (Cubitt *et al*., 1995; Schlatterer *et al*., 2001). It was demonstrated that altering intracellular Ca^{2+} concentration can exert effects on morphogenesis; for instance, elevated intracellular Ca^{2+} levels in the presence of a Ca^{2+} ionophore promoted prestalk pathways, whereas application of EGTA to cells (to buffer Ca^{2+} to low levels) interfered with the differentiation of both cell types (Baskar *et al*., 2000; Cubitt *et al*., 1995; Cubitt *et al.,*

1998). The transcription of prespore genes almost disappears when extracellular Ca^{2+} is chelated (Pinter and Gross, 1995), perhaps due to depletion of Ca^{2+} from intracellular Ca^{2+} stores.

Two penta-EF-hand Ca^{2+} binding proteins (PEF1 and PEF2) show cell-type specific expression as both are expressed in the anterior prestalk region, and PEF-1 is also expressed in the posterior prespore region of mound and early culminants (Ohkouchi *et al*., 2001). This implies an importance for controlling Ca^{2+} concentration both in prespore cells and in prestalk cells in *Dictyostelium*. In the late developmental stages, Ca^{2+} is again elevated in the sorus (the spore cell region of a fruiting body), suggesting there is still active Ca^{2+} signalling going on until the very end of development (Cubitt *et al*., 1995).

The method of using EGTA to chelate extracellular Ca^{2+} contains a degree of uncertainty as to the extent of its effects on intracellular Ca^{2+} stores, and may produce additional unforeseen events due to changes in basal levels of Ca^{2+}, therefore complicating the interpretation of the various results reported so far in the literature. For example, chelation of extracellular Ca^{2+} has been reported to inhibit movement of chemotacting cells in some reports (Malchow *et al*., 1982), but in other cases this appears to be without effect (Van Duijn and Van Haastert, 1992). Such difficulties limit the amount of useful information provided by studies using Ca^{2+} chelators.

Therefore, genetic manipulation may be a better technique to study Ca^{2+} signalling mechanisms in *Dictyostelium*. *Dictyostelium* is known to possess genes encoding intracellular Ca^{2+} channels, including one putative IP_3 receptor, mucolipin and TPC2,

all of which are proteins predicted to be localized to intracellular organelles (Wilczynska *et al*., 2005).

Gene expression of *iplA* (analogous to the IP_3 receptor) is the highest of the intracellular Ca^{2+} channels during aggregation, as quantified by RNA-seq (dictyExpress; Figure 1.5). *IplA* null cells chemotax normally, in spite of the loss of Ca^{2+} influx induced by extracellular cAMP (Traynor *et al*., 2000). In this paper, Ca^{2+} uptake into starving cells following cAMP pulsing was measured either by uptake of $^{45}Ca^{2+}$, or the response to cAMP stimulation was determined by measurement of Ca^{2+} transients in single amoebae using fura 2-dextran. The authors of this study suggested that Ca^{2+} signalling is not required for chemotaxis in *Dictyostelium*.

Although IplA or cAMP-mediated Ca^{2+} influx appears not to be essential for *Dictyostelium* development, this does not rule out an importance for Ca^{2+} transients in the developmental process, since there are other transporters or channels that could potentially compensate for the role of IplA in Ca^{2+} signalling at later stages. Indeed, *mucolipin* and *tpc2*, which are predicted to be prespore genes, are also expressed during aggregation, although mRNA-seq data (dictyExpress) show that expression levels are much lower than that of *iplA*, and rise to a peak at 12 - 14 hours and 16 hours of development, respectively (Figure 1.5).

The lack of effect of disruption of Ca^{2+} influx on *Dictyostelium* development raises the possibility that Ca^{2+} release from acidic organelles may play an important role in the developmental process. HGR8 (a disphosphonate-resistant mutant) and *lvsA*$^-$ strains are impaired in acidic Ca^{2+} store function, the former due to the impaired

proton gradient, and the latter due to loss of the gene encoding large volume sphere A (LvsA), which causes the failure of calmodulin to associate with the CV. In both mutants, calcium induced extravesicular calcium change (CIC) in vesicles from cells harvested at 2 - 4 hours of development was reduced (Malchow *et al*., 2008). The generation time of HGR8 was found to be 1.6 times longer than that of Ax2, whereas the *lvsA* mutant was not defective in development (Bof *et al*., 1992; Kwak *et al*., 1999). The authors suggested that mucolipin might be operating CIC, as gene expression of *mucolipin* begins earlier than *Dd*tpc2 during aggregation. However, further data is not available regarding this, and no developmental studies have been carried out on *mucolipin* null strains. Therefore, it has not yet been established whether mucolipin, TPC2 or both are required for chemotaxis.

4.2. Aims

The aim of this study was to analyze the role of TPC2 in *Dictyostelium* development by investigating protein expression levels during the developmental cycle, and the localization of both endogenous and homologously/heterologously expressed *Dd*TPC2. To gain further insight into the function of *Dd*TPC2 in *Dictyostelium*, NAADP binding to membrane fractions of Ax2 cells was studied at different stages of development (four and twenty hours), and the development of a strain in which *Dd*TPC2 was disrupted was also examined.

4.3. Results

4.3.1. Putative TPC2 in *Dictyostelium*

A BLAST search of *Dictyostelium* predicted proteins with human TPC2 (*Hs*TPC2) homology revealed one open reading frame with significant homology. The predicted protein sequence for *Dd*TPC2 shows 30% identity and 48% similarity to human TPC2. *Dd*TPC2 also shows high homology to *Mus musculus* TPC2 (*Mm*TPC2), *Danio rerio* TPC3 (*Dr*TPC3), *Equus caballus* TPC3 (*Ec*TPC3), and *Gallus gallus* TPC3 (*Gg*TPC3). Alignment of protein sequences is shown in Figure 4.1A and B.

The open reading frame predicts a protein of 2060 amino acids with an expected molecular weight of 237 kDa. Bioinformatic analysis (the list of web resources is shown in Appendix 7) reveals that *Dd*TPC2 possesses a Ca^{2+}-binding EF-hand motif (Friedrich *et al*., 2006), an ion transfer domain (Pfam) (Bateman *et al*., 2002), and 2x5 (10 total) predicted transmembrane domains (TMHMM) (Figure 4.2). Alignment of the EF-hand motif in comparison to those found in other species is shown in Figure 4.3: all TPCs examined are 12 transmembrane domain proteins, except for *Dd*TPC2 (Krogh *et al*., 2001). A repetitive sequence of TAA (42 x TAA) appears at 2949 bp downstream of the putative start codon, which is not found in *tpc*s of other species.

N-glycosylation sites have been reported in *Hs*TPC1 at residues 599, 611, and 616, in *Hs*TPC2 at residues 611 and 618, and in *Mm*TPC2 at residues 594 and 601 (Hooper *et al*., 2011). There are no glycosylation sites predicted in *DdTPC2*, but protein alignment shows that N273 and N618 are conserved in *Dictyostelium* (Figure 4.1A and B, respectively). In other organisms, leucine L265 (*Hs*TPC2) is highly conserved

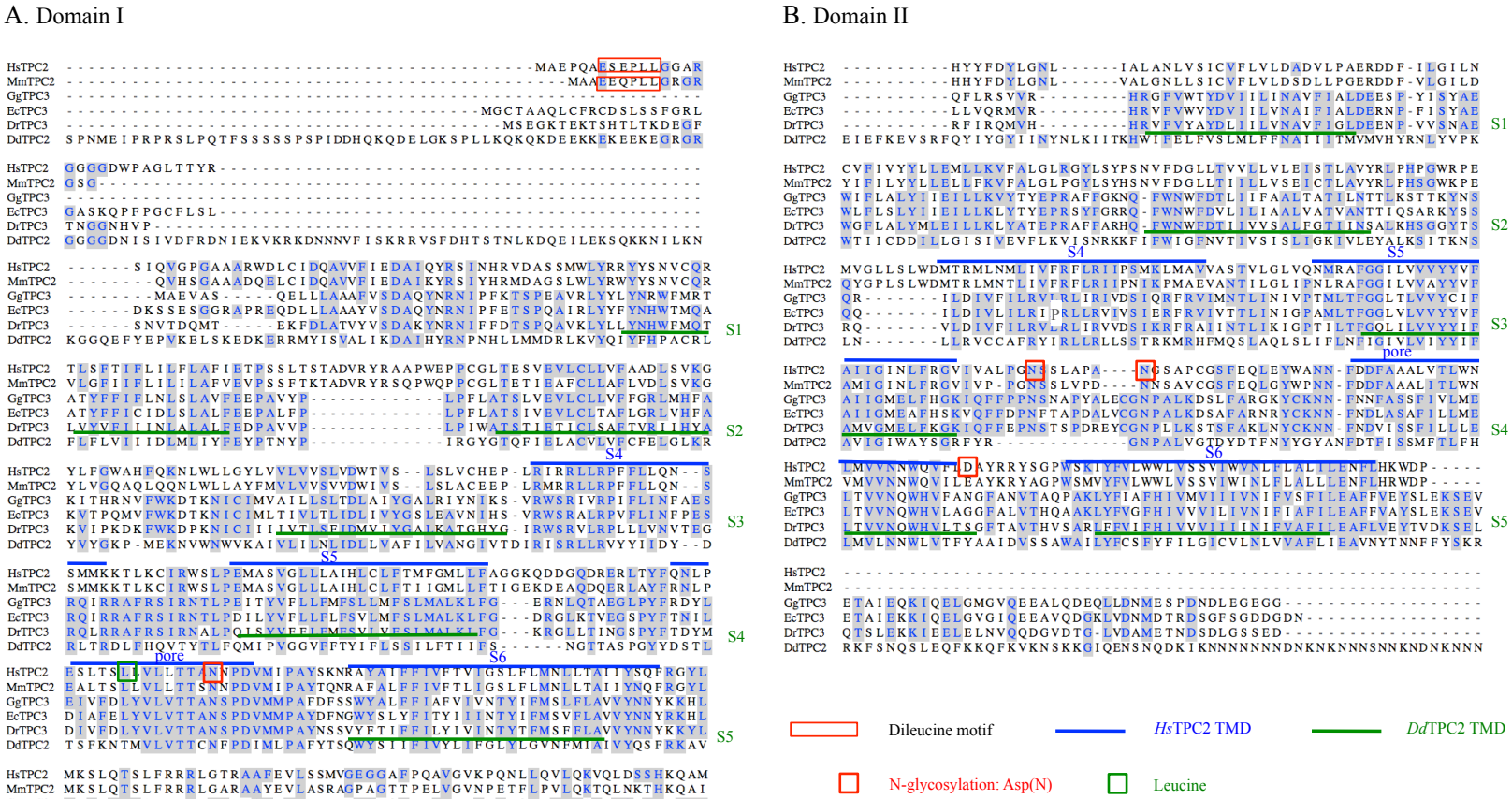


Figure 4.1. Protein alignment of TPC2 and TPC3 in various species

Protein sequences of *Homo sapiens* TPC2 (*Hs*TPC2), *Mus musculus* TPC2 (*Mm*TPC2), *Gallus gallus* TPC3 (*Gg*TPC3), *Equus caballus* TPC3 (*Ec*TPC3), *Danio rerio* TPC3 (*Dr*TPC3) *and Dictyostelium discoideum* TPC2 (*Dd*TPC2) were aligned using ClustauW (and identical residues to consensus are highlighted with blue text and light grey background using Mobyle portal. The first half of each predicted transmembrane domain (TMD) for *Hs*TPC2 (blue bars) and for *Dd*TPC2 (green bars) is shown in A, and the second half is shown in B. Aspartic acid (N) residues, which are the sites of N-glycosylation in *Hs*TPC2, are enclosed with red squares. A leucine (L), conserved in most species and proposed to be important for the pore region, is enclosed with a green square.

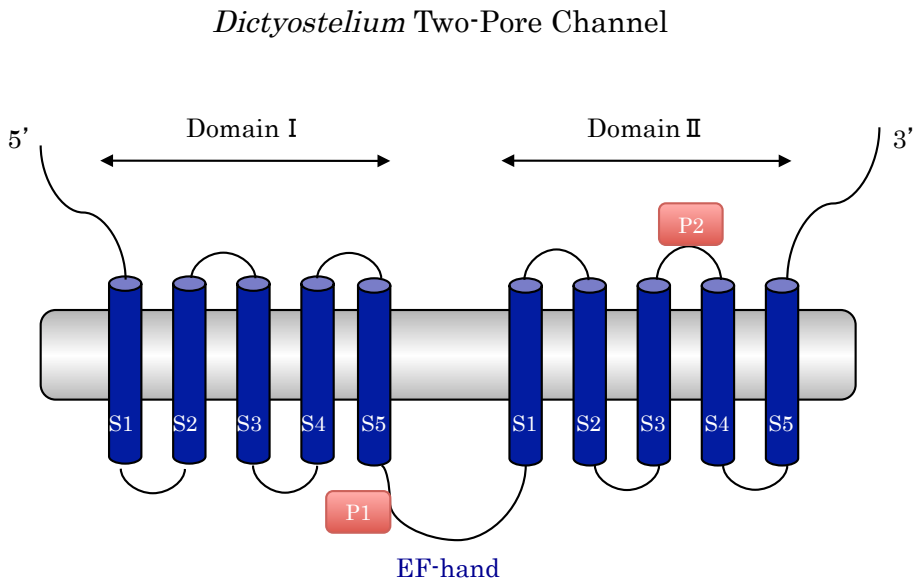


Figure 4.2. Topology of putative *Dd*TPC2
The predicted topology of *Dd*TPC2 is shown. *Dd*TPC2 consists of 2060 amino acids and is predicted to contain a Ca^{2+}-binding EF-hand and 2 x 5 (10 total) putative transmembrane domains (blue cylinders). The expected molecular weight is 237 kDa. The positions of two peptides, P1 and P2, selected to raise anti-*Dd*TPC2 antibodies are shown as red rectangles, and their sequences are shown below. P1 had an extra cysteine residue (shown in red) added at the N terminus to facilitate coupling.



Figure 4.3. The EF-hands
Putative EF hand regions (aligned for comparison) found in *Dictyostelium discoideum (DdTPC2), Arabidopsis thaliana (AtTPC1), Oryza sativa* (*Os*TPC1) *and Triticum aestivum* (*Ta*TPC1). The identical residues to consensus are indicated with red and the number of amino acids from M1 is shown on the right hand side

and is located in the pore region. Replacing L273 in *Hs*TPC1, which is equivalent to L265 in *Hs*TPC2, with proline was found to abrogate Ca^{2+} release by NAADP (Patel *et al*., 2010). In *Dictyostelium*, this residue is not conserved, and instead threonine is found at this position (Figure 4.1A and B). Instead, the leucine at L268 is conserved throughout the species examined. A dileucine motif responsible for lysosomal targeting of *Hs*TPC2 (Brailoiu *et al*., 2010b) is not apparent in the N or C-terminal region of *Dd*TPC2 (Figure 4.4). However, *Dd*TPC2 is predicted to be on the CV (Wilczynska *et al*., 2005), based upon the findings of a paper showing that *At*TPC1 localizes to the CV (Peiter *et al*., 2005).

4.3.2. Developmental delay in GPN-treated *Dictyostelium* cells

As a means to assess rapidly whether Ca^{2+} responses involving acidic stores might be involved in development, *Dictyostelium* cells were treated with glycyl-1-phenylalanine-β-naphthylamide (GPN). GPN is a cell permeable compound that is hydrolysed by cathepsin C inside lysosomes and causes disruption of lysosomes via osmotic swelling (Churchill *et al*., 2002; Galione and Churchill, 2002). It has been reported previously that GPN inhibits NAADP-induced Ca^{2+} release from acidic stores in mouse pancreatic acinar cells (Yamasaki *et al*., 2004). Therefore, the effect of GPN on the development of *Dictyostelium* was examined here by developing *Dictyostelium* Ax2 cells on filters soaked in increasing concentrations of GPN. At concentrations of GPN above 800 μM, the development was blocked at mounds stage and delayed in fruiting body formation (Figure 4.5). In contrast, no effects of bafilomycin A1, a V-type H^+-ATPase inhibitor (Aubry *et al*., 1993), and cis-Ned-19, an antagonist of NAADP (Rosen *et al*., 2009), were seen (data not shown). The ED_{50}

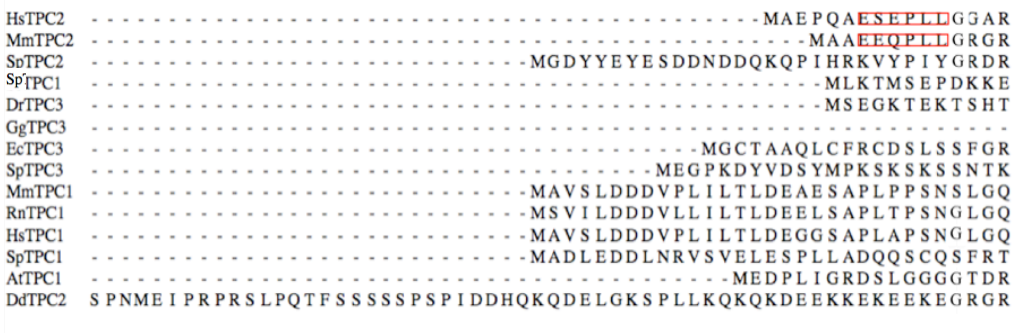


Figure 4.4. Dileucine motifs responsible for lysosomal targeting of TPC2
The dileucine motif (D/E)XXXL(L/I), believed to be responsible for lysosomal targeting of *Hs*TPC2, is highlighted for both *Hs*TPC2 and *Mm*TPC2 with a red rectangle. Protein sequence of *Danio rerio* TPC3 (*Dr*TPC), *Gallus gallus* TPC3 (*Gg*TPC3), *Equus caballus* TPC3 (*Ec*TPC3), *Rattus norvegicus* TPC1 (*Rn*TPC1) and *Arabidopsis thaliana* TPC1 (*At*TPC1) were aligned using ClustalW.

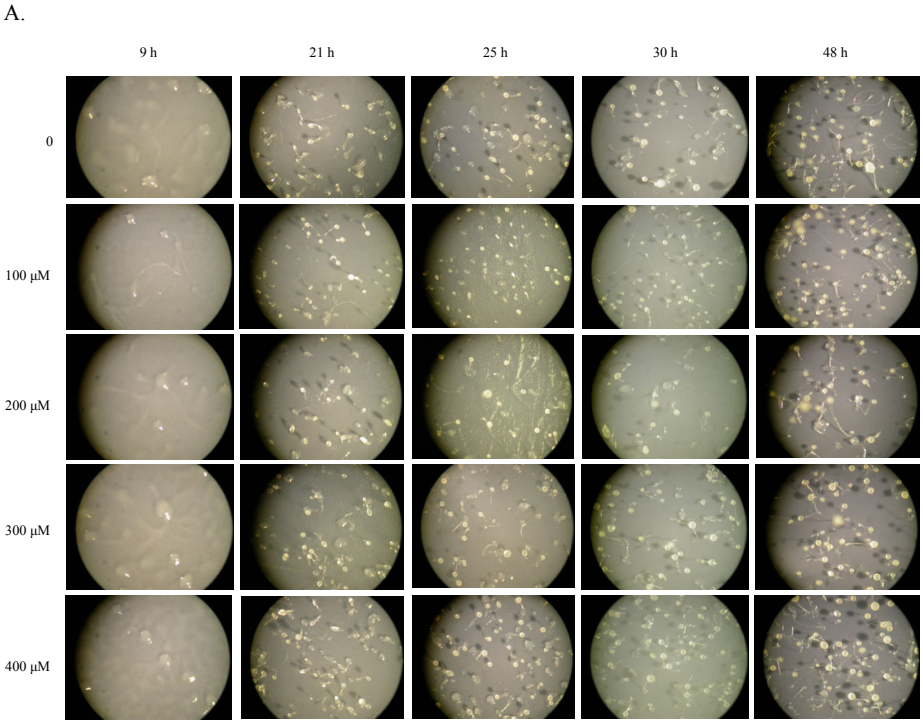
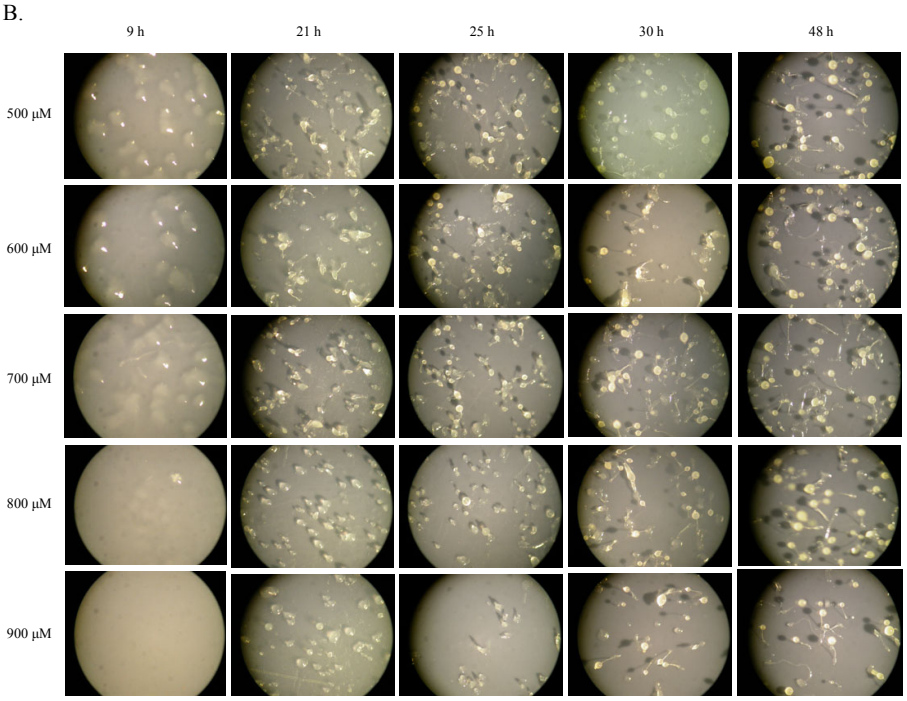
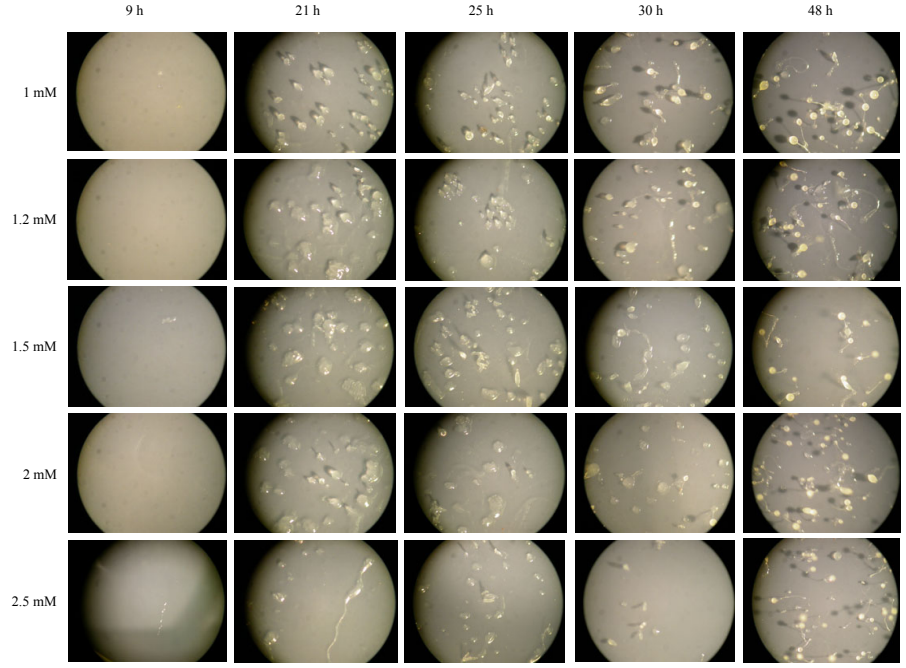


Figure 4.5. The effect of GPN on the development of *Dictyostelium discoideum*
Exponentially growing cells were plated on filters at a density of 2.2 x 10^6 cells/cm^2 to initiate development. The GPN concentrations used are shown to the left of the relevant set of images. Panel A, B and C show data for GPN concentrations of 0 – 400 µM, 500 – 900 µM and 1 – 2.5 mM, respectively. GPN was dissolved in DMSO at the final concentration of 1%.

B.


9 h
21 h
25 h
30 h
48 h
500 µM
600 µM
700 µM
800 µM
900 µM

C.


9 h
21 h
25 h
30 h
48 h
1 mM
1.2 mM
1.5 mM
2 mM
2.5 mM

values of many drugs for *Dictyostelium* are 10-100 times higher than those for other species (Alexander *et al*., 2003; Dhar and Lippard, 2009; Terbach *et al*., 2011), and the maximum concentrations of bafilomycin A1 and Ned-19 which could be applied in these experiments (due to practical considerations) were 10 μM and 100 μM, respectively. These concentrations may not be high enough to inhibit development of *Dictyostelium*.

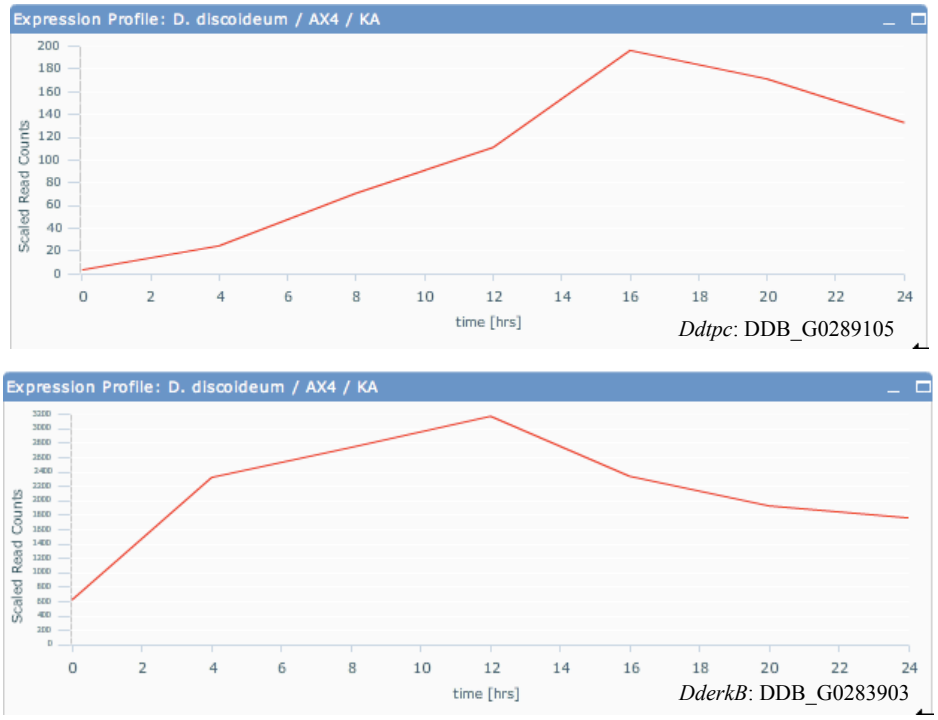
4.3.3. Levels of *Dd*TPC2 mRNA during development

Understanding the timing of gene transcription and protein expression is helpful to characterize the function of a target protein, especially since *Dd*TPC2 is predicted to function as a Ca^{2+} channel, and since the intracellular Ca^{2+} level is controlled during *Dictyostelium* development, the concentration depending on the cell type (Cubitt *et al*., 1995). The timing of protein expression may help to reveal whether the protein may be involved in growth, early development including chemotaxis, or late development when cell differentiation occurs.

To investigate this, Northern blotting was carried out using a 783 bp fragment (*Appendix 5.6*) as a probe labelled with [α-^{32}P]dCTP or [α-^{32}P]dATP. Total RNA was extracted from Ax2 cells at different stages of development; however, *Ddtpc2* was not detectable (data not shown). The subsequent to these experiments, the expression profile for *Dd*TPC2 mRNA levels quantified by RNA-seq became available on dictyBase (dictyExpress) (Parikh *et al*., 2010). The time course of the expression profile represents the abundance of mRNA in the cell population at different stages of development on nitrocellulose filters. *Dd*TPC2 mRNA levels are low in growing cells, increase gradually during development and reach a peak 16 hours after

starvation; this is followed by a downward trend (Figure 4.6A). In order to confirm expression throughout the developmental life cycle in Ax2 cells, RT-PCR was performed. Total RNA from Ax2 cells at different developmental stages was used to amplify a 783 bp fragment (F3), which is 1979 bp downstream from a putative ATG start codon. *ErkB* mRNA expression was also examined as a control. The primer sets used are shown in Appendix 5.6. PCR products obtained with 40 cycles and 30 cycles of amplification for *Ddtpc2* and *erkB* respectively were resolved on an agarose gel to determine the presence of transcripts by visual comparison during exponential amplification. The mRNA expression of *Ddtpc2* was detected during vegetative growth and throughout development (Figure 4.6B). DNA sequencing confirmed that the band in lane T20 was amplified from *Ddtpc2*. The *erkB* control also confirmed that these bands were dependent on reverse transcriptase (RT), since there are two introns within the gene, therefore the smaller fragment obtained here was derived from cDNA. The RT-PCR products of *erkB* from mRNA and gDNA have different sizes, 1108 bp and 1426 bp respectively. The size detected here is consistent with there being no introns present. This result is in agreement with the RNA-seq data on dictyBase, showing transcription of *Ddtpc2* throughout development. Attempts to examine the expression pattern by Northern blot were not successful (data not shown), although other transcripts could be detected. This would be consistent with low expression levels of *Ddtpc2* mRNA, as suggested by the RNAseq data. The prespore/prestalk RNA-seq data shows that the *Ddtpc2* transcript is highly enriched in prespore cells, indicating that *Dd*TPC2 may have a role at late developmental stages, especially in prespore cells.

A.



B.

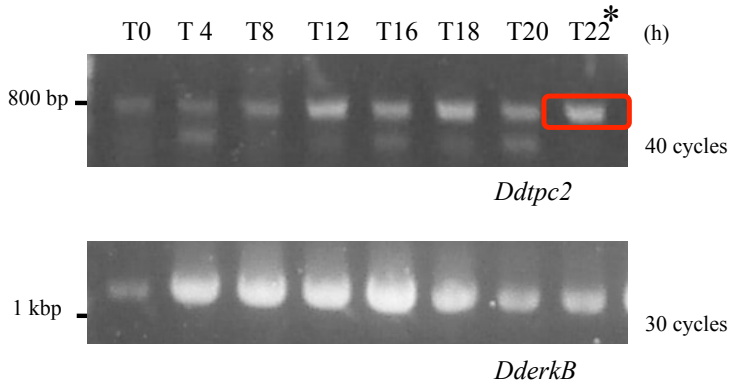


Figure. 4.6. Developmental expression of *Dd*TPC2 mRNA
RNA-seq data from dictyBase (Parikh *et al*., 2010) is shown in (A). Ax2 cells were developed on 2% agar and total RNA was extracted at various times during development (T0 - T22). RNA isolated at different developmental stages was treated with DNase, followed by one-step RT-PCR (B). A part of *Ddtpc2* (783 bp) and full-length *erkB* (1108 bp) were amplified by RT-PCR using the primer sets KW56/KW57 and ERK-F5/ERK-R2, respectively. The cycle number for PCR is indicated. PCR products were resolved on 1% agarose gel and visualized by staining with ethidium bromide (N=1). The RT-PCR product highlighted in red in the upper panel of B was confirmed to be amplified from *Ddtpc2* by sequencing. The primer details are given in *Appendix 5.6*. * TX designates the time (hours) after initiation of development.

4.3.4. NAADP binding activity in *Dictyostelium* cells

To investigate the involvement of *Dd*TPC2 in NAADP-mediated Ca^{2+} signalling in *Dictyostelium*, NAADP binding to membranes, enriched in intracellular vesicles, was examined.

4.3.4.1. Fractionation of intracellular Ca^{2+} stores

Vesicle preparation to generate 2 membrane fractions (P0, P1) was adapted from the procedure described by Malchow (Malchow *et al*., 2008) (Figure 4.7). These authors suggested that P0 was enriched in vesicles derived from the contractile vacuole (CV), and that P1 was enriched in endoplasmic reticulum (ER), although the percentage of CV and ER were reported to be 42% and 34% for P0, and 34% and 43% for P1, respectively (Malchow *et al*., 2006). Firstly, vesicle fractions, P0 and P1, were prepared from Ax2 *Dictyostelium* cells expressing dajumin-GFP or calnexin-GFP developed for 4 hours in shaking suspension (T4), to allow examination of the distribution of the CV and ER as potential intracellular Ca^{2+} stores (Gabriel *et al*., 1999; Müller-Taubenberger *et al*., 2001). As shown in Figure 4.8, the dajumin-GFP fusion protein, a CV marker, was mainly detected in the P1 fraction, whereas calnexin-GFP, an ER marker, was detected in both P0 and P1 fractions. As P1 contained both membranes, it was used for most of the NAADP binding assays.

4.3.4.4. NAADP binding to membrane fractions

It has been proposed that mammalian TPC2 proteins are NAADP-dependent Ca^{2+} channels. We therefore investigated the ability of membranes from *Dictyostelium* to bind to NAADP using radioligand binding techniques (Lewis *et al*., 2007). P0 and P1

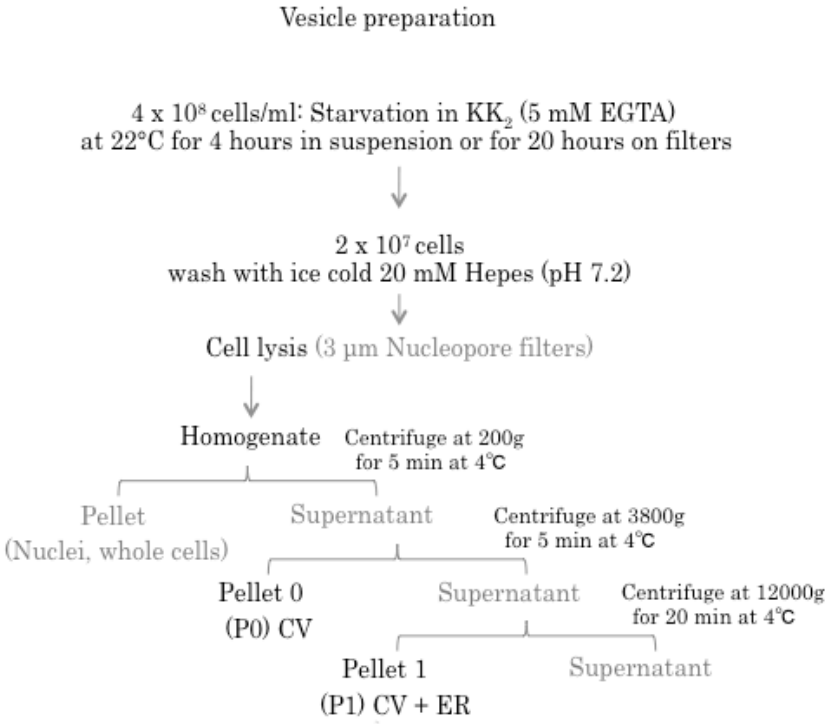


Figure 4.7. Flow chart to illustrate membrane preparation methodology
Dictyostelium cells were harvested at different developmental stages. Pellet 0 (P0) and pellet 1 (P1) were resuspended in 60 and 50 µl, respectively, of Buffer 2. All processes were carried out in a cold room (4°C) and on ice. Method adapted from Malchow *et al*., 2007.

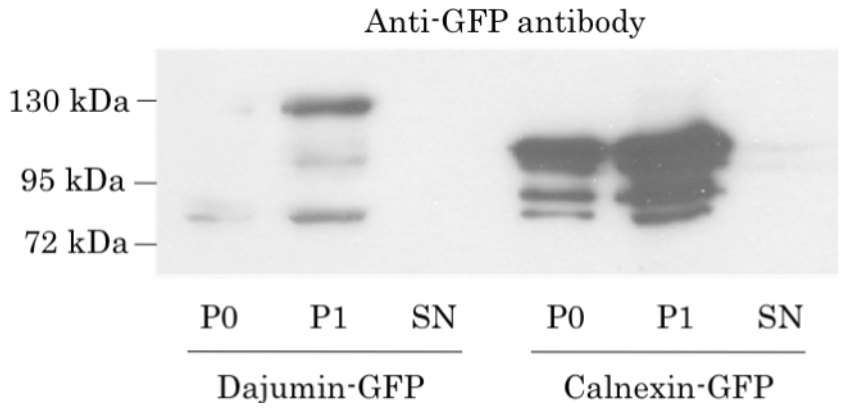


Figure 4.8. Separation of CV and ER membrane fractions
Membrane fractions P0 and P1, and supernatant (SN) were prepared from Ax2 cells expressing GFP fusions of dajumin or calnexin, following 4 hours of starvation. 15 μg of protein was loaded on a 10% SDS polyacrylamide gel and subjected to western blot using anti-GFP antibody (1:200). The expected molecular weight of each protein is 86 kDa for GFP-dajumin and 87 kDa for GFP-calnexin (Muller-Taubenberger *et al*., 2001). A high MW band observed at 130 kDa is likely to be O-glycosylated dajumin (Gabriel *et al*., 1999).

membrane preparations were isolated from cells at T4, as this is when Ca^{2+} signalling has been shown to occur in response to cAMP (Malchow *et al*., 2006), and at T18 - T20 (named T20), as this is when *Dd*TPC2 expression levels are higher than that of T4. Membrane fractions P0 and P1 were prepared from Ax2 cells, which had been starved in KK_2 buffer with 5 mM EGTA for 4 hours as described in Figure 4.7, and incubated with [^{32}P]NAADP for 40 min, with and without pre-incubation with unlabelled NAADP (1 mM). When T4 membranes were used, higher specific binding of [^{32}P]NAADP was observed in P1 membrane fractions relative to P0 (Figure 4.9A). The plot of competitive displacement was consistent with a low affinity binding site with an IC_{50} for NAADP of 2.14 ± 0.60 μM (n = 3: duplicate/each) and a Hill slope of -0.58 ± 0.40, as shown in Figure 4.9B. In view of the Hill slope having a value substantially different from -1, the possibility of another higher affinity binding site cannot be ruled out.

It was also examined whether heating or proteinase treatment of *Dictyostelium* membrane would affect binding of NAADP. P1 membranes isolated from T4 Ax2 cells were either incubated at 40°C or 100°C, or treated for 10 min with proteinase K at 80°C or trypsin at 37°C, prior to the binding assay (Figure 4.10). NAADP binding was not inhibited by heat treatment of membranes. A slight reduction in NAADP binding was seen with proteinase K treatment, whereas trypsin was found to increase non-specific binding. Therefore, the NAADP binding site in *Dictyostelium* membranes appears to be heat and proteinase resistant.

The P1 fraction from T20 showed a much higher level of specific binding of [^{32}P]NAADP than that from T4 (Figure 4.11A) and than that of the P0 fraction from

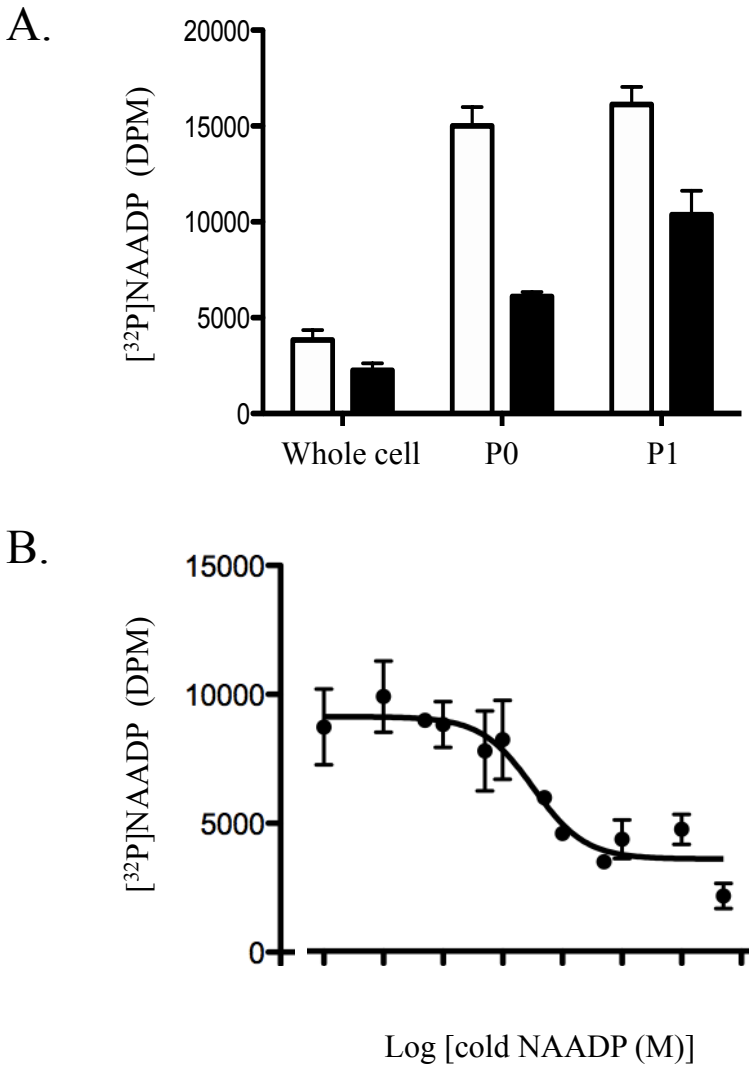


Figure 4.9. [^{32}P]NAADP binding assay applied to T4 cells
A. 4 hours after starvation in KK_2 buffer with 5 mM EGTA, P0 and P1 membrane fractions were obtained from *Dictyostelium* (Ax2) cells, and a [^{32}P]NAADP binding assay was performed either in the presence (black) or absence (grey) of 1 mM unlabelled NAADP. Specific binding is shown as black bars, with non-specific binding shown as grey bars.
B. A competitive displacement binding assay was performed on the P1 fraction from T4 cells, using varying concentrations of unlabelled NAADP from 1 nM to 10 mM. The binding reaction was terminated by quick filtration using a manifold or harvester with ice cold washing buffer. The IC_{50} for NAADP was measured to be 2.1 ± 0.60 μM (n = 2), with a Hill slope of -0.58 ± 0.40. 250 μg of membrane/reaction was used for all experiments. The mean ± S.E.M. of three independent experiments is shown. □: Non-specific binding, ■: Specific binding

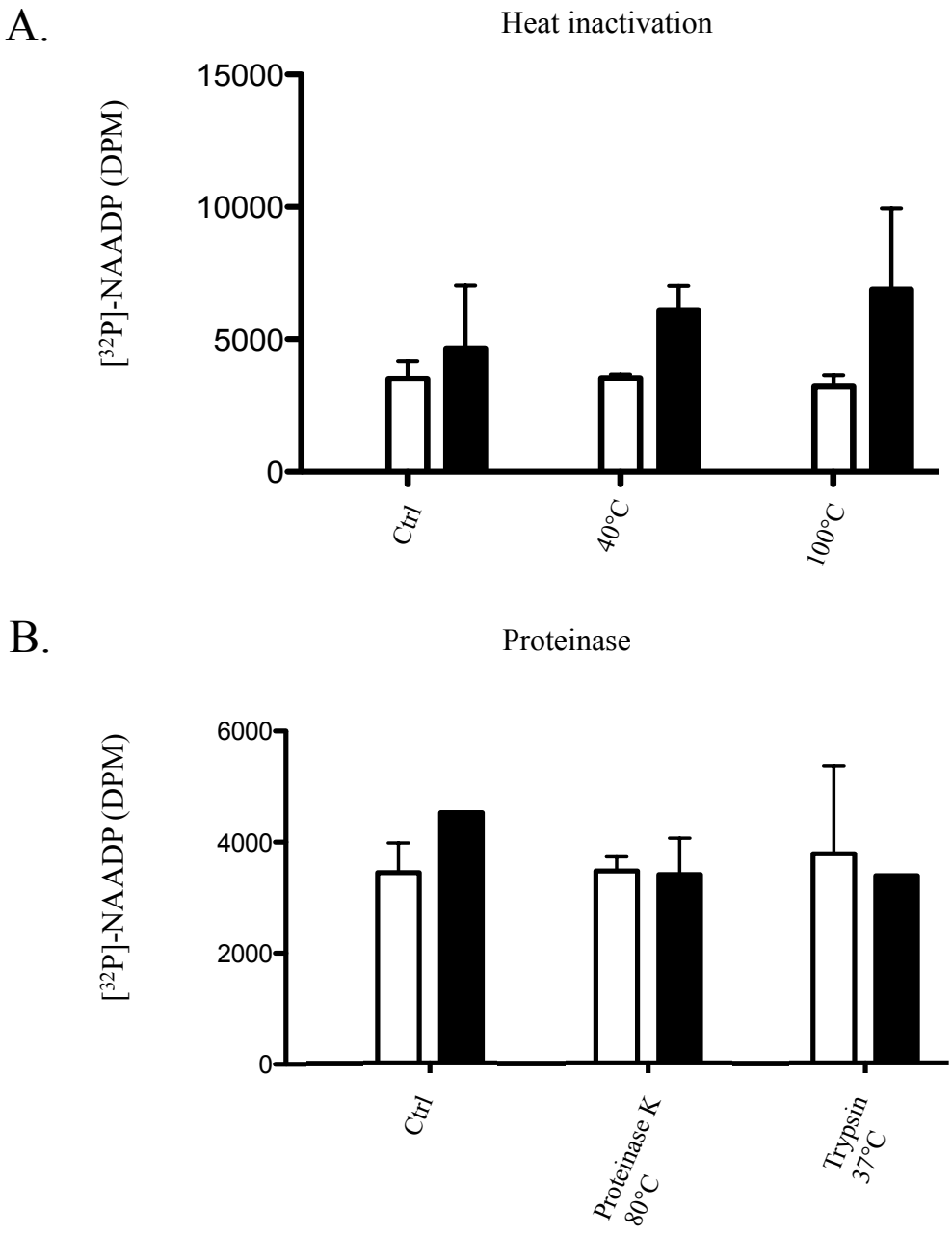


Figure 4.10. [^{32}P]NAADP binding to membranes treated with heat or proteinase

250 µg of T4 P1 membranes were incubated at 40°C or 100°C for 10 min (A), or treated with proteinase K at 80°C or trypsin at 37°C for 15 min (B), prior to the binding assay being performed. Membranes were preincubated with 1 mM unlabelled NAADP before adding [^{32}P]NAADP, and the reaction was terminated with quick filtration using a manifold. Specific binding is shown as black bars, with non-specific binding shown as grey bars. In Ctrl, untreated membrane was used. The data represent the mean ± S.E.M. of three independent experiments.

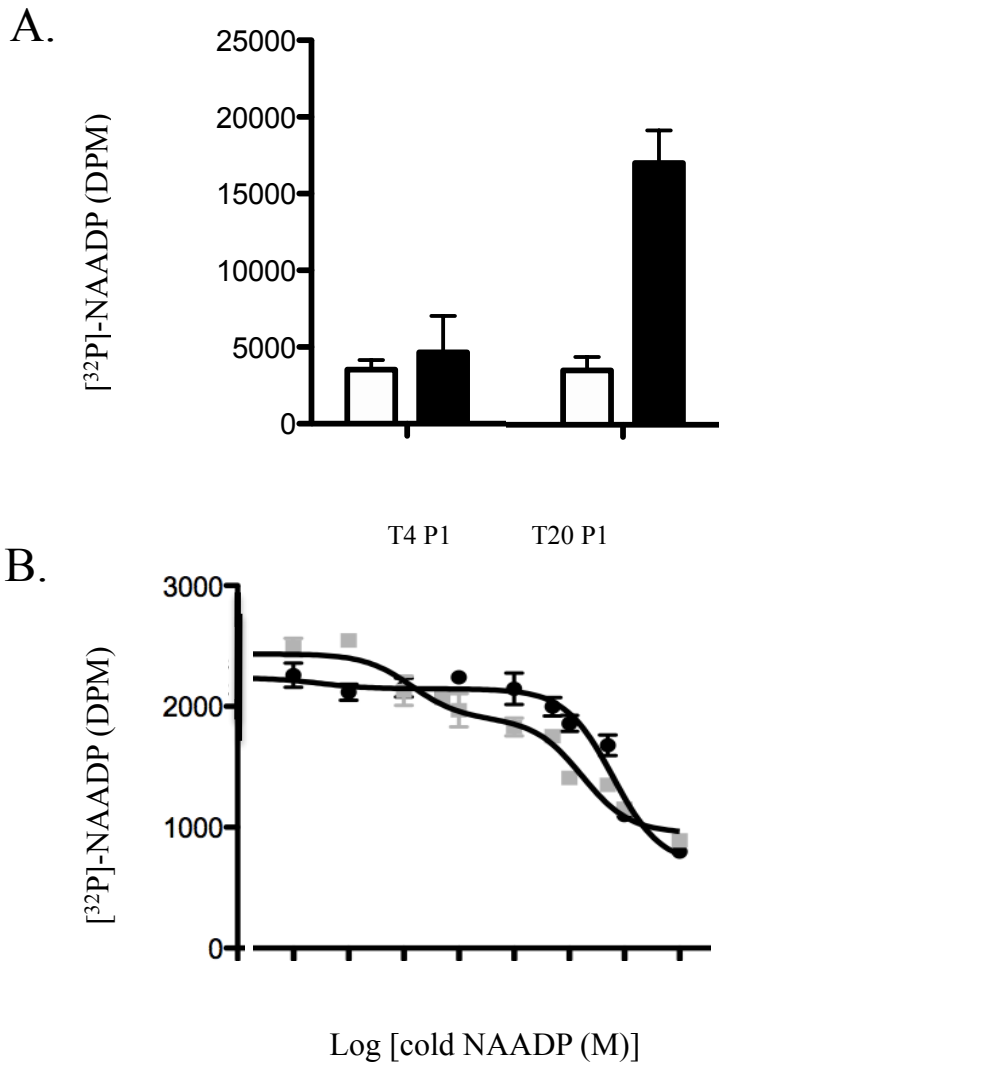


Figure 4.11. [^{32}P]NAADP binding to T20 cell membrane preparations
A. P0 and P1 fractions were prepared from T20 cells developed on 2% KK_2 agarose at 22°C, and [^{32}P]NAADP binding was compared to the T4 P1 fraction in the presence and absence of excess unlabelled NAADP (1 mM).
□: Non-specific binding, ■: Specific binding.
B. Binding of NAADP to the P1 fraction was examined in the presence of the indicated concentrations of unlabelled NAADP or NADP. The binding reaction was terminated by quick filtration using a manifold or harvester with ice cold washing buffer. The P1 fraction contained a single apparent binding site for NAADP with an IC_{50} of 72 ± 14 μM (n = 3), whereas this membrane fraction contained two apparent binding sites for NADP with IC_{50} values of 12 ± 5.2 nM and 14 ± 4.6 μM (n = 2). 250 μg of membrane/reaction was used for all experiments. The data represent the mean ± S.E.M. NAADP contamination with NADP was found to be significant (NAADP 86%, NADP 14 %), whereas contamination of NADP with NAADP was minimal (NADP 88%, NAADP 0.27 %). ■: NAADP, ■: NADP.

T20 (data not shown). A ligand competition assay was carried out using the P1 (T20) fraction in the presence of various concentrations of unlabelled NAADP or NADP. As shown in Figure 4.11B, there was a single binding site for NAADP with low affinity, with an IC_{50} value of 72 ± 14 μM (n = 3). In contrast, there was a high affinity binding site for NADP with an IC_{50} value of 12 ± 5.2 nM, and a low affinity binding site with an IC_{50} value of 14 ± 4.6 μM (n = 2). HPLC analysis of the preparations of NAADP and NADP used revealed that cold NAADP contained 14 % contamination with NADP, whilst NADP had a low 0.27 % contamination with NAADP. This suggested that the low affinity binding of NAADP may in fact be due to contaminating NADP.

Therefore, no high affinity NAADP binding sites were detected in P0 or P1 membranes from *Dictyostelium* at T4 or T20.

4.3.5. Detection of endogenous *Dd*TPC2 at the protein level

The protein expression pattern of *Dd*TPC2 is not known (Gaudet *et al*., 2009). In order to examine the correlation between mRNA abundance and protein expression, it was first necessary to raise an antibody that recognized endogenous *Dd*TPC2.

4.3.5.1. Production of anti-*Dd*TPC2 polyclonal antibody

Anti-*Dd*TPC2 polyclonal antibody was generated using the custom antibody service from Eurogentec (Southampton, UK). Two immunogenic peptides were designed, one from the loop between domains I and II (P1) and a second between transmembrane segments S3 and S4 in domain II (P2) (Figure 4.2). These regions

were chosen as they are predicted to be immunogenic, are hydrophilic to allow antibody access, and are in non-domain regions to avoid cross-reactivity with other proteins. One extra cysteine residue was added to the N terminus of P1 to aid future antibody purification, and 5 mg of each purified peptide was coupled with the carrier proteins, KLH (keyhole limpet haemocyanin) with MBS (*m*-maleimidobenzoyl-*N*-hydroxysuccinimide ester), followed by co-immunization. Rabbit antisera to the peptide-KLH conjugates were raised in two SPF (specific pathogen free) rabbits (Rb1 and Rb2). After harvesting pre-immune serum, both peptides were injected into each rabbit on day 0, 7, 10 and 18, and serum was taken on day 21 and 28. The latter was used for all experiments.

4.3.5.2. Antigen peptide synthesis in *E.coli*

Due to limited amounts of immunizing peptide, it was necessary to synthesize a GST (glutathione S-transferase) gene fusion peptide for future purification of the antisera and analysis. Annealed double-stranded oligonucleotides coding for P1 and P2 were cloned into the *E.coli* expression vector, pGEX-KG (Figure 4.12). Expression of GST-tagged peptides was examined by Western blotting using anti-GST antibody. One hour after IPTG (isopropyl β-D-1-thiogalactopyranoside**)** induction, GST-fusion peptides was successfully expressed in almost equal amounts to that expressed 3 and 7 hours after induction in *E. coli* (Figure 4.13A: data for Peptide 2 is not shown).
A program for annealing oligonucleotides is shown in Table 12.

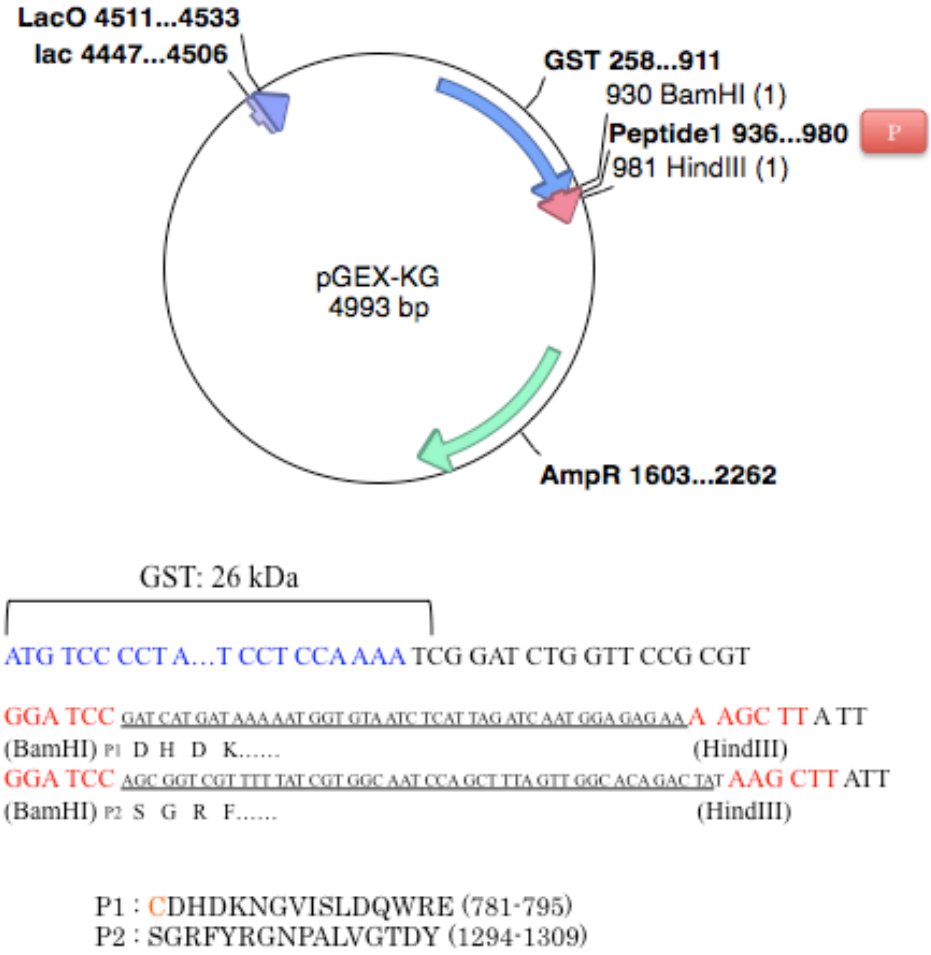


Figure 4.12. Antigen peptide expression plasmid
Double stranded oligonucleotides encoding P1 or P2 were synthesized. Restriction enzyme sites were included at either end to facilitate cloning. Annealed oligonucleotides were ligated into pGEX-KG digested with HindIII and BamHI. This generated an in-frame fusion between GST and the peptide.

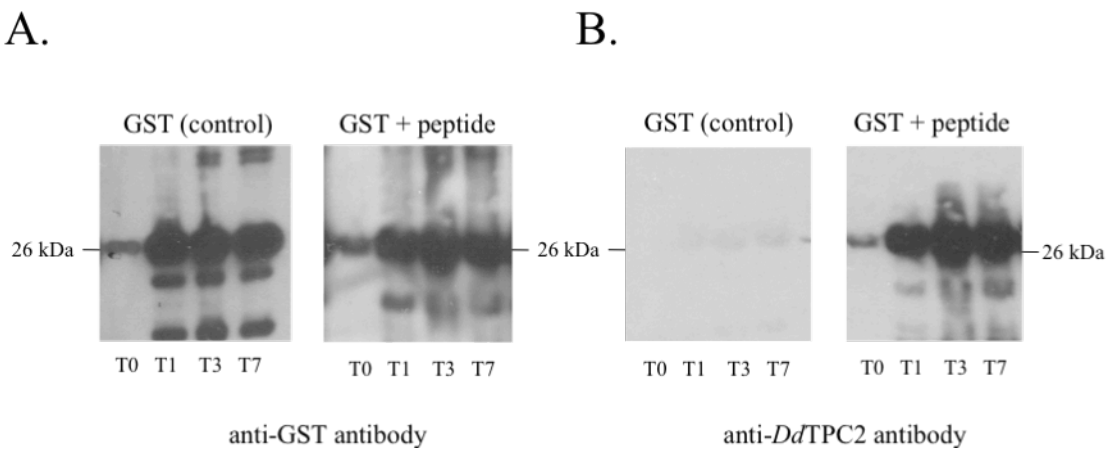


Figure 4.13. Expression of GST-P1 fusion protein
Annealed oligonucleotides encoding a peptide antigen were inserted into the *E. coli* expression vector, pGEX-KG. GST-tagged peptide was expressed in the *E. coli* strain, T7 Express lysY/I^q (New England Biolabs, Hitchin, UK). Cells containing plasmid driving the expression of either GST alone or GST-P1 fusion protein were collected 0, 1, 3 and 7 hours after induction with 0.4 mM IPTG and analyzed by Western blotting. GFP-P1 was detected by anti-GST antibody (SIGMA, G1160, 1:5000) (A) and by antibody purified from elution fraction (EF) 1 (1:100) (B). See Figure 4.15 for further details.

Table 12. Annealing oligonucleotides

1 µl or 2 µl of oligonucleotides (200 µM) were used in the annealing buffer in a total volume of 20 µl.

Temperature (ºC)	Time (sec/min)
95	3 min
94	1 min
92-62	2 min at -2ºC
60	30 min
58-30	2 min at -2ºC
15	2 min
4	Hold

4.3.5.3. Reactivity of serum to endogenous or heterologous antigens

In order to determine whether the antiserum reacted with the peptides, Western dot blotting was used to test the reactivity of unpurified rabbit serum against the GST-peptide fusion proteins produced in *E. coli* (data not shown), against immunogenic peptides and against whole cell lysate prepared from *Dictyostelium* cells developed on filters for 20 hours (T20) (Figure 4.14). This time was chosen as mRNA level of *Dd*TPC2 is close to the peak at this stage. The reactivity of serum (containing antibodies) from both rabbits against peptide P1 was high, but reactivity against peptide P2 was low, suggesting that P2 was not very immunogenic. Immune serum and pre-immune serum from Rb1 equally recognized whole cell lysate, suggesting that this was not a specific reaction. On the other hand, immune serum from Rb2 showed a strong signal against whole cell lysate, but less reactivity was observed with pre-immune serum. This is consistent with serum from Rb2 containing antibodies specific to P1, hence this serum was chosen for further analysis.

4.3.5.4. Antibody purification

In order to increase specificity, antibodies were affinity purified from the serum of Rb2 using SulfoLink Coupling Resin (Pierce, Thermo Scientific, Cramlington, UK), which was coupled via the N-terminal cysteine residue to immobilized peptide, P1. Antibody bound to the column was eluted using 8 ml of elution buffer (as described previously in *Chapter 2*) and collected in separate 1 ml fractions (elution fractions 1 to 8). The purification efficiency was firstly tested by dot-blotting assay. Purified antibody still recognized peptide P1 and was enriched in elution fractions (EF) 1 and 2, whereas an unrelated protein, here mammalian lymphoblast lysate, was not recognized (Figure 4.15A). Whole cell lysates from Ax2 cells at various late

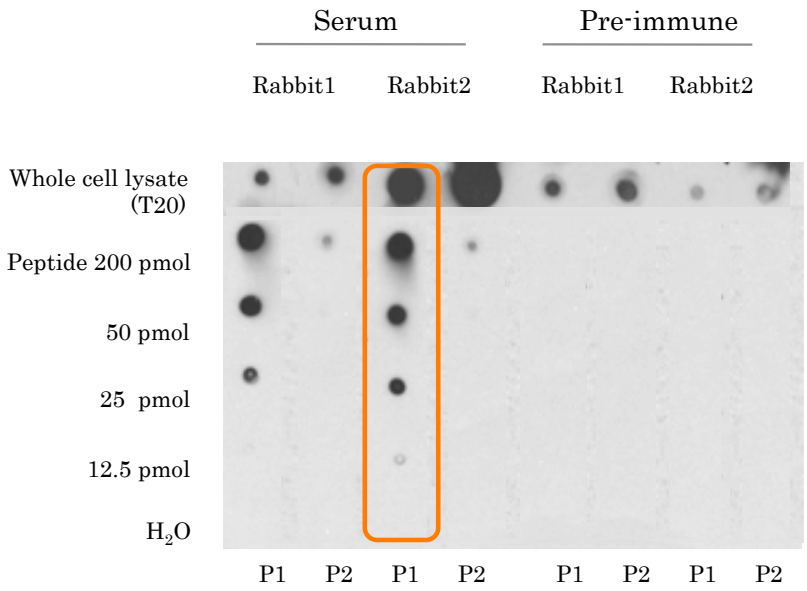


Figure 4.14. Dot blot analysis to determine reactivity of serum from Rb1 and Rb2
Whole cell lysate from Ax2 cells at a late developmental stage (T20), and two peptides (P1 and P2) at the various concentrations indicated, were spotted on nitrocellulose membrane. Biomolecules were detected by serum (1:500) from two rabbits (Rb1 and Rb2), shown on the left hand side of the figure, or by pre-immune serum as shown on the right hand side.

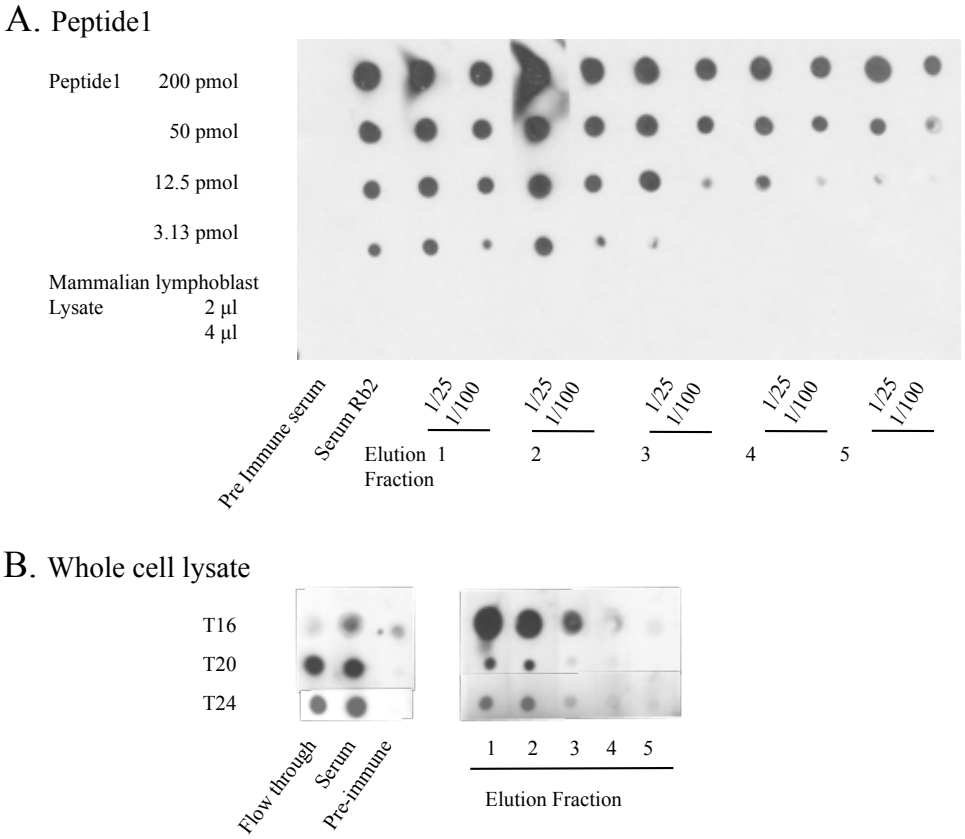


Figure 4.15. Affinity purification of Anti-*Dd*TPC2 antibody
A. Peptide1 was immobilised on SulfoLink coupling resin and serum from Rb2 was affinity purified by passing through the column. After washing ten times, purified antibody was eluted using 8 ml of Elution Buffer and collected in separate 1 ml fractions (Elution Fraction 1 to 8), and neutralized by adding 50 µl of Neutralization Buffer. Samples were taken at each step and the purification efficiency was determined by Western dot blotting different amounts of peptide with Elution Fraction (EF) 1 to 5 at the dilutions indicated. Mammalian lymphoblast lysate was used as a negative control. B. Ax2 cells were developed on filter paper for the time indicated (hours), and whole cell lysate spotted onto nitrocellulose was immunoblotted using EF1 at a 1 in 10 dilution.

developmental stages were also tested (Figure 4.15B) and purified antibody from EF1 and EF2 showed reactivity, especially with T16, suggesting that this antibody purification step retained detection of endogenous protein.

4.3.5.5. Endogenous protein recognized by purified antibody throughout development of *Dictyostelium*

In order to determine if endogenous protein could be detected by purified antibody, and establish the time course of protein expression, whole cell lysate prepared from different stages of *Dictyostelium* development was analyzed by Western blot (Figure 4.16). Multiple bands were observed. One major band at approximately 270 kDa, another at 200 kDa and a third at 130 kDa, all increased towards the late-stages of development with maximal expression of all 3 proteins at 20 hours of development. A number of strongly reacting lower molecular weight bands were also detected from the early stages of development. It is not known whether these lower bands were degradation products or unrelated proteins. The predicted molecular weight of *Dd*TPC2 is 237 kDa, and potential glycosylation could increase this.

To determine the specificity of purified antibody, a blocking experiment using an immunizing peptide was performed. Prior to Western blotting, the antibody was neutralized with an excess of peptide (100 μM) that corresponded to the epitope recognized by the antibody. The intensities of the high molecular weight bands all decreased after peptide blocking, with the bands at 270 kDa, 200 kDa and 130 kDa reduced in intensity compared to that of antibody alone (Figure 4.17). Therefore, anti-*Dd*TPC2 antibody is likely to be recognizing *Dd*TPC2.

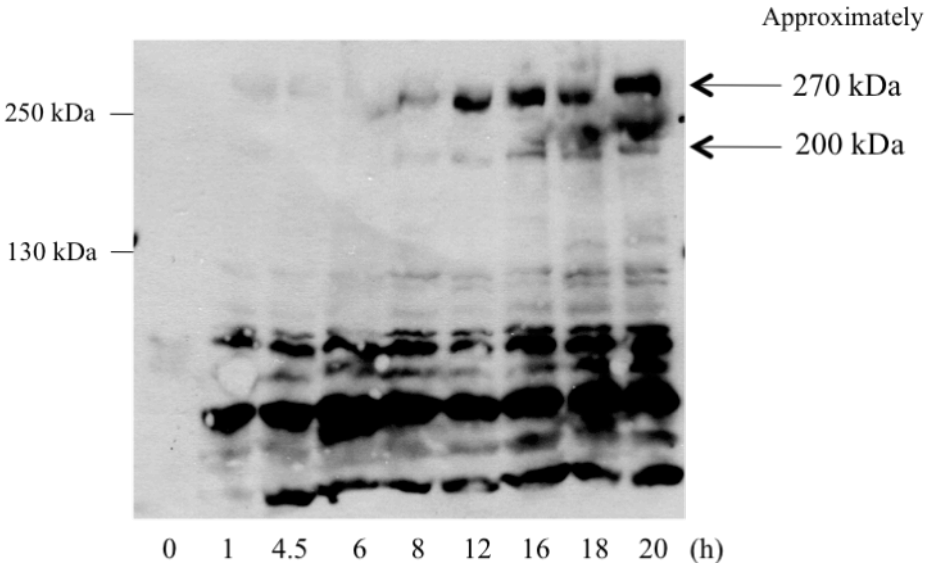


Figure 4.16. Western blot showing the time course of *Dd*TPC2 expression during development

Exponentially growing Ax2 cells were harvested and plated at a density of 3.25 x 10^6 cells/cm^2 on filters to initiate development. Plates were incubated at 22°C and samples were taken at each time point indicated (hours). Extracts were resolved on a 7% SDS polyacrylamide gel and subjected to Western blot using EF2 from the purification at a 1 in 10 dilution. Arrows show bands which increased in intensity during development, as predicted for *Dd*TPC2.

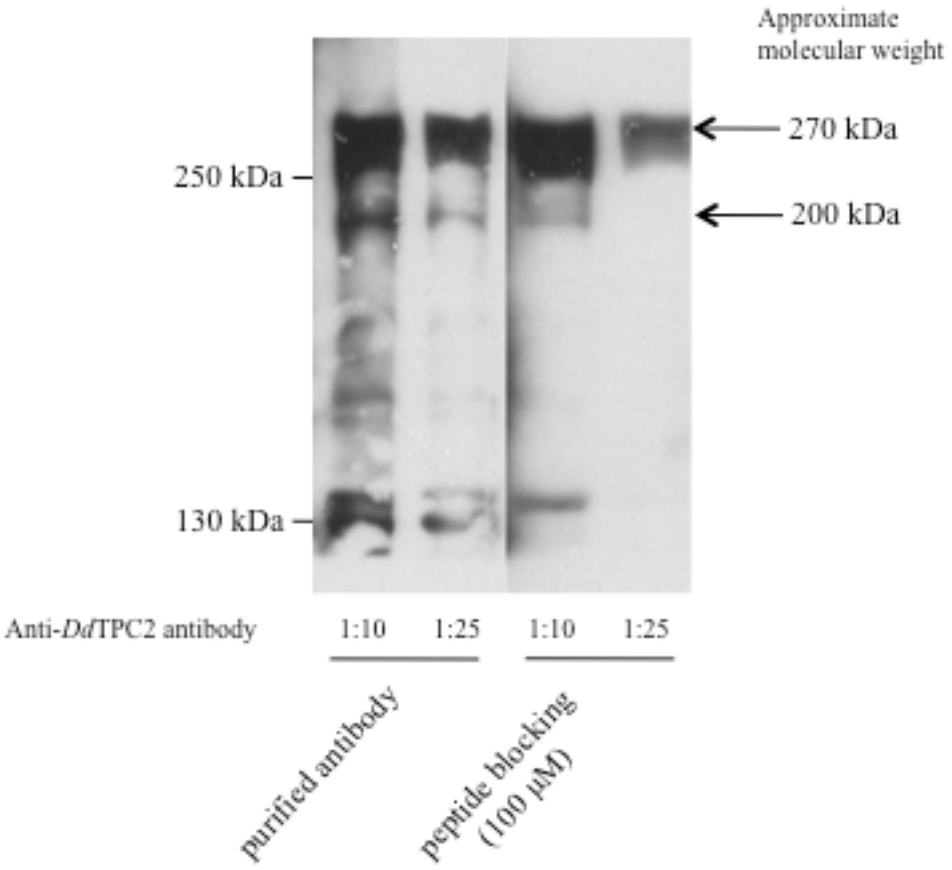


Figure 4.17. Peptide competition with anti-*Dd*TPC2 antibody from purified serum

Protein extracts were prepared from T20 cells and resolved on a 7% SDS polyacrylamide gel, followed by Western blot. Purified anti-*Dd*TPC2 antibody (at the indicated dilution) was pre-incubated with or without 100 μM peptide1 prior to incubating with membrane for 2 hours at room temperature. The indicated bands (arrows) were reduced in intensity by the presence of the blocking peptide. The molecular weights of major bands indicated at 270 and 200 kDa are approximations. The blots were exposed for the same time.

4.3.6. The localization of endogenous *Dd*TPC2

Immunohistochemistry techniques were utilized, using the purified antisera, in order to investigate the localization of endogenous *Dd*TPC2. No detectable immunofluoresence was observed in Ax2 cells at various developmental stages using purified antibody (data not shown), consistent with expression of low protein levels in these cells, as would be predicted from low mRNA levels.

4.3.7. Overexpression of *Dd*TPC2

In order to overcome problems with specificity of antibody recognition and low protein expression levels, it was decided to overexpress recombinant *Dd*TPC2 protein with an easily accessible epitope tag. The gene encoding *Dd*TPC2 is large (the open reading frame is 6183 bp, Appendix 10.1) and contains a number of repeat sequences. Therefore, as a cloning strategy, *Dd*TPC2 coding sequences were split into several smaller fragments, at restriction sites in the gene, to be separately amplified by PCR. Most of the fragments, except 1 kbp at the 5' end and the repetitive sequence of TAA (42 x TAA), were successfully amplified by PCR and cloned in a cloning vector, pSCA (StrataClone PCR cloning kit: Stratagene Europe, Leicestershire, UK), then verified by DNA sequence analysis (Figure 4.18). However, despite repeated attempts, these two remaining fragments could not be amplified. Therefore, the entire coding sequence was produced synthetically by DNA2.0 Inc (California, USA). This provided an optimized clone, in which parts of the gene that were difficult to amplify were modified to overcome this issue, whilst ensuring that the gene still coded for the same amino acids (Appendix 10.2). The first 20 codons and Kozak-like sequence were kept the same in the synthetic sequence as in the endogenous sequence, since these regions are known to be important for protein expression (Vervoort *et al*., 2000).

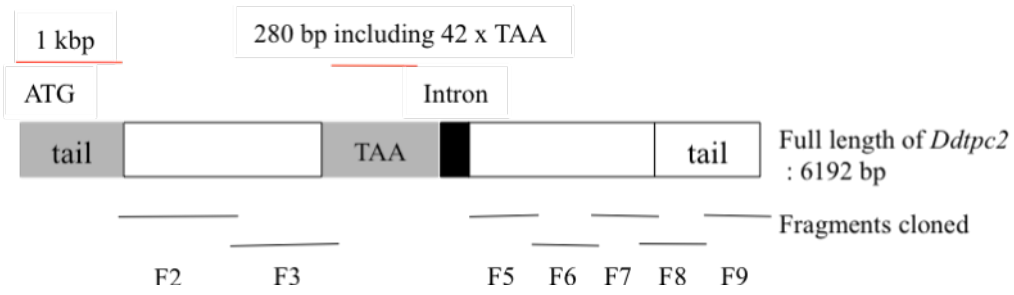


Figure 4.18. Fragments of *Ddtpc2* cloned
Total RNA from T20 cells was treated with DNase, followed by one-step RT-PCR. Fragments obtained (grey lines) were cloned into the TA cloning vector, pSC-A (StrataClone PCR cloning kit from Stratagene), and the sequence was confirmed by DNA sequencing. The red bars indicate the fragments missing. 'Tail' corresponds to an extra 1 kbp found in *tpc*s of other species, and TAA indicates a repetitive region of TAA. The primer details are given in *Appendix 5.6.*

4.3.7.1. Expression of synthetic recombinant *Dd*TPC2

*Dd*TPC2 dual use clone was designed and ordered from DNA2.0 Inc (California, USA). The original start and stop codon, and SpeI site, were omitted and appropriate restriction sites, Kozak sequence for mammalian cells and *Dictyostelium*, and sequence to code for an epitope FLAG tag at the 5' end, were introduced as shown in Figure 4.19. The mRFPmars coding sequence was already present in the donor plasmids as a C terminal tag. In order to express this in *Dictyostelium*, the coding sequence with a FLAG tag at its N terminus was cloned into the vector pDM341, to allow tetracycline-inducible expression (Veltman *et al*., 2009). The 6219 bp fragment was sub-cloned into the BglII/SpeI double-digested vector, pDM341, to produce the over-expression vector, pDM341.FLAG.*Dd*TPC2 (mRFPmars) (Figure 4.20A). The fragment containing the coding sequence of FLAG.*Dd*TPC2 was inserted into pcDNA5TO with a C terminal mRFPmars tag using BamHI and NotI sites (Figure 4.20B). The integrity of the insertion was confirmed by restriction analysis (data not shown).

Ax2 cells were transformed by electroporation with pDM341.FLAG.*Dd*TPC2.mRFPmars and selected in HL5 medium supplemented with 10 μg/ml of G418 to obtain a stable cell line. pDM341 vector was used to generate a control cell line. Pools of resistant colonies were grown in HL5 medium containing 10 μg/ml of G418, washed with HL5 once, and protein expression was induced by addition of doxycycline at 0, 0.5 or 10 μg/ml. Expression levels at 0, 3 and 6 hours of induction were examined by Western blot analysis using anti-mRFPmars antibody. Recombinant protein was detectable at 3 hours, and the intensity of the band increased at 6 hours (Figure 4.21A). Since lower levels of

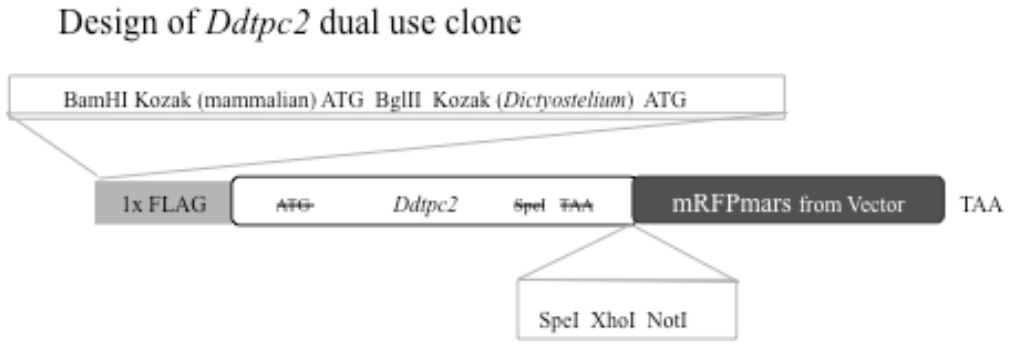
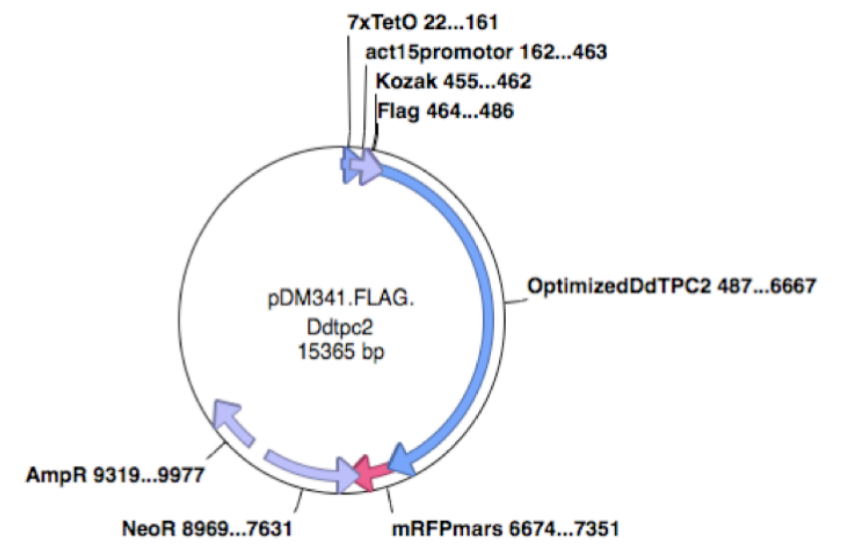


Figure 4.19. Synthetic gene coding for *Dd*TPC2
The coding sequence of *Ddtpc2* was optimized using multiple codon-optimization algorithms, except for the first 20 amino acids downstream of the endogenous ATG. Kozak sequences (*Dictyostelium*: AAAAAA**ATG**, Mammalian: CCACC**ATG**G) and sequences coding for a FLAG tag (GATTATAAAGATGATGATGATAAG) were introduced upstream of, and in frame with, the predicted ATG. The endogenous start codon, SpeI sites and stop codon were deleted. Appropriate restriction sites, either BglII and SpeI, or BamHI and NotI, were introduced for future subcloning. The mRFPmars coding sequence was inserted into the donor vector prior to the insertion of the *Ddtpc2* fragment.

A. *Dictyostelium* expression vector



B. Mammalian expression vector

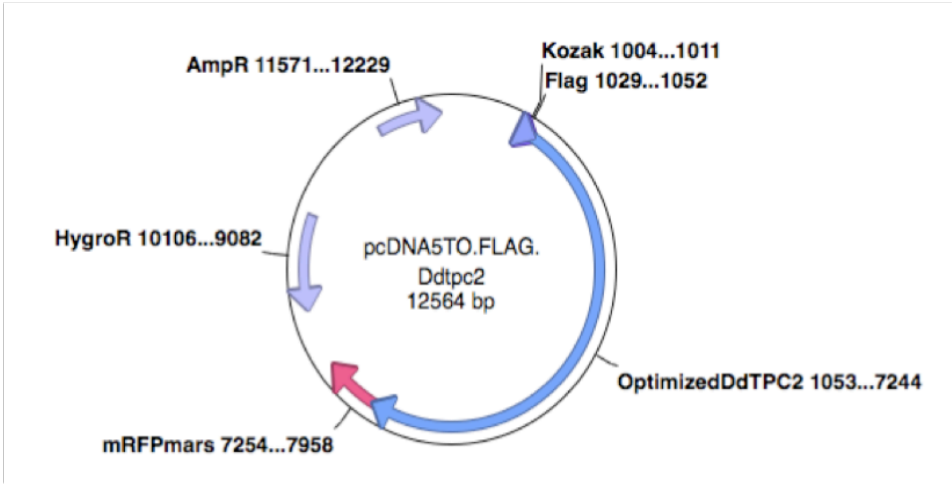


Figure 4.20. *D*dTPC2 expression plasmids
The fragment encoding FLAG-*Ddtpc2* was excised with either BglII and SpeI, or BamHI and NotI, to insert into either pDM341 (A) or pcDNA5TO (B) vectors, respectively. The pDM341 vector (9.1 kbp) contained a G418 cassette, and a coding sequence for mRFPmars at the 3' side of the cloning site (Veltman *et al*. 2009). Transcription of the gene of interest was under the control of the inducible promoter TRE-Pmin, which consists of 7 repeats of the TetO operator fused to a minimal fragment of the act15 promoter to allow it to be induced by doxycycline in a concentration-dependent manner. pcDNA5TO (Sigma-Aldrich) is a 5.7 kbp expression vector, designed for tetracycline-regulated expression in mammalian host cells expressing the Tet repressor (TetR). The hybrid promoter consisted of a human cytomegalovirus (CMV) immediate-early promoter and tetracycline operator 2 (TetO2) sites for high-level tetracycline-regulated expression.

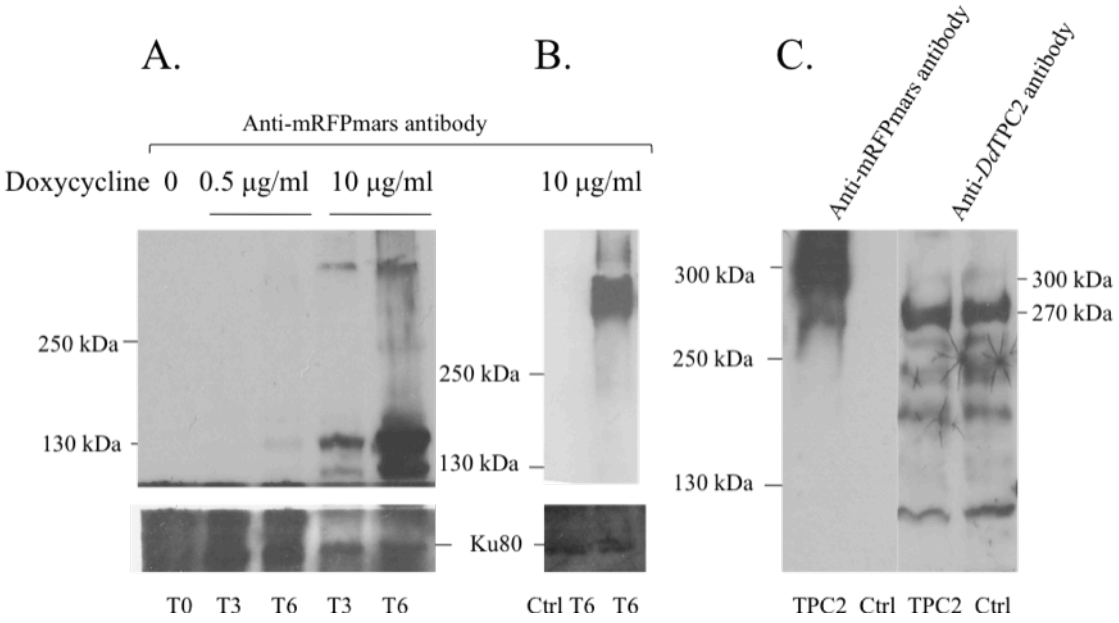


Figure 4.21. Ax2 cells stably expressing FLAG.*Dd*TPC2.mRFPmars
A. pDM341.FLAG.*Ddtpc2*.mRFPmars was transfected into Ax2 cells by electroporation, followed by selection with 10 µg/ml of G418, and 0.5 or 10 µg/ml of doxycycline was used to induce *Dd*TPC2 expression in pools of cells at a density of 3 x 10^6 cells/ml; this was followed by harvesting of cells after 3 and 6 hours incubation. Whole cell extract was resolved on an 8% SDS polyacrylamide gel, and immuno-blotted with a 1:100 dilution of anti-mRFP primary antibody in 0.5% skimmed milk. The blot was reprobed with anti-Ku80 serum to show equal loading (see the lower panel).
B. Ax2 cells expressing either mRFPmars (Ctrl) or FLAG.*Dd*TPC2.mRFPmars were induced with 10 µg/ml doxycycline for 6 hours, prior to Western blot analysis with anti-mRFPmars antibody. Samples were denatured at low temperature (65 - 70°C).
C. Lysates from cells induced for 6 hours with 10 µg/ml doxycycline were blotted with indicated primary antibodies, either anti-mRFPmars antibody or anti-*Dd*TPC2 antibody at 1:10 dilution in 1% skimmed milk. Lysate from mRFPmars expressing cells (Ctrl) was loaded as a control.
Approximate molecular weights of bands of interest are indicated at 270 and 300 kDa.

doxycycline gave lower induction, a concentration of 10 μg/ml was used for the remainder of the experiments. The immuno-reactive bands detected were at approximately 300 kDa, which is larger than the expected molecular weight for the FLAG.*Dd*TPC2.mRFPmars protein, 263.78 kDa. However, no band was evident in the control lane, suggesting that it is likely that recombinant *Dd*TPC2 was successfully expressed in Ax2 cells, despite a higher than predicted molecular weight (Figure 4.21B). This would indicate that *Dd*TPC2 protein runs at a higher molecular weight than expected on SDS gels and suggests that the band seen at 270 kDa with anti-TPC2 antibody represents the endogenous protein. Since the full length of FLAG.*Dd*TPC2.mRFPmars protein was successfully expressed without truncation, this also implies that there is no cleavage site within this protein. This allows examination of the subcellular distribution of exogenously expressed protein using RFP.

Lysates from cells expressing FLAG.*Dd*TPC2.mRFPmars were then blotted with purified anti-*Dd*TPC2 anti-serum. This recognized several bands which also appeared in the control lane (Figure 4.21C). In addition, the strongest band at 270 kDa was slightly smaller in MW than the one detected by anti-mRFPmars antibody at 300 kDa. This could represent the endogenous *Dd*TPC2 protein which would be slightly smaller due to the fact that it lacks the tags. This suggests that either the endogenous protein is expressed at a higher level than the induced protein, since the band detected by anti-*Dd*TPC2 antibody at 300 kDa was faint compared to that at 270 kDa (Figure 4.21C) or simply the quality of anti-*Dd*TPC2 antibody is not sufficient.

When the sample was prepared as gently as possible, fewer smaller bands were observed (Figure 4.21B). The lower bands observed at 130 kDa in Figure 4.21A and

C were likely to be segments of recombinant *Dd*TPC2 protein, as these were half the size of full length *Dd*TPC2, and were detected by both anti-mRFPmars antibody and anti-*Dd*TPC2 antibody. However, whether this 130 kDa product is a truncated protein of *Dd*TPC2 or due to degradation during sample preparation was not clarified.

4.3.8. Localization of exogenously-expressed *Dd*TPC2 in *Dictyostelium*

To investigate the localization of tagged *Dd*TPC2, pDM341.FLAG.*Dd*TPC2.mRFPmars was electroporated into Ax2 cells expressing dajumin-GFP or calnexin-GFP to visualize the CV (Gabriel *et al*., 1999) or ER (Muller-Taubenberger *et al*., 2001), respectively. 15 hours after transfection, 0.5 μg/ml or 10 μg/ml doxycycline was added to induce *Dd*TPC2 expression, and this was followed by fixation after 0, 3 and 6 hours. The localization of mRFPmars-tagged *Dd*TPC2 was examined using fluorescence microscopy, in comparison to GFP-labelled protein in either the CV or ER (Figure 4.22A or B). RFP was found to be associated with intracellular membranes, but was not apparent in the plasma membrane or cytosol. It was found co-localized with both dajumin-GFP and calnexin-GFP and so was apparent in both the CV and ER.

4.3.9. The localization of *Dd*TPC2 in HeLa cells

Since *Dd*TPC2 appeared in both the CV and ER, it was decided to express *Dd*TPC2 heterologously in HeLa cells to see if the localization might be more clearly defined. Expression of *Dd*TPC2 in HeLa cells would also allow future comparison of NAADP-binding and Ca^{2+} release with HeLa cells expressing other TPC proteins such as human TPC2 (Calcraft *et al*., 2009).

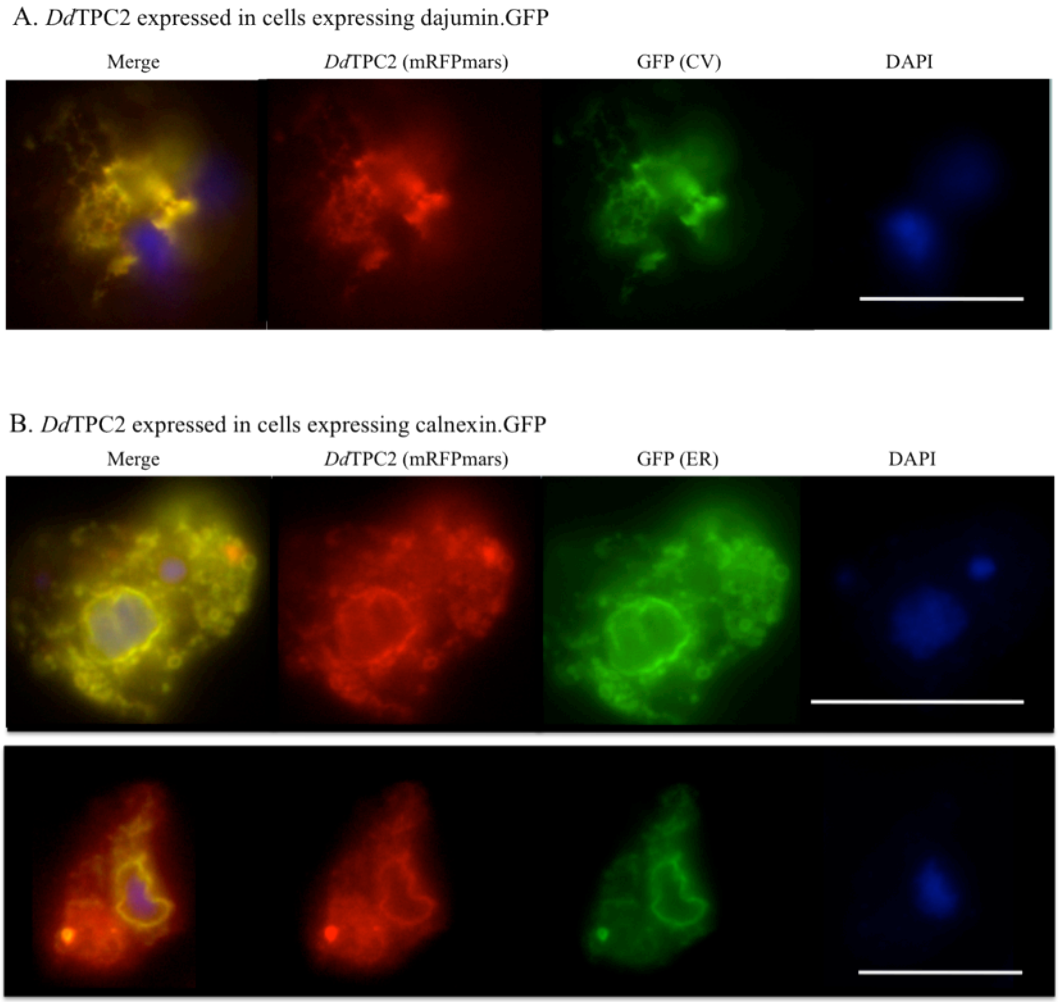


Figure 4.22. Localization of *Dd*TPC2 expressed in GFP-labelled strains
Cells transiently expressing FLAG.*Dd*TPC2.mRFPmars (red). A. Stably expressing C terminal GFP-dajumin (green) on the contractile vacuole (CV), or B. C terminal GFP-calnexin (green) on the ER, were visualized by fluorescence microscopy. The yellow colour in merged images corresponds to co-localisation of the mRFPmars-tagged protein with that of GFP. *Dd*TPC2 was found in intracellular compartments, the CV and ER.
Cell lines used were: [act15]:gppA:GFP(DBS026186) (Gabriel *et al*., 1999) and [act15]: cnxA:GFP(DBS0236184) (Muller-Taubenberger *et al*., 2001).
Scale bars, 10 μm.

pcDNA5TO.FLAG.*Dd*TPC2.mRFPmars, and plasmids to drive expression of GFP-tagged proteins specific for different organelles, were co-transfected into HeLa cells using jetPEI (as described previously in *Chapter 2*). Recombinant proteins, Lamp1-~~m~~GFP, GFP-KDRL, EEA1-GFP, TGN38-GFP or TfR-GFP were expressed as organelle markers for lysosomes, ER, early endosomes, trans-Golgi or recycling endosomes, respectively. *Dd*TPC2 was found to co-localize with the lysosomal marker and trans-Golgi marker, but not with markers for the ER or endosomes (Figure 4.23). There is no dileucine motif found in the *Dd*TPC2 coding sequence, nonetheless *Dd*TPC2 is predicted to localize to the CV (Wilczynska *et al*., 2005), which is equivalent to the lysosome in animal cells. Heterologously expressed *Dd*TPC2 was localized to lysosomes, i.e. acidic stores, consistent with *Dd*TPC2 being a protein associated with acidic organelles.

As *Dd*TPC2 was localized to the acidic CV in *Dictyostelium* and to lysosomes in HeLa cells, the function of *Dd*TPC2 was further investigated by experiments in which the gene was disrupted.

4.3.10. Generation of *tpc2*$^-$ cells

To examine the function of *Dd*TPC2, and in particular the developmental stages in which *Dd*TPC2 may play an important role, it was necessary to disrupt the gene coding for *Dd*TPC2.

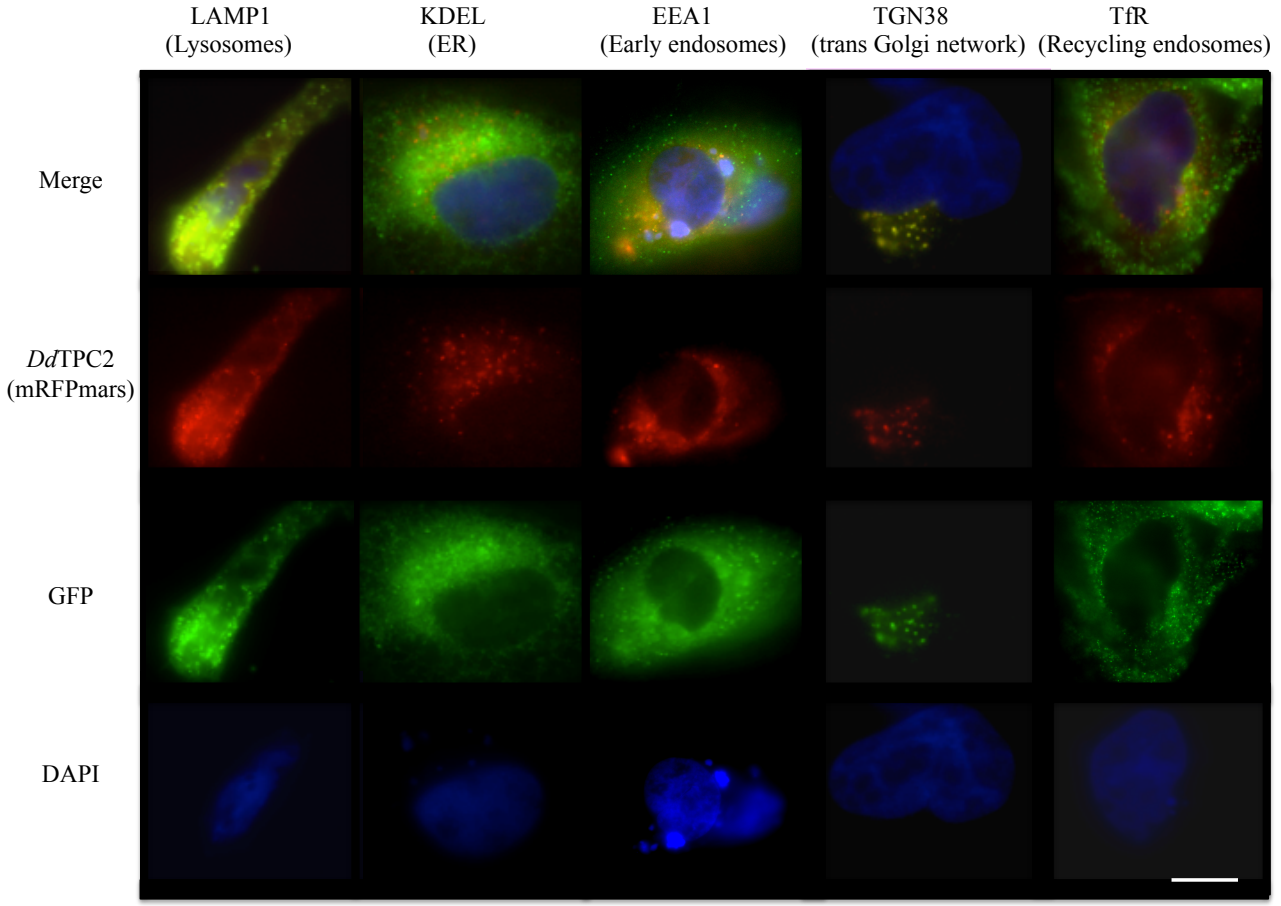


Figure 4.23. Localisation of *Dd*TPC2 in HeLa cells
Typical examples of HeLa cells transiently expressing FLAG.*Dd*TPC2.mRFPmars (red) and plasmids to derive expression of GFP-tagged ptoteins to label different organelles (green) are shown. Lamp1-mGFP, GFP-KDRL, EEA1, TGN38-eGFP and TfR-GFP were used as organelle markers for lysosomes, ER, early endosomes, trans Golgi network and recycling endosomes respectively. 1 - 2 µg of pcDNA5TO.FLAG.*Dd*TPC2.mRFPmars and 0.5 - 1 µg of plasmids express organelle marker plasmids were used. 24 - 30 hours after transfection, cells were fixed with 4 % PFA. Imaging was performed using a fluorescence microscope (Olympus IX71) with a 100x oil immersion objective, and images analyzed using HCImage (Hamamatsu Photonics UK Ltd, Hertfordshire). Yellow color in the merged (uppermost) images corresponds to co-localization of the mRFPmars-tagged protein with that of GFP. Blue color corresponds nuclei. *Dd*TPC2 co-localized with the lysosomal marker (LAMP1) and the trans Golgi marker (TGN38), but not with markers for ER or endosomes. Scale bars, 10 µm.

4.3.10.1. Construction of *Ddtpc2* disruption vector

A strategy to disrupt the endogenous gene by homologous recombination was devised, as a null strain would allow investigation of the importance of the protein. pLPBLP.*Ddtpc2* disruption vectors, KO1, KO2 and KO3, were constructed to cause disruption of the *Ddtpc2* locus on chromosome 5 (coordinates 2361958 to 2368217) by insertion of a blasticidin resistance (bsR) cassette through homologous recombination (Faix *et al*., 2004). As shown in Figure 4.24A, KO1 and KO2 were designed to delete 1 kbp and 3 kbp, respectively, downstream of the putative start codon, and a KO3 disruption vector was designed to replace the whole gene by targeted insertion of the bsR cassette. A KO4 knockout vector, in which the 5' arm of the KO3 construct was replaced with the 3' arm of KO1, was also generated. KO4 was designed to ablate 332 bp downstream from the putative ATG to the stop codon (Figure 4.24B).

Ax2 cells were transformed by electroporation with linearized disruption vector and 100 μM of specific primers (5'arm forward and 3'arm reverse), which have been reported to increase targeted insertion (Kuwayama *et al*., 2008). Electroporated cells were cultured at varying dilutions in 96 well plates in HL5 medium supplemented with 10 μg/ml blasticidin so as to yield clonal transformants. Blasticidin-resistant colonies formed a monolayer after approximately 14 days and transformants were screened by PCR to identify clones with integration of the bsR cassette at the *Ddtpc2* locus using appropriate primers (Figure 4.24A).

4.3.10.2. Screening potential disruptant clones

A number of potential disruption clones were shown to have correct integration on the

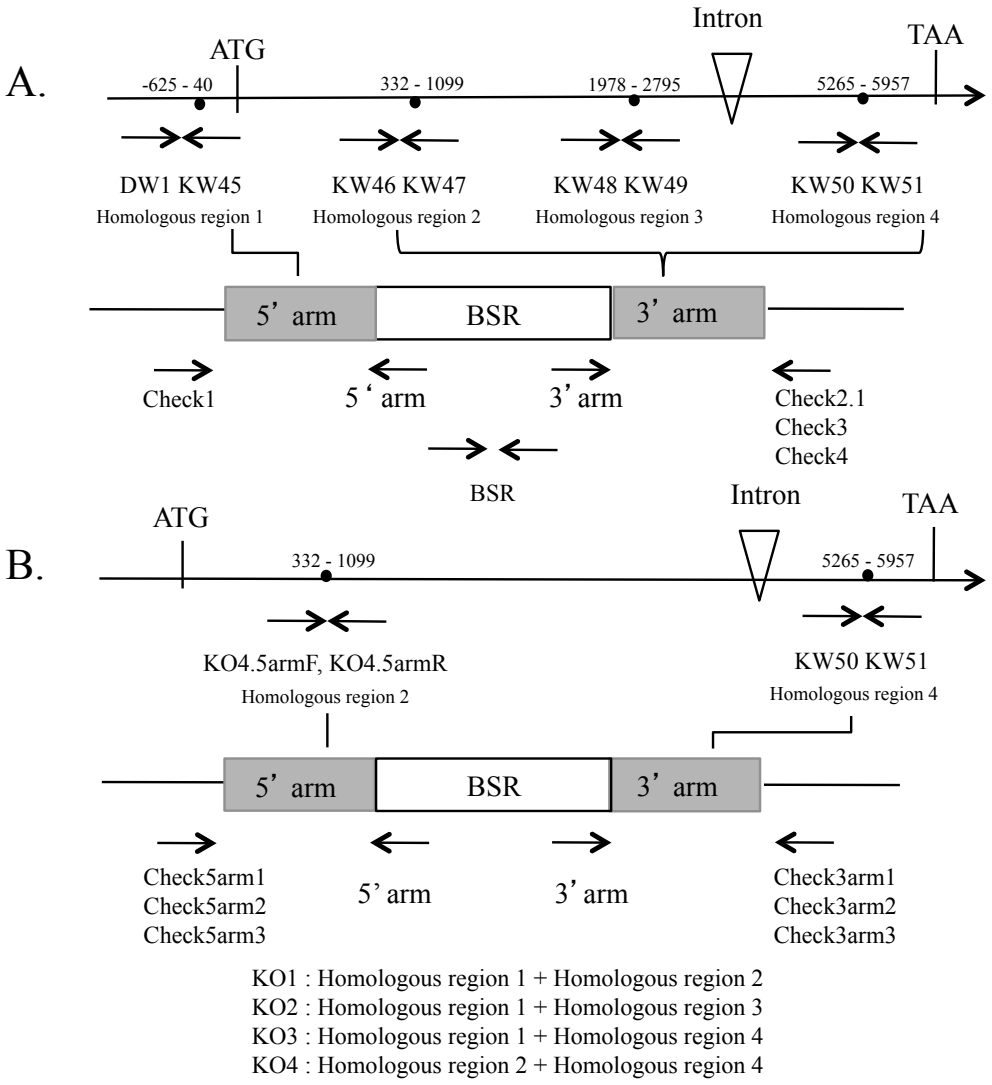


Figure 4.24. Design of *Dd*TPC2 disruption vectors and the screening strategy

A. Fragments of homologous regions 1, 2, 3 and 4 were obtained by PCR. Homologous region 1 was inserted using KpnI and HindIII for the 5' arm, and homologous region 2,3 or 4 was inserted using PstI and BamHI for the 3' arm into the pLPBLP vector. B. KO4 vector was constructed from previously produced KO1 and KO3. Homologous region 2 was produced by PCR-based modification using KO1 as a template and inserted into KO3, in which homologous region 1 had been removed beforehand. Successful insertion of the 5' arm was confirmed by PCR sequencing.

KO1 and KO3 were linearized with BamHI and KpnI, and KO2 was linearized with BamHI and PvuII, prior to electroporation into Ax2 cells. PCR using a bsR check primer set (bsRF, bsER) confirmed the insertion of the bsR cassette using genomic DNA extracted from resistant clones. The 5' side targeted insertion was screened using a primer set, Check1 and 5'arm. Similarly, the 3' side was screened using 3'arm primer and either Check2.1, Check3 or Check4 primers for KO1, 2 and 3 respectively.

3' side, however, 5' side integration could not be detected (Figure 4.25). This could simply be because of a problem with the PCR reaction of this unique sequence. Therefore, in order to confirm targeted insertion of the bsR cassette at the *Ddtpc2* locus, 6 potential *Ddtpc2* knockout clones were examined by Southern blot. A 540 bp fragment at the 3' end of *Ddtpc2* was used as a probe. No clones with *Ddtpc2* gene disruption were identified (data not shown).

At this stage of the experiments, *Ddtpc2* null cells became available (kindly provided by Dr. Wanessa de Lima and Dr. Pierre Cosson), and so no further attempts were made to generate this strain.

Three independent clones of *Ddtpc2*$^-$ cells were provided (11, 12 and 20) which had been generated in DH1 cells (Figure 4.26A). These cells were plated on SM Ka plates at different dilutions to obtain single colonies, and the growing edges were harvested and cultured in HL5 medium containing 10 μg/ml blasticidin and penicillin/streptomycin in culture dishes. PCR screening confirmed that the *Ddtpc2* gene was deleted (shown for clones 12-5 and 20-3, data not shown for other clones; see Figure 4.26B).

4.3.10.3. Development of the *Ddtpc2*$^-$ cells

In order to determine if *Dd*TPC2 has a role in development, clones 12-5 and 20-3 were observed forming colonies. On SM Ka plates, clone 12-5 was unable to form multicellular structures and clone 20-3 was less efficient at fruiting (Figure 4.27B). When developed on buffered filter paper, both mutant clones were able to form fruiting bodies (Figure 4.27A). However, as an abnormal phenotype, some

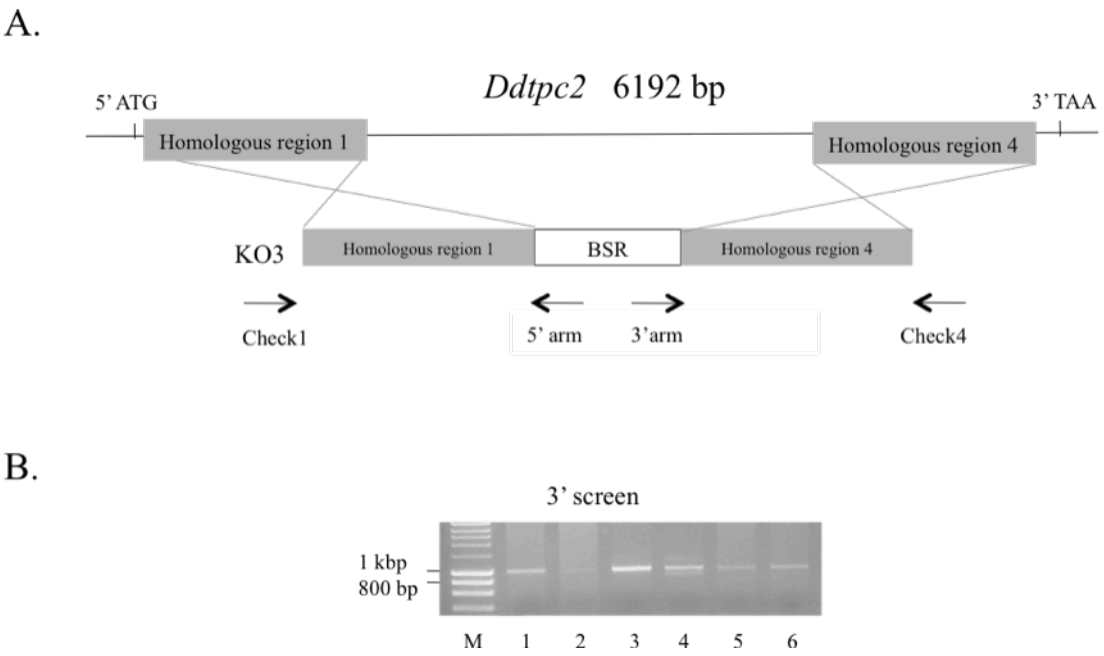


Figure 4.25. PCR screening of potential *Ddtpc2* disruptants
A. Schematic representation of the homologous recombination event.
B. Genomic DNA (gDNA) was prepared from each colony and used in a diagnostic PCR screen to confirm integration of the bsR cassette at the *Ddtpc2* locus. A primer set (3'arm, Check4) was used in a PCR reaction to check for targeted insertion of the bsR cassette at the 3'side. A random insertion of the bsR cassette would show no PCR product, only targeted insertion of 3' side clones would produce a 956 bp band. Similarly, 5'side target insertion was tested using 5'arm primer and Check1 primer (752 bp). Clones 1, 2, 3, 4, 5 and 6 had successful insertion of the 3' side. This band was sent for sequencing and it was confirmed that this band was the result of specific amplification by the primer set (3'arm, Check4). DNA ladder was loaded in the lane shown on the left hand side (M). On the other hand, 5'side PCR screening was not successful and no specific band was obtained from clones 1, 2, 3, 4, 5 and 6 (data not shown). Targeted insertion of the 5'side could not be confirmed by PCR (data not shown).

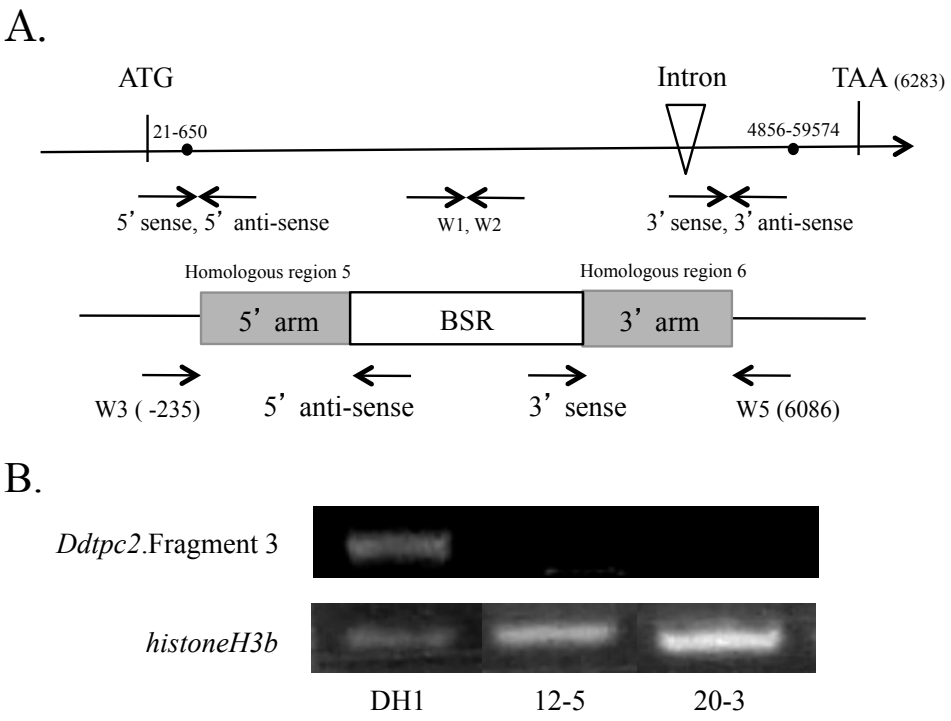


Figure 4.26. Confirmation of gene disruption
A. Construct used to generate the *Ddtpc2* null strain (by Dr. Lima). Fragments of homologous regions 5 and 6 were obtained by PCR using the indicated primer sets (see *Appendix 5.6*) and inserted into pLPBLP vector (obtained from dictyBase) using KpnI and HindIII for the 5' arm, and PstI and BamHI for the 3' arm. Genomic DNA extracted from resistant clones and PCR using a primer set (W1, W2) confirmed the disruption of the middle of *Dd*TPC2. 5' or 3' side targeted insertion was screened with the primer sets, W3 and 5'anti-sense, or 3'sense and W5, respectively.
B. Confirmation of *Ddtpc2* gene disruption.
gDNA was extracted from DH1 and single colonies 12-5 and 20-3, grown in HL5 medium with 10 μg/ml blasticidin. Fragment 3 in *Ddtpc2* or *histoneH3b* was amplified by PCR using a primer set KW56, KW57 or H3bF, H3bR respectively (*Appendix 5.6*). After 45 cycles of amplification, the PCR product of F3 was not obtained in 12-5 and 20-3 (shown on the upper lane) whereas that of *histoneH3b* was seen in all clones (shown on the lower lane), demonstrating the successful disruption of *Ddtpc2* and gDNA extraction, respectively.

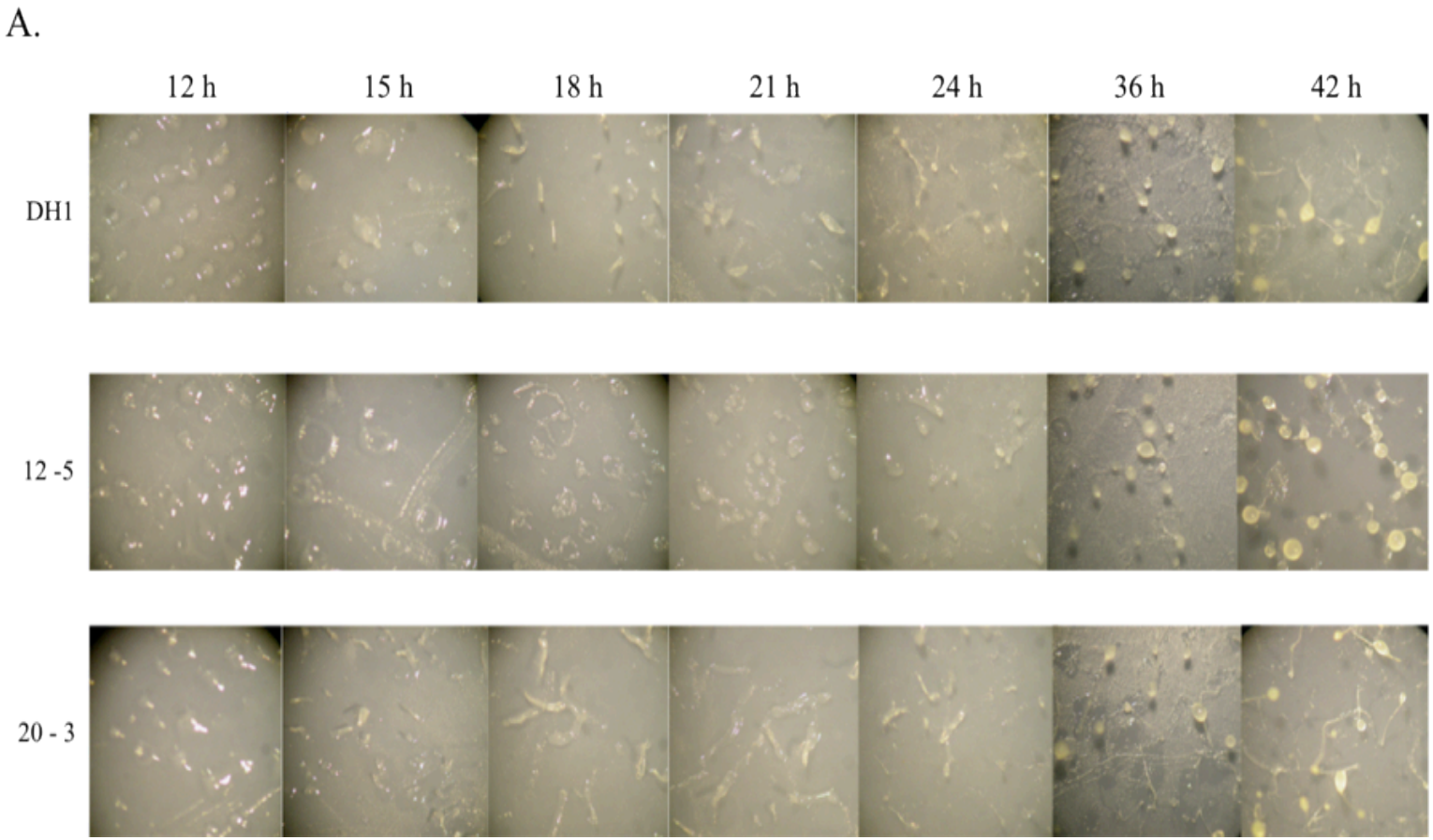


Figure 4.27. Development of *Ddtpc2* null clones
A. DH1 (Parental strain) or *Ddtpc2* null cells (clone 12-5 and 20-3) were grown on a 15 cm dish in HL5 medium supplemented with 10 µg/ml blasticidin. 2 x 10^7 cells were washed twice with KK_2 buffer and plated on 3.4 cm millipore filter paper. Starved cells were incubated on paper pre-soaked with KK_2 at 22°C. Developmental structures were observed using a Nikon SMZ-2B stereoscopic microscope and photographed using a Coolpix 4500 digital camera mounted on a light microscope (NIKON SMZ-2B stereoscopic microscope).

B.

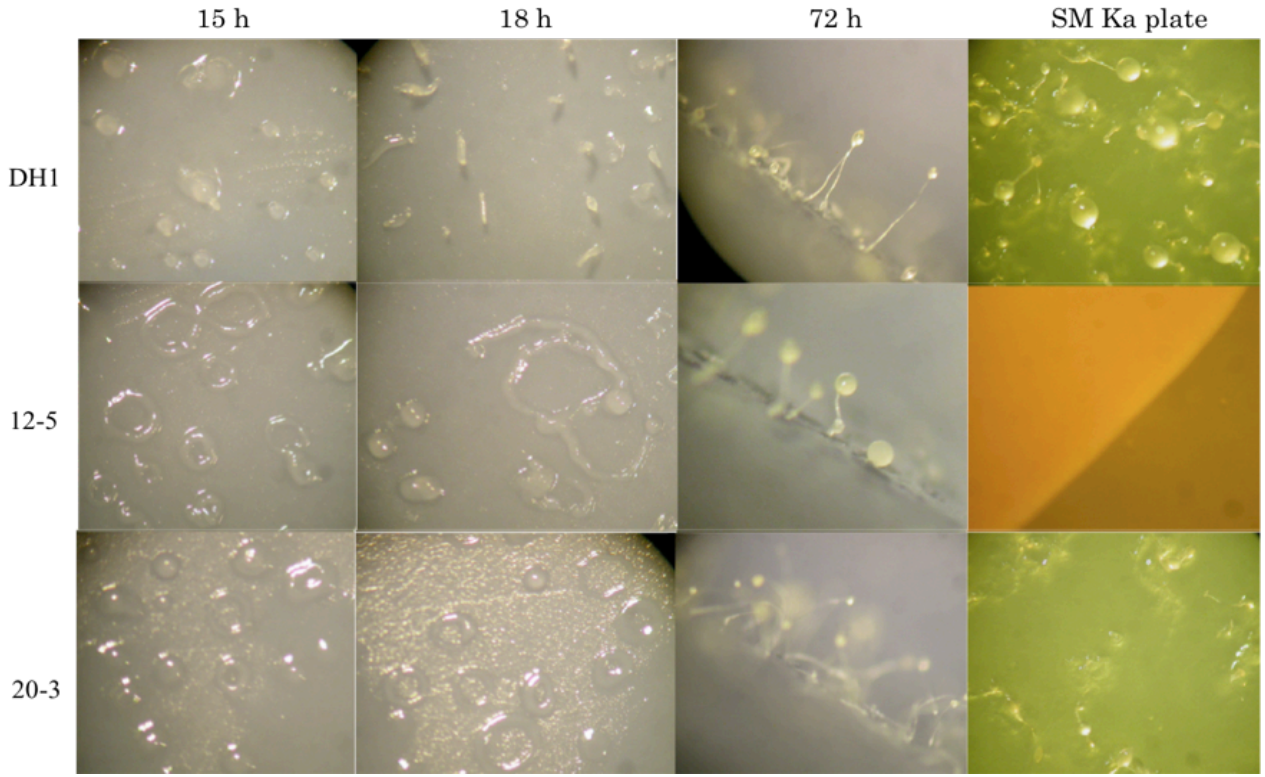


Figure 4.27B. Development of *Ddtpc2* null clones
B. Doughnuts-shaped mounds (clone 12-5 and 20-3) and fruiting bodies are shown at higher magnification. SM Ka plate shows the *Dictyostelium* cells developed on bacterial loan.

developmental delay was observed. After 12 hours of starvation, DH1 cells formed tight aggregates. In contrast, mutant strains continued to form loose aggregates, subsequently developing into doughnut-shaped mounds (Figure 4.27B). Clone 12-5 tended to make larger doughnut-shaped mounds, which split into small mounds before returning to the normal tight aggregates, therefore resulting in 8 - 10 hours developmental delay. On the other hand, although the 20-3 mutant formed doughnut-shaped mounds, the frequency of these was lower and the doughnuts were mainly small, and only up to 2 hours developmental delay was observed.

4.4. Discussion

There is increasing evidence suggesting that TPC2 is a NAADP-sensitive Ca^{2+} channel. For instance, purified recombinant protein of *Hs*TPC2 reconstituted into artificial membranes has been shown to behave as a NAADP-sensitive Ca^{2+} release channel (Pitt *et al*., 2010). In addition, overexpression of *Hs*TPC2 in HEK cells enhanced NAADP binding (Calcraft *et al*., 2009). *Dictyostelium* possesses only a single coding sequence for TPC and this shows higher homology to *Hs*TPC2 than to *Hs*TPC1. This suggests that *Dd*TPC2 may be involved in Ca^{2+} signalling.

4.4.1. The involvement of acidic Ca^{2+} stores in *Dictyostelium* development

The role of Ca^{2+} stored in acidic vesicles for *Dictyostelium* development is unknown. Therefore as a first step to investigate its importance, the effect of GPN on development was determined. GPN disrupts lysosomes by osmotic lysis in the presence of the lysosomal exopeptidase, cathepsin C, in sea urchin eggs (Churchill *et al*., 2002). Ax2 cells treated with GPN during development on filter paper exhibited a

few hours delay in forming slugs at concentrations above 800 μM GPN. This result is consistent with a role for acidic compartments in the development of *Dictyostelium*, and suggests that Ca^{2+} transients generated (at least in part) with the involvement of acidic compartments may be important. In sea urchin egg, 200 μM GPN bursts lysosomes (Churchill *et al*., 2002). However the specificity of GPN effect on acidic compartments in *Dictyostelium* is not clear, and it should be noted that a gene coding for cathepsin C is not found in the *Dictyostelium* genome, although it has been reported that *Dictyostelium* possesses a cathepsin D-like protein (Journet *et al*., 1999).

4.4.2. *Ddtpc2* mRNA levels are developmentally regulated

The expression pattern of *Ddtpc2* was released on the RNA-seq database on dictyExpress, showing that expression of *Ddtpc2* mRNA is developmentally regulated. The results from Northern blotting are consistent with low mRNA abundance predicted from RNAseq data, since the mRNA levels of *Ddtpc2* are lower (<200 scaled read counts) than those of abundant genes. For example, *erkB* has 3000 normalized reads at its peak of expression, whereas the mRNA levels of Ca^{2+} channels in general are lower, with normalized reads of 150, 95 and 50 for *iplA*, *mucolipin* and *polycystin-2*, respectively, at the peak of expression.

At stages (~12 hours), the role of Ca^{2+} may be important since prestalk/prespore genes begin to be expressed, and the levels of *tpc2* mRNA peak later at 16 hours. It was therefore important to know whether the transcript was expressed throughout the life cycle of *Dictyostelium* Ax2 cells under our laboratory conditions, as *Dd*TPC2 may also have a role during growth or early development. Amplifying a 783 bp-fragment

(F3: see *Appendix 5.6*) by RT-PCR confirmed that mRNA expression of *Ddtpc2* was detectable at all stages of development, including the vegetative stage.

4.4.3. Protein levels

Although *Dd*TPC2 protein existence is predicted, no evidence has been reported previously concerning *Dd*TPC2 expression at the protein level (Gaudet *et al*., 2009).

The expected molecular weight for endogenous *Dd*TPC2 and for the FLAG.*Dd*TPC2.mRFPmars protein are 237 kDa and 263.78 kDa, respectively. Endogenous proteins, with molecular weights of about 270 kDa, 200 kDa and 130 kDa, were detected by purified anti-*Dd*TPC2 antibody and increased in abundance towards the late stages of development. This trend is similar to that observed for mRNA abundance. The intensities of these bands were reduced on Western blot by competition with peptide, suggesting that they are specific to *Dd*TPC2. Although it is approximately 35 kDa larger than the predicted mass, the band at 270 kDa is likely to be *Dd*TPC2. A 300 kDa protein was detected by anti-mRFPmars antibody when expression of mRFPmars-tagged *Dd*TPC2 was induced by doxcycline. Furthermore, no such band was detected in the absence of *Dd*TPC2.mRFPmars, whereas a band with a molecular weight of 270 kDa was detected by anti-*Dd*TPC2 antibody in both the presence and absence of recombinant protein. A possible explanation is that the expression level of recombinant mRFPmars.*Dd*TPC2 was very low, so only endogenous *Dd*TPC2 was detected with the anti-*Dd*TPC2 antibody. Low expression levels may be due to the altered codon usage, or to the fusion protein being less stable or less well expressed than *Dd*TPC2 alone. It is possible that *Dd*TPC2 requires accessory proteins that are not abundant in vegetative cells when endogenous

*Dd*TPC2 is at a low level. A strong promoter was used to drive expression of FLAG. *Dd*TPC2.mRFPmars, thus it would be expected to drive higher expression than the endogenous promoter, especially as this was a multi-copy extrachromosomal plasmid; the length of time of induction with doxycycline might also lead to low expression levels, and hence use of longer times might be better.

The lower bands at around 130 kDa seen in Figure 4.16 and 4.17 may represent cleaved or degraded *Dd*TPC2 (compare with Figure 4.21A and B), since this band was not seen when cell lysate was prepared very gently or heated at low temperature (65-70°C) to minimize the possibility of degradation and cleavage.

*Hs*TPC2 is N-glycosylated (Hooper *et al*., 2011) and protein alignment shows that N273 and N618 are conserved in *Dicytostelium*. The band sizes detected by anti-mRFPmars antibody and anti-*Dd*TPC2 antibody in *Dictyostelium* are consistent with glycosylation, as occurs with human TPCs.

To conclude, the generated anti-*Dd*TPC2 antibody recognized endogenous *Dd*TPC2 at approximately 270 kDa, which confirmed that protein expression of *Dd*TPC2 is developmentally regulated. In addition, a protein product of approximately 300 kDa was successfully expressed without truncation or cleavage, since the mRFPmars-tag was at the C terminus, suggesting that it is likely to be a recombinant protein of *Dd*TPC2. This result allowed investigation of the subcellular distribution of *Dd*TPC2 in *Dictyostelium*.

4.4.4. Localization study

*Dd*TPC2 does not contain the dileucine lysosomal targeting signal peptide, namely a dileucine motif, which is found in *Hs*TPC1 and *Hs*TPC2 (Brailoiu *et al*., 2010b). However, acidic clusters of amino acids, which transfer transmembrane proteins to the CV (Mercanti *et al*., 2006), are found in *Dictyostelium* TPC2. Two putative sorting motifs are a diaromatic motif and an acidic motif, which are [Y]xxx[FW] and $[DE]_{2-3}$[F]xxΦ (where Φ is a hydrophobic residue). A similar amino acid sequence, repetition of $[DE]_2$, is present in *Dd*TPC2 at aa 91-99 (91 aa downstream from M1) (Figure 4.28). Although the [F] residue is further away than in the consensus, it would be very interesting to carry out mutagenesis studies or to express truncated versions of *Dd*TPC2 to explore the importance of this motif on targeting.

The subcellular localization of exogenously expressed *Dd*TPC2 in Ax2 cells was observed in intracellular compartments, both in the CV and in the ER. Unfortunately, the imaging of GFP expressed on the CV was not satisfactory, and this may have been due to the fixation technique I used, since visualization of the CV has been successfully demonstrated using a different fixation protocol, in addition, immunocytochemistry techniques allowed labelling the vacuolar proton pump with an appropriate antibody and have provided an excellent image of the CV (Kypri *et al*., 2007, Shaner *et al*., 2005). On the other hand, heterologously expressed *Dd*TPC2 was found to co-localize with a lysosomal marker and a trans-Golgi marker in HeLa cells, revealing useful information about the targeting of this protein.

Properly folded newly synthesized proteins are transferred from the ER to the Golgi apparatus. Proteins modified in the ER and Golgi apparatus exit through the trans Golgi network (TGN) and move to their next destination: lysosomes, secretory

A. Acidic motifs [DDEEE, DDEEED]

```
Rh50a     AGGDDEEEGVGKEH 488
Rh50b     LPSDDEEEDEFKQE 525
Furin     CPSDSEEDEGRGER 783
HIV-Nef   WLEAQEEEEVGFPV  70
Ent3a     DEEEDDDDEFSEFQ 276
```

B.

```
DdTPC2 MWKNNLNRNRGILTSTDEDSNDINNNNNDNINSPNSIKSHKSSKSGSSTKTNKSTKTIKS  60
       ASSSLQSRQIDLGFLKKLDTLPNEHSDDSYEEEDEDEDDYETHSYDSFDQSCDDCDENNI 120
       EDSEDSCELADDEDSENLSENDNNNNNNNNNNDNDNNEFNFGEGEEENNEENNEEEYNED 180
       NEDNEDNYETVNKIKKHDVFRKNQLKNILEFDDTFVGNKYNKHKTFNKFAYNNGAKTSLE 240
       SIIEKSESSITQRSNGSSPIPKRKKSITSNVDNNNNNNNINNNGNNNNNINDNGNNNKSP 300
       FLHQIKIPHSYKEKLISPHYNYNRTRGSLNLPPNGGTYSSPSSSSSSYSSISTTSSIFPT 360
       SPNMEIPRPRSLPQTFSSSSSPSPIDDHQKQDELGKSPLLKQKQKDEEKKEKEEKEGRGR 420

HsTPC2 ----------------------------------------MAEPQAESEPLLGGAR  16
```

Figure 4.28. Acidic clusters (Mercanti *et al*., 2006)
A. Acidic motifs found in *Dictyostelium* proteins (Rh50a, Rf50b, Furin and HIV-Nef), which are localized to contractile vacuole and a yeast protein (Ent3a) are coloured with red. B. The sequences similar to these acidic clusters found in *Dd*TPC2 are coloured in red. Methionine and identical residues are indicated with a red box and blue letters, respectively. The number shown on the right hand side represents the number of amino acids from the methionine coded by the putative start codon.

vesicles, the cell surface, or return to the ER. Therefore, it might be expected that lysosomal or CV proteins would be detectable in the ER and Golgi also.

The maturation time ($t_{0.5}$) of RFP is 40 min (Merzlyak *et al*., 2007), and RFP starts off green in colour (Wachter *et al*., 2010), therefore immature mRFPmars-tagged *Dd*TPC2, which has just been inserted into the trans Golgi network may appear green. The nature of RFP could explain why *Dd*TPC2 colocalized with the trans Golgi marker in addition to the marker for lysosomes, although it does not eliminate the possibility that *Dd*TPC2 is localized to the trans Golgi network also.

Furthermore, the results from the localization studies in HeLa cells broadens the choice of systems available to investigate the biochemical role of *Dd*TPC2 in comparison with other TPCs and to carry out functional studies, for instance, Ca^{2+} imaging or physiological analysis using whole cells, since the pharmacological approaches are more reliable and established in mammalian systems. The studies on *Sp*TPCs or *Hs*TPCs published previously from our laboratory have employed HEK cells (Calcraft *et al*., 2009; Galione *et al*., 2010; Ruas *et al*., 2010); however, HeLa cells recently have become the first choice for Ca^{2+} imaging studies. This is especially interesting as *Dd*TPC2 possesses EF-hands, which is an unusual feature of *Dd*TPC2, and CICR has been reported to operate through the CV in *Dictyostelium* (Malchow *et al*., 2008).

4.4.5. The role of *Dd*TPC2 during development

It is interesting that at least 4 different putative Ca^{2+} channels are expressed with different timing during development, increasing the complexity of Ca^{2+} signalling. The expression level of each gene throughout development is shown in Figure 1.4D.

The pattern of global Ca^{2+} changes during the development of *Dictyostelium* has been visualized using jellyfish apoaequorin (Cubitt *et al*., 1995), as shown in Figure 1.4C, with a high Ca^{2+} level detected in the prestalk cell region in multicellular structures. However, a higher sensitivity of Ca^{2+} detection is required to measure transient Ca^{2+} elevations in individual cells. The generation of Ca^{2+} channel ablation strains will allow for further understanding of the Ca^{2+} signalling mechanisms and their functional importance in *Dicyostelium*.

Ddtpc2 is not an essential gene since mutants have been isolated in a DH1 parental strain; furthermore, *Ddtpc2* deletion strains were capable of growing normally and forming aggregates without significant delay. However, it is interesting that *Ddtpc2* null cells exhibited doughnut-shaped mounds, which appeared after the formation of loose aggregates; this caused about 2 - 10 hours developmental delay. The mechanism underlying the formation of the doughnut-shaped mounds is unknown.

4.4.6. NAADP binding activity in *Dictyostelium* cells

NAADP binding to P1 membrane fractions prepared from T4 Ax2 cells, showed a significant amount of specific binding which was enhanced when samples were prepared from T20 cells, developed on filter paper. These results suggest some correlation between NAADP binding and protein expression levels of *Dd*TPC2.

However, the IC_{50} for NAADP was 2.1 ± 0.6 μM (a Hill slope of -0.58 ± 0.40), which is extremely high compared to that of sea urchin egg, which is 0.54 ± 0.07 nM (with a Hill coefficient of 1.1 ± 0.003) (Patel *et al*., 2000a). In mammalian cells, the IC_{50} of NAADP binding in mouse/rat brain membranes was 200 ± 17 nM, with a Hill coefficient of 0.76 ± 0.04, which indicates that multiple binding sites for NAADP may exist in mammalian cells (Patel *et al*., 2000b). Indeed, membranes prepared from HEK293 cells, overexpressing *Hs*TPC2, had two sites with different affinities for NAADP, with dissociation constant (K_d) values of 5.0 ± 4.2 nM and 7.2 ± 0.8 μM. Similarly, mouse liver membranes had two binding sites for NAADP with K_d values of 6.6 ± 3.5 nM and 4.6 ± 2.4 μM (Calcraft *et al*., 2009). Since the Hill slope derived from NAADP binding to *Dictyostelium* membranes is not close to unity, this may indicate that another higher affinity binding site is also present in these membranes.

The binding specificity was further examined using heat or proteinase treatment on T4 membrane, since DIF-1 binding has been shown to be completely destroyed when samples were treated with 1 mg/ml pronase (a proteinase mixture) at 22°C for 20 min (Insall and Kay, 1990). However, heat inactivation of membrane proteins or incubation with proteinase did not disrupt NAADP specific binding. Trypsin cleaves peptide chains mainly at the carboxyl side of the amino acids lysine or arginine, except when either is followed by proline, therefore trypsinization may not be sufficient to disrupt NAADP binding. Alternatively, the binding seen may not be due to a protein, thus autoclave or NaOH treatment may have been necessary for the clarification.

A competitive equilibrium NAADP binding assay on T20 membrane confirmed the presence of a single NAADP binding site with IC_{50} of 73 ± 14 μM and no higher affinity site. In contrast, NADP exhibited two binding sites with IC_{50} values of 11 ± 5.2 nM and 14 ± 4.6 μM. The purity of NAADP is very important for interpretation of the binding assay, as there may be some contaminating NADP in the NAADP. Unlabelled NAADP used for all experiments contained 86 % NAADP and 24 % NADP, whereas the composition of NADP purchased from Sigma-Aldrich was 87.5 % NADP and 0.27 % NAADP. It is possible that NADP contamination of NAADP is sufficient to inhibit labelled NAADP binding to *Dictyostelium* membranes (Patel *et al*., 2000a).

Another point to note is that endogenous NAADP level in *Dictyostelium* is not measured, if *Dictyostelium* synthesizes NAADP and the receptors have already occupied by endogenous NAADP in the first place, it could prevent exogenous unlabelled/labelled NAADP added in the present assay from binding to NAADP receptor in the situations that irreversible NAADP binding or the self-desensitization of NAADP receptor occurs.

In conclusion, it was not possible to demonstrate the existence of a high affinity NAADP binding site in *Dictyostelium*. Now that the protein has been expressed in HeLa cells, this may prove useful for further analysis since techniques and procedures for NAADP binding assays are more established in this mammalian system than in *Dictyostelium*.

4.5. Summary

Developmentally expressed *Dd*TPC2 has been identified at the endogenous protein level, and its distribution in intracellular compartments, the CV and ER in *Dicytostelium*, and in lysosomes and Golgi apparatus in HEK cells, was determined by detecting exogenously expressed *Dd*TPC2. Potentially disrupting acidic Ca^{2+} stores using GPN caused a few hours delay in the formation of mounds at concentrations of GPN above 800 μM. Some defects in the development of *tpc2*$^{-}$ cells at the late stages of aggregation were also seen, consistent with a role for TPC2 in late development. However, no high affinity NAADP binding site could be detected in T4 or T20 cells.

CHAPTER 5

CALCIUM RELEASE FROM INTRACELLULAR VESICLES ISOLATED FROM SEA URCHIN EGGS AND *DICTYOSTELIUM*

5.1. Introduction

5.1.1. Ca^{2+} release in sea urchin egg homogenate

Sea urchin eggs provide an excellent model system in which to study Ca^{2+} release mechanisms from intracellular Ca^{2+} stores, including those induced by NAADP, IP_3 and cADPR (Churchill *et al.*, 2002; Genazzani *et al.*, 1997; Genazzani *et al.*, 1996). NAADP releases Ca^{2+} from acidic stores that are quite distinct from those sensitive to IP_3 and cADPR, since the ER SERCA inhibitor, thapsigargin (Tg), inhibits Ca^{2+} release from the ER, while NAADP-induced Ca^{2+} release is only partially reduced by Tg in intact sea urchin eggs or in egg homogenate (Genazzani and Galione, 1996; Churchill and Galione, 2001). In addition, only the NAADP response was abolished by pretreatment of vesicles with GPN, which causes osmotic lysis of the vesicles (Churchill *et al.*, 2002).

There have been no published reports of AA-induced Ca^{2+}release from sea urchin egg homogenate. One publication mentioned that AA inhibited Ca^{2+}release induced by NADP and alkali-NADP with half-maximal inhibition occurring at 5 μM (Clapper *et al.*, 1987), although the specific data were not shown in the paper. This result could be interpreted as an inhibitory effect on NAADP-induced Ca^{2+}release, since NAADP was later found to be a contaminant of NADP (Lee and Aarhus, 1995).

5.1.2. Ca^{2+} release from *Dictyostelium* membranes

There have been many studies to investigate Ca^{2+} transients in *Dictyostelium* using whole cells, including one describing cAMP or AA-induced Ca^{2+} influx, which has been suggested to be store operated Ca^{2+} influx (Schaloske *et al.*, 1997; Schaloske *et*

al., 1998). An alternative approach has been to visualize changes in cytosolic Ca^{2+} levels by monitoring Ca^{2+}-dependent luminescence in intact cells expressing jellyfish apoaequorin (Cubitt *et al.*, 1995). However, apoaequorin is not sensitive enough to detect the small Ca^{2+} transients observed in response to cAMP; it only detects the larger, more stable changes seen later in development. These studies successfully demonstrated the relationship between the prestalk/prespore ratio and intracellular Ca^{2+} events triggered by the applied molecules.

The signalling cascades activated by the binding of cAMP to its cell surface receptors, including PLA_2 activation which is proposed to induce Ca^{2+} changes through fatty acid (FA) production together with PIP_3 signalling, are considered to be essential for chemotaxis. Intracellular vesicles prepared from *Dictyostelium*, starved for about 4 hours, respond to Ca^{2+} and AA by releasing Ca^{2+}, as judged by increased fluorescence of Ca^{2+} sensitive dyes such as Fluo-3 (Malchow *et al.*, 2006; Malchow *et al.*, 2008). Ca^{2+} release from intracellular Ca^{2+} stores induced by FAs, especially AA, is relatively well characterized. AA is thought to release Ca^{2+} from acidic stores, that is, the contractile vacuole (CV), since AA-induced Ca^{2+}-release is reduced in *lvsA*$^-$, a mutant strain in which the CV is impaired (Malchow *et al.*, 2006). *Dictyostelium* possesses two main intracellular Ca^{2+} stores, a concanamycin A (CMA) sensitive store and a Tg sensitive store, the latter is thought to be responsible for IP_3-induced Ca^{2+}-release. Many studies have suggested that Ca^{2+} signalling through the acidic stores plays an important role in chemotaxis (Chen *et al.*, 2007; Schaloske *et al.*, 1998; Schaloske *et al.*, 2007). To date, only AA (representing fatty acids in general) has been reported to mobilize Ca^{2+} from acidic stores in *Dictyostelium,* with the exception of Ca^{2+} itself using CICR mechanisms (Malchow *et al.*, 2008). The

presence of an AA-sensitive Ca^{2+} transient mechanism is implied by the latter finding, but whether the Ca^{2+} signalling mechanism is operated by arachidonate-regulated Ca^{2+}-selective (ARC) channels remains to be established.

5.2. Aims

The aims of this chapter were to gain further insights into NAADP- and arachidonic acid (AA)-induced Ca^{2+} release in *Dictyostelium*, and study AA responses in sea urchin egg cell extracts. To address these questions, a cell free system to analyze Ca^{2+} uptake and release in *Dictyostelium* was established and the pharmacology of Ca^{2+} release mechanisms in sea urchin egg homogenates and *Dictyostelium* was compared. In addition, Ca^{2+} responses were examined in *tpc2*$^{-}$ *Dictyostelium* cells.

5.3. Results

5.3.1. Ca^{2+} release studies in vesicle preparations from *Dictyostelium*

5.3.1.1. Ca^{2+} uptake into intracellular Ca^{2+} stores requires ATP

Intracellular P1 vesicles were prepared from Ax2 cells starved for 4 hours (T4) in a shaking suspension following the protocol described for the NAADP binding assay (see *Chapter2* and Figure 4.7). 200 - 400 µg of membrane were resuspended in Ca^{2+} uptake buffer without ATP, in the presence of the Ca^{2+}-sensitive fluorescent dye Fluo-3. Ca^{2+} uptake was initiated by the application of 1.5 mM ATP as determined by loss of the Ca^{2+} signal outside the vesicles. Free ionized Ca^{2+} was measured by monitoring emission at 535 nm (490 nm excitation) using a fluorometer (NovoStar). In the absence of ATP, no Ca^{2+} uptake was detected (Figure 5.1). ATP is required for

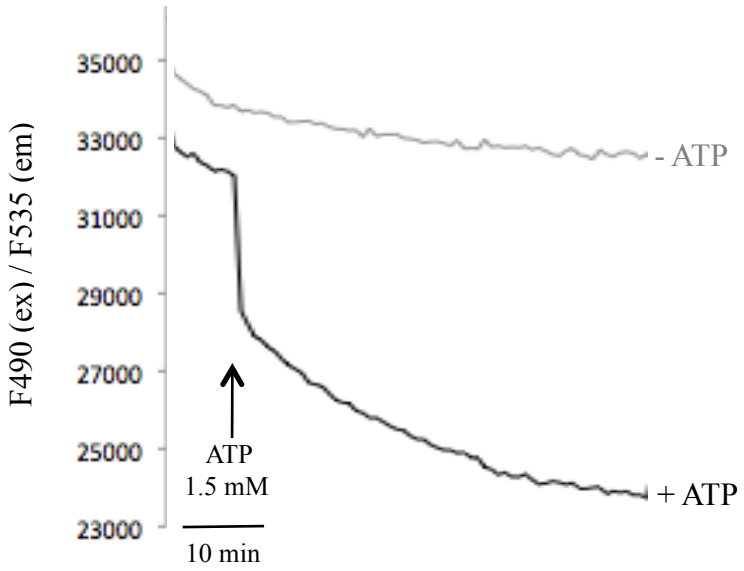


Figure 5.1. Ca^{2+} uptake into intracellular vesicles
200 µg of the P1 fraction prepared from T4 Ax2 cells was added to a total volume of 50 µl Ca^{2+} uptake buffer supplemented with 100 µM NaN_3 and 6 µg/ml oligomycin A. Free ionized Ca^{2+} was measured by monitoring the fluorescence emission of 6.6 µM fluo-3 (490 nm excitation wavelength and 535 nm emission wavelength) using a Fluorometer (NovoStar). Representative fluorimetric traces of Ca^{2+} uptake are shown. Ca^{2+} uptake was initiated by adding 1.5 mM ATP to the reaction in the trace shown in black.

Ca^{2+} uptake into intracellular Ca^{2+} compartments in *Dictyostelium*, as has also been reported in sea urchin egg homogenate (Churchill *et al.*, 2002). The same result was obtained using vesicles prepared from *Dictyostelium* cells at vegetative (T0) and late developmental (T20) stages (data not shown).

5.3.1.2. Arachidonic acid-induced Ca^{2+} release

Previously, it has been reported that AA can induce Ca^{2+} release from these vesicle fractions (Malchow *et al.*, 2006). Therefore, the Ca^{2+}mobilizing ability of AA was examined to determine whether the vesicle preparations were capable of releasing Ca^{2+}. AA-induced Ca^{2+} release from P1 membrane fractions prepared from T4 cells (T4P1) occurred in a concentration-dependent manner (Figure 5.2). Release was triggered by 2.5 μM AA and was maximal at 15 μM. Ca^{2+} uptake was observed after its release, suggesting that the stores remained intact, and the stores were responsive to a second application of AA at 5 μM (Figure 5.2). Previous experiments that demonstrated AA-induced Ca^{2+} release had only been carried out using vesicles isolated from T4 cells. However, *Dd*TPC2 is maximally expressed late in development. Therefore, P1 vesicles were prepared in the same way from T20 cells developed on buffered agar. These vesicles also exhibited ATP-dependent Ca^{2+} uptake and AA-induced Ca^{2+} release over a similar concentration (5 - 20 μM) range (Figure 5.3). The mechanism of AA-induced Ca^{2+} release is unknown, but it is of relevance that the genes coding for orthologues of Orai, STIM and TRP channel proteins have not been found in the *Dictyostelium* genome sequence.

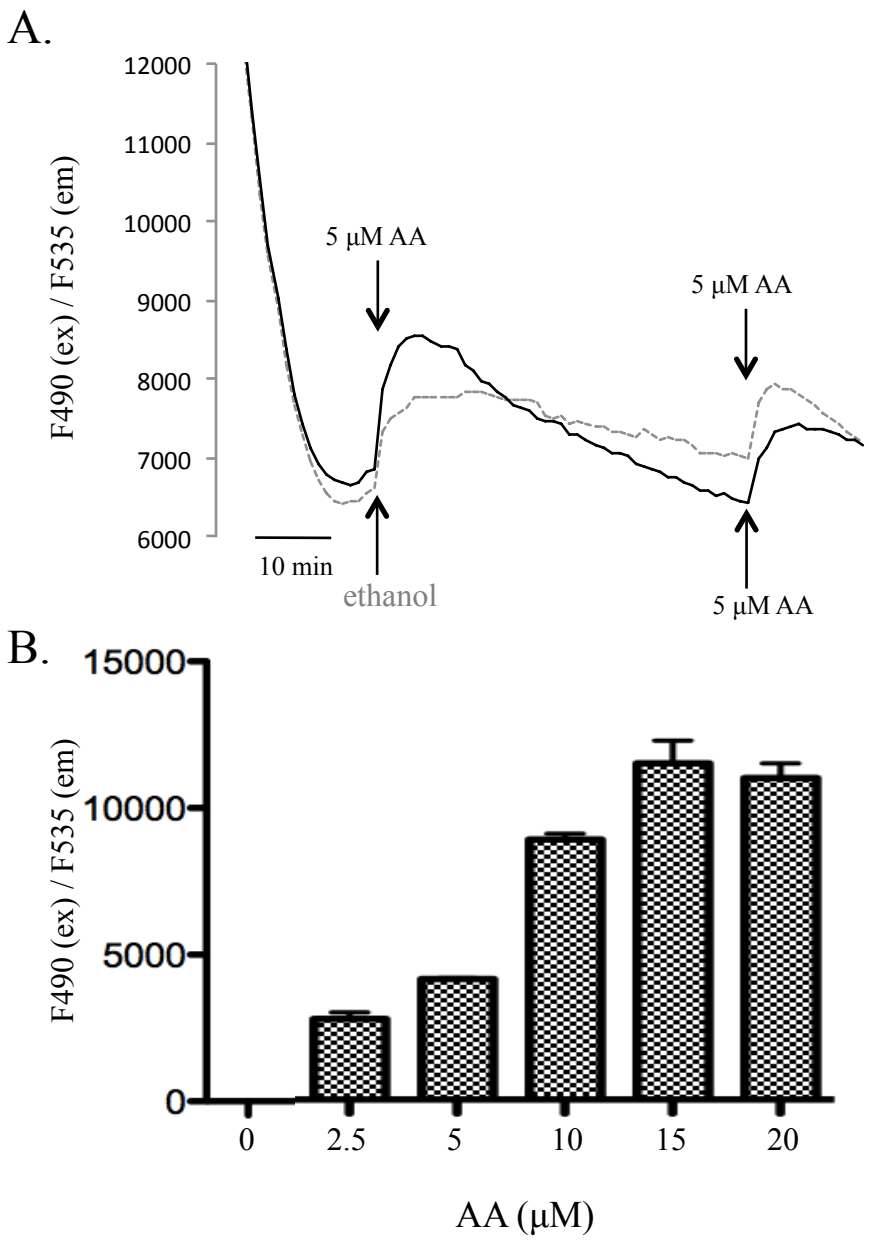


Figure 5.2. Ca^{2+} mobilizing activity of AA in P1 vesicles prepared from cells developed for 4 hours (T4)

200 - 400 µg of the P1 fraction prepared from T4 Ax2 cells was added to a total volume of 100 µl Ca^{2+} uptake buffer supplemented with 100 µM NaN_3, 1.5 mM ATP and 6 µg/ml oligomycin A. A. Representative fluorimetric trace of AA-induced Ca^{2+} release. B. AA-mobilized Ca^{2+} release was quantified for a range of AA concentrations in 3 independent experiments (mean ± S.E.M., $n = 3$).

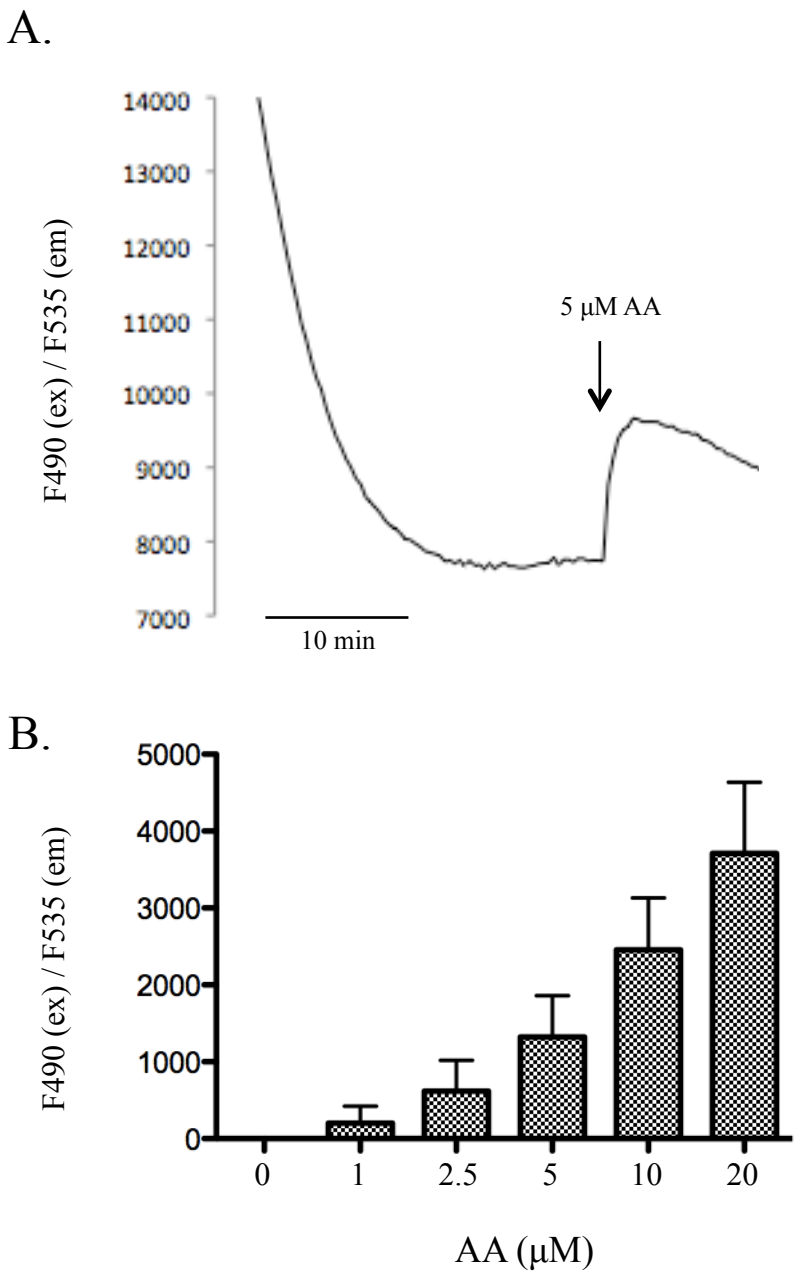


Figure 5.3. Ca^{2+} mobilizing activity of AA (T20)
Ax2 cells were developed on 2% KK_2 agar and harvested at early culminant stages (T20). 200 µg of P1 was added to a total volume of 100 µl Ca^{2+} uptake buffer supplemented with 100 µM NaN_3, 1.5 mM ATP and 6 µg/ml oligomycin A to allow calcium uptake into vesicles. Free ionized Ca^{2+} was measured with 6.6 µM fluo-3. A. Representative fluorimetric trace of AA-induced Ca^{2+} release. B. AA-mobilized Ca^{2+} release was quantified for a range of AA concentrations in 6 independent experiments (mean ± S.E.M., $n = 6$).

5.3.1.3. Ability of other FAs to cause Ca^{2+} release from T4P1 vesicles

AA is not synthesized endogenously in *Dictyostelium* (Weeks, 1976). Therefore, octadehydroarachidonic acid (ETYA), a non-metabolizable analogue of AA, and other fatty acids, including those already reported to have Ca^{2+} mobilizing activity in *Dictyostelium* (Schaloske *et al.*, 1998), palmitic acid (PA), oleic acid (OA), linoleic acid (LA) and 5,8,11-eicosatriynoic acid (ETI), were tested on T4P1 membrane preparations (Figure 5.4). The chemical structures of these FAs are shown in Figure 5.5. ETYA-induced Ca^{2+} release was at least equal to that induced by AA, suggesting AA-induced Ca^{2+} release was not dependent on metabolism. OA, which is endogenously synthesized in *Dictyostelium,* elicited comparable Ca^{2+} mobilizing activity to that of ETYA. PA also caused release of Ca^{2+}, but increasing the concentration of PA to 10 mM did not change the amount of Ca^{2+} released. LA and ETI also induced comparable Ca^{2+} release at 5 μM, although a concentration of 10 μM was not tested. Care must be taken when comparing the levels of Ca^{2+} mobilizing ability since Ca^{2+} contamination is often found in FAs; however, in these experiments, all FAs were equally treated with chelex before use to chelate any contaminating Ca^{2+}.

5.3.1.4. Release of Ca^{2+} from vesicles by NAADP

Membranes prepared from T4 and T20 showed significant Ca^{2+} release in response to AA; therefore, the ability of NAADP to release Ca^{2+} was tested. NAADP was unable to mobilize detectable levels of Ca^{2+} from either P0 or P1 membranes, even though these preparations were able to uptake Ca^{2+}, and release Ca^{2+} in response to 8 μM AA (P1: Figure 5.6; P0: data not shown). This was true for vesicles prepared from both T4 and T20 cells, and for a range of NAADP concentrations from 50 pM to 10 μM.

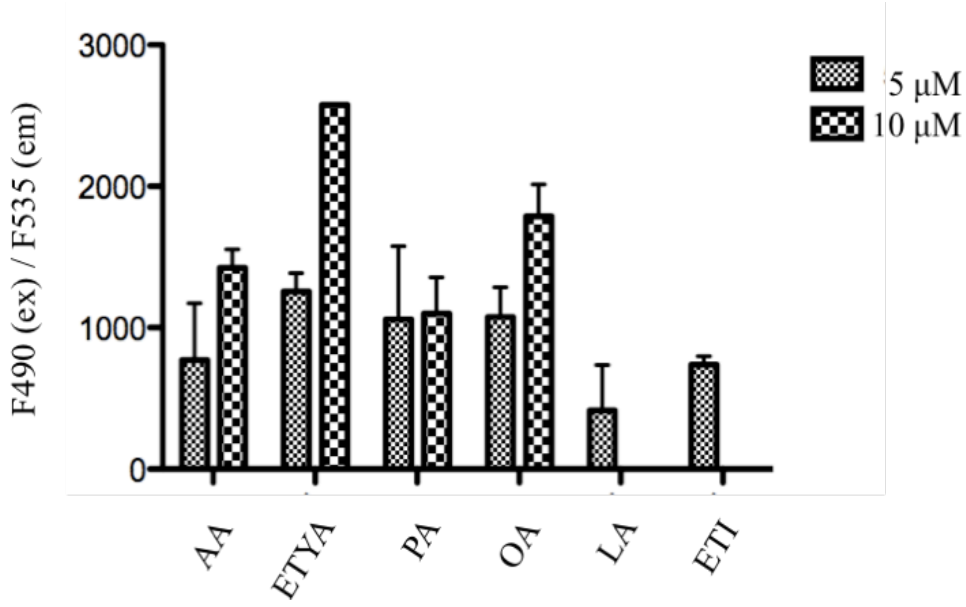


Figure 5.4. Ca^{2+} mobilizing activity of fatty acids
The P1 fraction was prepared from Ax2 cells at T4. Indicated concentrations of fatty acids, dissolved in ethanol, were applied to reaction mixtures containing 300 µg of membrane. Ca^{2+} release was measured with 6.6 µM fluo-3. All dissolved fatty acids were vortexed with chelex for 15 - 20 min at room temperature prior to experiments and it was confirmed that there was no contamination with Ca^{2+}. Data are represented as the mean ± S.E.M. of 3 independent experiments. LA (10 µM) and ETI (10 µM) were not tested.
Fatty acids used were arachidonic acid (AA), octadehydroarachidonic acid (ETYA), palmitic acid (PA), oleic acid (OA), linoleic acid (LA) and eicosatriynoic acid (ETI).

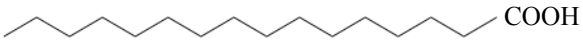
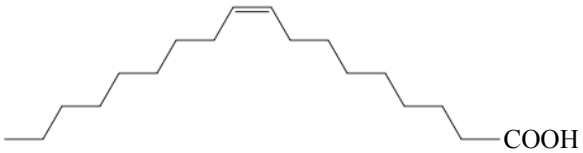
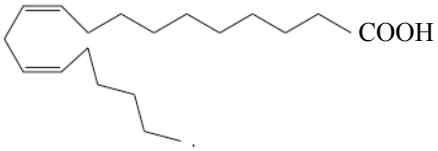
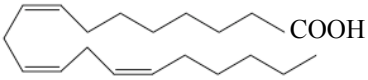
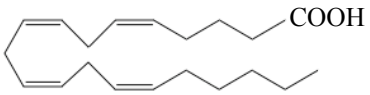
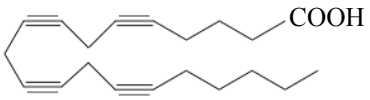
Fatty acid	Number of C / double bond	Chemical structure
PA	C16 / 0	
OA	C18 / 1	
LA	C18 / 2	
ETI	C20 / 3	
AA	C20 / 4	
ETYA	C20 / 4	

Figure 5.5. Chemical structures of fatty acids

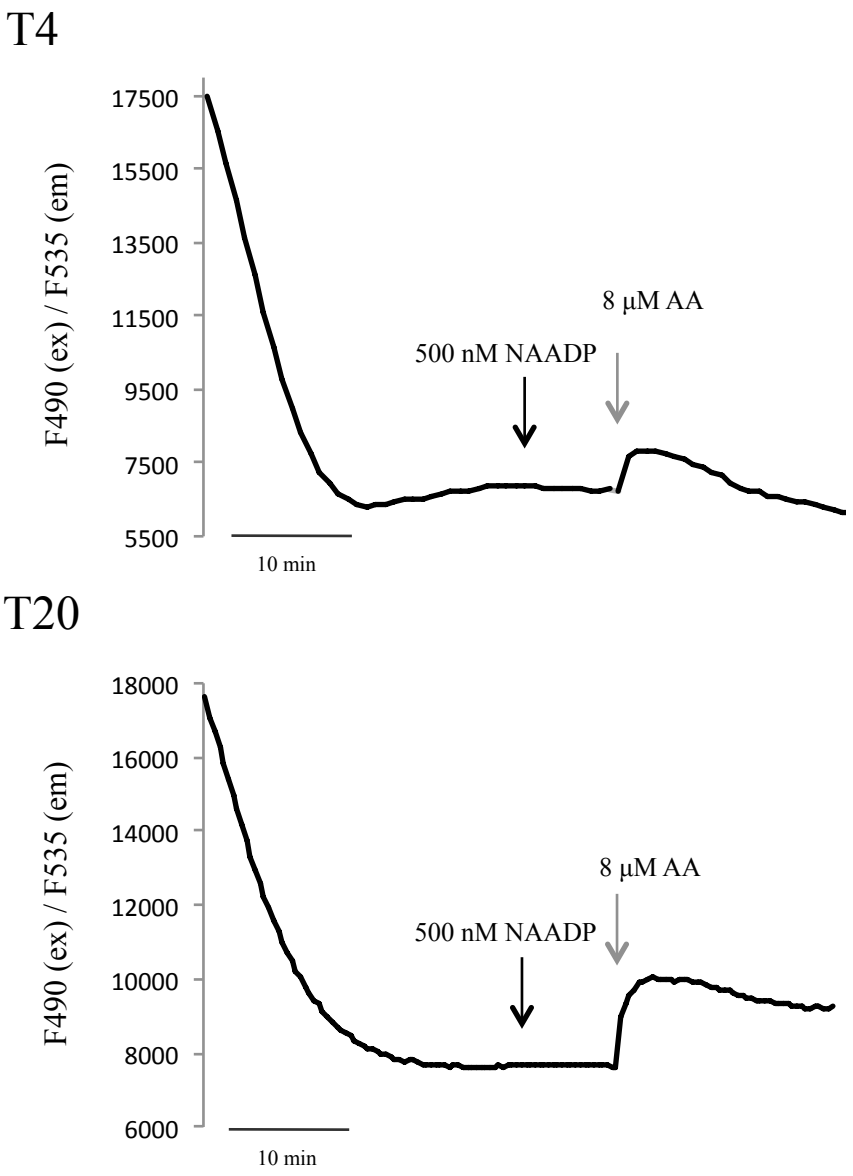


Figure 5.6. Ca^{2+} mobilizing ability of NAADP in P1 from T4 and T20 cells
500 nM NAADP was applied to 200 - 400 μg of P1 membrane after Ca^{2+} uptake into the vesicles in the presence of 1.5 mM ATP, and the Ca^{2+} changes measured with 6.6 μM fluo-3. AA 8 μM was later added to confirm the integrity of vesicles. Representative fluorimetric traces of P1 fractions from T4 and T20 cells are shown.

Unexpectedly, a small amount of NAADP-induced Ca^{2+} release was detected in the P0 fraction from vegetative cells (Figure 5.7A). Concentrations of NAADP from 50 pM to 10 μM were tested for their ability to induce Ca^{2+} release. The concentration-response relationship for NAADP was characterised as a bell-shaped curve – a shape often observed in other systems e.g. Jurkat T-cells (Berg *et al.*, 2000) and pancreatic β-cells (Masgrau *et al.*, 2003) (Figure 5.7B and data not shown). Preliminary results revealed similar NAADP-induced Ca^{2+} release in P0 from vegetative stable cell lines expressing FLAG.*Dd*TPC2.mRFPmars (n = 1 out of 2) or mRFPmars (n = 2 out of 2). A representative trace of NAADP-induced Ca^{2+} release and a concentration-response curve for NAADP-mediated Ca^{2+} mobilization in the stable cell line expressing mRFPmars are shown in Figure 5.7. The Ca^{2+} release was small, and in some preparations release was not detectable, perhaps due to the levels of Ca^{2+} being below the limits of detection.

5.3.1.5. The role of *Dd*TPC2 in NAADP-induced Ca^{2+} release

In order to determine if the NAADP-induced Ca^{2+} release was dependent on *Dd*TPC2, experiments were carried out in two independent *Ddtpc2*$^-$ strains, 12 and 20. P0 fractions were prepared from vegetatively growing cells, *Ddtpc2*$^-$ clones 12-6 and 20-1. NAADP-evoked Ca^{2+} release was detected in both clones 12-6 and 20-1, showing a similar concentration-response relationship to wild type cells with maximal Ca^{2+} release at NAADP concentrations of 125 nM and 250 nM, respectively (n=1 out of 3) (Figure 5.8).

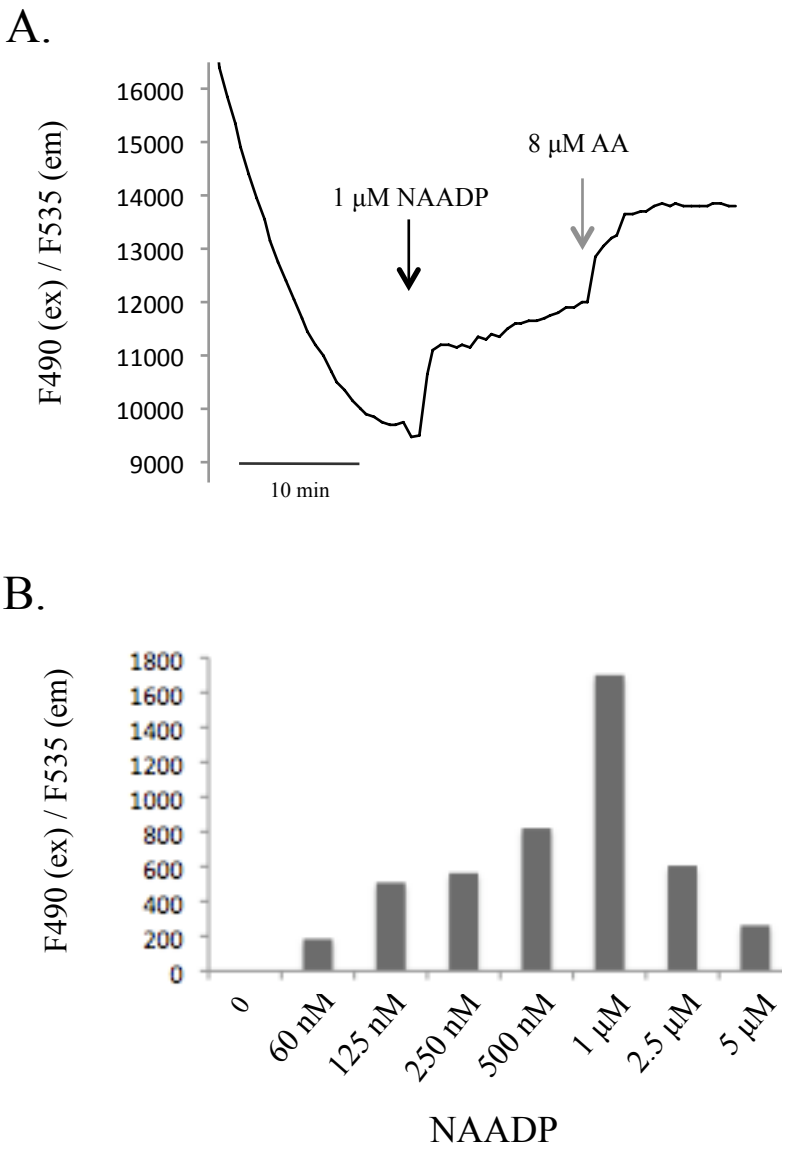


Figure 5.7. Concentration-dependence of NAADP-induced Ca^{2+} mobilization in P0 fractions from vegetative cells (T0)
A. 400 µg of P0 from vegetatively growing cells, in Ca^{2+} uptake buffer as in Figure 5.1, was incubated in the presence of fluo-3 (6.6 µM), and either NAADP or H_2O (not shown) was added to the reaction after Ca^{2+} uptake. Ca^{2+} re-uptake was not seen after the addition of NAADP; therefore, 8 µM AA was added to show that the vesicles were still active. B. Different concentrations of NAADP were tested for Ca^{2+} mobilizing activity as in A. One representative experiment is shown using Ax2 cells which stably expressing mRFPmars.

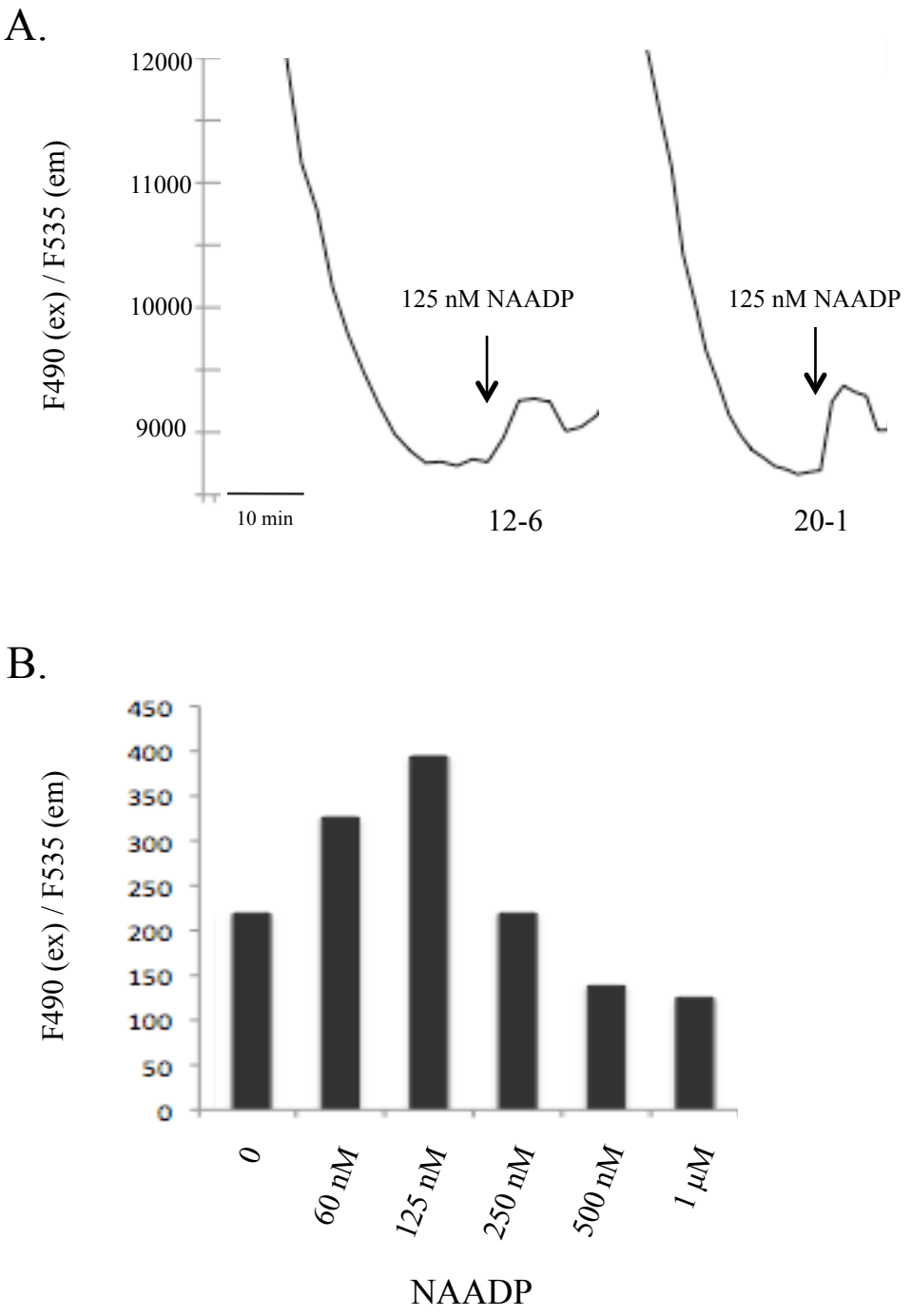


Figure 5.8. NAADP-induced Ca^{2+} release in the T0P0 fraction prepared from *Ddtpc2* knockout strains (12–6 and 20–1)
Cells grown on plates were harvested just before reaching 80% confluency and intracellular vesicles were extracted. After Ca^{2+} uptake, up to 1 μM NAADP was applied to the P0 membranes (400 μg/reaction), followed by 8 μM AA. A. Representative fluorimetric traces are shown. B. The Ca^{2+} release in response to different concentrations of NAADP was quantified. One representative experiment is shown.

5.3.1.6. The role of *Dd*TPC2 in AA-induced Ca^{2+} release

5 μM and 10 μM AA were tested on the P0 fraction from vegetatively growing *Ddtpc2*$^{-}$ clones 12-5, and 20-3, and compared to effects on the parental strain, DH1. A small level of AA-induced Ca^{2+} release was observed in the T0P0 fraction from DH1; however, the equivalent preparation of *Ddtpc2*$^{-}$ did not respond to AA, even though it did respond to NAADP (Figure 5.9). This result suggests an involvement of *Dd*TPC2 in AA-mediated Ca^{2+} signalling in *Dictyostelium.*

5.3.1.7. Ca^{2+} mobilising activity of differentiation inducing factor (DIF) in T4P1 vesicles

The effect of DIF-1 on stalk gene expression is mediated by an elevation of the intracellular Ca^{2+}concentration (Schaap *et al.*, 1996) with STATc tyrosine phosphorylation being controlled by the Ca^{2+} concentration (Araki *et al.*, 2010). Therefore, the ability of DIF-1 to cause Ca^{2+} release directly from vesicles was tested. Endogenous DIF-2 and DIF-3 have been identified as pentan-1-one and monochloro analogues of DIF-1 respectively (Morris *et al.*, 1988), and have been reported to possess dramatically reduced biological activity (the chemical structures of DIF-1, 2 and 3 are shown in Figure 1.6).

The Ca^{2+} mobilizing activities of DIF-1, DIF-2 and DIF-3 were examined using the P1 fraction from T4 Ax2 cells (Figure 5.10). Concentrations between 10 nM and 100 nM were tested, and ~ 50 nM of DIF-1, 2 and 3 induced small amounts of Ca^{2+} release from T4P1 vesicles. These concentrations are within the physiological range, as physiological levels of DIF-1 have been shown to be ~70 nM (Kay, 1998);

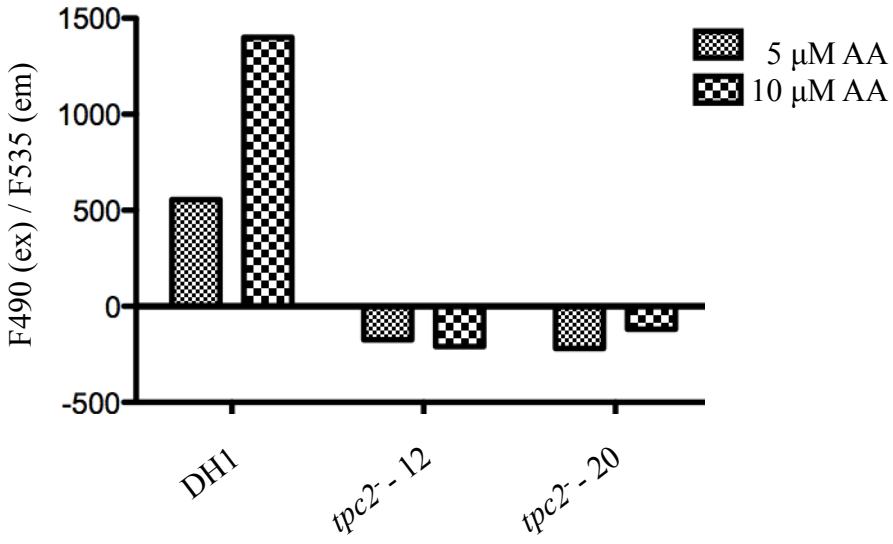


Figure 5.9. AA-induced Ca^{2+} release in the P0 fraction prepared from T0 *tpc2*$^{-}$ cells

Vegetatively growing *tpc2*$^{-}$ cells and the parental strain, DH1 cells, were harvested and P0 membranes isolated. Either 5 μM or 10 μM AA was applied to the reaction buffer containing 400 μg of P0 membrane, and free ionized Ca^{2+} was measured using 6.6 uM fluo-3. Ca^{2+} release caused by disruption of the vesicles by the vehicle (ethanol) was subtracted from each measurement (N=1).

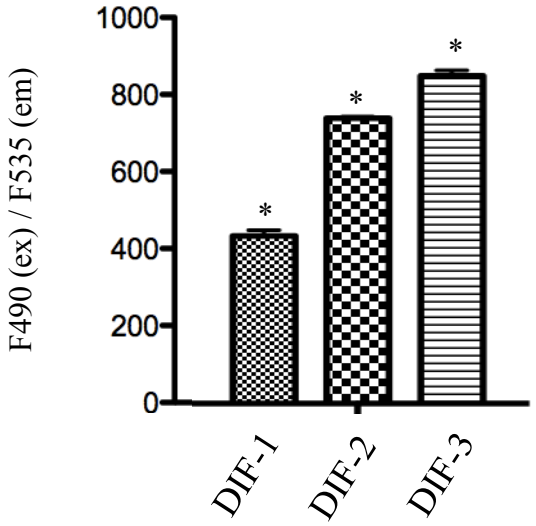


Figure 5.10. Ca^{2+} mobilization caused by DIF analogues
300 µg of T4P1 membranes were suspended in reaction buffer as described in Figure 5.1 and 50 nM DIF-1, 2 and 3 were added after Ca^{2+} uptake into vesicles. Ca^{2+} changes were measured using 6.6 µM fluo-3.
The mean ± S.E.M. of three independent experiments is shown. Data were analysed by ANOVA followed by Dunnett's test.
Indicates statistically significance difference relative to the control (ethanol) in the absence of DIFs, $P < 0.05$. Ca^{2+} release by disruption of vesicles caused by vehicle (ethanol) was subtracted from each measurement.

interestingly, DIF-2 and DIF-3 showed similar activity to DIF-1.

5.3.2. Ca^{2+} release studies in sea urchin eggs

The results described above from *Dictyostelium* preparations suggested a role for TPC proteins in AA-induced Ca^{2+} release. However, the low level of Ca^{2+} release seen in

membranes prepared from vegetative cells made these observations difficult to study further. Therefore, I investigated whether AA could induce Ca^{2+} release in sea urchin egg extracts, and if so, whether this release was from the same stores targeted by NAADP. This approach would also enable one to take advantage of the well-established pharmacology in this system, compared to that in *Dictyostelium* where the efficacy of pharmacological reagents is relatively unknown.

5.3.2.1. NAADP-induced Ca^{2+} release in sea urchin egg homogenate

In order to verify our experimental system, NAADP-induced Ca^{2+} release was firstly confirmed. *L. pictus* egg homogenate was incubated in Ca^{2+} uptake buffer prior to the application of a range of NAADP concentrations (50 pM - 1 μM). Transient Ca^{2+} release was measured with Fluo-3 (490 nm excitation and 535 nm emission). NAADP potently triggered Ca^{2+} release from vesicles in egg homogenate in a concentration-dependent manner (EC_{50} ~90 nM, maximal release ~500 nM), as shown in Figure 5.11A. A bell-shaped concentration-response curve has been reported as a unique property of NAADP-induced Ca^{2+} release in various models (Zong *et al.*, 2009). For all NAADP concentrations, released $Ca^{2+}$was re-sequestered into stores as determined by the return of Fluo-3 fluorescence to near basal levels. In addition, a

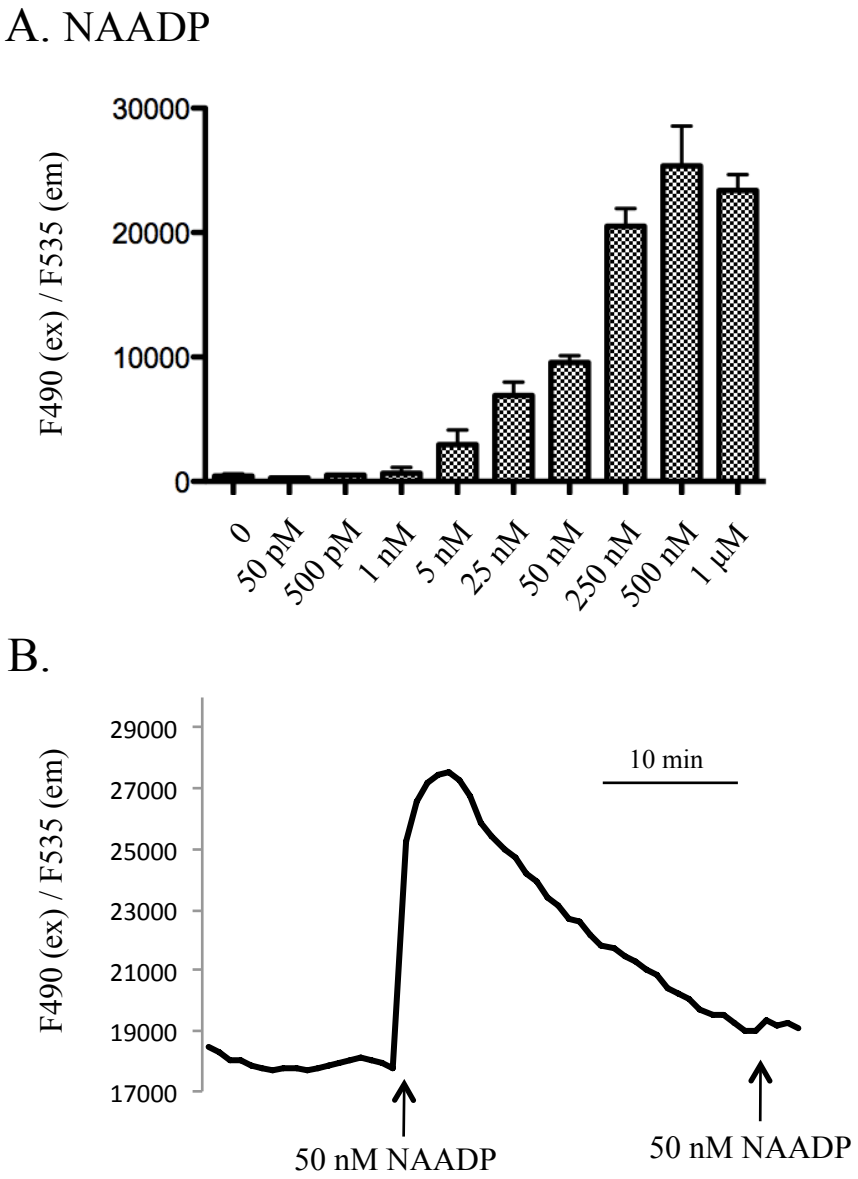


Figure 5.11. Ca^{2+} mobilizing activity of NAADP in egg homogenate
The reaction mixture containing 5% sea urchin egg homogenate and the ATP regenerating system (*see Chapter 2*), which induces Ca^{2+} uptake into vesicles, was used for each experiment. A. A range of NAADP concentrations was applied to the homogenate and free ionized Ca^{2+} measured using 3 µM fluo-3 (490 nm excitation and 535 nm emission) at 17°C in a fluorometer (NovoStar) (each from 1 - 6 determinations). The mean ± S.E.M. is shown. B. Representative fluorimetric trace showing NAADP-induced Ca^{2+} release, and desensitization following a second addition of NAADP.

subsequent application of NAADP following the re-sequestration of Ca^{2+}, failed to induce a significant second Ca^{2+} release (Figure 5.11B), indicating desensitization of the NAADP-response by NAADP itself, as previously reported (Genazzani *et al.*, 1996). Therefore, this system, employing fluorometric measurements of Ca^{2+} transients in sea urchin egg homogenate using a plate-reader (NovoStar), successfully reproduced previously reported data.

To demonstrate that the ER (targeted by IP_3 and cADPR) and acidic stores were functional in this preparation, the Ca^{2+} mobilizing activity of other ligands, namely IP_3 and cADPR (data not shown) at various concentrations were examined. Homogenates released Ca^{2+} in response to these agents in a concentration-dependent manner (Figure 5.12), consistent with the preservation of all the Ca^{2+} recruitment and release systems previously reported in this preparation. These results demonstrated that the homogenate contained Ca^{2+} stores sensitive to these reagents and capable of releasing Ca^{2+}.

5.3.2.2. Ca^{2+} mobilizing ability of AA

Having demonstrated the integrity of the preparation, these vesicles were tested for the ability of AA to induce Ca^{2+} release. AA induced a concentration-dependent Ca^{2+} release, with a threshold concentration of 5 μM, similar to that seen in vesicle preparations from *Dictyostelium* (Figure 5.13A). Since the mechanism of AA-induced Ca^{2+}release in sea urchin egg is unknown, ETYA was tested in egg homogenate for its ability to release Ca^{2+} compared to that of AA. Both AA and ETYA induced a transient Ca^{2+} release, though AA may be slightly more potent

IP_3

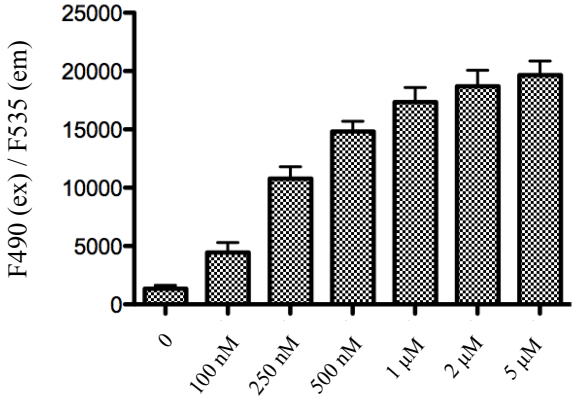


Figure 5.12. Concentration-response relationships for IP_3 in sea urchin egg homogenate

Ca^{2+} mobilizing agents IP_3 at the indicated concentrations were applied to egg homogenate prepared in an ATP regenerating buffer. Ca^{2+} transients were quantified in 6 - 12 independent experiments (the mean ± S.E.M. for each concentration is shown).

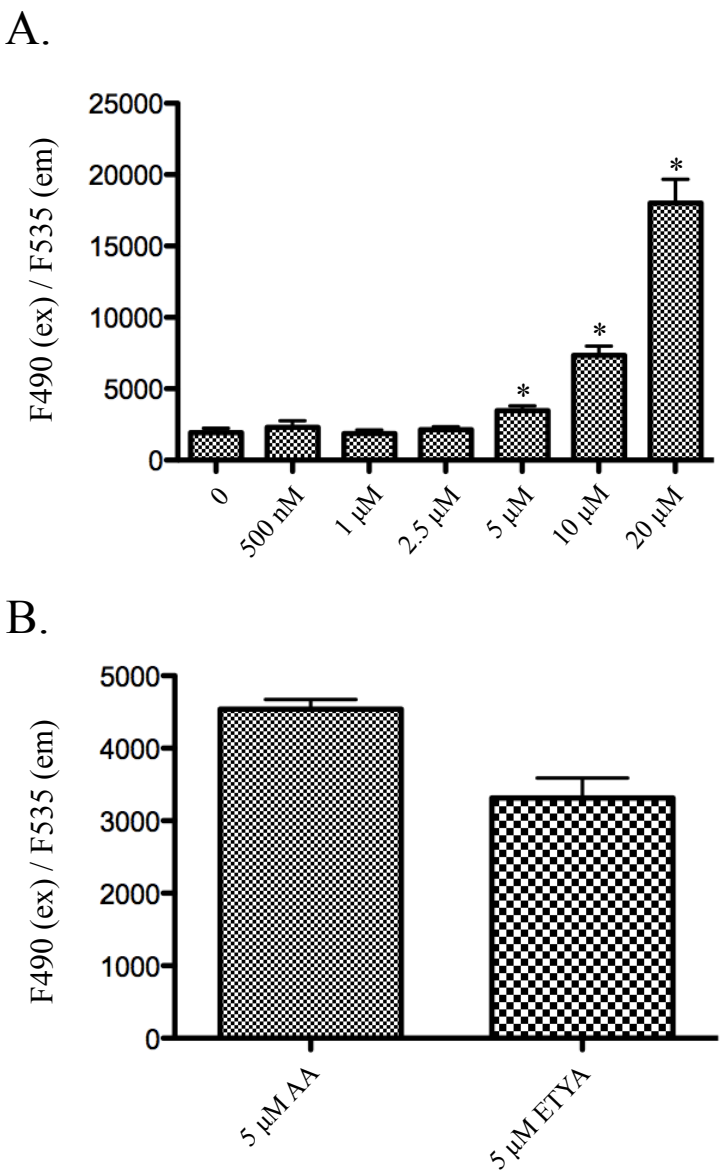


Figure 5.13. Fatty acid-induced Ca^{2+} release in egg homogenate
A. Concentration-response relationship for AA. At indicated concentrations AA was applied to egg homogenate prepared in an ATP regenerating buffer. Ca^{2+} transients were quantified for a range of concentrations of Ca^{2+} mobilizing agents in 6 - 12 independent experiments.
B. The Ca^{2+} mobilizing ability of AA and ETYA. AA and eicosatetraynoic acid (ETYA) at 5 µM were applied to 100 µl of egg homogenate and released Ca^{2+} was measured with 3 µM fluo-3. Both reagents were dissolved in 100% ethanol. Each data point was obtained from 6 - 12 determinations and the mean ± S.E.M. is shown. * Indicates statistical significance against vehicle (ethanol) control, $P < 0.05$

(Figure 5.13B), a result which indicates that AA itself is acting on Ca^{2+} stores and does not need to be metabolized further.

5.3.2.3. Ca^{2+} stores targeted by NAADP, IP_3 and AA

To determine which stores these agonists were releasing Ca^{2+} from, GPN and Tg were preincubated with egg homogenate to disrupt lysosomes and the ER respectively. GPN, a highly selective lysosomal lytic agent, virtually abolished the NAADP response, but had little or no effect on that of the other compounds (Figure 5.14A). In contrast, Tg, an inhibitor of ER Ca^{2+}-ATPase (SERCA), caused a reduction in the IP_3 response but had no effect on NAADP-induced Ca^{2+} release (Figure 5.14B). These results are consistent with the Ca^{2+} released in response to NAADP originating in lysosomes, and the IP_3 sensitive stores being derived from the ER. Since neither GPN nor Tg reduced the AA response, the store targeted by AA remains unknown.

5.3.2.4. The effect of Ca^{2+} channel blockade on AA responses in sea urchin egg homogenate

In an alternative approach to identifying the AA-sensitive stores, the inhibitory effect of the L-type Ca^{2+} channel blocker, diltiazem, and the IP_3 receptor antagonist, heparin (Perez-Terzic *et al.*, 1995), were tested, initially on Ca^{2+} release induced by NAADP and IP_3, respectively (Figure 5.15 and 5.16). NAADP-induced Ca^{2+} release was effectively inhibited by diltiazem (Figure 5.15A) but not by heparin, which is a selective blocker of IP_3-mediated Ca^{2+}release, consistent with previous data (Genazzani *et al.*, 1996; Genazzani *et al.*, 1997). Heparin effectively abolished IP_3-induced Ca^{2+} release, while diltiazem had no effect (Figure 5.16). From these

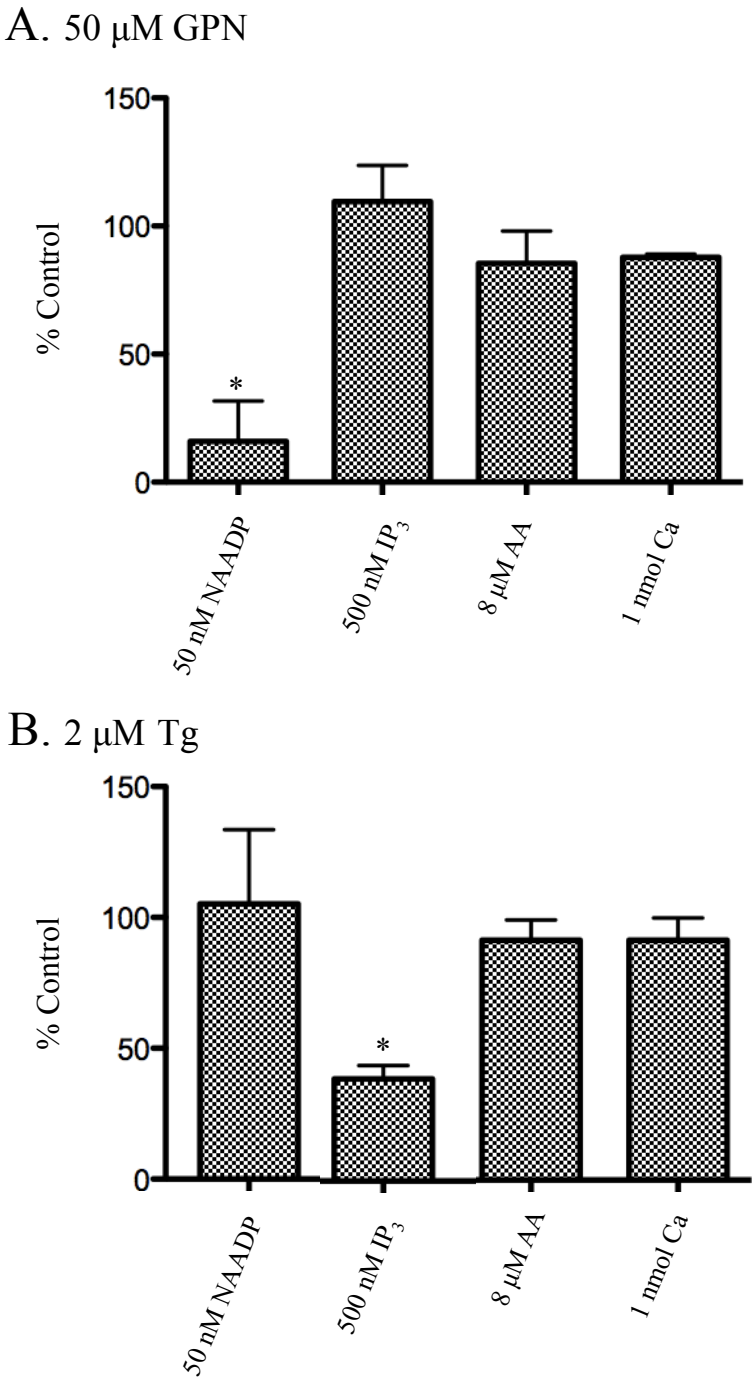


Figure 5.14. Origin of released Ca^{2+}
A. 50 μM GPN was added to the egg homogenate and just after released Ca^{2+} reached its maximum, the indicated concentrations of NAADP, IP_3, Ned19 and AA were applied. B. 2 μM thapsigargin (Tg) was applied and the level of Ca^{2+} store depletion monitored by the response to IP_3. After an average incubation time of 60 - 70 min, the indicated concentrations of Ca^{2+} mobilizing agents were applied. Released Ca^{2+} is expressed as a percentage of the vehicle control. Linearity of the fluorescent dye was measured by adding 1 nM Ca^{2+} to the reaction. The mean ± S.E.M. of three experiments is shown. The data is represented as a % of control release in the absence of inhibitor and * indicates a statistically significant difference relative to the control, $P < 0.02$

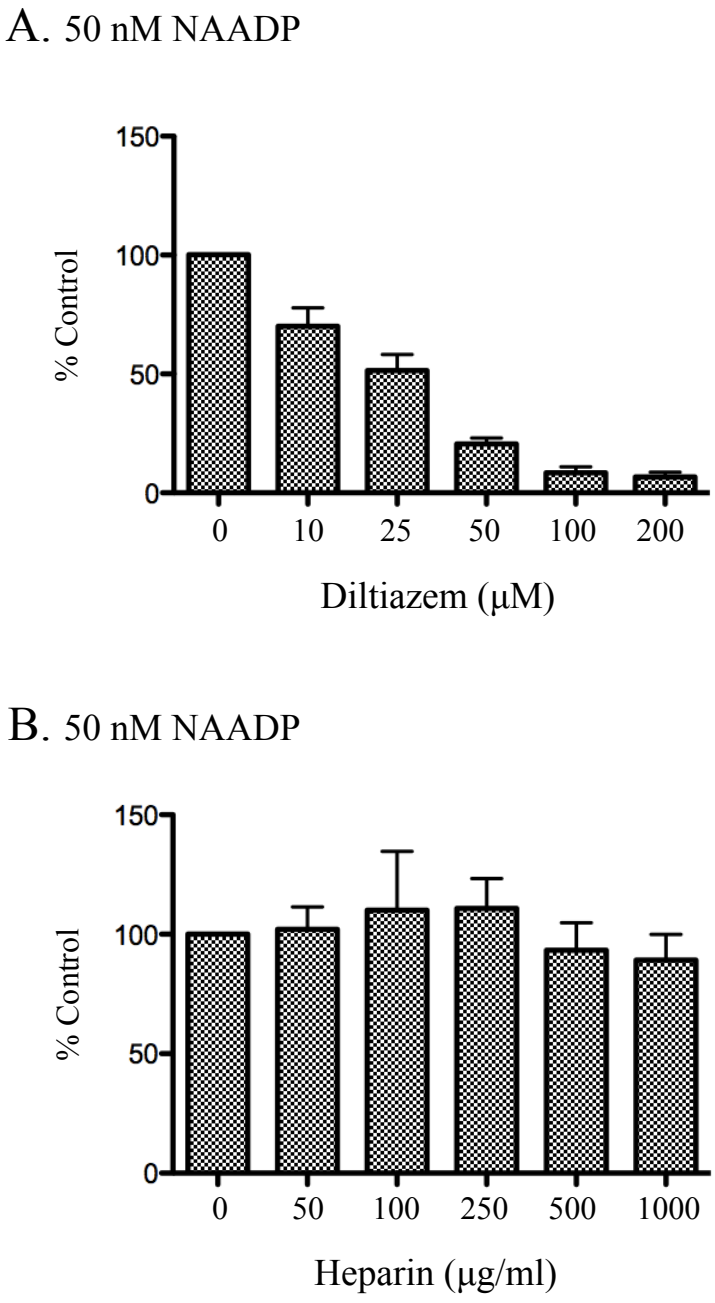


Figure 5.15. Effect of diltiazem and heparin on NAADP-induced Ca^{2+} release The indicated concentrations of A. diltiazem or B. heparin were applied to egg homogenate and, after allowing the baseline to settle, 50 nM NAADP was added to the reaction. Released Ca^{2+} was measured with 3 μM fluo-3. Both diltiazem and heparin were dissolved in chelated H_2O. The data is represented as a % of the control release in the absence of inhibitor. The mean ± S.E.M. of 5 - 7 experiments is shown.

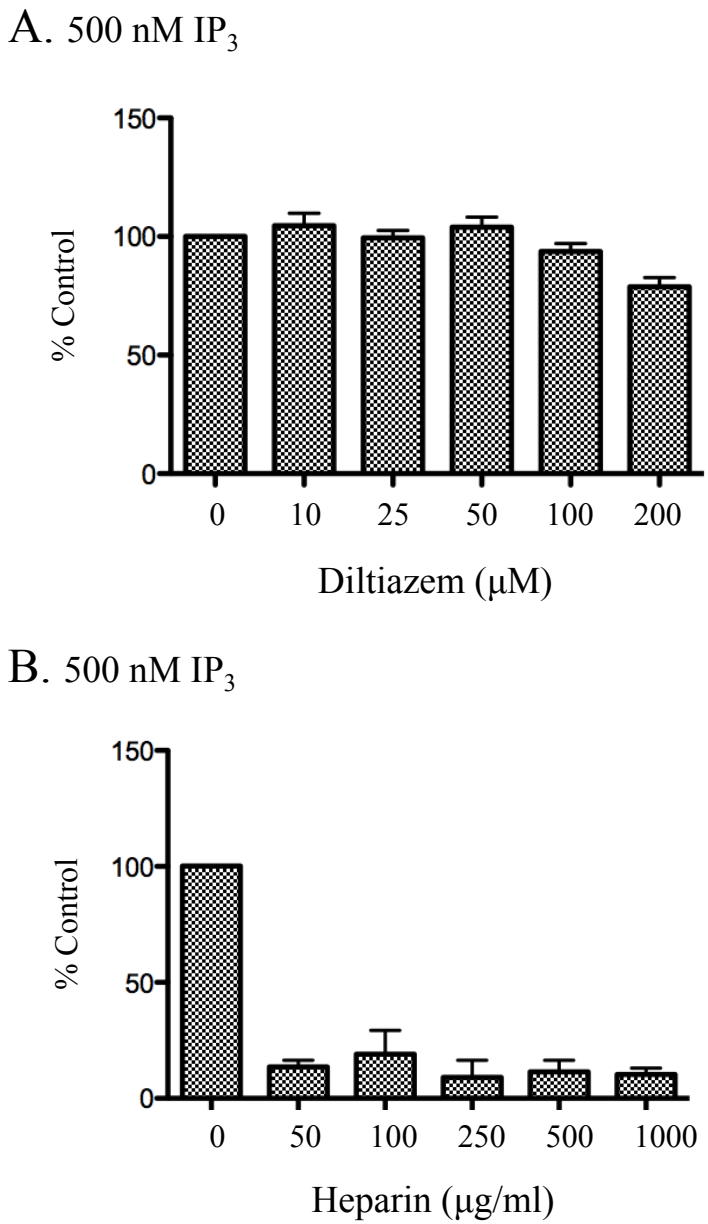


Figure 5.16. Effect of diltiazem and heparin on IP_3-induced Ca^{2+} release
The indicated concentrations of A. diltiazem or B. heparin were applied to egg homogenate and, after allowing the baseline to settle, 500 nM IP_3 was added to the reaction. Released Ca^{2+} was measured with 3 μM fluo-3. Both diltiazem and heparin were dissolved in chelated H_2O. The data is represented as a % of the control release in the absence of inhibitor. The mean ± S.E.M. of 5 - 7 independent experiments is shown.

experiments, 50 μM diltiazem and 50 μg/ml heparin were chosen in order to examine their effects on AA-induced Ca^{2+} release.

IP_3- and AA-induced Ca^{2+} release were not reduced by pre-treatment with 50 μM diltiazem (Figure 5.17A). On the other hand, the IP_3 receptor antagonist, heparin, greatly reduced IP_3-induced Ca^{2+}release, but had no significant effect on Ca^{2+} release induced by other compounds (Figure 5.17B). Ca^{2+} release in response to AA appeared to be slightly inhibited by diltiazem; however, the inhibition was not statistically significant, indicating that it is unlikely that AA releases Ca^{2+} from stores that require L-type Ca^{2+} channels. To examine these findings further, the interactions between AA and either NAADP or IP_3 were examined.

5.3.2.5. Effect of AA on NAADP and IP_3-induced Ca^{2+} release

Different concentrations of AA were applied to the egg homogenate, and after the re-sequestration of Ca^{2+} into stores (approximately 10 - 15 min), Ca^{2+} release induced by either 50 nM NAADP or 500 nM IP_3 was examined. NAADP-induced Ca^{2+} release was reduced by AA in a concentration-dependent manner, and 2.5 μM AA effectively inhibited NAADP-induced Ca^{2+} release, although this concentration of AA was not sufficient to cause significant Ca^{2+} release by itself. This finding shows that the loss of NAADP-induced responses was not a consequence of depletion of a common Ca^{2+} store or of a lack of sensitivity of Fluo-3 to detect the second round of Ca^{2+} release (Figure 5.18A). On the other hand, IP_3-induced Ca^{2+} release was unaffected by AA at a concentration of 2.5 μM, and only slightly reduced at 5 μM AA (Figure 5.18B). Therefore, AA appears to desensitize, selectively, NAADP-induced Ca^{2+} release in

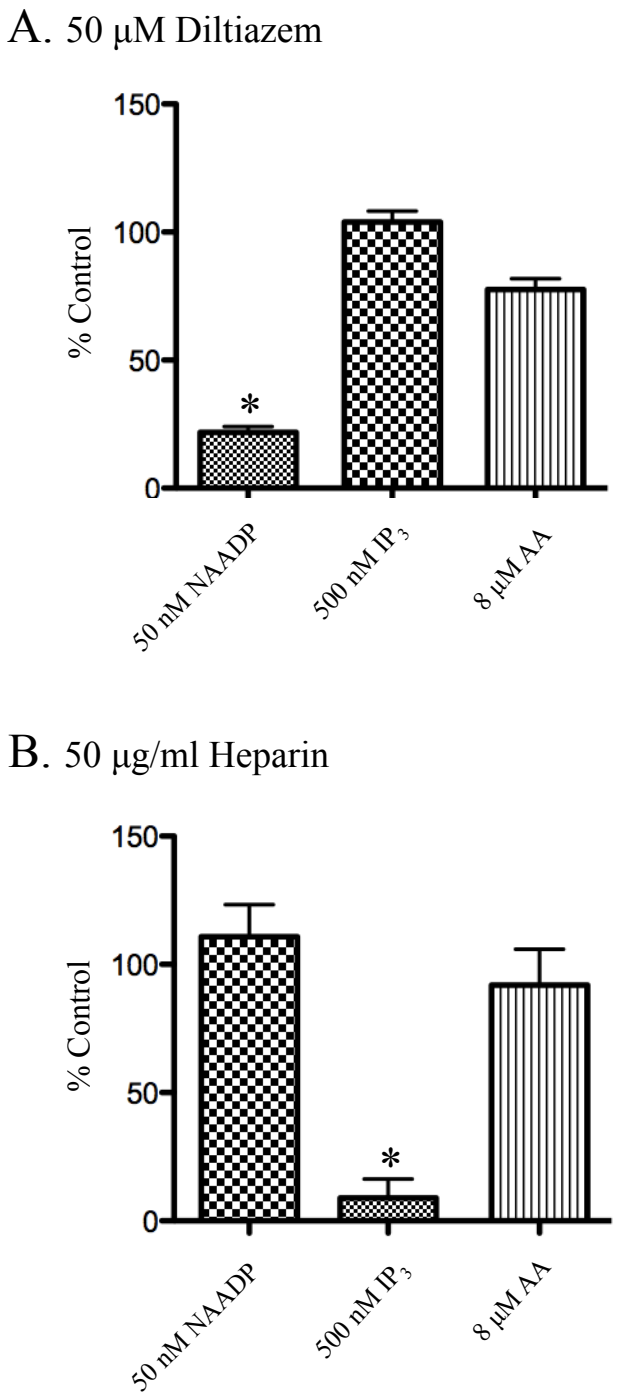


Figure 5.17. Effect of diltiazem and heparin on NAADP, IP_3 and AA-induced calcium release

The indicated concentrations of Ca^{2+} mobilizing agents were applied to egg homogenate after pre-incubation either with or without 25 μM diliazem (A) or 50 μg/ml heparin (B). Released Ca^{2+} is shown as a percentage of control (untreated homogenate). The mean ± S.E.M. of 5 independent experiments is shown. * Indicates statistical significance relative to control (100%) in the absence of inhibitor, $P < 0.05$

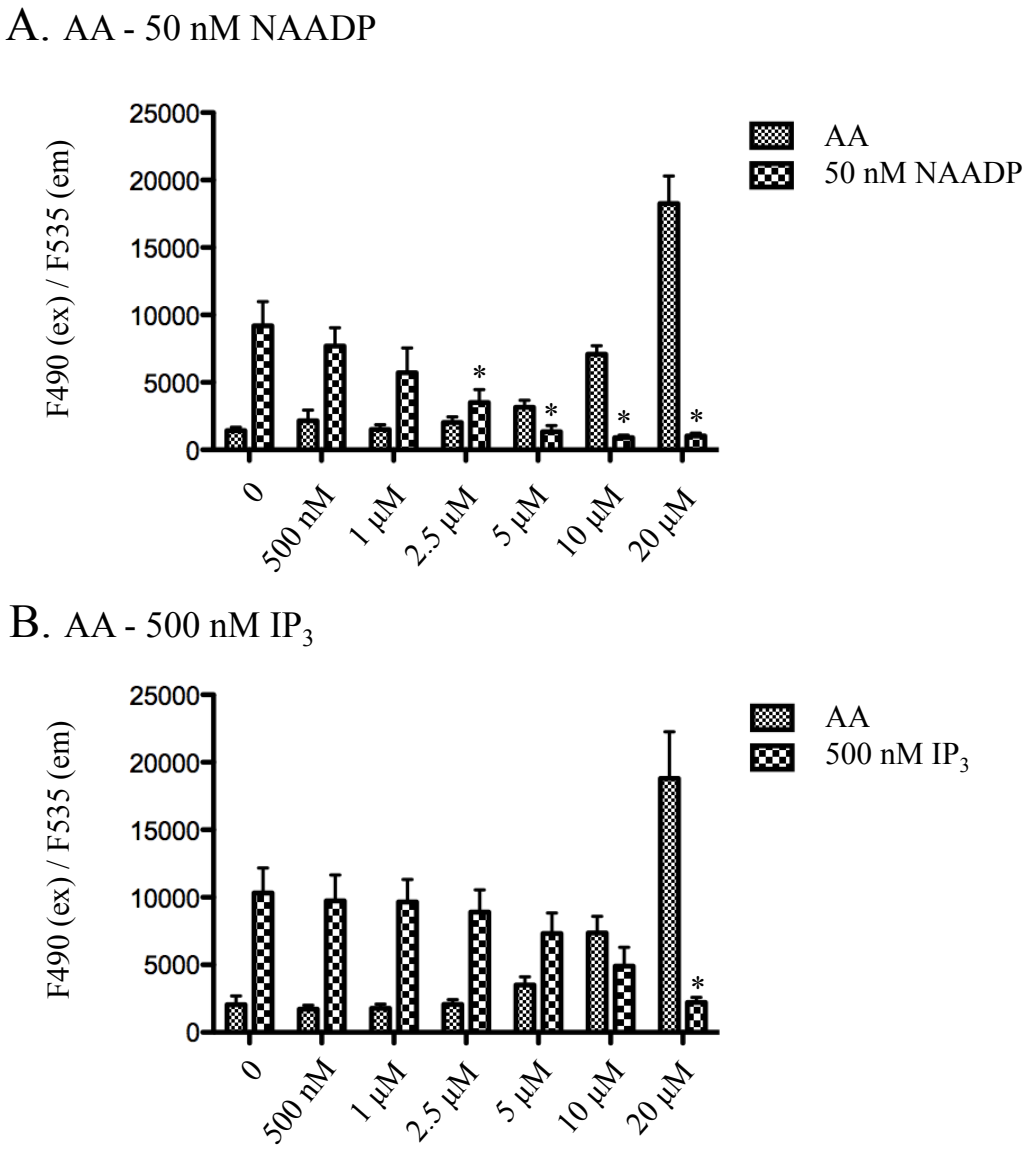


Figure 5.18. Effect of arachidonic acid (AA) on NAADP or IP_3-induced Ca^{2+} release

The indicated concentrations of AA were applied to egg homogenate and peak Ca^{2+} release measured. After released Ca^{2+} was re-sequestered into stores, as determined by the return to near basal fluo-3 fluorescence. Ca^{2+} release in response to either A. 50 nM NAADP or B. 500 nM IP_3 was measured in 6 -12 determinations (the mean ± S.E.M. is shown). Data were analysed by ANOVA followed by Dunnett's test. * Indicates statistical significance against vehicle (ethanol) control, $P < 0.02$

sea urchin egg homogenate, although high concentrations of AA (20 μM) reduced both the NAADP and IP_3 responses.

To investigate further the mechanism of AA-induced Ca^{2+} release, the effects of Ned-19, an NAADP antagonist, on AA-induced Ca^{2+} responses were investigated.

5.3.2.6. Inhibitory effect of Ned-19 on Ca^{2+} release in sea urchin egg homogenate

Ned-19 has been shown to inhibit NAADP-induced Ca^{2+} release (Rosen *et al.*, 2009). Therefore, 50 nM NAADP, 500 nM IP_3 and 8 μM AA were applied to egg homogenate after Ca^{2+} released by Ned-19 had been re-sequestered into stores as determined by the return of Fluo-3 fluorescence to near basal levels. As expected, Ned-19 showed a strong inhibitory effect on NAADP-induced Ca^{2+} release; however, no effect was detected on release induced by IP_3 or AA (data not shown). Although AA- induced Ca^{2+}release was not affected by Ned-19, it is still possible that AA may act on the NAADP receptor in a manner that is not antagonised by Ned-19.

5.4. Discussion

5.4.1. Ca^{2+} release studies using *Dictyostelium* vesicles

NAADP-mediated Ca^{2+} release was demonstrated using the vesicle fraction (P0) prepared from vegetatively growing cells, although the amount of Ca^{2+} released was small and on occasions could not be detected. The response (when present) did exhibit a bell-shaped concentration-response curve, as reported in other systems, and peaked at an NAADP concentration of 125 nM. This concentration is comparable to an EC_{50} of 100 nM NAADP in Jurkat T cells and mouse insulinoma cells (MIN6

cells) (Berg *et al.*, 2000; Masgrau *et al.*, 2003). 1 μM and 100 nM NAADP effectively elicit Ca^{2+} release from starfish oocytes and pancreatic β-cells, respectively (Masguau *et al.*, 2003; Lim *et al.*, 2001), and in plants, an EC_{50} value of 96 nM has been reported for microsomal vesicles from red beet and cauliflower (Navazio *et al.*, 2000). Furthermore, the concentrations of NAADP which elicited Ca^{2+} release in SKBR3 and HEK cells expressing *Hs*TPC2 or *Sp*TPCs were 10 nM and 100 nM, respectively (Brailoiu *et al.*, 2010b; Ruas *et al.*, 2010). Therefore the concentrations of NAADP releasing Ca^{2+} in the *Dictyostelium* P0 fraction are similar to those seen in all other systems. Unexpectedly, the NAADP response was also observed in the P0 fraction at T0 using two independent clones of *Ddtpc2* null cells. This finding might suggest that the NAADP response is not via TPC2 homologue in contrast to that noted in other systems. Pancreatic β-cells from *tpc*$^{-}$ mice were insensitive to NAADP and HEK cells silencing *Hs*TPC2, by short hairpin RNA interference (shRNAi), abolished the NAADP-activated cation current (Calcraft *et al.*, 2009).

5.4.2. Biological role of DIFs in *Dictyostelium*

Dictyostelium possesses a single class of DIF-1 binding site, found in the membrane fractions, with a K_d value of 1.8 nM, (Insall and Kay, 1990). DIF-1 effectively induces stalk cell differentiation and prestalk-specific gene expression, and represses spore and prespore differentiation, at nanomolar concentrations. DIF-1 is a small, hydrophobic molecule thought to be able to diffuse across the plasma membrane without requiring a carrier protein. DIF responses have been shown to be dependent on changes in Ca^{2+} (Araki *et al.*, 2008; Schaap *et al.*, 1996).

In the present study, 50 nM DIFs released Ca^{2+} from intracellular vesicles prepared from T4 *Dictyostelium* cells. The Ca^{2+} mobilising activity between DIF analogues were DIF-3 > DIF-2 > DIF-1, which order is different from their activity in inducing prestalk differentiation, i.e. DIF-1 > DIF-2 >> DIF-3 (Masento *et al.*, 1988). It should also be noted that the change in fluorescence measured was very small, and thus a more sensitive method for measuring Ca^{2+} may be necessary to confirm the hypothesis that DIF-1 acts physiologically to release Ca^{2+} from intracellular stores.

5.4.3. Biological role of AA in *Dictyostelium*

In *Dictyostelium*, AA effectively induced Ca^{2+} release from intracellular Ca^{2+} stores prepared from T4 cells, as previously reported (Schaloske *et al*., 1998). Efficient release from vesicles prepared from T20 cells was also demonstrated, and the range of effective AA concentrations was the same as reported in an earlier study (Schaloske *et al.*, 1998). AA was also able to elicit Ca^{2+} release from vesicles prepared from vegetative cells, though the level of release was generally much lower. Although AA is not synthesized endogenously in *Dictyostelium* (Davidoff and Korn, 1963; Weeks, 1976), it appears that it does not need to be metabolized to elicit Ca^{2+} release because 5 μM ETYA was also effective in releasing Ca^{2+} from vesicles prepared from T4 cells. The mono-unsaturated fatty acid, oleic acid (18:1), and the saturated fatty acid, palmitic acid (16:0), released Ca^{2+} in a similar manner to AA, suggesting that this effect is not limited to unsaturated compounds of a specific length, and further demonstrating that FAs other than AA may well be the endogenous release factors. In an experiment performed on whole cells, linoleic acid also induced an influx of Ca^{2+}across the plasma membrane (Schaloske *et al.*, 1998), and the authors suggested that the effects on Ca^{2+} homeostasis were not specific to AA, but could be generally

induced by fatty acids. As AA is not endogenously produced in *Dictyostelium*, other polyunsaturated fatty acids, such as OA, may be the messengers inducing Ca^{2+} release in *Dictyostelium* (Davidoff and Korn, 1963; Weeks, 1976).

There are numerous reports from the 1980s that document the effects of FAs on ion channels. The results varied, depending on the channels studied, the cell types, experimental procedures, the types of FAs studied, the concentrations used, and the manner of application (i.e. intracellularly or extracellulary) reviewed by Meves (1994). If a response to the saturated fatty acid, palmitic acid (PA), was observed, it *could be* a detergent effect. However, in some cases, Ca^{2+} re-uptake was detected which would not be consistent with the latter assertion. Moreover, in GH_3 pituitary cells, even 1 μM PA was sufficient to have effects on Ca^{2+} channels, which would be a very low concentration to be acting as a detergent. Recent studies have shown direct effects of AA on TRP and ARC channels (Meves, 2008). In the present study, different kind of FAs, including saturated or unsaturated species, were examined in *Dictyostelium* vesicles, and a concentration-response curve was obtained using AA. Non-specific effects of AA are often distinguished by using PA, which may mimic the AA effect on membranes as it acts like a detergent (Chyb *et al.*, 1999). The fact that the quantity of Ca^{2+} released by PA was not increased when the concentration of PA was raised from 5 μM to 10 μM might be consistent with this idea. However, after the release of Ca^{2+} in response to FAs, Ca^{2+} was re-sequestered into vesicles, and furthermore, the Ca^{2+} mobilizing ability of PA has been reported in *Dictyostelium*; however, the mechanism(s) remain unknown (Schaloske *et al.*, 1998).

Previous studies have shown that AA can elicit Ca^{2+}release from acidic stores (Malchow *et al.*, 2006; Schaloske *et al.*, 1998). The molecular basis for AA-induced Ca^{2+} fluxes in *Dictyostelium* is not known, but Ca^{2+} release was observed in both *iplA*$^-$ and *polycystin2*$^-$ cells, suggesting that these putative channels are not required for this response, consistent with a previous report regarding the *iplA*$^-$ strain (Schaloske *et al.*, 2005). Interestingly, Ca^{2+} entry triggered by AA was reduced in a phospholipase C null strain, suggesting the participation of the IP_3 pathway (Schaloske *et al.*, 1998). However, most studies suggest that acidic stores are responsible for AA-mediated Ca^{2+} transients, since the *lvsA*$^-$ strain, which does not have functional CVs, shows reduced AA responses (Malchow *et al.*, 2006). The reduced AA response observed in *Ddtpc2* null strains and localization of *Dd*TPC2 to the CV, might imply that disruption of *Ddtpc2* affects the function of acidic stores responsible for AA-mediated Ca^{2+} signalling.

5.4.4. AA-induced Ca^{2+} release in sea urchin egg homogenate

All Ca^{2+} mobilizing systems known to be active in sea urchin egg homogenate (ER and lysosomes) were successfully demonstrated in the system *outlined here*. In particular, NAADP, IP_3 and cADPR-induced Ca^{2+} release was shown. The NAADP response had an EC_{50} of 90 nM and the concentration-response curve was similar to those previously reported (Lee and Aarhus, 1995); the effective concentration range was the same as that demonstrated in permeabilised pancreatic islets (Wolf *et al.*, 1986). It was reported that AA has no Ca^{2+} mobilizing ability in sea urchin eggs; however, 5 μM AA inhibited NADP or alkaline-NAADP responses, but not those of IP_3 or cADPR (Clapper *et al.*, 1987). On the other hand, in my study, AA triggered Ca^{2+} release from intracellular stores in sea urchin egg homogenate with an EC_{50} of

~10 μM. ETYA, a non-metabolizable analogue of AA, was able to mobilize Ca^{2+} in a similar manner to AA, suggesting the AA effect was not due to metabolites of AA *per se* but to AA itself. GPN, which disrupts lysosomes, virtually abolished the NAADP response but had little or no effect on the AA response; Tg also had no effect on AA-induced Ca^{2+} release. Diltiazem, an L-type Ca^{2+} channel blocker, effectively inhibited the NAADP response, but again was without significant effect on AA-induced Ca^{2+} release. These results are consistent with the NAADP-sensitive and AA-sensitive Ca^{2+} stores being distinct, although it cannot be ruled out that AA targets more than one store.

The clearest evidence for an interaction between NAADP- and AA-induced Ca^{2+} release was the observation that treatment with low concentrations of AA desensitized egg homogenate to subsequent treatment with NAADP. 2.5 μM AA inhibited NAADP- induced Ca^{2+}release but had no effect on IP_3-mediated Ca^{2+}release at this concentration. Possible explanations are that AA disrupts acidification of lysosomes and consequently selectively inhibits NAADP responses or AA affects on NAADP receptor directly, for instance, sealing the pore-forming region. High concentrations of AA (20 μM) reduced both the NAADP and/ IP_3 responses, possibly due to a lack of sensitivity of the dye after AA-induced Ca^{2+} release. However, the observation that AA responses are lost in the *tpc*$^-$ *Dictyostelium* cells would also be consistent with a more direct relationship and might even suggest that AA responses are directly dependent on TPCs, though this hypothesis will require further investigation. This latter observation suggests that the previous report of AA desensitizing NADP-induced Ca^{2+} responses might well have been due to the presence of contaminating levels of NAADP (Lee and Aarhus, 1997). It is also noteworthy that low

concentrations of NAADP, insufficient to trigger Ca^{2+} release on thier own, also desensitize homogenate to the subsequent addition of higher concentrations of NAADP (Lee and Aarhus, 1995, Lee and Aarhus, 1997).

In conclusion, AA-targeting stores are not clear, however AA is affecting to NAADP-sensitive channel.

5.5. Summary

ATP-dependent Ca^{2+} uptake in a cell free system was successfully established using vesicles prepared from *Dictyostelium* cells at different stages of development. AA-induced Ca^{2+} release from vesicles prepared from T0, T4 and T20 cells was also demonstrated. In addition, T4 cells exhibited sensitivity to several FAs, namely ETYA, PA, OA, LA and ETI. Vesicles from vegetative *tpc2*$^{-}$ cells failed to respond to AA, suggesting TPC2 may be responsible for AA-induced Ca^{2+} release, although this idea requires further experimental analysis.

It was not possible to observe NAADP-induced Ca^{2+} release using vesicles prepared from T4 and T20 cells, although levels of TPC2 protein would be expected to be high at these times, especially at T20. Interestingly, NAADP elicited small amounts of Ca^{2+} release from vesicles extracted from T0 cells, including Ax2 cells expressing mRFPmars or *Dd*TPC2.mRFPmars, and cells lacking *Dd*TPC2. However, it was difficult to record these very low levels of NAADP responses consistently, and a more sensitive Ca^{2+} detection system will be required for future experimental analysis.

Nanomolar concentrations of DIFs were able to mobilize small amounts of Ca^{2+} from intracellular Ca^{2+} stores, which is consistent with the biological activity reported (Insall and Kay, 1990).

In sea urchin egg homogenate, Ca^{2+} was released in response to AA in a concentration-dependent manner and did not require metabolism of AA, since a non-metabolizable analogue of AA, ETYA, also effectively mobilized Ca^{2+} from intracellular compartments. AA-induced Ca^{2+} release was inhibited neither by GPN nor by diltiazem. Interestingly, pretreatment with low concentrations (2.5 μM) of AA greatly inhibited NAADP-induced Ca^{2+} release, but had no effect on IP_3-induced Ca^{2+} release. The mechanisms underlying AA-induced Ca^{2+} release and the inhibitory effect on NAADP-induced Ca^{2+} release remain to be determined.

CHAPTER 6

GENERAL DISCUSSION

Independent work on *Strongylocentrotus purpuratus* (*Sp*) and *Dictyostelium discoideum* (*Dd*) has highlighted the importance of acidic Ca^{2+} stores (ACS) in cell signalling. Central features of how we think the ACS functions are shown in Figure 1.2 for sea urchin egg, and in Figure 1.6 for *Dictyostelium*. Ca^{2+} is pumped into the ACS by a mechanism that requires acidification of the ACS by a V-type H^+-ATPase. There may not be a direct exchange of H^+ and Ca^{2+}, but in either case efficient sequestration is promoted by low vesicle pH (Churchill *et al*., 2002; Patel and Docampo, 2010). Ca^{2+} is released from the ACS in response to a Ca^{2+} releasing agent, e.g. NAADP or FA (equivalent to IP_3 and cADPR for the ER), that is produced in response to extracellular signals and which opens specific Ca^{2+} channels on the stores (Chini *et al.*, 1995; Churchill *et al.*, 2003, Schaloske *et al*., 1998).

In sea urchin eggs, the key events leading to the realization of the importance of the acidic stores were the discovery of a store released by a novel Ca^{2+}-releasing agent, NAADP (Clapper *et al.*, 1987) and the demonstration that this store was acidic (lysosomes) (Churchill *et al*., 2002). Furthermore, in sea urchin eggs, the evidence is that NAADP releases Ca^{2+} by opening a two-pore channel, TCP1 or TPC2 (Ruas *et al*., 2010).

In *Dictyostelium,* key findings included evidence for the importance of an acidic compartment in regulating the choice between prestalk and prespore developmental pathways, and the observation that vesicle acidity influences the choice of pathway by controlling the storage and release of vesicular Ca^{2+} (Gross, 2009). In *Dictyostelium,* Malchow has presented substantial evidence that release of Ca^{2+} from acidic stores can be triggered by FAs (such as AA). The authors demonstrated the existence of a

Ca^{2+} store sensitive to CMA (a V-H^+-type ATPase inhibitor) that was distinct from the BHQ-sensitive store (presumed to be the ER). Furthermore, a CV-deficient strain (*lvsA*$^-$) showed reduced Ca^{2+} release in response to AA (Malchow *et al*., 2006; Shaloske *et al*., 1998). *Dictyostelium* also possesses a two pore channel, one of several candidate Ca^{2+} channels encoded by the genome, which also include an IP_3 receptor like protein, mucolipin, polycystin-2-like receptor and P2X receptors.

6.1. Are TPCs NAADP receptors?

NAADP is reported to be the most potent Ca^{2+} releasing agent known. Accumulating evidence suggests that NAADP is targeting TPCs on acidic stores (lysosomes).

When NAADP responses were first studied, it was shown that IP_3- and cADPR-mediated Ca^{2+} release was abolished by SERCA inhibitors (such as Tg) whereas NAADP-sensitive Ca^{2+} release was unaffected (Chini *et al*., 2002; Churchill and Galione, 2001). In addition, stratification studies, in which intact eggs were centrifuged resulting in elongated structures with different organelles separating to different 'poles', demonstrated that NAADP mobilized Ca^{2+} from the 'pole' containing the mitochondria and acidic vesicles, but not from the 'pole' containing ER (Lee and Aarhus, 2000). Soon after, Churchill and colleagues performed Percoll gradient centrifugation to purify a particulate fraction of the sea urchin egg homogenate in which Ca^{2+} release was sensitive to NAADP; this fraction was also found to contain the greatest amount of specific [^{32}P]NAADP binding protein (Churchill *et al*., 2002). Furthermore, GPN, which causes osmotic lysis of lysosomes, abolished the NAADP response both in this fraction and in intact eggs (Churchill *et al*., 2002). Ca^{2+} uptake into the NAADP-sensitive stores was dependent on ATP (as is

the case for Ca^{2+} uptake into the ER), but was insensitive to Tg and vanadate (a P-type Ca^{2+}-ATPase inhibitor). NAADP-mediated Ca^{2+} release was also sensitive to FCCP and nigericin, suggesting that a Ca^{2+}-ATPase was not involved, but rather a proton gradient that may be dependent on a V-type H^{+}-ATPase. Indeed, bafilomycin A1 (a vacuolar H^{+}-ATPase inhibitor) prevented Ca^{2+} uptake into NAADP-sensitive stores (Churchill *et al*., 2002; Galione and Churchill, 2002). These results are all consistent with NAADP triggering Ca^{2+} release from acidic stores.

In pancreatic acinar cells, NAADP elicits Ca^{2+} release from secretory granules, but not from lysosomes (Gerasimenko *et al*., 2006), whereas in a pancreatic β cell line (MIN6), NAADP does not act on either the ER or on RyRs (Mitchell *et al*., 2003). It has been reported that NAADP may mobilize Ca^{2+} via direct action on RyRs, including RyR1 in skeletal muscle SR vesicles (Hohenegger *et al*., 2002), and RyR2 in dog cardiac microsomes (Mojžišová *et al*., 2001). However, the latter study required micromolar concentrations of NAADP for an effect, whereas it is not thought that NAADP concentrations ever reach such levels, as these are believed to cause desensitization of NAADP receptors. Furthermore, another group has demonstrated that NAADP had no effect on the probability of opening of isolated RyR1 and RyR2 channels (Copello *et al*., 2001). It has also been reported that NAADP causes Ca^{2+} release from the ER via RyRs in T-lymphocytes, since the RyR agonist ruthenium red efficiently blocked NAADP-induced Ca^{2+} release (Langhorst *et al*., 2004), and the NAADP response was abolished when RyR expression was knocked down in Jurkat T cells (Dammermann and Guse, 2005). On the other hand, RyR3 on the SR has been reported to co-localize with markers for lysosomal compartments, and this arrangement proposed to form a specialized 'trigger zone' for NAADP-induced Ca^{2+}

signalling in pulmonary arterial smooth muscle cells. This suggests that NAADP does not act on RyRs directly; instead, it has been proposed that NAADP-induced Ca^{2+} release triggers CICR via RyRs (Kinnear *et al*., 2004), but not via IP_3Rs (Boittin *et al*., 2002).

The best candidates for NAADP receptors are the TPC proteins, as it has been reported that pancreatic β-cells derived from *TPC2*$^{-/-}$ mice were insensitive to NAADP, and short hairpin RNA interference (shRNAi) studies have shown that detectable NAADP-mediated Ca^{2+} release was not observed in hepatocellular carcinoma (HepG2) cells when *Hs*TPC2 expression was reduced (Calcraft *et al*., 2009). However, it is not clear whether TPC proteins bind NAADP directly or via another protein. Results presented that immunoprecipitates of *Sp*TPCs expressed in HEK cells showed enhanced NAADP binding (Ruas *et al*., 2010). However, it remains possible that the TPC proteins are not the NAADP receptors themselves, but associate with another protein with binding activity. I was unable to show that *Sp*TPCs and *Hs*TPCs, expressed in Sf9 cells, enhanced NAADP binding (*Chapter 3*), although others have shown that expression of *Hs*TPC2 in HEK cells enhanced NAADP binding (Calcraft *et al*., 2009). *Dictyostelium* expresses TPC2 proteins, but I found no evidence for specific NAADP binding in *Dictyostelium* extracts from cells developed for either 4 or 20 hours. These times were chosen because the mRNA expression level of *Dd*TPC2 reaches its peak at 16 hours after the initiation of development, and a specific antibody that I raised and purified showed that TPC2 protein was expressed at both of these times, with higher levels at T20. I also did not see NAADP-induced Ca^{2+} release using vesicle preparations from cells developed for the same times. However, I show preliminary evidence for NAADP-induced Ca^{2+}

release from vesicles prepared from growing cells. Although conditions required to demonstrate Ca^{2+} release need to be optimized, these initial experiments show a typical bell-shaped concentration-response curve, similar to that seen in Jurkat T-cells, with maximal release occurring at 100 nM NAADP, a concentration similar to that reported in sea urchin eggs (an EC_{50} of 30 nM) (Berg *et al*., 2000; Lee and Aarhus, 1995). These results suggest that NAADP-induced Ca^{2+} release may be present in *Dictyostelium* vesicle preparations; however, the Ca^{2+} release seen in *tpc2*$^-$ cells is not consistent with this release being dependent on *Dd*TPC2.

6.2. Fatty acid-induced Ca^{2+} release

Saturated and unsaturated fatty acids consistently induced Ca^{2+} release from *Dictyostelium* vesicle preparations, including FAs that are not metabolized further (ETYA), and FAs known to be synthesized by *Dictyostelium* (palmitoleic acid and oleic acid). Ca^{2+} release induced by AA, linoleic acid and palmitic acid was seen in cells developed for 4 hours, as previously reported (Schaloske *et al*., 1998). No previous studies to investigate FA-induced Ca^{2+} release have been carried out in cells developed for 20 hours, and in growing cells. However, the current study suggests that the response system is expressed at both of these stages, and perhaps throughout growth and development. Preliminary data indicate that the FA response is lost in *Ddtpc2* null cells, although this has only been examined in vegetative cells and not during development as yet. These results suggest that *Dd*TPC2 is required for FA-induced Ca^{2+} release.

In sea urchin eggs, I was also able to demonstrate an association between NAADP-dependent and AA-dependent stores, as pre-incubation with AA (2.5 μM) effectively

inhibited NAADP-induced Ca^{2+} release from sea urchin egg homogenate. However, pharmacological studies were not able to identify the store targeted by AA.

On the basis of the available evidence, FAs are probably responsible for Ca^{2+} release from the ACS in *Dictyostelium*, though a role for NAADP cannot be excluded. It has been suggested that FAs are rapidly formed in response to cAMP binding (Schaloske *et al*., 1998), although there is, as yet, no direct evidence for NAADP production. Furthermore, there is no orthologue of the protein most likely to be responsible for NAADP synthesis apparent in the *Dictyostelium* genome sequence.

One possibility that merits future study is that TPC2 could be the target for AA-induced Ca^{2+} release in *Dictyostelium*. In sea urchin eggs, FAs may also be involved in Ca^{2+} release and perhaps may target two stores – one NAADP-sensitive and one insensitive, as AA responses were not substantially affected by agents that completely blocked NAADP-dependent Ca^{2+} release. AA may act on the NAADP release system directly, as low levels of AA were able to desensitize the NAADP receptor in a manner similar to low levels of NAADP.

Experiments on *Ddtpc2* null cells showed that development was delayed by up to 10 hours, with the appearance of abnormal multicellular structures and the formation of doughnut-shaped mounds. Therefore, whether the role played by *Dd*TPC2 in *Dictyostelium* development involves NAADP and/or FAs as the Ca^{2+} mobilizing agents requires further investigation, as does the relationship between *Dd*TPC2, Ca^{2+} mobilizing agents and Ca^{2+} signalling in *Dictyostelium*.

6.3. Future directions

Currently, there are numerous questions arising in the field of *Dictyostelium* Ca^{2+} signalling, including the identity of the mechanism for FA-induced Ca^{2+} release. Now that *Dd*TPC2 has been expressed successfully in HeLa cells (as described in this thesis), where it localizes to lysosomes, this will allow the detailed pharmacological characterization of *Dd*TPC2 in live cells, using Ca^{2+} imaging methods or patch clamp techniques. It may even be possible to analyze *Dd*TPC2 function by the reconstitution of *Dd*TPC2 into a lipid bilayer. It would be interesting to test all agents, including NAADP, FAs and DIFs, to provide insights into the mechanisms of Ca^{2+} release, including the nature of the stores targeted, and whether *Dd*TPC2 is capable of responding to FAs such as AA, as ARC channels do. Further understanding of the role of *Dd*TPC2-mediated Ca^{2+} signalling in cell differentiation, and the relevance of Ca^{2+} stores including acidic stores, would be my favoured area of future research.

Appendices

Appendix 1. Solutions

All solutions were made with distilled water, sterilized either by autoclaving (125°C for 12 min) or filtration (0.2 μm filter, Millipore Ltd., Watford, U.K.) and stored at 4°C unless indicated.

Unless otherwise specified, all reagents were purchased from Sigma-Aldrich Limited (Poole, UK). Deionized water was produced by a Purite reverse osmosis unit with a Still Plus polisher (Purite Ltd., Thame, UK) and a Milli-Q Water Purification System (Millipore).

Annealing Buffer (10x TE buffer + 500 mM NaCl)

100 mM Tris-NaCl
10 mM EGTA
500 mM NaCl
pH 7.4

Binding Standard Buffer for Sea Urchin Egg

GluIM : 1.5M $HClO_4$: 2M $KHCO_3$ = 1 : 1 : 2

Binding Buffer for HEK cells

20 mM Hepes
140 mM Potassium acetate
pH 7.2 with NaOH

Binding Buffer (HisTrap HP)

20 mM Sodium phosphate
0.5 M NaCl
20 mM Imidazole (optional 20 - 40 mM)
pH 7.4

Blocking Buffer (Western blot)

5% Dried skimmed milk in 1xTBS (Tris-buffered saline containing 0.2% Tween-20)

Ca^{2+}-free artificial sea water (ASW)

470 mM NaCl

27 mM $MgCl_2.6H_2O$

28 mM $MgSO_4.7H_2O$

10 mM KCl

2.5 mM $NaHCO_3$

pH 8.0

(1 mM EGTA for the first two washes)

Calcium Uptake Buffer for Dictyostelium

10 mM HEPES

50 mM KCl

2 mM $MgCl_2$

3% Sucrose

pH 7.2

(The following chemicals were added just before use)

100 nM NaN_3

6.6 µM Fluo-3

0.4 mM Mg^{2+}-ATP

12 µg/ml Oligomycin A

Coomassie Blue

0.25% Coomassie brilliant blue

50% Methanol

10% Acetic acid

Destain

5% Methanol

7.5% Acetic acid

Coomassie Blue (Quick)

0.25% Coomassie brilliant blue

50% Trichloracetic acid (R-250)

Destain

Water

or

25% Methanol

7% Acetic acid

DNA Loading Dye

10xDNA loading dye

30% Glycerol

0.1M EDTA

1% SDS

0.25% Bromophenol Blue

ECL (Luminol : Fluka, 09253); stock 250 mM in DMSO (-20°C, in shade)

Solution1

1 ml Luminol

0.44 ml Coumaric acid

10 ml of 1 M Tris.HCl (pH 8.5)

to 100 ml with ddH2O

Solution2

10 ml Tris.HCl (pH 8.5)

90 ml ddH_2O

64 µl 30% H_2O_2

ECL plus/Advance Western Blotting Detection Kit (Amersham Biosciences RPN2132/2135)

0.5 M EDTA

EDTA disodium salt dihydrate: Sigma-Aldrich, E5134

pH 8.0 with NaOH

(autoclaved for sterilization)

0.5 M EGTA (pH 7.5 - 8.0) stock 20 ml

(Sigma-Aldrich, E4378. MW 380.35)

3.8 g EGTA in 10 ml ddH_2O

1.56 g KOH

pH adjusted to 7.5 - 8.0, and solution made up to a final volume of 20 ml with distilled water

(Filtered through a 0.2 μm filter (Millipore) before use)

Elution Buffer (PIERCE cobalt resin)

50 mM Sodium phosphate

300 mM Sodium chloride

150 mM Imidazole

pH 7.4

Elution Buffer (HisTrap HP)

20 mM Sodium phosphate

0.5 M Sodium chloride

40 - 500 mM Imidazole

pH 7.4

gDNA Extraction

Crude Genomic DNA extraction Lysis Buffer for PCR screening

50 mM KCl
10 mM Tris
2.5 mM $MgCl_2$
0.45% NP-40
0.45% Tween-20
0.8 µg/ml proteinase K
pH 8.3

High quality Genomic DNA extraction Buffer
Nuclear Lysis Buffer
10 mM MgOAc
10 mM NaCl
30 mM HEPES
10% Sucrose
2% NP-40
pH 7.5

HMK Buffer
50 mM Hepes
40 mM MgOAc
20 mM KCl
pH 7.5

GluIM
250 mM N-methyl glutamine
250 mM Potassium gluconate
20 mM Hepes (free acid)
1 mM $MgCl_2$
pH 7.2 with acetic acid

HBS for HEK cells transfection

(origin of mammalian cell lines is listed in Appendix 2.1)

280 mM NaCl

50 mM HEPES

1.5 mM Na_2HPO_4

pH 7.10 - 7.15 with NaOH

(Filtered for sterilization)

HEPES washing buffer (4 L) for sea urchin egg binding studies

20 mM Hepes (free acid) [19.4 g in 4 L]

500 mM Potassium acetate [196 g in 4 L]

pH 7.4 with KOH

HL5 medium

53 mM Maltose

1.4% Bacteriological peptone (Oxoid)

0.7% Yeast extract (Oxoid)

4 mM Na_2HPO_4

3.5 mM KH_2PO_4

340 μM Dihydrostreptomycin sulphate

74 μM Vitamin B12 (cyanocobalamin)

82 μM Biotin

532 μM Riboflabin

pH 6.5

(Autoclaved, stored at room temperature for no more than 6 weeks)

H5O

50 mM KCl

20 mM HEPES

10 mM NaCl

5 mM $NaHCO_3$

1 mM NaH_2PO_4

1 mM $MgSO_4$

pH 7.0 with HCl or NaOH

(Filtered for sterilization, stored at -20°C)

Hypotonic Buffer for HEK293 cells, HEK293T cells and Sf9 cells

20 mM Hepes

1 mM EDTA

pH 7.2 with NaOH

PMSF or Proteinase Inhibitor Cocktail added just before use

KK_2 Buffer

19 mM KH_2PO_4

3.6 mM K_2HPO_4

(Autoclaved, stored at room temperature)

KK_2 agar

19 mM KH_2PO_4

3.6 mM K_2HPO_4

1.5 - 2.0% Agar

Laemmli Buffer, 1x Sodium Dodecyl Sulphate (SDS) Sample Buffer

63 mM Tris.HCl (pH 6.8)

10% Glycerol

2% SDS

0.02% Bromophenol blue

5% β-mercaptoethanol

(or 100 mM DDT was used instead of 5% β-mercaptoethanol)

(Stored at -20°C)

LB Agar

1% Bactotryptone

0.5% Yeast Extract

85 mM NaCl

1.5% Agar (weight/volume)

As an alternative, LB Agar (Mellford) was used.

(Autoclaved, stored at room temperature)

LB Broth (Lysogeny Broth)

1% Bactotryptone

0.5% Yeast Extract

85 mM NaCl

As an alternative, LB Broth (Mellford) was used.

(Autoclaved, stored at room temperature)

MAC (Sf9 Lysis Buffer)

20 mM Tris.HCl (pH 8.0)

0.3 M NaCl

10% Glycerol

0.5% Tween20

10 mM Imidazole

± 0.2 mM EDTA

MES Buffer (PIERCE Cobalt Resin)

20 mM 2-(N-morpholine)-ethanesulfonic acid

0.1 M NaCl

pH 5.0

Nonidet P-40 (Sigma-Aldrich: no longer sold)

Nonionic, non-denaturing detergent

Sigma-Aldrich claims that IGEPAL CA-630 is chemically indistinguishable from Nonidet P-40.

4% Paraformaldehyde (PFA)

20 g PFA in 500 mL ddH2O

Heated up to 60°C (but not exceeding 65°C), small quantities of 0.1 M NaOH (approx. 1 ml) added, and stirring maintained until solution became clear.

Filtered through a 0.2 µm filter (Millipore)

Phosphate buffer

Cocktail (Oxoid, BR0014G)

pH 7.2

1 M Phosphate (sodium) Buffer

1 M NaH_2PO_4

1 M Na_2HPO_4

Autoclaved, stored at room temperature

(various pH values are compounded by changing the ratio)

Proteinase Inhibitor

Complete, EDTA-free (Roche, 11 873 580 001)

Regeneration Medium for Sea Urchin Egg

Charcoal filtered GluIM 10 ml

10 mM Phosphocreatine

10,000 U Creatine phosphokinase

100 mM Mg^{2+}-ATP

10 µM Fluo-3

Sf9 Lysis Buffer

10 mM Tris.HCl

150 mM NaCl

1% CHAPS

1x Proteinase Inhibitor (Roche)

pH 8.0

SM agar (saccharose mannitol agar)

1% Bactopeptone (Gibco)

56 mM Glucose

16 mM KH_2PO_4

5.5 mM K_2HPO_4

4 mM $MgSO_4$

0.1% Yeast extract

1.2% Agarose

Autoclaved, stored at room temperature

Solubilization Buffer for HEK293 cells and HEK293T cells

1% CHAPS

150 mM NaCl

20 mM HEPES

Proteinase Inhibitor

pH 7.2

Starving buffer

1x KK_2 medium

5 mM EGTA

Stripping Buffer

62.5 mM Tris.HCl

100 mM β-mercaptoethanol

2% SDS

pH 7.6

50x TAE

2 M Tris.HCl

50 mM EDTA

5.71% (1 M) Glacial acetic acid

Transfer Buffer (Western blot)

50 mM Tris.HCl

500 mM Glycine

20% Methanol

0.1% SDS

pH 8.3

Transformation Buffer for E. coli

TFB I Buffer

30 mM Potassium acetate

100 mM RbCl

10 mM $CaCl_2.2H_2O$

50 mM $MnCl_2.4H_2O$

Glycerol to 15%

pH 5.8 with 0.2 M Acetic acid

Filtered for sterilization

TFB II Buffer

10 mM PIPES or 0.2313 g/100 ml MOPS

75 mM $CaCl_2.2H_2O$

10 mM RbCl

Glycerol to 15%

pH to 6.8 using 0.1 M HCl (if using PIPES) or 0.1 M NaOH (if using MOPS)

Filtered for sterilization

Tris-Glycine Electrophoresis Buffer

25 mM Tris.HCl

250 mM Glycine

0.1% SDS

pH 8.3

Tris-Buffered Saline (TBS)

2.48 mM Tris.HCl

137 mM NaCl

pH 7.4

Autoclaved, stored at room temperature

Vesicle Preparation for Dictyostelium

Washing Buffer

20 mM HEPES

pH 7.2

2x Buffer 1

100 mM KCl

2 mM $MgCl_2$

6% Sucrose

x2 Proteinase Inhibitor (Roche)

1x Buffer 2 (TKS)

10 mM Tris.HCl

50 mM KCl

1 mM $MgCl_2$

3% Sucrose

x2 Proteinase Inhibitor (Roche)

Washing Buffer for HEK binding studies

20 mM HEPES

pH 7.2 with NaOH

Washing Buffer (PIERCE Cobalt Resin)

50 mM Sodium phosphate

300 mM Sodium chloride

10 mM Imidazole (2 or 5 mM was also used)

pH 7.4

Washing Buffer (Western blot)

1x TBS

0.2% Tween20

Appendix 2.1 Cell lines

Strain name	Source / dictyBase ID	University / description	Resistance	Genetic modification
HEK293	Professor D. Blake	Dept of Pharmacology, Oxford University, UK		
HEK293T	Dr MX Zhu	The Ohio State University		
Hela	Dr AM Maison (Cox lab)	Dept of Biochemistry, Oxford University, UK		
Sf9	Dr MA Cohn	Dept of Biochemistry, Oxford University, UK		
Dictyostelium				
Ax2	Dr RR Kay	Cambridge University		
DH1	Dr WC Lima (Professor P Cosson)	Centre Medical Universitaire, Geneva, Switzerland		
csaA:gppA	DBS0236187	dajumin-GFP expressed on the CV	G418	Exogenous mutation
cnxA:GFP	DBS0236184	calnexin-GFP expressed on the ER	G418	Exogenous mutation
iplA$^-$	DBS0236187	IP_3 receptor-like protein null cells (Ax2 cells)	blasticidin	Endogenous insertion
lvsA$^-$	DBS0236519	Large volume sphere A null cells (DH1 cells)	blasticidin	Endogenous insertion
polycystin2$^-$	Professor Chris Thompson	The University of Manchester Polycystin-2-like protein null cells (Ax4 cells)	blasticidin	Endogenous insertion
tpc2$^-$	Dr WC Lima (Professor P Cosson)	Centre Medical Universitaire, Geneva, Switzerland (DH1 cells)	blasticidin	
E.coli				
TOP10	Invitrogen			
XL-10 Gold	Stratagene			
DH10Bac	Invitrogen	1. Bacmid 2. Donor plasmid 3. Helper plasmid	1. lacZ, kanamycin 2. gentamicin, ampicillin 3. tetracycline	
Bacmid	Dr MA Cohn	1. Bacmid 2. Donor plasmid 3. Helper plasmid	1. lacZ, kanamycin 2. gentamicin, ampicillin 3. tetracycline	
T7 Express lysY/I^q	Biolabs	*E. coli* expression		

Appendix 2.2 Plasmids

Name of plasmid	Source / dictyBase ID	Description	Resistance gene
pcDNA5TO	Invitrogen	Mammalian expression vector Tet On system	Ampicillin Hygromycin
pCRXLTOPO	Invitrogen	PCR cloning vector	Ampicillin Kanamycin lacZ
pCRIITOPO.XL	Invitrogen	PCR cloning vector for long insertion	Kanamycin lacZ
pSC-A	Stratagene	PCR cloning vector	
pFast. HT.A	Invitrogen	Sf9 expression vector with N terminal 6xHis tag TEV recognition site	Ampicillin Gentamicin
pLPBLP	dictyBase ID: 9	Plasmid for generating multiple gene disruptions	Blasticidin
pDM341	dictyBase ID: 526	Extrachromosomal, inducible expression vector (doxycycline). C terminal mRFPmars tag.	G418
pGEX-KG	Dr Pears, Biochemistry Department, Oxford	E.coli expression vector with N terminal GST tag. IPTG inducible system	Ampicillin
Vectors for organelle markers			
Details unknown		GFP-EEA1 (Early Endosome Antigen1: Early Endosome marker)	
Details unknown	Dr. S Grinstein, Tront	GFP-KDEL [Lys-Asp-Glu-Leu (KDEL) protein: ER marker]	G418
pEGFP-N1.*Hs*TfR	Professor P Woodman, Manchester University	TfR-GFP (Recycling endosome marker)	Kanamycin Neomycin
pEGFP-N3.*Hs*Lamp1	Dr C Esteban, Dell'Angelica, UCLA Dept of Human Genetics	Lamp1-mGFP (Lysosomal marker)	Kanamycin Neomycin
pCB6.*Rn*TGN38	Professor G Banting, Bristol University	TGN38-eGFP (trans-Golgi marker)	Ampicillin

Appendix 3. Overview of kits used for genetic modifications

Protocol	Company name	Kit name	Catalogue number
Plasmid preparation	Qiagen	Qiagen Plasmid Mini Kit	12125
Plasmid preparation	Qiagen	HiSpeed Plasmid Maxi Kit	12663
Plasmid purification	Qiagen	QIAquick Gel Extraction Kit	28704
PCR Purification	Qiagen	QIAquick PCR Purification Kit	28104
Phosphatase reaction	Roche Applied Science	Alkaline phosphatase, Shrimp	11 758 250 001
Ligation	Roche Applied Science	Rapid DNA Ligation Kit	11 635 379 001
RNA preparation	Sigma-Aldrich	RNA: TRI Reagent	T9424
PCR	Roche Applied Science	Expand Long Range dNTPack	04 829 034 001
PCR	Sigma-Aldrich	Taq polymerase	D4545
DNase	Applied Biosystems	TURBO DNA-free™ Kit	AM1907
RT-PCR	Sigma-Aldrich	Enhanced Avian HS RT-PCR Kit	HSRT100
Restriction enzymes	Roche Applied Science or New England Biolabs		

Appendix 4. IMAGE clone

	IMAGE clone ID	Gene Bank accession
*Hs*TPC1	40148827	BC150203
*Hs*TPC2	5214862	IRAT83-E04

Appendix 5. PCR primers

Appendix 5.1. Primers for pcDNA5TO.mRFPmars.SpTPCs

Primer set	Primer	F/R	5'-primer sequence-3'
*Sp*TPC1	MR282	R	GATCGCGGCCGCGGCGGATTTGGAGGACGACCTA
*Sp*TPC1	MR283	F	GATCGGGCCCTCATAACTCATCTCCAAGAATATC
*Sp*TPC2	MR123	F	GATCGCGGCCGCGGGAGACTACTACGAGTA
	MR110	R	GATCTCTAGATTAGTCCCAGGATGTGATGAAAT
*Sp*TPC3	MR289	F	GATCGCGGAGGGGCCAAAGGATTATGTT
	MR290	R	GATCGGGCCCTCATGCTATGTTATCCACGGA
N'mRFPmars	MR276	F	GATCGCGGCCGCGATGGTGAGCAAGGGCGAGGAG

Appendix 5.2. Primers for pcDNA5TO.SpTPCs.mRFPmars

Primer set	Primer	F/R	5'-primer sequence-3'
*Sp*TPC1	KW3	F	GATCGGATCCGCCATGGCGGATTTGGAGGACGAC
	KW4	R	GATCGCGGCCGCTAACTCATCTCCAAGAATATC
*Sp*TPC2	TMF1	F	GATCAAGCTTGACATGGGAGACTACTACGAGTAT
	TMF2	R	GATCGCGGCCGCGAAGCGCAGGTTTTGTATGTG
*Sp*TPC3	KW1	F	GATCGGATCCGCCATGGAGGGGCCAAAGGATTATG
	KW2	R	GATCGCGGCCGCTGCTATGTTATCCACGGAAAG
C'mRFPmars	KW6	F	GATCGCGGCCGCGGTGAGCAAGGGCGAGGAGG
	KW7	R	GATCGGGCCCCTACTTGTACAGCTCGTCCATG

Appendix 5.3. Primers for pCRIITOPO.mRFPmars.SpTPCs

Primer set	Primer	F/R	5'-primer sequence-3'
*Sp*TPC1	MR283	R	GATCGGGCCCTCATAACTCATCTCCAAGAATATC
*Sp*TPC2	MR110	R	TTAGAAGCGCAGGTTTTGTAT
*Sp*TPC3	MR290	R	GATCGGGCCCTCATGCTATGTTATCCACGGA
N'mRFPmars	MR276	F	GATCGCGGCCGCGATGGTGAGCAAGGGCGAGGAG

Appendix 5.4. Primers for pCRIITOPO.SpTPCs.mRFPmars

Primer set	Primer	F/R	5'-primer sequence-3'
*Sp*TPC1	KW3	F	GATCGGATCCGCCATGGCGGATTTGGAGGACGAC
*Sp*TPC2	TMF1	F	GATCAAGCTTGACATGGGAGACTACTACGAGTAT
*Sp*TPC3	KW1	F	GATCGGATCCCGCCATGGAGGGGCCAAAGGATTATG
C'mRFPmars	KW7	R	GATCGGGCCCCTACTTGTACAGCTCGTCCATG

Appendix 5.5. Primers for pFastHT.A

Primer set	Primer	F/R	5'-primer sequence-3'
*Sp*TPC1	KW8	F	GATCGCGGCCGCTGTAAACATGGCGGATTTGG
	KW9	R	GATCCTCGAGTCATAACTCATCTCCAAGAAT
*Sp*TPC2	KW10	F	GATCGCGGCCGCTGGGAGACTACTACGAGTAT
	KW11	R	GATCTCTAGATTAGAAGCGGAGGTTTTGTAT
*Sp*TPC3	KW12	F	GATCGCGGCCGCTGGAGGGGCCAAAGGATTAT
	KW13	R	GATCCTCGAGTCATGCTATGTTATCCACGGA

Appendix 5.6. Primers for Dictyostelium

Primer set	Primer	F/R	5'-primer sequence-3'
ERK	ERK-F5		CGCGGATCCATGTCATCTGAAGATATAGATA
	ERK-R2		ACCAGATACAACTGCTCCAACTTTATCAACAGA ATTCTAACTCGAGCGG
HR1	DW1		GTACCGATCCAACTGTTGGAGCATG
	KW45		GATCACTATCCTCATCAGTTGAGG
HR2	KW46		GATCCTGCAGGTTGTGATGACTGTGACGAG
	KW47		GATCGGATCCGAGGTAATGATCTTGGTCTCGG
HR3	KW48		GATCCTGCAGCAAATGATACCGGTTGGTGGTG
	KW49		GATCGGATCCTAGTTGCAGGTGGTAAGATTGG
HR4	KW50		GATCCTGCAGCTAGACCTCCAACACCTCAATC
	KW51		GATCGGATCCGCGTCAAAATGTTGTTGGGG
HR2.5'	KO4.5armF		GATCGGTACCGTTGTGATGACTGTGAC
	KO4.5armR		GATCAAGCTTGAGGTAATGATCTTGGTCTC
Primer set	Primer	F/R	5'-primer sequence-3'
Histone	HH3bF		GTGGCCCGTACAAAACAAAC
	HH3bR		TTAAGCACGTTCACCTCTGAT
BSR	Check1	F	GCGACAGAGAAGATTACAATGC
	Check2	R	CGTAGTTTTGACTAACTTGCC
BSR5arm		R	GCTATACGAAGTTATCCGTGG
BSR3arm		F	CGAAGTTATCATATGCCGCATGG
Check4		R	CCAATACCGATACTGGAAATGAGAAAAAATAA
Check1		F	GGGAGGTCGTTTTTACCC
Check2.1		R	GATGATCATCAATTGGTGATGGAG
Check3		R	CCAATTGAGATACAAGTTGC
Check5arm1		F	TCGAAATAGAGGGATTCTAACCTCAA
Check5arm2		F	CCTCAACTGATGAGGATAGTAATG
BSR cassette	BSR5' anti-sense	R	TTCAAATAATAATTAACCAACCCAAG
	BSR3' sense	F	GCATTAGATGTAAAACAGCCAAAGAG
	W5	R	TCACCAGTGACAGCACCAATTACA

Primer set (Size bp)	Primer	F/R	5'-primer sequence-3'
F1	KW52	F	AAGCTTGGATCCATGTGGAAAAATAATTTAAATCG
(1017)	KW53	R	GGAGTATGTACCACCATTAGGCGG
F2	KW54	F	CCGCCTAATGGTGGTACATACTCC
(1082)	KW55	R	CCTGGACTAGCGGTGGTACC
F3	KW56	F	GGTACCACCGCTAGTCCAGG
(775)	KW57	R	GTAAAGTACTATTGATAGTTGCAGGTGG
F4	KW58	F	CCACCTGCAACTATCAATAGTACTTTAC
(973)	KW59	R	GTCTCATTTTTCTAGTTGATGATAATAATC
F5	KW60	F	CTAGAAAAATGAGACATTTTATGCAATC
(295)	KW61	R	GCACTTGATACATCGATTGCAGC
F6	KW62	F	GCTGCAATCGATGTATCAAGTGC
(437)	KW63	R	CCACTACCACCTCCGCCTCCACC
F7	KW64	F	GGTGGAGGCGGAGGTGGTAGTGG
(812)	KW65	R	GAGGTGTTGGAGGTCTAGAAATA
F8	KW66	F	TATTTCTAGACCTCCAACACCTC
(567)	KW67	R	GGGCCCCTCTTCCTACCACTAGTACCAC
F9	KW69	F	GTGGTACTAGTGGTAGGAAGAG
(388)	KW70	R	GCGGCCGCTTTTTTCTCATTTCCAGTATCGG
Southern Prove 3'	KW50	F	GATCCTGCAGCTAGACCTCCAACACCTCAA
(562)	KW67	R	GGGCCCCTCTTCCTACCACTAGTAGGAC
Lima5arm	5' sense	F	TCGAAATAGAGGGATTCTAACCTCA
	5' anti-sense	R	CCAACAAATGTATCATCAAATTCCAA
Lima3arm	3' sense	F	TGAACTCAATGGAACTCAACATCAAA
	3' anti-sense	R	CGTCAAAATGTTGTTGGGGATCTT
screen	W1	F	AAATGTTTGGAATTGGGTTAAAGC
	W2	R	TGCAGGTGGTAAGATTGGTAAATGA
	W3	F	AAAACACAACCCACACCACTATCAA

	BSR5' anti-sense	R	TTCAAATAATAATTAACCAACCCAAG
	BSR3' sense	F	GCATTAGATGTAAAACAGCCAAAGAG
	W5	R	TCACCAGTGACAGCACCAATTACA

Appendix 6. Software

4Peask 1.7.2 (http://www.mekentosj.com/science/4peaks)
EnzymeX3 (http://www.mekentosj.com/science/enzymex)
Serial cloner (http://serialbasics.free.fr/Serial_Cloner.html)
ApE (http://biologylabs.utah.edu/jorgensen/wayned/ape/)
ChemBioDraw Ultra (http://www.cambridgesoft.com/software/chembiodraw/)

Appendix 7. Bioinformatics

S. purpuratus (*Strongylocentrotus purpuratus*) Genome Browser Gateway
http://genome.ucsc.edu/cgi-bin/hgGateway?clade=other&org=C.+intestinalis&db=strPur1

dictyBase
http://dictybase.org/

National Center for Biotechnology Information
http://www.ncbi.nlm.nih.gov/

European bioinformatics institute
http://www.ebi.ac.uk/

Center for Biological Sequence Analysis
http://www.cbs.dtu.dk/services/

TMHMM

A membrane protein topology prediction method based on a hidden Markov model; it predicts transmembrane helices and discriminates between soluble and membrane proteins with a high degree of accuracy.

http://www.cbs.dtu.dk/services/TMHMM/

Phobius

The prediction gives the most probable location and orientation of transmembrane helices in the sequence. It is found by an algorithm called N-best (or 1-best in this case) that sums over all paths through the model with the same location and direction of the helices

http://phobius.sbc.su.se/

Protein families, domains and structures

SMART

http://smart.embl-heidelberg.de/

Pfam (curated protein domains)

http://pfam.sanger.ac.uk/search

Motifs

EFhand (PROSITE)

http://expasy.org/prosite/

Motif scan

http://myhits.isb-sib.ch/cgi-bin/motif_scan

Aligment

EBI-ClustalW

http://www.ebi.ac.uk/Tools/msa/clustalw2/

Boxshade

http://mobyle.pasteur.fr/cgi-bin/portal.py#welcome

BCM search launcher

http://searchlauncher.bcm.tmc.edu/multi-align/multi-align.html

Appendix 8. Drugs and chemicals used

Drug	**Abbrev.**	**Effect**	**Source**	Catalogue Number
Concanamycin A	CMA	V-type H^+ ATPase inhibitor. CMA has 20 times the inhibitory effect on the V-type ATPase compared to bafilomycin A	Sigma-Aldrich	C9705
Bafilomycin A1	Baf	V-type H^+ ATPase inhibitor	LC laboratories	B-1080
Nigericin sodium salt	Nig	Ion-selective electrode, which disrupts membrane potential and stimulates ATPase activity	Sigma-Aldrich	N7143
Thapsigargin	Tg	IP_3-independent intracellular calcium releaser	Sigma-Aldrich	T9033
Gly-Phe β-naphthylamide	GPN	Substrate for cathepsin C, causes osmotic lysis of lysosomes	Sigma-Aldrich	(GPN): G9512
ß-Nicotinamide adenine dinucleotide phosphate, oxidised form, monosodium salt	NADP	A co-enzyme used in anabolic reactions, such as lipid and nucleic acid synthesis, which require NADPH as a reducing agent.	Melford	B3013
Nicotinic acid adenine dinucleotide phosphate	NAADP, $NAADP^+$	Calcium signalling messenger molecules	Homemade Dr Churchill, or made in our laboratory	
Nifedipine		L-type Ca^{2+} channel blocker	Sigma-Aldrich	N7634
Heparin		IP_3 receptor antagonist	Sigma-Aldrich	H3149
Diltiazem		L-type Ca^{2+} channel blocker	Sigma-Aldrich	D2521
Differentiation Inducing Factor-1	DIF-1	Induces cell differentiation	Enzo Life Sciences	BML-GR324-0100
Differentiation Inducing Factor-2	DIF-2	Induces cell differentiation	Dr Kay RR University of Cambridge	
Differentiation Inducing Factor-3	DIF-3	Induces cell differentiation	Dr Kay RR University of Cambridge	
Tert-Butylhydroquinone	tBHQ	SERCA inhibitor	Sigma-Aldrich	19986

Appendix 9. Fatty acids

A. Saturated fatty acids

Drug	**Abbrev.**		Source	Catalogue number
Palmitic acid	PA	$CH_3(CH_2)_{14}COOH$	SIGMA	P5585

B. Unsaturated fatty acids

Drug	**Abbrev.**	**Effect**	**Source**	**Catalogue number**
Arachidonic acid	AA	$CH_3(CH_2)_4(CH=CHCH_2)_4CH_2CH_2CO_2H$	SIGMA	A3555
Linoleic acid	LA	$CH_3(CH_2)_4CH=CHCH_2CH=CH(CH_2)_7COOH$	SIGMA	L1376
Oleic acid	OA	$CH_3(CH_2)_7CH=CH(CH_2)_7COOH$	Enzo	FA-045
5,8,11,14-Eicosatetraynoic acid	ETYA	$CH_3CH_2CH=CHCH_2CH=CHCH_2CH=CHCH_2CH=CH(CH_2)_3COOH$	SIGMA	E1768
5,8,11-Eicosatriynoic acid	ETI	$CH_3CH_2CH=CHCH_2CH=CHCH_2CH=CH(CH2)_6COOH$	SIGMA	E3140

Appendix 10. Sequence

Appendix 10.1. Coding sequence of putative DdTPC2

> putative *Ddtpc2* (*Putative *intron: 3768 - 3844*)

ATGTGGAAAAATAATTTAAATCGAAATAGAGGGATTCTAACCTCAACTGATGAGGA
TAGTAATGATATAAATAATAACAATAATGATAATATTAATAGTCCAAATAGTATTAA
AAGTCATAAATCAAGTAAAAGTGGTAGTAGTACAAAAACAAATAAAAGTACAAAA
ACAATTAAATCTGCATCATCTTCATTACAAAGTAGACAAATTGATTTAGGTTTTTTA
AAGAAATTAGATACACTACCCAATG
AACATTCAGATGATTCATACGAAGAAGAAGACGAAGACGAAGACGACTATGAAAC
CCATTCATATGATTCTTTTGATCAAAGTTGTGATGACTGTGACGAGAATAATATAGA
AGATTCAGAAGATTCATGTGAATTGGCAGATGATGAAGATTCTGAAAATTTAAGTG
AAAATGATAATAATAATAATAATAATAATAATAATAATGATAATGATAATAATGAA
TTTAACTTTGGTGAAGGTGAAGAAGAGAATAATGAAGAAAATAATGAAGAAGAATA
TAATGAAGATAATGAAGATAACGAAGATAATTATGAAACTGTAAATAAAATAAAAA
AACATGATGTATTTAGAAAGAATCAATTAAAGAATATTTTGGAATTTGATGATACAT
TTGTTGGAAATAAATATAATAAACACAAAACATTTAATAAATTTGCCTATAACAATG
GTGCCAAAACTTCATTGGAATCTATTATAGAGAAATCGGAATCATCAATAACTCAAC
GTAGTAATGGTTCTTCACCAATACCAAAAAGAAAAAAATCAATAACTTCAAATGTT
GATAATAATAATAATAATAATAATATTAATAATAATGGAAATAATAATAATAATATT
AATGATAATGGAAATAATAATAAAAGTCCATTTTTACATCAAATTAAAATTCCACAT
TCTTATAAAGAAAAATTAATTTCACCTCATTATAATTATAACAGAACAAGAGGTTCA
TTAAATTTACCGCCTAATGGTGGTACATACTCCTCACCATCATCATCTTCTTCTTCAT
ACTCATCTATTAGTACGACAAGTTCAATATTTCCAACATCTCCAAATATGGAAATAC
CGAGACCAAGATCATTACCTCAAACATTTTCTTCTTCTTCTTCTCCATCACCAATTGA
TGATCATCAAAAACAAGATGAATTAGGAAAATCACCATTATTAAAACAAAAACAAA
AAGATGAAGAAAAAAAAGAAAAAGAAGAAAAAGAAGGGAGAGGGAGAGGAGGAG
GAGGAGATAATATTAGTATTGTTGATTTTAGAGATAATATTGAAAAAGTTAAAAGA
AAAGATAATAATAATGTTTTTATAAGTAAGAGAAGAGTTAGTTTTGATCACACATCA
ACCAATTTAAAAGATCAAGAAATTTTGGAAAAATCACAAAAAAAAAATATATTAAA
AAATAAAGGTGGTCAAGAATTTTATGAACCTGTTAAAGAATTATCAAAAGAAGATA
AAGAGAGGAGAATGTATATATCAGTGGCATTAATAAAAGATGCCATTCATTATCGT
AATCCAAATCATCTTTTAATGATGGATCGATTAAAAGTTTATCAAATTTATTTTCACC
CAGCTTGTAGATTATTTTTATTTTTAGTGATTATAATAGATTTAATGTTGATTTATTTC
GAATATCCTACCAATTATCCAATTAGAGGATATGGTACACAATTTATAGAGTTGGCT
TGTGTATTGGTGTTTTGTTTTGAGTTGGGTTTAAAAAGGTATGTCTATGGTAAACCAA
TGGAAAAAAATGTTTGGAATTGGGTTAAAGCTATAGTTTTAATACTGAATCTTATAG
ATTTATTGGTTGCTTTTATATTGGTTGCTAATGGTATAGTTACTGATATTAGAATTTC
AAGATTACTTAGAGTTTATTATATCATTGATTATGATCGATTAACTAGAGATTTATTT
CATCAAGTTACCTACACTCTATTTCAAATGATACCGGTTGGTGGTGTATTCTTTACCT

ATATTTTCCTATCATCAATACTTTTCACTATTATTTTTTCAAATGGTACCACCGCTAG
TCCAGGTTATTATGATAGTACATTAACATCATTCAAAAACACAATGGTATTGGTAAC
AACTTGTAATTTCCCTGATATTATGCTACCTGCATTTTATACAAGTCAATGGTATTCA
ATCATATTCATAGTTTATTTAATATTTGGATTGTATTTAGGTGTTAATTTTATGATTG
CAATTGTTTATCAAAGTTTTAGAAAAGCAGTATTAGGTGAAACTAAAAATAATTTTA
GAACTAGAAGAACTGCTTTATTGGCAGCTTTTATCATTATGGATCATGATAAAAATG
GTGTAATCTCATTAGATCAATGGAGAGAAATGTATAAAGAAATCGTACCAAAATCA
ACATCCTATGAAGCAAATGTTGCGTTTGAATTAGTTGATACAGATAGTAATGGTTAT
TTAAATGCTCGTGAATTTTTTGCAATGTGTGATGTATTTGTCACTGGTAGAAAAGAA
GTTAGAAAATTAGCTAAAAGAAGATTAGAACGTGAAAAAAGAAAAAGAGAATATC
TAATCCGTAAAAATGAAAAACTATTACATAGAAAAAAAAAACAAAAAAAAATTAA
AAAAGAACAAGAACAATTACAAGAAAATGAAAAAGAACAAGTTCAACAACAACAA
GTTGAGGAAACAAATAACCAAAACGATTTAAAAGAATTTTTTCAAAAAAGAAAAAC
AATTATTAGAAAACCTAATGAACCAAAAACTACCAATGATCATTTACCAATCTTACC
ACCTGCAACTATCAATAGTACTTTACAAGATAGTCAAGCAACTTGTATCTCAATTGG
TAATTCACCTCAAATTTCAGATTTAAATTATAAATTGCCCCAACAAAAAAATGTTGA
AATTTCAATACCAGAATCTACAAAATCAAATAATAATAATAATAATAATAATAATA
ATAATAATAATAATAATAATAATAATAATAATAATAATAATAATAATAATAATAAT
AATAATAATAATAATAATAATAATAATAATAATAATAATAATAATAGTTTTAATAAT
AAATATGATGATAATGATAATAATATAAATGATAATAATAATTATAAAAATGAAGA
AAAAAATTTCTTAGAGGATGTGGATAATGATGGTGATAATGTCTCAAATGAGATTA
ATCAAGATAAAAATAGTATTGATGAATTACCACAATCACAAAAACATCAAGATAAA
AGTTTAGAGAAAAAACAACATATTCATATACTACATCATAATCATAGTCATATTCAT
CATCACCATCATCGTCATAAAAAAGAAATTGAATTTAAAGAAGTTTCTCGTTTTCAA
TATATTTATGGTTATATTATAAATTACAATTTAAAAATAATTACAAAACATTGGATTT
TTGAATTATTTGTTTCTTTAATGTTATTTTTTAATGCAATAATCATTACAATGGTAAT
GGTTCATTATAGAAATTTATATGTCCCAAAGTGGACAATCATTTGTGATGATATTTT
ATTAGGAATTTCAATTGTTGAAGTTTTTTTAAAAGTAATTTCAAATAGAAAGAAATT
CATTTTTTGGATTGGTTTTAATGTTACCATAGTTTCAATCTCATTAATTGGTAAAATC
GTATTGGAATATGCATTAAAATCAATAACTAAAAATAGTTTAAATTTATTAAGAGTT
TGTTGTGCTTTTAGATATATTAGATTATTAAGATTATTATCATCAACTAGAAA

**GTAAGTAAAAATATAACATAATAATAATAAATGATGATAATAATAATAATAATACTAATAATA*
ATAATTTTTTTTAG

AATGAGACATTTTATGCAATCATTAGCACAACTATCACTTATATTCCTAAATTTTATT
GGAATTGTATTGGTAATTTATTATATTTTTGCAGTTATTGGAATTTGGGCTTATAGCG
GTCGTTTTTATCGTGGCAATCCAGCTTTAGTTGGCACAGACTATGATACTTTTAATTA
TTATGGATATGCAAATTTCGATACATTCATTAGTTCAATGTTTACATTATTTCATTTA
ATGGTTTTAAATAATTGGTTGGTTACATTTTATGCTGCAATCGATGTATCAAGTGCAT

GGGCTATATTATATTTTTGTTCTTTCTACTTCATTCTAGGTATTTGTGTTTTAAATTTA
GTTGTTGCATTCTTAATTGAAGCTGTAAACTATACAAATAATTTCTTTTATTCAAAAC
GTAGAAAGTTTTCAAATCAAAGTTTAGAACAATTTAAAAAACAATTTAAAGTGAAA
AACAGTAAAAAAGGTATTCAAGAAAACTCAAATCAAGATAAAATTAAAAATAATAA
TAATAATAATAATGACAACAAAAATAAAAATAATAATAGTAATAATAAAAATGATA
ATAAAAATAATAATAGTAACAATGATAATAATAATAATGATAAAAATCGTAGTGAC
AGCAGTAGTGATGATAATGATGGAAAAGGTAGAGGTGGAGGTGGTGGAGGTGGAG
GCGGAGGTGGTAGTGGTGAAAATAGTTTTGGATTTAATCATCTTGGTTCAATAAATG
GGTCAATATTTACAAATGACGAATTAAAATGTTGTGATATTGACGATAGAGGAGATT
ATCGTTTACCAATACAATCATTAAGAAATGATGGTTCATTAAAATTTTTAGATATGA
CACATAACCATTTTTCTCCACCAACTAAAAAAGCTCATAAAAAGATATCACCTGAAA
CTATTAAAAAAAATTTCGTTGGTTTTGAAGAAACTAAAAAAGATTCAAATGTAAATC
CAACTAGGGGCGACTATTCCAGTATTGAAGATGTTGAAGAATTTATACCACAAGATT
ATTTATTAGAACAAATAAAAGATTTAAAAACTGATAGTGGTTTAGGATATGTTAGTG
ATGATGAACTCAATGGAACTCAACATCAAACATTTCCAAAATATTCAAGTGATATTG
GTAGTGTATTTAGAAAGGAATATAGTCAAAGAAGAAGACAATCAATTAGACATAAT
TCATTAGGTCACATTTTAAAACCATCTGAATCTCAAACAATTAATCAAAATAAAGTT
TTTTCAAACCCACTTTCAAGAACTCATCCAATTCAAGAAGGAATTGAATCAGAACCT
ATTGATTTTTCAAATTTTAATGGAAATAATAATAATAATAATAATAATAATAATAAT
AATAATAATAATAATTATAATAATAATAATAATAATAATAATATTGTAAAAAATCCA
TTACCAAAAACAATGCCATCATCAAAATTATTACCACAATCAACATTACAACCTAGT
GATAAAATTATTTCTAGACCTCCAACACCTCAATCAAATGTAAAACAACAACAGTCA
ATATTAAATAAAAGTAGTAGTAATAATCCGATATTAAATAAGAGTGGAAATAATTT
ATCTTCATCACCATCATCACCAATTTTATCAGATGTAAGGAAAAGTGTTAAACTTGT
AAATGAATCATCAAAAGCATCTTTTTCGAAAAAGGATTTATTAAAATCAAAAAAGC
TAAGATTAGAGAAAAAGATAAAAGACATTGAAAAGGAATTAGAGAAAGAAAGTAA
AGAATATAAATTAAAAATGAAAGAGAGAAGGAAAAATAGTAACACTGATTGCGAT
GATGATGATGGTGATGTAGATAATGACGACGATGGTTCTGATATCGATGGCGATAA
TAATGTCTTTGATGACGACGACTCTGTAGATTTTGAACCAACATTAAGAAAAAGTAA
AATAAAGAAAGAAATTAAACGAAAATCAAATGTAAGTGCTGGTTTAGGTTTTGAAG
AATCAAATCATGGTTTTGACGACAATGATTATGATAATGATAATACAAGTGGTACTA
GTGGTAGGAAGAGTAATAACAAGAAGAATAACCACAAAAACACTCCAATCGAAAC
TGACACAAGTAGAGAAGATTTTACAGATTTAAATGATGAGTCAGATTTTACTGAAG
GTGAAATAAGAAGGTTTAGAAAGAAAAAAGATCCCCAACAACATTTTGACGCTCAT
GATTTAGAAACTAAAATGTTTGGTAAAGAACTAAAAGATGTAAATCTAGAAGAGAT
CAACTTTGATCAATTCTTGGAGAATAATGTAATTGGTGCTGTCACTGGTGATAAAAT
ATTAAAAAATCCAATAATAGAAACCGATACTGATAGTGATACCGATAACAATACCA
AAACCAATACCGATACTGGAAATGAGAAAAAATAA

Appendix 10.2. Optimized sequence of DdTPC2 for synthetic gene

>*Ddtpc2*_dual use_opt_V3modifiedbyK

GGATCCGCCACCATGGAAAGATCTAAAAAAATGGATTATAAAGATGATGATGATAA
GGGTTGGAAAAATAATTTAAATCGAAATAGAGGGATTCTAACCTCAACAGATGAGG
ATTCAAATGATATCAATAACAACAATAACGATAACATCAATTCACCAAATTCTATCA
AGTCTCACAAGTCATCAAAATCAGGTAGTTCAACAAAGACCAACAAATCAACTAAA
ACTATCAAGTCTGCATCTTCATCATTACAATCACGTCAAATTGATCTTGGTTTCTTAA
AAAAGCTTGATACTCTTCCAAACGAACATTCAGATGATAGTTATGAGGAAGAGGAT
GAAGATGAGGATGATTACGAGACACATTCATATGATAGTTTCGATCAATCATGCGAT
GATTGCGATGAGAATAACATAGAAGATTCAGAGGATTCATGTGAATTAGCAGATGA
TGAAGATAGTGAGAATTTGAGTGAGAACGATAACAACAACAACAACAATAACAATA
ACAACGATAATGATAACAATGAGTTCAATTTCGGAGAGGGTGAAGAGGAGAATAAC
GAAGAGAACAACGAGGAGGAATACAATGAGGATAATGAGGATAATGAGGATAACT
ATGAAACTGTAAACAAAATCAAAAAGCATGATGTATTCCGTAAAAACCAATTGAAA
AACATTTTGGAATTCGATGATACTTTCGTTGGTAACAAGTATAACAAACACAAGACC
TTCAACAAGTTTGCCTATAACAATGGAGCTAAGACCAGTTTAGAGAGTATCATAGA
GAAATCAGAATCTAGTATTACACAACGTTCTAATGGATCTTCACCAATTCCTAAGCG
TAAAAAGTCAATAACTTCTAATGTAGATAACAACAACAACAACAATAACATAAACA
ACAATGGAAACAACAACAACAATATCAATGATAATGGAAACAATAACAAGTCACCA
TTCCTTCATCAAATCAAAATCCCTCACTCATACAAAGAGAAGCTTATCAGTCCACAC
TATAACTATAACCGTACTCGTGGTAGTCTTAATCTTCCACCAAATGGTGGAACCTAT
AGTAGTCCATCAAGTTCAAGTTCAAGTTACTCATCAATTTCAACAACTTCAAGTATC
TTCCCAACTTCACCAAACATGGAGATCCCAAGACCAAGATCATTACCTCAAACATTT
TCATCTTCATCTAGTCCTTCTCCTATCGATGATCATCAAAAACAAGATGAGCTTGGA
AAATCACCATTACTTAAACAAAAGCAAAAAGATGAGGAGAAAAAGGAGAAGGAGG
AGAAGGAGGGTAGAGGTAGAGGTGGTGGAGGAGATAACATCTCAATTGTAGATTTC
AGAGATAACATTGAAAAGGTTAAACGTAAGGATAACAATAACGTTTTCATCAGTAA
GCGTCGTGTATCTTTTGATCACACCTCAACCAATTTGAAGGATCAAGAGATATTGGA
GAAGTCACAAAAGAAAAACATCTTGAAAAATAAGGGAGGACAAGAGTTTTACGAA
CCAGTAAAAGAGCTTTCAAAGGAGGATAAAGAGCGTAGAATGTATATCTCAGTAGC
ATTGATCAAAGATGCAATTCACTACAGAAATCCTAATCACTTACTTATGATGGATCG
TTTGAAAGTTTATCAAATCTACTTTCACCCAGCATGTAGACTTTTCCTTTTCCTTGTT
ATCATTATCGATTTGATGTTGATATACTTCGAATATCCAACAAACTATCCAATTAGA
GGTTATGGTACCCAATTCATAGAATTAGCCTGCGTTTTAGTATTCTGTTTTGAGTTGG
GTTTGAAACGTTATGTTTATGGAAAACCAATGGAGAAAAACGTATGGAACTGGGTT
AAGGCCATCGTTTTGATCTTAAACTTGATCGATCTTTTAGTTGCCTTTATCCTTGTTG
CTAACGGAATCGTAACTGATATACGTATTTCTCGTTTACTTCGTGTTTACTACATTAT
CGATTACGATAGACTTACACGTGATTTGTTTCACCAAGTTACCTACACACTTTTCCAA
ATGATCCCTGTTGGTGGTGTTTTCTTTACCTATATTTTCCTTTCATCAATCTTATTCAC
AATCATCTTCAGTAATGGAACCACAGCCTCACCAGGATACTACGATTCTACATTGAC

CAGTTTCAAAAACACAATGGTATTGGTAACCACATGCAATTTCCCTGATATCATGTT
ACCAGCCTTTTACACAAGTCAATGGTACTCAATCATATTCATAGTATACCTTATCTTC
GGACTTTATCTTGGAGTTAACTTTATGATCGCTATTGTATATCAATCTTTTCGTAAAG
CTGTATTAGGAGAAACCAAAAACAATTTCCGTACACGTAGAACTGCATTGTTAGCCG
CCTTCATCATAATGGATCATGATAAAAATGGAGTTATCTCATTGGATCAATGGAGAG
AGATGTATAAGGAGATTGTTCCAAAATCAACTTCATACGAGGCTAATGTTGCATTCG
AGTTGGTTGATACAGATTCAAACGGTTACCTTAACGCCAGAGAGTTTTTCGCCATGT
GTGATGTTTTCGTAACTGGTAGAAAAGAGGTTAGAAAGTTGGCAAAGCGTAGATTA
GAAAGAGAGAAACGTAAACGTGAGTATCTTATCCGTAAGAACGAGAAGCTTTTACA
CCGTAAAAAGAAGCAAAAAAAGATCAAAAAGGAGCAAGAGCAATTACAAGAGAAC
GAAAAAGAGCAAGTACAACAACAACAAGTAGAGGAGACTAACAATCAAAATGATC
TTAAGGAGTTTTTCCAAAAGCGTAAAACCATCATCAGAAAACCAAACGAGCCTAAG
ACAACAAATGATCATTTGCCAATACTTCCACCAGCCACAATCAATTCAACATTGCAA
GATAGTCAAGCAACATGTATAAGTATAGGTAATTCTCCACAAATCTCAGATTTGAAT
TACAAATTGCCTCAACAAAAGAATGTTGAGATTAGTATTCCAGAGTCTACAAAAAG
TAACAACAACAATAACAACAACAACAATAACAACAACAATAACAACAACAATAAC
AACAATAACAATAACAACAACAATAACAACAATAACAATAACAACAACAATAACA
ACAATAACAACAACAATAACAGTTTCAACAATAAGTATGATGATAATGATAACAAC
ATAAACGATAACAATAACTACAAAAACGAGGAGAAAAACTTTTTGGAGGATGTTGA
TAATGATGGTGATAATGTTTCAAATGAGATCAATCAAGATAAAAATTCAATTGATGA
ACTTCCACAATCACAAAAACACCAAGATAAGTCTTTAGAGAAAAAGCAACATATTC
ATATACTTCACCATAACCACTCTCACATTCACCACCATCACCATAGACACAAAAAGG
AAATTGAGTTCAAAGAGGTTTCACGTTTCCAATACATCTACGGTTACATCATTAACT
ACAATCTTAAGATCATTACCAAGCATTGGATTTTCGAGCTTTTTGTAAGTCTTATGTT
GTTTTTCAACGCCATTATCATTACTATGGTTATGGTTCACTATAGAAACCTTTATGTT
CCAAAGTGGACCATCATTTGCGATGATATCTTGCTTGGAATTTCAATTGTTGAGGTTT
TCCTTAAAGTAATCTCTAACAGAAAGAAATTCATCTTCTGGATTGGATTCAACGTTA
CAATCGTAAGTATATCACTTATTGGAAAGATCGTATTAGAATATGCATTGAAATCAA
TCACCAAAAACAGTTTGAACTTACTTAGAGTTTGCTGTGCTTTCCGTTACATTAGATT
ACTTAGACTTTTGTCTAGTACTCGTAAGATGAGACATTTCATGCAAAGTTTAGCTCA
ATTGAGTTTGATCTTTTTGAACTTCATCGGTATTGTATTAGTTATCTACTACATTTTCG
CAGTTATCGGTATTTGGGCTTACAGTGGTAGATTCTACCGTGGTAATCCAGCATTAG
TAGGTACAGATTATGATACCTTCAACTACTATGGATATGCCAATTTCGATACTTTCAT
AAGTTCAATGTTTACTTTGTTTCATCTTATGGTATTGAACAATTGGCTTGTAACCTTC
TATGCTGCAATTGATGTAAGTTCAGCATGGGCTATACTTTACTTTTGCAGTTTCTACT
TCATCCTTGGTATATGCGTATTGAATCTTGTAGTTGCTTTCCTTATCGAAGCCGTAAA
CTACACTAACAACTTTTTCTATTCTAAGCGTAGAAAGTTCAGTAATCAATCATTAGA
ACAATTCAAAAAGCAATTCAAGGTTAAGAATAGTAAAAAGGGTATTCAAGAGAACT
CTAATCAAGATAAGATCAAAAACAACAATAACAACAATAACGATAACAAAAACAA
AAACAATAACTCAAACAACAAAAACGATAACAAAAACAATAACTCAAACAACGAT

AACAACAACAATGATAAAAATCGTTCAGATTCAAGTAGTGATGATAATGATGGTAA
AGGTAGAGGAGGTGGTGGTGGAGGTGGTGGAGGAGGAGGATCTGGTGAAAACTCTT
TCGGATTCAATCACTTGGGAAGTATCAATGGATCAATCTTCACTAATGATGAGCTTA
AGTGTTGTGATATTGATGATCGTGGTGATTACAGATTGCCAATTCAATCATTGAGAA
ACGATGGATCTCTTAAGTTTTTGGATATGACTCATAATCACTTTTCACCTCCAACCAA
AAAGGCACACAAAAAGATATCACCAGAAACAATCAAGAAGAACTTTGTTGGTTTCG
AGGAAACCAAAAAGGATTCAAATGTTAATCCAACTCGTGGAGATTACAGTTCAATA
GAAGATGTAGAAGAGTTCATCCCACAAGATTACCTTTTGGAGCAAATCAAGGATCTT
AAGACAGATTCTGGTCTTGGTTACGTAAGTGATGATGAGCTTAATGGTACACAACAT
CAAACTTTCCCAAAGTACAGTAGTGATATTGGATCTGTATTTCGTAAGGAGTATTCA
CAACGTCGTAGACAATCAATCAGACACAACTCATTAGGACACATATTGAAACCAAG
TGAATCACAAACCATTAACCAAAACAAAGTTTTCTCTAATCCATTAAGTCGTACACA
TCCTATCCAAGAGGGTATCGAAAGTGAGCCAATTGATTTCTCTAACTTCAATGGAAA
CAACAATAACAACAATAACAATAACAACAACAACAACAATAACAATTACAACAAC
AACAACAATAACAATAACATTGTTAAAAATCCACTTCCAAAAACAATGCCTTCATCA
AAACTTTTACCACAATCTACTCTTCAACCTAGTGATAAGATTATCTCAAGACCACCA
ACTCCTCAAAGTAATGTTAAGCAACAACAAAGTATCTTGAATAAGTCATCATCTAAC
AACCCTATCTTGAACAAGTCAGGTAACAATTTGAGTTCATCACCAAGTAGTCCAATC
TTGTCAGATGTTAGAAAAAGTGTAAAGTTGGTTAACGAATCTTCAAAAGCAAGTTTT
TCAAAGAAGGATTTGCTTAAGAGTAAAAAGTTACGTTTAGAGAAAAAGATCAAAGA
TATTGAAAAAGAGTTGGAGAAAGAGTCAAAAGAGTATAAGTTGAAGATGAAGGAG
CGTCGTAAGAACTCTAATACAGATTGTGATGATGATGATGGTGATGTTGATAACGAT
GATGATGGATCTGATATTGATGGTGATAACAATGTATTCGATGATGATGATTCAGTT
GATTTCGAGCCAACACTTAGAAAATCAAAGATCAAAAAGGAGATAAAGAGAAAGA
GTAACGTATCTGCCGGATTAGGTTTTGAAGAGAGTAATCATGGATTTGATGATAATG
ATTATGATAATGATAACACATCAGGAACTTCTGGTCGTAAAAGTAACAACAAAAAG
AACAATCACAAAAACACTCCTATTGAAACTGATACATCTAGAGAAGATTTCACTGAT
CTTAACGATGAATCAGATTTCACTGAAGGAGAAATTCGTCGTTTTAGAAAAAAGAA
AGATCCTCAACAACACTTCGATGCACATGATTTGGAAACCAAAATGTTCGGTAAAG
AGTTAAAGGATGTTAATCTTGAAGAGATCAACTTCGATCAATTCCTTGAGAACAATG
TAATTGGAGCTGTTACCGGAGATAAGATATTGAAAAACCCAATCATTGAAACAGAT
ACTGATTCAGATACAGATAACAATACCAAAACCAACACTGATACTGGAAATGAGAA
AAAGACTAGTCTCGAGGCGGCCGC

REFERENCES

Aarhus R, Graeff RM, Dickey DM, Walseth TF & Lee HC (1995). ADP-ribosyl cyclase and CD38 catalyze the synthesis of a calcium-mobilizing metabolite from NADP. *Journal of Biological Chemistry* **270**: 30327-30333.

Aarhus R, Dickey DM, Graeff RM, Gee KR, Walseth TF & Lee HC (1996). Activation and Inactivation of Ca^{2+} Release by $NAADP^{+}$. *Journal of Biological Chemistry* **271**: 8513-8516.

Alexander H, Vomund AN & Alexander S (2003). Viability assay for *Dictyostelium* for use in drug studies. *BioTechniques* **35**: 464-6, 468, 470.

Araki T, Langenick J, Gamper M, Firtel RA & Williams JG (2008). Evidence that DIF-1 and hyper-osmotic stress activate a *Dictyostelium* STAT by inhibiting a specific protein tyrosine phosphatase. *Development* **135**: 1347-1353.

Araki T, Van Egmond WN, Van Haastert PJ & Williams JG (2010). Dual regulation of a *Dictyostelium* STAT by cGMP and Ca^{2+} signalling. *Journal of Cell Science* **123**: 837-841.

Aksoy P, Escande C, White TA, Thompson M, Soares S, *et al*. (2006). Regulation of SIRT 1 mediated NAD dependent deacetylation: a novel role for the multifunctional enzyme CD38. *Biochemical and Biophysical Research Communications* **349**: 353-359.

Aubry L, Klein G, Martiel JL & Satre M (1993). Kinetics of endosomal pH evolution in *Dictyostelium discoideum* amoebae. Study by fluorescence spectroscopy. *Journal of Cell Science* **105**: 861-866.

Aubry L, Maeda M, Insall R, Devreotes PN & Firtel RA (1997). The *Dictyostelium* mitogen-activated protein kinase ERK2 is regulated by ras and cAMP-dependent protein kinase (PKA) and mediates PKA function. *Journal of Biological Chemistry* **272**: 3883-3886.

Bach G, Chen CS & Pagano RE (1999). Elevated lysosomal pH in Mucolipidosis type IV cells. *Clinica Chimica Acta* **280**: 173-179.

Bach G (2001). Mucolipidosis Type IV. *Molecular Genetics and Metabolism* **73**: 197-203.

Baskar R, Chhabra P, Mascarenhas P & Nanjundiah V (2000). A cell type-specific effect of calcium on pattern formation and differentiation in *Dictyostelium discoideum*. *International Journal of Developmental Biology* **44**: 491-498.

Bateman A, Birney E, Cerruti L, Durbin R, Etwiller L, *et al*. (2002). The Pfam protein families database. *Nucleic Acids Research* **30**: 276-280.

Berg I, Potter BVL, Mayr GW & Guse AH (2000). Nicotinic acid adenine dinucleotide phosphate ($NAADP^+$) is an essential regulator of T-lymphocyte Ca^{2+}-signaling. *The Journal of Cell Biology* **150**: 581-588.

Berridge MJ, Lipp P & Bootman MD (2000). The versatility and universality of calcium signalling. *Nature Reviews Molecular Cell Biology* **1**: 11-21.

Berridge MJ, Bootman MD & Roderick HL (2003). Calcium signalling: Dynamics, homeostasis and remodelling. *Nature Reviews Molecular Cell Biology* **4**: 517-529.

Beutner G, Sharma VK, Giovannucci DR, Yule DI & Sheu SS (2001). Identification of a ryanodine receptor in rat heart mitochondria. *Journal of Biological Chemistry* **276**: 21482-21488.

Billington RA & Genazzani AA (2000). Characterization of $NAADP^+$ binding in sea urchin eggs. *Biochemical and Biophysical Research Communications* **276**: 112-116.

Bof M, Brenot F, Gonzalez C, Klein G, Martin JB & Satre M (1992). *Dictyostelium discoideum* mutants resistant to the toxic action of methylene diphosphonate are defective in endocytosis. *Journal of Cell Science* **101**: 139-144.

Boittin FX, Galione A & Evans AM (2002). Nicotinic acid adenine dinucleotide phosphate mediates Ca^{2+} signals and contraction in arterial smooth muscle via a two-pool mechanism. *Circulation Research* **91**: 1168-1175.

Bolourani P, Spiegelman GB & Weeks G (2008). Rap1 activation in response to cAMP occurs downstream of Ras activation during *Dictyostelium* aggregation. *Journal of Biological Chemistry* **283**: 10232-10240.

Bominaar AA & Van Haastert P (1994). Phospholipase C in *Dictyostelium discoideum*. Identification of stimulatory and inhibitory surface receptors and G-proteins. *Biochemical Journal* **297**: 189-193.

Bosanac I, Alattia JR, Mal TK, Chan J, Talarico S, *et al.* (2002). Structure of the inositol 1, 4, 5-trisphosphate receptor binding core in complex with its ligand. *Nature* **420**: 696-700.

Bosanac I, Yamazaki H, Matsu-Ura T, Michikawa T, Mikoshiba K & Ikura M (2005). Crystal Structure of the Ligand Binding Suppressor Domain of Type 1 Inositol 1,4,5-Trisphosphate Receptor. *Molecular Cell* **17**: 193-203

Brailoiu E, Churamani D, Cai X, Schrlau MG, Brailoiu GC, *et al.* (2009). Essential requirement for two-pore channel 1 in NAADP-mediated calcium signaling. *The Journal of Cell Biology* **186**: 201-209.

Brailoiu E, Hooper R, Cai X, Brailoiu GC, Keebler MV, *et al.* (2010a). An ancestral deuterostome family of two-pore channels mediates nicotinic acid adenine dinucleotide phosphate-dependent calcium release from acidic organelles. *Journal of Biological Chemistry* **285**: 2897-2901.

Brailoiu E, Rahman T, Churamani D, Prole DL, Brailoiu GC, *et al.* (2010b). An NAADP-gated two-pore channel targeted to the plasma membrane uncouples triggering from amplifying Ca^{2+} signals. *Journal of Biological Chemistry* **285**: 38511-38516.

Buck E, Zimanyi I, Abramson JJ & Pessah IN (1992). Ryanodine stabilizes multiple conformational states of the skeletal muscle calcium release channel. *Journal of Biological Chemistry* **267:** 23560-24567.

Buhl AM, Johnson NL, Dhanasekaran N & Johnon GL (1995). Gα12 and Gα13 Stimulate Rho-dependent Stress Fiber Formation and Focal Adhesion Assembly. *The Journal of Biological Chemistry* **270**: 24631-24634.

Calcraft PJ, Ruas M, Pan Z, Cheng X, Arredouani A, *et al.* (2009). NAADP mobilizes calcium from acidic organelles through two-pore channels. *Nature* **459**: 596-600.

Cancela JM, Churchill GC & Galione A (1999). Coordination of agonist-induced Ca^{2+}-signalling patterns by NAADP in pancreatic acinar cells. *Nature* **398**: 74-76.

Caterina MJ, Devreotes PN, Borleis J & Hereld D (1995). Agonist-induced loss of ligand binding is correlated with phosphorylation of cAR1, a G protein-coupled chemoattractant receptor from *Dictyostelium*. *Journal of Biological Chemistry* **270**: 8667-8672.

Chandra M, Zhou H, Li Q, Muallem S, Hofmann SL & Soyombo AA (2011). A Role for the Ca^{2+} Channel TRPML1 in Gastric Acid Secretion, Based on Analysis of Knockout Mice. *Gastroenterology* **140**: 857-867.

Charette SJ & Cosson P (2004). Preparation of genomic DNA from *Dictyostelium discoideum* for PCR analysis. *Biotechniques* **36**: 574-575.

Chen SR, Ebisawa K & Zhang L (1997). Functional characterization of the recombinant type 3 Ca^{2+} release channel (ryanodine receptor) expressed in HEK293 cells. *Journal of Biological Chemistry* **272**: 24234-24246.

Chen YH, Li MH, Zhang Y, He LL, Yamada Y & Yang J (2004). Structural basis of the alpha1-beta subunit interaction of voltage-gated Ca^{2+} channels. *Nature* **429**: 675–680.

Chen L, Iijima M, Tang M, Landree MA, Huang YE, *et al*. (2007). PLA_2 and PI3K/PTEN Pathways Act in Parallel to Mediate Chemotaxis. *Developmental Cell* **12**: 603-614.

Chini EN, Beers KW & Dousa TP (1995). Nicotinate adenine dinucleotide phosphate (NAADP) triggers a specific calcium release system in sea urchin eggs. *Journal of Biological Chemistry* **270**: 3216-3223.

Chini EN, Chini CC, Kato I, Takasawa S & Okamoto H (2002). CD38 is the major enzyme responsible for synthesis of nicotinic acid–adenine dinucleotide phosphate in mammalian tissues. *Biochemical Journal* **362**: 125–130.

Churchill GC & Galione A (2001). NAADP induces Ca^{2+} oscillations via a two-pool mechanism by priming IP_3- and cADPR-sensitive Ca^{2+} stores. *The EMBO Journal* **20**: 2666-2671.

Churchill GC, Okada Y, Thomas JM, Genazzani AA, Patel S & Galione A (2002). NAADP Mobilizes Ca^{2+} from Reserve Granules, Lysosome-Related Organelles, in Sea Urchin Eggs. *Cell* **111**: 703-708.

Churchill GC, O'Neill JS, Masgrau R, Patel S, Thomas JM, *et al.* (2003). Sperm deliver a new second messenger: NAADP. *Current Biology* **13**: 125-128.

Chyb S, Raghu P & Hardie RC (1999). Polyunsaturated fatty acids activate the *Drosophila* light-sensitive channels TRP and TRPL. *Nature* **397**: 255-259.

Clapham DE (2003). TRP channels as cellular sensors. *Nature* **426**: 517-524.

Clapham DE (2007). Calcium Signaling. *Cell* **131**: 1047-1058.

Clapper DL & Lee H (1985). Inositol trisphosphate induces calcium release from nonmitochondrial stores in sea urchin egg homogenates. *Journal of Biological Chemistry* **260**: 13947-13954.

Clapper DL, Walseth T, Dargie P & Lee H (1987). Pyridine nucleotide metabolites stimulate calcium release from sea urchin egg microsomes desensitized to inositol trisphosphate. *Journal of Biological Chemistry* **262**: 9561-9568.

Copello JA, Oi Y, Jevakumar LH, Ogunbunmi E & Fleischer S (2001). Lack of effect of cADP-ribose and NAADP on the activity of skeletal muscle and heart ryanodine receptors. *Cell Calcium* **30**: 269-284.

Cubitt AB, Firtel RA, Fischer G, Jaffe LF & Miller AL (1995). Patterns of free calcium in multicellular stages of *Dictyostelium* expressing jellyfish apoaequorin. *Development* **121**: 2291-2301.

Cubitt AB, Reddy I, Lee S, McNally JG & Firtel RA. (1998). Coexpression of a Constitutively Active Plasma Membrane Calcium Pump with GFP Identifies Roles for Intracellular Calcium in Controlling Cell Sorting during Morphogenesis in *Dictyostelium*. *Developmental Biology* **196**: 77-94.

Dammermann W and Guse AH. (2005). Functional ryanodine receptor expression is required for NAADP-mediated local Ca^{2+} signaling in T-lymphocytes. *Journal of Biological Chemistry* **280**: 21394-21399.

Darmon M, Brachet P & Da Silva LH (1975). Chemotactic signals induce cell differentiation in *Dictyostelium discoideum*. *Proceedings of the National Academy of Sciences of the United States of America* **72**: 3163-3166.

Davidoff F & Korn ED (1963). The biosynthesis of fatty acids in the cellular slime mold, *Dictyostelium discoideum*. *Journal of Biological Chemistry* **238**: 3210-3215.

Desbuquois B & Aurbach GD (1972). Distribution of free and antibody-bound peptide hormones in two-phase aqueous polymer systems. *Biochemical Journal* **126**: 717-726.

Dhar S & Lippard SJ (2009). Mitaplatin, a potent fusion of cisplatin and the orphan drug dichloroacetate. *Proceedings of the National Academy of Sciences of the United States of America* **106**: 22199-22204.

Dickinson GD & Patel S (2003). Modulation of NAADP (nicotinic acid adenine dinucleotide phosphate) receptors by K^+ ions: Evidence for multiple NAADP receptor conformations. *Biochemical Journal* **375**: 805-812.

Dolphin AC (2006). A short history of voltage-gated calcium channels. *British Journal of pharmacology* **147**: S45-S62.

Drayer AL, Van der Kaay J, Mayr GW & Van Haastert P (1994). Role of phospholipase C in *Dictyostelium*: formation of inositol 1, 4, 5-trisphosphate and normal development in cells lacking phospholipase C activity. *The EMBO Journal* **13**: 1601-1609.

Eichinger L, Pachebat JA, Glöckner G, Rajandream MA, Sucgang R, *et al.* (2005). The genome of the social amoeba *Dictyostelium discoideum*. *Nature* **435**: 43-57.

Europe-Finner GN & Newell PC (1986). Inositol 1,4,5-trisphosphate induces calcium release from a non-mitochondrial pool in amoebae of *Dictyostelium*. *Biochimica et Biophysica Acta (BBA) - Molecular Cell Research* **887**: 335-40.

Faix J, Kreppel L, Shaulsky G, Schleicher M & Kimmel AR (2004). A rapid and efficient method to generate multiple gene disruptions in *Dictyostelium discoideum* using a single selectable marker and the Cre-*loxP* system. *Nucleic Acids Research* **32**: e143.

Feske S, Gwack Y, Prakriya M, Srikanth S, Puppel SH, *et al.* (2006). A mutation in Orai1 causes immune deficiency by abrogating CRAC channel function. *Nature* **441**: 179-185.

Flaadt H, Jaworski E & Malchow D (1993a). Evidence for two intracellular calcium pools in *Dictyostelium*: the cAMP-induced calcium influx is directed into a NBD-Cl-and 2, 5-di-(tert-butyl) 1, 4-hydroquinone-sensitive pool. *Journal of Cell Science* **105**: 1131-1135.

Flaadt H, Jaworski E, Schlatterer C & Malchow D (1993b). Cyclic AMP- and Ins(1,4,5)P3-induced Ca^{2+} fluxes in permeabilised cells of *Dictyostelium discoideum*: cGMP regulates Ca^{2+} entry across the plasma membrane. *Journal of Cell Science* **105**: 255-261.

Fountain SJ, Parkinson K, Young MT, Cao L, Thompson CRL & North RA (2007). An intracellular P2X receptor required for osmoregulation in *Dictyostelium discoideum*. *Nature* **448**: 200-203.

Fox AP, Cahill AL, Currie KPM, Grabner C & X Xie (2008). N- and P/Q-type Ca^{2+} channels in adrenal chromaffin cells. *Acta Physiologica* **192**: 247-261

Friedrich T, Pils B, Dandekar T, Schultz J & Müller T (2006). Modelling interaction sites in protein domains with interaction profile hidden Markov models. *Bioinformatics* **22**: 2851-2857.

Fruen BR, Bardy Jm, Byrerm TM, Strasburg Gm & Louis CF (2000). Differential Ca^{2+} sensitivity of skeletal and cardiac muscle ryanodine receptors in the presence of calmodulin. *American Journal of Cell Physiology* **297**: 724-733.

Fukuzawa M, Araki T, Adrian I & Williams JG (2001). Tyrosine Phosphorylation-Independent Nuclear Translocation of a *Dictyostelium* STAT in Response to DIF Signaling. *Molecular Cell* **7**: 779-788.

Furuichi T, Yoshikawa S, Miyawaki A, Wada K, Maeda N & Mikoshiba K (1989). Primary structure and functional expression of the inositol 1, 4, 5-trisphosphate-binding protein P400. *Nature* **342**: 32-38.

Furuichi T, Kohda K, Miyawaki A & Mikoshiba K (1994). Intracellular channels. *Current Opinion in Neurobiology* **4**: 294-303.

Gabriel D, Hacker U, Köhler J, Müller-Taubenberger A, Schwartz JM, *et al*. (1999). The contractile vacuole network of *Dictyostelium* as a distinct organelle: its dynamics visualized by a GFP marker protein. *Journal of Cell Science* **112**: 3995-4005.

Galione A & Churchill GC (2002). Interactions between calcium release pathways: Multiple messengers and multiple stores. *Cell Calcium* **32**: 343-354.

Galione A, Morgan AJ, Arredouani A, Davis LC, Rietdorf K, *et al.* (2010). NAADP as an intracellular messenger regulating lysosomal calcium-release channels. *Biochemical Society Transactions* **38**: 1424-1431.

Gaudet P, Lane L, Fey P, Bridge A, Poux S, *et al*. (2009). Collaborative annotation of genes and proteins between UniProtKB/Swiss-Prot and dictyBase. *Database: The Journal of Biological Databases and Curation* 2009.

Genazzani AA, Empson RM & Galione A (1996). Unique inactivation properties of NAADP-sensitive Ca^{2+} release. *Journal of Biological Chemistry* **271**: 11599-11602.

Genazzani AA & Galione A (1996). Nicotinic acid-adenine dinucleotide phosphate mobilizes Ca^{2+} from a thapsigargin-insensitive pool. *Biochemical Journal* **315**: 721-725.

Genazzani A, Mezna M, Dickey D, Michelangeli F, Walseth T & Galione A (1997). Pharmacological properties of the Ca^{2+} release mechanism sensitive to NAADP in the sea urchin egg. *British Journal of Pharmacology* **121**: 1489-1495.

Geng L, Segal Y, Peissel B, Deng N, Pei Y, *et al.* (1996). Identification and localization of polycystin, the PKD1 gene product. *Journal of Clinical Investigation* **98**: 2674-2682.

Gerasimenko JV, Maruyama Y, Yano K, Dolman NJ, Tepikin AV, *et al*. (2003). NAADP mobilizes Ca^{2+} from a thapsigargin-sensitive store in the nuclear envelope by activating ryanodine receptors. *The Journal of Cell Biology* **163**: 271-282.

Gerasimenko JV, Sherwood M, Tepikin AV, Peterson OH & Gerasimenko OV (2006). NAADP, cADPR and IP_3 all release Ca^{2+} from the endoplasmic reticulum and an acidic store in the secretory granule area. *Journal of Cell Science* **119**: 226-238.

Gerisch G & Hess B (1974). Cyclic-AMP-controlled oscillations in suspended *Dictyostelium* cells: their relation to morphogenetic cell interactions. *Proceedings of the National Academy of Sciences of the United Stated of America* **71**: 2118-2122.

Giannini G, Conti A, Mammarella S, Scrobogna M & Sorrentino V (1995). The ryanodine receptor/calcium channel genes are widely and differentially expressed in murine brain and peripheral tissues. *The Journal of Cell Biology* **128**: 893-904.

Gross JD (2009). Acidic Ca^{2+} stores, excitability, and cell patterning in *Dictyostelium discoideum*. *Eukaryotic Cell* **8**: 696-702.

Guerini D, Coletto L & Carafoli E (2005). Exporting calcium from cells. *Cell Calcium* **38**: 281-289.

Guse AH (2009). Second messenger signaling: multiple receptors for NAADP. *Current Biology* **19**: 521-523.

Hanlon MR, Berrow NS, Dolphin AC & Wallace BA (1999). Modelling of a voltage-dependent Ca^{2+} channel β subunit as a basis for understanding its functional properties. *FEBS letters* **445**: 366–370.

Hardie RC (2007). TRP channels and lipids: from *Drosophila* to mammalian physiology. *Journal of Physiology* **578**: 9-24.

Heuser J, Zhu Q & Clarke M (1993). Proton pumps populate the contractile vacuoles of *Dictyostelium* amoebae. *The Journal of Cell Biology* **121**: 1311-1327.

Hohenegger M, Suko J, Gscheidlinger R, Drobny H & Zidar A. (2002). Nicotinic acid-adenine dinucleotide phosphate activates the skeletal muscle ryanodine receptor. *Biochemical Journal* **367:** 423-431.

Hooper R, Churamani D, Brailoiu E, Taylor CW & Patel S (2011). Membrane topology of NAADP-sensitive two-pore channels and their regulation by N-linked glycosylation. *Journal of Biological Chemistry* **286**: 9141-9149.

Hoppe UC (2010). Mitochondrial calcium channels. *FEBS letters* **584**: 1975-1981.

Howard PK, Ahern KG & Firtel RA (1988). Establishment of a transient expression system for *Dictyostelium discoideum*. *Nucleic Acids Research* **16**: 2613-1623.

Hu HZ, Xiao R, Wang C, Gao N, Colton CK, Wood JD & Zhu MX (2006). Potentiation of TRPV3 channel function by unsaturated fatty acids. *Journal of Cell Physiology* **208**: 201–212.

Insall R & Kay RR (1990). A specific DIF binding protein in *Dictyostelium*. *The EMBO Journal* **9**: 3323-3328.

Insall R, Nayler O & Kay R (1992). DIF-1 induces its own breakdown in *Dictyostelium*. *The EMBO Journal* **11**: 2849-2854.

Insall R, Kuspa A, Lilly PJ, Shaulsky G, Levin LR, *et al.* (1994). CRAC, a cytosolic protein containing a pleckstrin homology domain, is required for receptor and G protein-mediated activation of adenylyl cyclase in *Dictyostelium*. *The Journal of Cell Biology* **126**: 1537-1545.

Ishibashi K, Suzuki M & Imai M (2000). Molecular cloning of a novel form (two-repeat) protein related to voltage-gated sodium and calcium channels. *Biochemical and Biophysical Research Communications* **270**: 370-376.

Iwai M, Tateishi Y, Hattori M, Mizutani A, Nakamura T, *et al.* (2005). Molecular cloning of mouse type 2 and type 3 inositol 1, 4, 5-trisphosphate receptors and identification of a novel type 2 receptor splice variant. *Journal of Biological Chemistry* **280**: 10305-10317.

Iwai M, Michikawa T, Bosanac I, Ikura M & Mikoshiba K (2007). Molecular basis of the isoform-specific ligand-binding affinity of inositol 1, 4, 5-trisphosphate receptors. *Journal of Biological Chemistry* **282**: 12755-12764.

Jaffe LF (1999). Organization of early development by calcium patterns. *BioEssays* **21**: 657-667.

Jin T, Amzel M, Devreotes PN & Wu L (1998). Selection of Gβ subunits with Point Mutations That Fail to Activate Specific Signaling pathways In Vivo: Dissecting Cellular Responses Mediated by a Heterotrimeric G protein in *Dictyostelium discoideum*. *Molecular Biology of the Cell* **9**: 2949-2961.

Johnson R, Saxe CL, Gollop R, Kimmel A & Devreotes P (1993). Identification and targeted gene disruption of cAR3, a cAMP receptor subtype expressed during multicellular stages of *Dictyostelium* development. *Genes & Development* **7**: 273-282.

Jörs S, Kazanski V, Foik A, Krautwurst D & Harteneck C (2006). Receptor-induced activation of *Drosophila* TRPγ by polyunsaturated fatty acids. *Journal of Biological Chemistry* **281**: 29693–29702.

Journet A, Chapel A, Jehan S, Adessi C, Freeze H, *et al*. (1999). Characterization of *Dictyostelium discoideum* cathepsin D. *Journal of Cell Science* **112**: 3833-3843.

Kawasaki T, Lange I & Feske S (2009). A minimal regulatory domain in the C terminus of STIM1 binds to and activates ORAI1 CRAC channels. *Biochemical and Biophysical Research Communications* **385**: 49-54.

Kay RR, Gadian DG & Williams SR (1986). Intracellular pH in *Dictyostelium*: a 31P nuclear magnetic resonance study of its regulation and possible role in controlling cell differentiation. *Journal of Cell Science* **83**: 165-179.

Kay, R.R. (1992). Cell differentiation and patterning in *Dictyostelium*. *Current Opinion in Cell Biology* **4:** 934-938.

Kay RR (1998). The biosynthesis of differentiation-inducing factor, a chlorinated signal molecule regulating *Dictyostelium* development. *Journal of Biological Chemistry* **273**: 2669-2675.

Kay RR, Flatman P & Thompson CRL (1999). DIF signalling and cell fate. *Seminars in Cell and Developmental Biology* **10**: 577-585.

Kay RR & Thompson CRL (2001). Cross-induction of cell types in *Dictyostelium*: evidence that DIF-1 is made by prespore cells. *Development* **128**: 4959-4966.

Kessen U, Schaloske R, Aichem A & Mutzel R (1999). Ca^{2+}/calmodulin-independent activation of calcineurin from *Dictyostelium* by unsaturated long chain fatty acids. *Journal of Biological Chemistry* **274**: 37821-37826.

King J, Keim M, Teo R, Weening KE, Kapur M, *et al.* (2010). Genetic control of lithium sensitivity and regulation of inositol biosynthetic genes. *PLoS ONE* ***5***: e11151.

Kinnear NP, Boittin FX, Thomas JM, Galione A & Evans AM (2004). Lysosome-sarcoplasmic reticulum junctions. A trigger zone for calcium signaling by nicotinic acid adenine dinucleotide phosphate and endothelin-1. *Journal of Biological Chemistry* **279**: 54319-54326.

Klein PS, Sun TJ, Saxe CL, Kimmel AR, Johnson RL & Devreotes PN (1988). A chemoattractant receptor controls development in *Dictyostelium discoideum*. *Science* **241**: 1467-1472.

Klugbauer N, Marais E & Hofmann F (2003). Calcium channel alpha2delta subunits: differential expression, function, and drug binding. *Journal of Bioenergetics and biomembranes* **35**: 639-647

Knetsch ML, Epskamp SJ, Schenk PW, Wang Y, Segall JE & Snaar-Jagalska BE (1996). Dual role of cAMP and involvement of both G-proteins and ras in regulation of ERK2 in *Dictyostelium discoideum*. *The EMBO Journal* **15**: 3361 -3368.

Koivusalo M, Steinberg BE, Mason D & Grinstein S (2011). In situ measurement of the electrical potential across the lysosomal membrane using FRET. *Traffic* **12**: 972-982.

Krogh A, Larsson B, von Heijne G & Sonnhammer ELL (2001). Predicting transmembrane protein topology with a hidden markov model: application to complete genomes. *Journal of Molecular Biology* **305**: 567-580.

Kubohara Y & Okamoto K (1994). Cytoplasmic Ca^{2+} and H^{+} concentrations determine cell fate in *Dictyostelium discoideum*. *The FASEB Journal* **8**: 869-874.

Kubohara Y, Arai A, Gokan N & Hosaka K (2007). Pharmacological evidence that stalk cell differentiation involves increases in the intracellular Ca^{2+} and H^{+} concentrations in *Dictyostelium discoideum*. *Development, Growth & Differentiation* **49**: 253-264.

Kuwayama H, Yanagida T & Ueda M (2008). DNA oligonucleotide-assisted genetic manipulation increases transformation and homologous recombination efficiencies: Evidence from gene targeting of *Dictyostelium discoideum*. *Journal of Biotechnology* **133**: 418-423.

Kuwayama H & Kubohara Y (2009). Differentiation-inducing factor-1 and-2 function also as modulators for *Dictyostelium* chemotaxis. *PLoS ONE* **4**: e6658.

Kwak E, Gerald N, Larochelle DA, Vithalani KK, Niswonger ML, *et al.* (1999). LvsA, a Protein Related to the Mouse Beige Protein, Is Required for Cytokinesis in *Dictyostelium*. *Molecular Biology of the Cell* **10**: 4429-4439.

Kypri E, Schmauch C, Maniak M & Lozanne AD (2007). The BEACH protein LvsB is localized on lysosomes and postlysosomes and limits their fusion with early endosomes. *Traffic* **8**: 774-83.

Langhorst MF, Schwarzmann N & Guse AH (2004). Ca^{2+} release via ryanodine receptors and Ca^{2+} entry: major mechanisms in NAADP-mediated Ca^{2+} signaling in T-lymphocytes. *Cell Signalling* **16**: 1283-1289.

Lee HC & Aarhus R (1995). A derivative of NADP mobilizes Ca^{2+} stores insensitive to inositol trisphosphate and cyclic ADP-ribose. *Journal of Biological Chemistry* **270**: 2152-2157.

Lee HC, Aarhus R & Graeff RM (1995). Sensitization of calcium-induced calcium release by cyclic ADP-ribose and calmodulin. *Journal of Biological Chemistry* **270**: 9060-9066.

Lee HC & Aarhus R (1997). Structural determinants of nicotinic acid adenine dinucleotide phosphate important for its calcium-mobilizing activity. *Journal of Biological Chemistry* **272**: 20378-20383.

Lee HC & Aarhus R (2000). Functional visualization of the separate but interacting calcium stores sensitive to NAADP and cyclic ADP-ribose. *Journal of Cell Science* **113**: 4413-4420.

Lewis AM, Masgrau R, Vasudevan SR, Yamasaki M, O'Neill JS, *et al*. (2007). Refinement of a radioreceptor binding assay for nicotinic acid adenine dinucleotide phosphate. *Analytical Biochemistry* **371**: 26-36.

Lewis RS (2001). Calcium signaling mechanisms in T lymphocytes. *Annual Review of Immunology* **19**: 497-521.

Lewis RS (2007). The molecular choreography of a store-operated calcium channel. *Nature* **446**: 284-287.

Li X, Zima AV, Sheikh F, Blatter LA & Chen J (2005). Endothelin-1-induced arrhythmogenic Ca^{2+} signaling is abolished in atrial myocytes of inositol-1, 4, 5-trisphosphate (IP_3)-receptor type 2-deficient mice. *Circulation Research* **96**: 1274 -1281.

Lilly P, Wu L, Welker DL & Devreotes PN (1993). A G-protein β-subunit is essential for *Dictyostelium* development. *Genes & Development* **7**: 986-995.

Lilly PJ & Devreotes PN (1994). Identification of CRAC, a cytosolic regulator required for guanine nucleotide stimulation of adenylyl cyclase in *Dictyostelium*. *Journal of Biological Chemistry* **269**: 14123-14129.

Lim D, Kyozuka H, Gragnaniello G, Garafoli E & Santella L (2001). $NAADP^+$ initiated the Ca^{2+} response during fertilization of starfish oocytes. *The FASEB Journal* **15**: 2257-2267.

Lima WC & Cosson P (2010). Role of mucolipin calcium channel in the endocytic pathway of *Dictyostelium discoideum*. *Annual International Dictyostelium Conference, Talk* **37.**

Lin P, Yao Y, Hofmeister R, Tsien RY & Farquhar MG (1999). Overexpression of CALNUC (nucleobindin) increases agonist and thapsigargin releasable Ca^{2+} storage in the Golgi. *Journal of Cell Biology* **145**: 279-289.

Liou J, Kim ML, Won DH, Jones JT, Myers JW, *et al.* (2005). STIM is a Ca^{2+} sensor essential for Ca^{2+}-store- depletion-triggered Ca^{2+} influx. *Current Biology* **15**: 1235-1241.

Louis JM, Ginsburg GT & Kimmel AR (1994). The cAMP receptor CAR4 regulates axial patterning and cellular differentiation during late development of *Dictyostelium*. *Genes & Development* **8**: 2086-2096.

Ludlow MJ, Traynor D, Fisher PR & Ennion SJ (2008). Purinergic-mediated Ca^{2+} influx in *Dictyostelium discoideum*. *Cell Calcium* **44**: 567-579.

Ludlow M, Durai L & Ennion S (2009). Functional characterization of intracellular *Dictyostelium discoideum* P2X receptors. *Journal of Biological Chemistry* **284**: 35227-35239.

Luo Y, Vassilev PM, Li X, Kawanabe Y & Zhou J (2003). Native polycystin 2 functions as a plasma membrane Ca^{2+}-permeable cation channel in renal epithelia. *Molecular and Cellular Biology* **23**: 2600-2607.

Lusche DF, Rotzer H, Merz R, Fink H, Mutzel R & Schlatterer C (2004). Multichannel apparatus for parallel monitoring of light scattering in *Dictyostelium discoideum* cell suspensions. *BioTechniques* **37**: 970-976.

McPherson SM, McPherson PS, Mathews L, Campbell KP & Lingo FI (1992). Cortical localization of a Ca^{2+} release channel in sea urchin eggs. *Journal of Cell Biology* **116**: 1111-1121.

Maeda N, Niinobe M, Nakahira K & Mikoshiba K (1988). Purification and characterization of P400 protein, a glycoprotein characteristic of Purkinje cell, from mouse cerebellum. *Journal of Neurochemistry* **51**: 1724-1730.

Mak DOD, McBride S & Foskett JK (1998). Inositol 1, 4, 5-tris-phosphate activation of inositol tris-phosphate receptor Ca^{2+} channel by ligand tuning of Ca^{2+} inhibition. *Proceedings of the National Academy of Sciences of the United States of America* **95**: 15821–15825.

Malchow D, Böhme R & Gras U (1982). On the role of calcium in chemotaxis and oscillations of *Dictyostelium* cells. *European Biophysics Journal* **9**: 131-136.

Malchow D, Mutzel R & Schlatterer C (1996). On the role of calcium during chemotactic signalling and differentiation of the cellular slime mould *Dictyostelium discoideum*. *International Journal of Developmental Biology* **40**: 135-139.

Malchow D, Lusche DF & Schlatterer C (2004). A link of Ca^{2+} to cAMP oscillations in *Dictyostelium*: the calmodulin antagonist W-7 potentiates cAMP relay and transiently inhibits the acidic Ca^{2+}-store. *BMC Developmental Biology* **4**: 1-42.

Malchow D, Lusche DF, Schlatterer C, De Lozanne A & Müller-Taubenberger A (2006). The contractile vacuole in Ca^{2+}-regulation in *Dictyostelium*: its essential function for cAMP-induced Ca^{2+}-influx. *BMC Developmental Biology* **6**: 31-38.

Malchow D, Lusche DF, De Lozanne A & Schlatterer C (2008). A fast Ca^{2+}-induced Ca^{2+}-release mechanism in *Dictyostelium discoideum*. *Cell Calcium* **43**: 521-530.

Malli R & Graier WF (2010). Mitochondrial Ca^{2+} channels: Great unknowns with important functions. *FEBS Letters* **584**: 1942-1947.

Masento MS, Morris HR, Taylor GW, Johnson SJ, Skapski AC & Kay RR (1988). Differentiation-inducing factor from the slime mould *Dictyostelium discoideum* and its analogues. Synthesis, structure and biological activity. *Biochemical Journal* **256:** 23-28.

Masgrau R, Churchill GC, Morgan AJ, Ashcroft SJH & Galione A (2003). NAADP: A new second messenger for glucose-induced Ca^{2+} responses in clonal pancreatic β cells. *Current Biology* **13**: 247-251.

Masento MS, Morris HR, Taylor GW, Johnson SJ, Skapski AC & Kay RR (1988). Differentiation-inducing factor from the slime mould *Dictyostelium discoideum* and its analogues. Synthesis, structure and biological activity. *Biochemical Journal* **256**: 23-28.

Matsumoto M, Nakagawa T, Inoue T, Nagata E, Tanaka K, *et al.* (1996). Ataxia and epileptic seizures in mice lacking type 1 inositol 1, 4, 5-trisphosphate receptor. *Nature* **379**: 168-171.

Mercanti V, Blanc C, Lefkir Y, Cosson P & Letourneur F (2006). Acidic clusters target transmembrane proteins to the contractile vacuole in *Dictyostelium* cells. *Journal of Cell Science* **119**: 837-845.

Merzlyak EM, Goedhart J, Shcherbo D, Bulina ME, Shcheglov AS, *et al*. (2007). Bright monomeric red fluorescent protein with an extended fluorescence lifetime. *Nature Methods* **4**: 555-557.

Meur G, Parker AKT, Gergely FV & Taylor CW (2007). Targeting and retention of type 1 ryanodine receptors to the endoplasmic reticulum. *Journal of Biological Chemistry* **282**: 23096-23103.

Meves H (1994). Modulation of ion channels by arachidonic acid. *Progress in Neurobiology* **43**: 175-186.

Meves H (2008). Arachidonic acid and ion channels: an update. *British Journal of Pharmacology* **155**: 4-16.

Mignen O & Shuttleworth TJ (2000). I_{ARC}, a novel arachidonate-regulated, noncapacitative Ca^{2+} entry channel. *Journal of Biological Chemistry* **275**: 9114-9119.

Mignen O, Thompson JL & Shuttleworth TJ (2003). Ca^{2+} selectivity and fatty acid specificity of the noncapacitative, arachidonate-regulated Ca^{2+} (ARC) channels. *Journal of Biological Chemistry* **278**: 10174-10181.

Mignen O, Thompson JL & Shuttleworth TJ (2008). Both Orai1 and Orai3 are essential components of the arachidonate-regulated Ca^{2+}-selective (ARC) channels. *The Journal of Physiology* **586**: 185-105.

Mikoshiba K, Huchet M & Changeux JP (1979). Biochemical and Immunological Studies on the P400 Protein, a Protein Characteristic of the Purkinje Cell from Mouse and Rat Cerebellum. *Developmental Neuroscience* **2**: 254-275.

Mitchell KJ, Lai FA & Rutter GA (2003). Ryanodine receptor type I and nicotinic acid adenine dinucleotide phosphate receptors mediate Ca^{2+} release from insulin-containing vesicles in living pancreatic β-cells (MIN6). *Journal of Biological Chemistry* **278**: 11057-11064.

Miyawaki A, Furuichi T, Maeda N & Mikoshiba K (1990). Expressed cerebellar-type inositol 1,4,5-trisphosphate receptor, P400, has calcium release activity in a fibroblast L cell line. *Neuron* **5**: 11-8.

Mojžišová A, Križanová O, Žáčiková Ľ, Komínková V & Ondriaš K (2001). Effect of nicotinic acid adenine dinucleotide phosphate on ryanodine calcium release channel in heart. *Pflügers Archiv European Journal of Physiology* **441**: 674-677.

Moniakis J, Coukell MB & Forer A (1995). Molecular cloning of an intracellular P-type ATPase from *Dictyostelium* that is up-regulated in calcium-adapted cells. *Journal of Biological Chemistry* **270**: 28276-28281.

Moniakis J, Coukell MB & Janiec A (1999). Involvement of the Ca^{2+}-ATPase PAT1 and the contractile vacuole in calcium regulation in *Dictyostelium discoideum*. *Journal of Cell Science* **112**: 405-414.

Morris HR, Taylor GW, Masento MS, Jermyn KA & Kay RR (1987). Chemical structure of the morphogen differentiation inducing factor from *Dictyostelium discoideum*. *Nature* **328**: 811-814.

Morris HR, Masento MS, Taylor GW, Jermyn KA & Kay RR (1988). Structure elucidation of two differentiation inducing factors (DIF-2 and DIF-3) from the cellular slime mould *Dictyostelium discoideum*. *Biochemical Journal* **249**: 903-906.

Müller-Taubenberger A, Lupas AN, Li H, Ecke M, Simmeth E & Gerisch G (2001). Calreticulin and calnexin in the endoplasmic reticulum are important for phagocytosis. *The EMBO Journal* **20**: 6772-6782.

Mullis KB (1993). The Polymerase Chain Reaction. *Kary Mullis' Nobel Lecture.*

Navazio L, Bewell MA, Siddiqua A, Dickinson GD, Galione A & Sanders D (2000). Calcium release from the endoplasmic reticulum of higher plants elicited by the NADP metabolite nicotinic acid adenine dinucleotide phosphate. *Proceedings of the National Academy of Sciences of the United States of America* **97**: 8693-8698.

Naylor E, Arredouani A, Vasudevan SR, Lewis AM, Parkesh R, *et al.* (2009). Identification of a chemical probe for NAADP by virtual screening. *Nature Chemical Biology* **5**: 220-226.

Nebl T, Kotsifas M, Schaap P & Fisher PR (2002). Multiple signalling pathways connect chemoattractant receptors and calcium channels in *Dictyostelium*. *Journal of Muscle Research and Cell Motility* **23**: 853-865.

Neumann CS, Walsh CT & Kay RR (2010). A flavin-dependent halogenase catalyzes the chlorination step in the biosynthesis of *Dictyostelium* differentiation-inducing factor 1. *Proceedings of the National Academy of Sciences of the United States of America* **107**: 5798-5803.

Nellen W, Silan C & Firtel RA (1984). DNA-mediated transformation in *Dictyostelium discoideum*: regulated expression of an actin gene fusion. *Molecular Cell Biology* **4**: 2890-2898.

Neves SR, Ram PT & Iyengar R (2002). G protein pathways. *Science* **296**: 1636-1639.

Newton CL, Mignery GA & Südhof TC (1994). Co-expression in vertebrate tissues and cell lines of multiple inositol 1, 4, 5-trisphosphate ($InsP_3$) receptors with distinct affinities for $InsP_3$. *Journal of Biological Chemistry* **269**: 28613-28619.

Nolta KV & Steck TL (1994). Isolation and initial characterization of the bipartite contractile vacuole complex from *Dictyostelium discoideum*. *Journal of Biological Chemistry* **269**: 2225-2233.

Ohkouchi S, Nishio K, Maeda M, Hitomi K, Adachi H & Maki M (2001). Identification and characterization of two penta-EF-hand Ca^{2+}-binding proteins in *Dictyostelium discoideum*. *Journal of Biochemistry* **130**: 207-215.

Ozawa T (2010). Modulation of ryanodine receptor Ca^{2+} channels. *Molecular Medicine Reports* **3**: 199-204.

Palade P (2007). The hunt for an alternate way to generate NAADP. Focus on "NAADP as a second messenger: neither CD38 nor base-exchange reaction are necessary for *in vivo* generation of NAADP in myometrial cells". *American Journal of Physiology Cell Physiology* **292**: 4-7.

Pang KM, Lynes MA & Knecht DA (1999). Variables controlling the expression level of exogenous genes in *Dictyostelium*. *Plasmid* **41**: 187-197.

Prakriya M, Feske S, Gwack Y, Srikanth S, Rao A & Hogan P (2006). Orai1 is an essential pore subunit of the CRAC channel. *Nature* **443:** 230–233.

Park CY, Hoover PJ, Mullins FM, Bachhawat P, Covington ED, *et al.* (2009). STIM1 Clusters and Activates CRAC Channels via Direct Binding of a Cytosolic Domain to Orai1. *Cell* **136**: 876-890.

Parikh A, Miranda ER, Katoh-Kurasawa M, Fuller D, Rot G, *et al*. (2010). Conserved developmental transcriptomes in evolutionarily divergent species. *Genome Biol* **11**: R35.

Parker AKT, Gergely FV & Taylor CW (2004). Targeting of inositol 1, 4, 5-trisphosphate receptors to the endoplasmic reticulum by multiple signals within their transmembrane domains. *Journal of Biological Chemistry* **279**: 23797-23805.

Patel S, Churchill GC & Galione A (2000a). Unique kinetics of nicotinic acid-adenine dinucleotide phosphate (NAADP) binding enhance the sensitivity of NAADP receptors for their ligand. *Biochemical Journal* **352**: 725-729.

Patel S, Churchill GC, Sharp T & Galione A (2000b). Widespread distribution of binding sites for the novel Ca^{2+}-mobilizing messenger, nicotinic acid adenine dinucleotide phosphate, in the brain. *Journal of Biological Chemistry* **275**: 36495-36497.

Patel S & Docampo R (2010). Acidic calcium stores open for business: expanding the potential for intracellular Ca^{2+} signaling. *Trends in Cell Biology* **20**: 277-286.

Patel S, Marchant JS & Brailoiu E (2010). Two-pore channels: Regulation by NAADP and customized roles in triggering calcium signals. *Cell Calcium* **47**: 480-490

Patel S, Ramakrishnan L, Rahman T, Hamdoun A, Marchant JS, *et al*. (2011). The endo-lysosomal system as an NAADP-sensitive acidic Ca^{2+} store: Role for the two-pore channels. *Cell Calcium* **50**: 157-167.

Peiter E, Maathuis FJM, Mills LN, Knight H, Pelloux J, *et al.* (2005). The vacuolar Ca^{2+}-activated channel TPC1 regulates germination and stomatal movement. *Nature* **434**: 404-408.

Perez-Terzic CM, Chini EN, Shen SS, Dousa TP & Clapham DE (1995). Ca^{2+} release triggered by nicotinate adenine dinucleotide phosphate in intact sea urchin eggs. *Biochemical Journal* **312**: 955-959.

Pérez CA, Huang L, Rong M, Kozak JA, Preuss AK, *et al*., (2002). A transient receptor potential channel expressed in taste receptor cells. *Nature Neuroscience* **5**: 1169-1176.

Pinter K & Gross J (1995). Calcium and cell type specific gene expression in *Dictyostelium*. *Differentiation* **59**: 201-206.

Pinton P, Pozzan T & and Rizzuto R (1998). The Golgi apparatus is an inositol 1,4,5-trisphosphate-sensitive Ca^{2+} store, with functional properties distinct from those of the endoplasmic reticulum. *The EMBO Journal* **17**: 5298-5308.

Piper RC & Luzio JP (2004). Coupling calcium to lysosomal biogenesis. *Trends in Cell Biology* **14**: 471-473.

Pitt SJ, Funnell TM, Sitsapesan M, Venturi E, Rietdorf K, *et al.* (2010). TPC2 is a novel NAADP-sensitive Ca^{2+} release channel, operating as a dual sensor of luminal pH and Ca^{2+}. *Journal of Biological Chemistry* **285**: 35039-35046.

Pozzan T, Reimann Fm Gribble FM & Luzio JP (2006). Molecular and cellular physiology of intracellular calcium stores. *Physiology Review* **74**: 595-636.

Pryor PR, Reimann F, Gribble FM & Luzio JP (2006). Mucolipin-1 is a lysosomal membrane protein required for intracellular lactosylceramide traffic. Traffic 7: 1388-1398.

Putney JW (2005)**.** Calcium Signaling, Second Edition: Methods in Signal Transduction. *CRC press.*

Quiviger B, de Chastellier C & Ryter A (1978). Cytochemical demonstration of alkaline phosphatase in the contractile vacuole of *Dictyostelium discoideum*. *Journal of Ultrastructure Research* **62**: 228-236.

Ramos IB, Miranda K, Pace DA, Verbist KC, Lin FY, *et al.* (2010). Calcium-and polyphosphate-containing acidic granules of sea urchin eggs are similar to acidocalcisomes, but are not the targets for NAADP. *Biochemical Journal* **429**: 485-495.

Raychowdhury MK, González-Perrett S, Montalbetti N, Timpanaro GA, Chasan B, *et al*. (2004). Molecular pathophysiology of mucolipidosis type IV: pH dysregulation of the mucolipin-1 cation channel. *Human Molecular Genetics* **13**: 617-627.

Reiken S, Lacampagne A, Zhou H, Kherani A, Lehnart SE, *et al*. (2003). PKA phosphorylation activates the calcium release channel (ryanodine receptor) in skeletal muscle: defective regulation in heart failure. *Journal of Cell Biology* **160**: 919-928.

Robinson R, Carpenter D, Shaw MA, Halsall J & Hopkins P (2006). Mutations in RYR1 in malignant hyperthermia and central core disease. *Human Mutation* **27**: 977-989.

Rooney EK & Gross JD (1992). ATP-driven Ca^{2+}/H^{+} antiport in acid vesicles from *Dictyostelium*. *Proceedings of the National Academy of Sciences of the United States of America* **89**: 8025-8029.

Rooney EK, Gross JD & Satre M (1994). Characterisation of an intracellular Ca^{2+} pump in *Dictyostelium*. *Cell Calcium* **16**: 509-522.

Roos J, DiGregorio PJ, Yeromin AV, Ohlsen K, Lioudyno M, *et al.* (2005). STIM1, an essential and conserved component of store-operated Ca^{2+} channel function. *Journal of Cell Biology* **169**: 435-445.

Rosen D, Lewis AM, Mizote A, Thomas JM, Aley PK, *et al.* (2009). Analogues of the nicotinic acid adenine dinucleotide phosphate (NAADP) antagonist Ned-19 indicate two binding sites on the NAADP receptor. *Journal of Biological Chemistry* **284**: 34930-34934.

Roux MM, Townley IK, Raisch M, Reade A, Bradham C, *et al.* (2006). A functional genomic and proteomic perspective of sea urchin calcium signaling and egg activation. *Developmental Biology* **300**: 416-433.

Ruas M, Rietdorf K, Arredouani A, Davis LC, Lloyd-Evans E, *et al.* (2010). Purified TPC isoforms form NAADP receptors with distinct roles for Ca^{2+} signaling and endolysosomal trafficking. *Current Biology* **20**:703-709.

Sambrook J & Russell DW (2001). Molecular Cloning: A Laboratory Manual, 3rd edition, *Cold Spring Harbor Laboratory Press*.

Saxe C, Johnson RL, Devreotes PN & Kimmel AR (1991). Expression of a cAMP receptor gene of *Dictyostelium* and evidence for a multigene family. *Genes & Development* **5**: 1-8.

Saxe CL, Ginsburg G, Louis J, Johnson R, Devreotes P & Kimmel A (1993). CAR2, a prestalk cAMP receptor required for normal tip formation and late development of *Dictyostelium discoideum*. *Genes & Development* **7**: 262-272.

Saxe III CL, Johnson R, Devreotes PN & Kimmel AR (1991). Multiple genes for cell surface cAMP receptors in *Dictyostelium discoideum*. *Developmental Genetics* **12**: 6-13.

Schaap P, Nebl T & Fisher PR (1996). A slow sustained increase in cytosolic Ca^{2+} levels mediates stalk gene induction by differentiation inducing factor in *Dictyostelium*. *The EMBO Journal* **15**: 5177-5183.

Schaloske R & Malchow D (1997). Mechanism of cAMP-induced Ca^{2+} influx in *Dictyostelium*: Role of phospholipase A_2. *Biochemical Journal* **327**: 233-238.

Schaloske R, Sonnemann J, Malchow D & Schlaherer C (1998). Fatty acids induce release of Ca^{2+} from acidosomal stores and activate capacitative Ca^{2+} entry in *Dictyostelium discoideum*. *Biochemical Journal* **332**: 541-548.

Schaloske R, Schlatterer C & Malchow D (2000). A xestospongin C-sensitive Ca^{2+} store is required for cAMP-induced Ca^{2+} influx and cAMP oscillations in *Dictyostelium*. *Journal of Biological Chemistry* **275**: 8404-8408.

Schaloske RH, Lusche DF, Bezares-Roder K, Happle K, Malchow D & Schlatterer C (2005). Ca^{2+} regulation in the absence of the ipIA gene product in *Dictyostelium discoideum*. *BMC Cell Biology* **6**: 13-30.

Schaloske RH, Blaesius D, Schlatterer C & Lusche DF (2007). Arachidonic acid is a chemoattractant for *Dictyostelium discoideum* cells. *Journal of Biosciences* **32**: 1281-1289.

Schieder M, Rötzer K, Brüggemann A, Biel M & Wahl-Schott CA (2010). Characterization of two-pore channel 2 (TPCN2)-mediated Ca^{2+} currents in isolated lysosomes. *Journal of Biological Chemistry* **285**: 21219-21222.

Schlatterer C, Walther P, Müller M, Mendgen K, Zierold K & Knoll G (2001). Calcium stores in differentiated *Dictyostelium discoideum*: prespore cells sequester calcium more efficiently than prestalk cells. *Cell Calcium* **29**: 171-182.

Shaner NC, Steinbach PA & Tsien RY (2005). A guide to choosing fluorescent proteins. *Nature Methods* **2**: 905-909.

Shaulsky G, Loomis WF (1995). Mitochondrial DNA replication but no nuclear DNA replication during development of *Dictyostelium*. *Proceeding of the National Academy of Science of the United States of America* **92**: 5660-5663.

Shaulsky G, Escalante R & Loomis WF (1996). Developmental signal transduction pathways uncovered by genetic suppressors. *Proceedings of the National Academy of Sciences of the United States of America* **93**: 15260-12565.

Shaulsky G, Fuller D & Loomis WF (1998). A cAMP-phosphodiesterase controls PKA-dependent differentiation. *Development* **125**: 691-699.

Sutherland EW & Rall T (1958). Fractionation and characterization of a cyclic adenine ribonucleotide formed by tissue particles. *Journal of Biological Chemistry* **232**: 1077-1091.

Shuttleworth TJ, Thompson JL & Mignen O (2007). STIM1 and the noncapacitative ARC channels. *Cell Calcium* **42**: 183-191.

Sitsapesan R & Williams AJ (1990). Mechanisms of caffeine activation of single calcium-release channels of sheep cardiac sarcoplasmic reticulum. *Journal of Physiology* **423**: 425-439.

Soares S, Thompson M, White T, Isbell A, Yamasaki M, *et al*. (2007). NAADP as a second messenger: neither CD38 nor base-exchange reaction are necessary for *in vivo* generation of NAADP in myometrial cells. *American Journal of Physiology Cell Physiology* **292**: 227-239.

Sodergren E, Weinstock GM, Davidson EH, Cameron RA, Gibbs RA, *et al.* (2006). The genome of the sea urchin *Strongylocentrotus purpuratus*. *Science* **314**: 941-952.

Sotoh K (1993). A transformation vector for *Dictyostelium discoideum* with a new selectable marker bsr. *Plasmid* **30**: 150-154.

Soyombo AA, Tjon-Kon-Sang S, Rbaibi Y, Bashllari E, Bisceglia J, *et al.* (2006). TRP-ML1 regulates lysosomal pH and acidic lysosomal lipid hydrolytic activity. *Journal of Biological Chemistry* **281**: 7294-7301.

Sparagna GC, Gunter KK, Sheu SS & Gunter TE (1995). Mitochondrial Calcium Uptake from Physiological-type Pulses of Calcium. *Journal of Biological Chemistry* **270**: 27510-27515.

Steen M, Kirchberger T & Guse AH (2007). NAADP mobilizes Ca^{2+} from the endoplasmic reticular Ca^{2+} store in T-lymphocytes. *Journal of Biological Chemistry* **282**: 18864-18871.

Steinberg BE, Huynh KK, Brodovitch A, Jabs S, Stauber T, *et al.* (2010). A cation counterflux supports lysosomal acidification. *The Journal of Cell Biology* **189**: 1171-1186.

Stathopulos PB, Zheng L, Li G-Y, Plevin MJ & Ikura M (2008). Structural and Mechanistic Insights into STIM1-Mediated Initiation of Store-Operated Calcium Entry. *Cell* **135**: 110-122.

Story GM, Peier AM, Reeve AJ, Eid SR, Mosbacher J, *et al*. (2003). ANKTM1, a TRP-like channel expressed in nociceptive neurons, is activated by cold temperatures. *Cell* **112**: 819-829.

Striessnig J, Bolz HJ & Koschak A (2010). Channelopathies in $Ca_v1.1$, $Ca_v1.3$, and $Ca_v1.4$ voltage-gated L-type Ca^{2+} channels. European Journal of Physiology **460**: 361-374.

Swann K & Parrington J (1999). Mechanism of Ca^{2+} release at fertilization in mammals. *Journal of Experimental Zoology* **285**: 267-275.

Takahashi M, Seager MJ, Jones JF, Reber BFX & Catterall WA (1987). Subunit structure of dihydropyridine-sensitive calcium channels from skeletal muscle. *Proceedings of the National Academy of Sciences of the United States of America* **84**: 5478–5482.

Takeshima H (1994). Excitation-contraction uncoupling and muscular degeneration in mice lacking functional skeletal muscle ryanodine-receptor gene. *Nature* **369**: 556-559.

Takeshima H, Komazaki S, Hirose K, Nishi M, Noda T & Iino M (1998). Embryonic lethality and abnormal cardiac myocytes in mice lacking ryanodine receptor type 2. *The EMBO Journal* **17**: 3309-3316.

Tasker PN, Taylor CW& Nixon GF (2000). Expression and distribution of $InsP_3$ receptor subtypes in proliferating vascular smooth muscle cells. *Biochemical and Biophysical Research Communications* **273:** 907-912.

Terbach N, Shah R, Kelemen R, Klein PS, Gordienko D, *et al*. (2011). Identifying an uptake mechanism for the antiepileptic and bipolar disorder treatment valproic acid using the simple biomedical model *Dictyostelium*. *Journal of Cell Science* **124**: 2267-2276.

Thomas JM, Masgrau R, Churchill GC & Galione A (2001). Pharmacological characterization of the putative cADP-ribose receptor *Biochemical Journal* **359**: 451-457.

Thomas JM, Summerhill RJ, Fruen BR, Churchill GC & Galione A (2002). Calmodulin dissociation mediates desensitization of the cADPR-induced Ca^{2+} release mechanism. *Current Biology* **12**: 2018-2022.

Thompson CRL & Kay RR (2000). The role of DIF-1 signaling in *Dictyostelium* development. *Molecular cell* **6**: 1509-1514.

Thompson JL, Mignen O & Shuttleworth TJ (2010). The N-terminal domain of Orai3 determines selectivity for activation of the store-independent ARC channel by arachidonic acid. *Channels* **4**: 398-410.

Thomason PA, Traynor D, Cavet G, Chang WT, Harwood AJ & Kay RR. (1998). An intersection of the cAMP/PKA and two-component signal transduction systems in *Dictyostelium*. *The EMBO Journal* **17**: 2838-2845.

Timerman AP, Ogunbumni E, Freud E, Wiederrecht G, Marks AR & Fleischer S (1993). The calcium release channel of sarcoplasmic reticulum is modulated by FK-506-binding protein: dissociation and reconstitution of FKBP-12 to the calcium release channel of skeletal muscle sarcoplasmic reticulum. *Journal of Biological Chemistry* **268**: 22992-22999.

Traynor D, Milne JLS, Insall RH & Kay RR (2000). Ca^{2+} signalling is not required for chemotaxis in *Dictyostelium*. *The EMBO Journal* **19**: 4846-4854.

Uchikawa T, Yamamoto A & Inouye K (2011). Origin and function of the stalk-cell vacuole in *Dictyostelium*. *Developmental Biology* **352**: 48-57.

Van Baelen K, Dode L, Vanoevelen J, Callewaert G, De Smedt H, *et al.* (2004). The Ca^{2+}/Mn^{2+} pumps in the Golgi apparatus. *Biochemica et Biophysica Acta* **1742**: 103-112.

Van Dijken P, de Haas JR, Craxton A, Erneux C, Shears SB & Van Haastert PJM (1995). A novel, phospholipase C-independent pathway of inositol 1, 4, 5-trisphosphate formation in *Dictyostelium* and rat liver. *Journal of Biological Chemistry* **270**: 29724-29731.

Van Duijn B & Van Haastert PJ. (1992). Independent control of locomotion and orientation during *Dictyostelium discoideum* chemotaxis. *Journal of Cell Science* **102**: 763-768.

Van Haastert PJM & Devreotes PN (2004). Chemotaxis: signalling the way forward. *Nature Reviews Molecular Cell Biology* **5**: 626-634.

Vasudevan SR, Galione A & Churchill GC (2008). Sperm express a Ca^{2+}-regulated NAADP synthase. *The Biochemical Journal* **411**: 63-70.

Veltman DM, Keizer-Gunnink I & Haastert PJ (2009). An extrachromosomal, inducible expression system for *Dictyostelium discoideum*. *Plasmid* **61**: 119-125.

Venkatachalam K & Montell C (2011). TRP Channels Annual Review Biochemistry **76**: 387-417.

Vervoort EB, Ravestein A, Peij NNME, Heikoop JC & Haastert PJM (2000). Optimizing heterologous expression in *Dictyostelium*: importance of 5 codon adaptation. *Nucleic Acids Research* **28**: 2069-2074.

Wachter RM, Watkins JL & Kim H (2010). Mechanistic diversity of red fluorescence acquisition by GFP-like proteins. *Biochemistry* **49**: 7417-7427.

Wang YX, Zheng YM, mei QB, Cooier ML, Fleischer S, *et al*. (2004). FKBP12.6 and cADPR regulation of Ca^{2+} release in smooth mscle cells. *American Journal of Physiology Cell Physiology* **286**: 538-546.

Watanabe H, Vriens J, Prenen J, Droogmans G, Voets T & Nilius B (2003). Anandamide and arachidonic acid use epoxyeicosatrienoic acids to activate TRPV4 channels. *Nature* **424**: 434-438.

Weeks G (1976). The manipulation of the fatty acid composition of *Dictyostelium discoideum* and its effect on cell differentiation. *Biochimica et Biophysica Acta (BBA)-Lipids and Lipid Metabolism* **450:** 21-32.

Wilczynska Z, Happle K, Müller-Taubenberger A, Schlatterer C, Malchow D & Fisher PR (2005). Release of Ca^{2+} from the endoplasmic reticulum contributes to Ca^{2+} signaling in *Dictyostelium discoideum*. *Eukaryotic Cell* **4**:1513-1525.

Williams JG (2006). Transcriptional regulation of *Dictyostelium* pattern formation. *The EMBO reports* **7**: 694-698.

Wojcikiewicz RJ & Luo SG (1998). Differences among type I, II, and III inositol-1,4,5-trisphosphate receptors in ligand-binding affinity influence the sensitivity of calcium stores to inositol-1,4,5-trisphosphate. *Molecular Pharmacology* **53**: 656-662.

Wolf BA, Turk J, Sherman W & McDaniel M (1986). Intracellular Ca^{2+} mobilization by arachidonic acid. Comparison with myo-inositol 1, 4, 5-trisphosphate in isolated pancreatic islets. *Journal of Biological Chemistry* **261**: 3501-3511.

Wurster B & Kurzenberger W (1989). Periodic cell aggregation in suspensions of *Dictyostelium discoideum*. *Differentiation* **41**: 1-4.

Wurster B & Kay RR (1990). New roles for DIF? Effects on early development in *Dictyostelium*. *Developmental Biology* **140**: 189-195.

Wuytack F, Raeymaekers L & Missiaen L (2003). PMR1/SPCA Ca^{2+} pumps and the role of the Golgi apparatus as a Ca^{2+} store. *Pflügers Archive European Journal of Physiology* **446**: 148-153.

Yamaguchi S, Jha A, Li Q, Soyombo AA, Dickinson GD, Churamani D, *et al*. (2011). TRPML1 and two-pore channels are functionally independent organellar ion channels. *Journal of Biological Chemistry* **286**: 22934-22942.

Yamasaki M, Masgrau R, Morgan AJ, Churchill GC, Patel S, *et al*. (2004). Organelle Selection Determines Agonist-specific Ca^{2+} Signals in Pancreatic Acinar and β-Cells. *Journal of Biological Chemistry* **279**: 7234-7240.

Yang J, McBride S, Mak DOD, Vardi N, Palczewski K, Haeseleer F & Foskett JK (2002). Identification of a family of calcium sensors as protein ligands of inositol trisphosphate receptor Ca^{2+} release channels. *Proceedings of the National Academy of Sciences of the United States of America* **99**: 7711-7716.

Yeromin AV, Zhang SL, Jiang W, Yu, Y, Safrina O & Cahalan M (2006). Molecular identification of the CRAC channel by altered ion selectivity in a mutant of Orai. *Nature* 443: 226–229.

Yoshikawa F, Morita M, Monkawa T, Michikawa T, Furuichi T & Mikoshiba K (1996). Mutational analysis of the ligand binding site of the inositol 1, 4, 5-trisphosphate receptor. *Journal of Biological Chemistry* **271**: 18277-18284.

Yoshikawa F, Iwasaki H, Michikawa T, Furuichi T & Mikoshiba K (1999). Trypsinized cerebellar inositol 1, 4, 5-trisphosphate receptor. *Journal of Biological Chemistry* **274**: 316-327.

Zhang Y, Hoon MA, Chandrashekar J, Mueller KL, Cook B, *et al*. (2003). Coding of sweet, bitter, and umami tastes: different receptor cells sharing similar signaling pathways. *Cell* **112**: 293-301.

Zhang F and Li PL (2007). Reconstitution and Characterization of a Nicotinic Acid Adenine Dinucleotide Phosphate (NAADP)-sensitive Ca^{2+} Release Channel from Liver Lysosomes of Rats. *The Journal of Biological Chemistry* **282**: 25259-25269.

Zong X, Schieder M, Cuny H, Fenske S, Gruner C, *et al*. (2009). The two-pore channel TPCN2 mediates NAADP-dependent Ca^{2+}-release from lysosomal stores. *Pflugers Archiv European Journal of Physiology* **458**: 891-899.

Zorzato F, Fujii J, Otsu K, Phillips M, Green N, *et al*. (1990). Molecular cloning of cDNA encoding human and rabbit forms of the Ca^{2+} release channel (ryanodine receptor) of skeletal muscle sarcoplasmic reticulum. *Journal of Biological Chemistry* **265**: 2244-2256.